université de BORDEAUX

THÈSE

PRÉSENTÉE À

L'UNIVERSITÉ DE BORDEAUX

ÉCOLE DOCTORALE DE MATHÉMATIQUES ET D'INFORMATIQUE

par **Benjamin Alzaix**

POUR OBTENIR LE GRADE DE

DOCTEUR

SPÉCIALITÉ : MATHÉMATIQUES APPLIQUÉES

Mathematical and numerical analysis of the Herberthson integral equation dedicated to electromagnetic plane wave scattering

---

Date de soutenance : le 25 avril 2017 à l'auditorium de l'Onera Toulouse

Devant la commission d'examen composée de :

M. Herberthson,	Professeur Linköping University ,	Rapporteur
T. Abboud,	Cherchuer IMACS/Polytechnique Palaiseau,	Examinateur
A. Bendali,	Professeur émérite INSA Toulouse ,	Examinateur
B. Michielsen,	Ingénieur de recherche Onera Toulouse ,	Encadrant
J.-R. Poirier,	Maître de conférences INPT-ENSEEIHT Toulouse ,	Co-directeur
L. Giraud,	Directeur de recherche Inria Bordeaux ,	Directeur

– 2017 –

Abstract This thesis is about the scattering of an electromagnetic plane wave incident on a perfectly conducting smooth surface. It presents the analysis of the properties of a new formulation of the three principal boundary integral equations of electromagnetic scattering theory (EFIE, MFIE and CFIE). The basic idea is to adapt the conventional integral equations to plane-wave scattering by supposing that the phase function of an incident plane wave determines the phase function of the induced boundary current distribution.
This idea of using the phase in plane wave scattering has previously been studied in high-frequency scattering, in particular in the theses by Zhou (1995) and Darrigrand (2002) who adapt the finite element approximation spaces. In this thesis, though, we follow a more recent formulation, given by Herberthson (2008), where the phase function is incorporated in the kernel distribution of the integral operators.
Presenting the modified version of the EFIE and the MFIE (denoted HEFIE and HMFIE) in appropriate function spaces, we prove the existence of a unique solution to this specific formulation and developp an original practical implementation which takes advantage of the gained experience on the EFIE/MFIE. Then, we explore another important property provided by the new formulations: the possibility to reduce the number of degrees of freedom required to get an accurate solution of the problem.

Keywords electromagnetic scattering, boundary integral equation, plane wave

Titre Analyse mathématique et numérique de l'équation intégrale de Herberthson dédié à la diffraction d'ondes planes

Résumé Cette thèse porte sur la diffraction d'une onde plane électromagnétique par une surface lisse parfaitement conductrice (PEC). Elle présente l'analyse des propriétés d'une nouvelle formulation des trois principales équations intégrales de frontières de la théorie de la diffraction électromagnétique (EFIE, MFIE et CFIE). L'idée est d'adapter les équations intégrales conventionnelles à la diffraction d'une onde plane en supposant que la fonction de phase de l'onde plane incidente détermine la fonction de phase de la distribution de courant induit sur la surface.
L'idée d'utiliser la phase dans la diffraction d'ondes planes a déjà été étudiée pour les hautes fréquences, notamment dans les thèses de Zhou (1995) et Darrigrand (2002) qui adaptèrent les espaces d'approximation des éléments finis. Dans cette thèse, cependant, nous suivons une formulation plus récente, donnée par Herberthson (2008), où la fonction de phase est incorporée dans la distribution du noyau des opérateurs intégraux.
En présentant les versions modifiées de l'EFIE et de la MFIE (dénommées HEFIE et HMFIE) dans des espaces fonctionnels appropriés, nous prouvons ici l'existence d'une solution unique à cette formulation spécifique et présentons une mise en œuvre pratique originale qui tire parti de l'expérience acquise sur l'EFIE/MFIE. Par la suite, nous explorons une propriété importante offerte par ces nouvelles formulations: la possibilité de réduire le nombre de degrés de liberté requis pour obtenir une solution précise du problème.

Mots-clés diffraction électromagnétique, équation intégrale de frontières, onde planes

Laboratoire d'accueil Onera Toulouse, 2 avenue Edouard Belin, 31400 Toulouse

Remerciements

Merci à vous tous!

Il est probablement de meilleures introductions à cette page de remerciements, tant il est difficile d'être juste, concis et exhaustif lorsque l'on souhaite témoigner telles gratitudes. Bien des personnes ont joué des rôles importants durant ces quatre dernières années, et ces quelques mots, à défaut d'une très longue liste, auront au moins le mérite d'en oublier aucune.

Tout d'abord, je souhaiterais remercier MM. Michielsen et Poirier d'avoir proposé cette thèse qui m'a permis de travailler pendant quelques années sur un sujet extrêmement intéressant et riche, tant sur les thèmes abordés que les domaines scientifiques explorés. Leurs visions du sujet, la dialectique qui en résulta, furent des plus intéressantes, et si quelques-unes des nombreuses pistes investies n'aboutirent pas, cette diversité fut la vraie richesse de cette thèse.

Je souhaiterais ensuite remercier M. Giraud d'avoir dirigé cette thèse, de s'être posé, parfois, en juge de paix et de manière générale pour ses conseils avisés. Il est fort probable que cette thèse n'aurait jamais abouti sans son implication, et à ce titre il doit être doublement remercié.

Je remercie MM. Herberthson, Darrigrand et Antoine d'avoir accepté d'examiner cette thèse et de la rapporter, ainsi que pour l'ensemble de leurs remarques sur mes travaux. Je remercierais enfin MM. Abboud, Bendali et Herberthson d'avoir participé au jury d'une soutenance qui ne s'est fait que trop longtemps attendre.

Pour conclure, j'aimerais aussi remercier toutes les personnes du DEMR pour leur accueil, le cadre et l'environnement de travail qui s'y trouvent. Je garderais toujours de très bons souvenirs des conversations de la pause-déjeuner, aux sujets aussi variés que passionnés. Enfin, je me permettrais de faire une mention toute spéciale au "Bureau 116", à l'ensemble des doctorants que j'ai pu côtoyer, à vous: "Bonjour!".

"We all change, when you think about it, we're all different people; all through our lives, and that's okay, that's good, you've gotta keep moving, so long as you remember all the people that you used to be. I will not forget one line of this, not one day, I swear."

S. Moffat

Introduction

The context

The simulation of electromagnetic scattering and the computation of radar signatures, for example, Radar Cross Section (RCS), of large structures is an important issue for industrial applications. Fields of application of such simulations are various; among them, we can find the technologies of radar stealthiness in defense activities, recognition and identification of aircraft, electromagnetic compatibility effect of a wind turbine farm on the operation of electromagnetic field, ... As the numerical methods used to simulate these phenomena require ever more resources, both in memory and in computation power, the simulation of such phenomena has been a very active domain of research in the last decades.
From a general point of view, an electromagnetic scattering problem is a radiation problem where a local current distribution, induced by an external current or field, has to be computed. To be more concrete, let us consider an object, an airplane for example, immersed in free space and submitted to an incident wave. This incident wave creates a distribution of current throughout the scattering object which in its turns generates the scattered field in the surrounding space.
From a mathematical point of view, to formalize and model this scattering phenomenon, the first tool at our disposal, is the system of Maxwell equations. These equations developed by Maxwell in 1865, reformulated in 1873, and developed in the vector calculus formalism by Heaviside a few years later, can be used to model and characterize the electromagnetic field solutions of the scattering problem that we described above.

. Partial Differential Equations

From the Maxwell equations and the establishment of boundary conditions, one can solve the scattering problem. Basically, from this point, either we can look for an analytical expression of the solution or we can discretize the Partial Differential Equations (PDE) that constitute the Maxwell equations. There are various methods to discretize the PDE; among them, we can cite two important classes: the finite difference discretization, mostly applied in the time-domain, and the finite element discretization, mostly used in the frequency-domain.

- Finite difference methods, for example the FDTD [1] (Finite Difference in Time Domain), are methods that calculate the electromagnetic field on a Cartesian grid of the space. Their main features enable the computation of fields anywhere on the grid for any time t from the value of the field at the previous time. With an explicit scheme, these methods are also characterized by the absence of a linear system to solve. However the time discretization is related to the space discretization by a Courant-Friedrichs-Lewy stability condition. One of the main limitations of this method is the use of a Cartesian grid which hardly respects the geometry of the scattering object and which sometimes introduces numerical dispersion problems which substantially reduce the quality of the solutions.

- Finite element methods [2] are also interesting. They allow, in contrast to finite difference methods, to follow the geometry of the object by meshing the surrounding space with tetrahedra. The resulting approximation leads to the solution of a sparse linear system (often very large) that describes the interactions between each tetrahedron and its neighbours. The linear system can be solved by means of iterative methods specific to sparse matrices. The main limitation of this kind of method is due to its important needs in terms of computing resources.

Discretizing the PDE is interesting for simulation in both the frequency and the time-domain, but also for heterogeneous objects and media. One of the advantages of time-domain methods is to obtain the scattering behaviour of the object for a range of frequencies from the results of a single computation. However, in general, these methods suffer from very serious theoretical difficulty: numerical solution can be established only on bounded domains. If we solve the exterior Maxwell problem, the domain of the solution field is unbounded, therefore the domain has to be truncated before being meshed. This operation is achieved by imposing conditions on the outer surface of the solution domain in order to simulate an infinite volume (see [1] for example).

. Integral Equations

Since PDE discretization methods can suffer from certain difficulties, one can also look for a fundamentally different approach. In fact, in homogeneous domains (constant coefficients in the Maxwell equations), we have integral representations of the electromagnetic field in the domain in terms of its values on the boundary of the domain (usually denoted as an electric surface current, j_S, and a magnetic surface current, m_S). Therewith, the problem of scattering by homogeneous objects, like perfectly conducting (PEC) objects, can be reduced to an integral equation on the object's boundary. The essential integral equations are established in Chapter 1. For PEC objects, for example, integral equation methods involve the computation of only the electric current j_S on the surface of the radiating object (the magnetic current m_S are known in this case). This problem is strictly equivalent to the determination of the electric field E and the magnetic field H in the surrounding domain Ω. From the currents j_S and m_S, by means of integral representations, the fields E and H can be determined throughout the volume and automatically satisfy the Maxwell equations and the radiation conditions at infinity. Since the exterior domain does not require to be meshed, integral methods, when applicable, are generally more accurate than partial differential equation methods and are often used as reference methods, see [3, 4, 5].

From a technical point of view, surface currents can be expanded in a basis of tangent-vector functions on the surface. These functions generally have a reduced support (of the order of $\lambda/10$ where λ is the wavelength). The main difficulty lies in the fact that local currents, represented by an element of this basis, radiate throughout the surrounding space and interact with all the other basis elements. This strong interaction leads to the solution of a linear system involving complex matrices, which are dense and can be ill-conditioned.
For objects with very large sizes, the solution of the linear system is a challenging problem requiring the use of large computing resources. The idea is then to use iterative solvers, such as CG, BiCG, QMRES, GMRES or TFQMR (see [6]), for the solution of the linear system. Measuring the computational complexity as $O(N_{iter}N^2)$, where N is the dimension of the matrix and N_{iter} the number of iterations required to obtain an approximate solution, which is generally required to be significantly smaller than the dimension of the problem.

Although these iterative methods only need matrix-vector products, the ill-conditioned matrices put in difficulty these numerical methods and increases significantly the CPU and storage

cost. Therefore, it appears necessary to add acceleration and preconditioning methods. Among the acceleration methods, we can mention for example IE-FMM [7, 8, 9] and IE-ACA [10] methods. They all aim to reduce the computational complexity and memory requirements. Preconditioners intend to improve the conditioning in order to facilitate the solution of the linear system, they can be applied before the assembly [11, 12] or after [13].
There is not yet a definitive and unique solution method, iterative solvers combined with preconditioning and acceleration might still exhibit slow convergence for realistic objects for various reasons (complexity of the geometry, local over-meshing ...).

. Asymptotic methods and integral equations

If there are a large number of solution methods, the scattering problem for high frequencies remains a very active field of research. For several decades, different authors proposed to combine different kind of solution methods, previously dissociated, in particular integral equations and asymptotic methods.
The latter, justified by pseudo-differential operator analysis, consists in considering a particular approximation of the solution, locating the propagation of waves along privileged directions and proposing a simpler problem. This family of methods includes various methods such as physical optics or geometric diffraction theory. These methods were for a long time the only ones to give results for high frequencies, since they have the advantage of presenting a complexity that does not increase with the frequency. However, they suffer several limitations. Among them, we can mention a complex implementation in the case of non-convex surfaces and of multiple reflections.
On the other hand, the integral equations are able to take into account the radiation condition and the geometry of the scattering object and are intended to be fairly simple to implement in non-convex cases. The main limitations are a complexity which increases with the frequency and the necessity to solve a full linear system, with large size with complex values, sometimes ill-conditioned.
Consequently, the idea was to combine these two methods to reduce the inherent difficulties, in particular to reduce the number of coefficients of the matrix resulting from the integral equations. If the two-dimensional case was fairly well treated, see [14, 15], adding the third dimension of space make it turn out more delicate and the expected gains turned out to be less important than hoped for.
In [16, 17, 18], B. Zhou directly uses the Kirchhoff approximation in its basic functions to reduce the size of the matrix. Under some conditions (notably the convexity of the scattering surface), the starting point consists in expressing the unknown of the scattering problem, the boundary current, by introducing an approximation of its phase by the phase of the incident plane wave. The idea is to limit the problem to finding the modulus of the current, which is a function less oscillating than the current itself. From there, Zhou proposes to couple this approximation with the method of integral equations by introducing new functional and approximation spaces, constituted of oscillating test functions. Furthermore, to reduce the number of degrees of freedom, he builds a technical system with a double mesh, called micro-local discretization, with a coarse mesh to represent the current and a fine mesh to correctly compute the oscillating integrals defining the Galerkin coefficients. The main drawback of this method is that the matrix is then dependent of the incidence direction.
In the same spirit, A. de la Bourdonnaye and M. Tolentino [19, 20] proposed another method which shares an idea previously formulated by F.X. Canning in [15]. This other method relies on a discretization of the unit sphere, parameterizing the propagation directions in the phase distribution of the unknown. Although this formulation applies under more general conditions

(non-convex domains and arbitrary direction of incidence) than the method presented by Zhou, it appears to be more difficult to implement.
Starting from differential calculus, they propose to approximate the current by a linear combination of plane waves with various directions of incidence, preselected and independent of the direction of the incident wave. Although this method does not significantly reduce the number of degrees of freedom, it leads to a very sparse linear system. However, in some cases, the matrix appears to be ill-conditioned and requires an efficient preconditioner. Finally, E. Darrigrand [21, 22, 23] proposed a formulation coupling a fast multipole method and the micro-local discretization method introduced by Zhou through the integral formulation of B. Després [23].

Outline of the thesis

The starting point for this thesis is the work of M. Herberthson, published between 2008 and 2010 ([24, 25, 26]). Herberthson proposed a new formulation of the three principal conventional integral equations, i.e., for the Electric (EFIE), the Magnetic (MFIE) and the Combined (CFIE) Field Integral Equation. The basic idea is the same as what inspired the work by Zhou and Darrigrand cited in the previous section: adapt the conventional integral equations to plane-wave scattering by supposing that the phase function of an incident plane wave will determine, to a high degree, the phase function of the induced boundary current distribution. The actual current distribution is then a complex vector-valued modulation of this phase function and we can make this modulation explicit as a pseudo-current by multiplying the actual current with the complex conjugate of that phase function (or, equivalently, representing the actual current as the pseudo current multiplied by the incident wave's phase function).
The second idea was also to do a phase conjugation of the whole equation and therewith, reducing the right hand side of the equation to the boundary trace of a constant polarisation vector. In Galerkin discretisation, this is equivalent to the techniques proposed by Zhou and Darrigrand when the current expansion functions are conventional finite elements multiplied by the incident field and the weight functions are the same finite elements multiplied by the complex conjugate phase function. In the presentation of Herberthson, however, a new integral equation for the pseudo current is defined by including the incident plane wave's phase function in the kernel distribution. The Helmholtz decomposition splitting the pseudo-current into a surface gradient and a surface curl component further transforms the original integral equation for a vector distribution into one for two scalar distributions. This last step, which is possible for boundaries with specific topologies only, will not be done in this thesis.

The basic equations

The basic system of equations studied in this thesis is the system of Maxwell equations. To respond to the invitation by Herberthson in his articles, we chose to take these equations in the formalism of differential forms and offer a complete modelling of the phenomenon using the same formalism. Despite its centenary existence (E. Cartan, 1899) and its general adoption in fundamental theoretical physics, the differential form formulation is still not well established in the world of electromagnetic modelling. However, the algebra and calculus of differential forms is ideally suited to the study of electromagnetism. As we show in Chapter 1 (and Appendix A), this formalism provides a simple, compact and elegant formulation of the boundary value problems of electromagnetics. In the same chapter, the basic boundary integral equations, namely the EFIE, the MFIE and the CFIE, are formally derived from the partial differential equations.

Adaptation of the Electric and Magnetic Field Integral Equations to plane wave scattering

In Chapter 2, we study the electromagnetic boundary integral equations from a mathematical point of view, that is, we consider a set of consistent function spaces for representing the physical quantities (the incident and diffracted fields, boundary currents, ...) and the operators defined on them. For each conventional equation, the literature provides us a well-suited set of function spaces to establish the existence and uniqueness of a solution of the scattering problem. Our objective is to describe, in a mathematical sense, the solution of the problem in order to give for each integral equation, both conventional and Herberthson's modified version, a strong and a weak formulation in suitable function spaces. The modified versions of the boundary integral equations are shown to be algebraically equivalent to there conventional counterparts. In this way, we obtain the conditions for the existence of a unique solution. Then we show that the HEFIE can also be described as the sum of the EFIE and a perturbation. This representation is advantageous for numerical implementations as will appear in the later chapters.

Numerical Implementation

In Chapter 3, we begin with the practical implementation of the integral equation. The aim here is to give all the elements needed to build the Galerkin matrices and form the linear systems. First, we consider the practical implementation of the HEFIE in an edge finite element space. The originality of our implementation is to take advantage of the gained experience on the EFIE, in terms of implementation and finite element code, and focus not on the HEFIE itself, but on the perturbation, with respect to the EFIE, that we exhibited previously. This approach leads us to introduce a new matrix to represent the perturbation on edge finite elements. We adopt the same strategy for the HMFIE.

In a second step, we study an implementation of the Helmholtz decomposition on edge finite element spaces. The goal was to move the system from the initial HEFIE on edge finite elements into the one suggested by Herberthson, which splits the current distribution into a divergent and a solenoidal part and leads to a right-hand side with a lot of null-terms. For this, we explore different tracks and notably study the link between cycles on the face-edge incidence graph of the mesh and linear combinations of edge function belonging to the kernel of the divergence. Finally, we formalize this decomposition by a sparse change-of-basis matrix in order to obtain the desired system.

With the given numerical implementation, we have done two distinct studies.

- The first concerns the study of the new linear systems (HEFIE/HMFIE) and their solution (cf. Chapter 4). The purpose, here, was to assess whether it is possible, using a Helmholtz decomposition, to accelerate the solution by focusing on a subspace of divergent or solenoidal pseudo-currents. In order to corroborate the results of this numerical study, we have carried out a detailed analytical study of the HEFIE in a spherical harmonic expansion on a sphere (cf. Chapter 6).

- The second study deals with the reduction of the degrees of freedom made possible by the fact that the pseudo-current is only weakly oscillating. This aspect had been studied by Zhou [16, 17, 18] and Darrigrand [21, 22, 23] and Herberthson [24, 25, 26]. In this thesis, though, we show the advantages of computing the discretised perturbation operator separately. Because the HEFIE operator is dependent on the direction of incidence, just like the modified finite element discretisations considered by Zhou and Darrigrand, it is

important to minimise the computational cost by handling multiple incidence directions. We show that combining the reduced number of degrees of freedom and recomputing only the perturbation part (which is the only part depending on the direction of incidence), can be more efficient than using the conventional EFIE or the system proposed by Zhou.

Computational analysis of the solution of the linear systems

With the implementation of the modified Herberthson version of the EFIE, MFIE and CFIE detailed, we establish in Chapter 4 some numerical properties of the Galerkin matrices and present some aspects of the solution of the associated linear systems. We have considered the scattering of a plane wave incident on perfectly conducting bodies: a sphere and an airplane. In order to choose an appropriate solution method, it quickly appears necessary to look at the interactions between divergent and solenoidal currents, which are reflected in the norms of some blocks of the matrices. These interactions are illustrated for the two examples: the scattering of a plane wave by a perfectly conducting sphere and by a perfectly conducting airplane over a range of frequencies.

Through this study, we attempt to highlight the performance of the HEFIE and the HMFIE and identify the situations where the new formulation will be the best suited one (in terms of structures, frequencies, ...). Then, we look at the solution of the linear systems and especially at possible algebraic preconditioners for the new linear systems. Therefore, to evaluate the advantages of our solution methods, we begin with the analysis of the additional costs generated by the construction of the HEFIE from the EFIE (and, by the same token, for obtaining the HMFIE from the MFIE). Choosing the Krylov iterative solver GMRES as a reference, we translate these costs into an equivalent minimal number of GMRES iterations to gain, in order to see whether Herberthson's versions are competitive. Then, we propose various preconditioners, based on our previous studies and experience, and compare, for the two chosen configurations, the number of GMRES iterations required to solve the system.

Reduction of the number of degrees of freedom

Apart from the analysis of linear systems and their solution, we are interested in another important property provided by Herberthson's equations: the possibility to reduce the number of degrees of freedom required to get an accurate solution of the problem. In Chapter 5, we develop this aspect of the modified equations. Considering the conventional equations and the scattering of a plane wave with a frequency f_0, a good approximation of the surface current requires the edges of the mesh to have a maximum size, h, smaller than, say, $\lambda_0/7$. Therefore, it seems interesting to see whether the HEFIE suffers from the same constraint. To test this, we study the quality of the current obtained from the HEFIE with meshes conforming and non-conforming to this constraint. It appears that the limitations of the HEFIE are the same as those of the EFIE, but for different reasons. Whereas the original EFIE suffers from both bad numerical integrations and a non-adapted mesh for the representation of the physical current, the HEFIE only suffers from bad numerical integrations.

In order to get a good solution in terms of surface current, we have shown that it is necessary to work on a fine mesh. However, as the size of the associated linear system increases, it is useful to look for an alternative to the linear system obtained from a fine mesh. Therefore, our objective is to create a linear system with a size as small as possible that can still give a good quality solution. The idea is then to consider two meshes: a coarse mesh adapted to the representation of the pseudo-current, but not necessarily conforming to the constraint "$h < \lambda/7$", and a fine mesh conforming to that constraint having a mesh size a factor two smaller than the coarse mesh. Noting that the interactions between local currents defined on the coarse mesh were

poorly described, we propose to compute the Galerkin coefficients of the coarse mesh matrix by using the integration rules associated with the fine mesh. We can then evaluate the reduced system for the HEFIE in terms of quality of the current solution, computational cost and number of GMRES iterations.

A reference case: the scattering of a plane wave by a perfectly conducting sphere

In addition to the above work, we also did an analytical study of Herberthson's version of the EFIE for the special case of scattering by a perfectly conducting sphere. The purpose of Chapter 6 is to get the expressions for the HEFIE operator coefficients in a basis of orthogonal vector spherical harmonics and then to study the operator norms, in particular those related to the coupling between the subspaces of divergent and solenoidal surface currents.
One of the objectives of this study is to give a completely explicit representation of the HEFIE operator in the vector spherical harmonics basis in the previously given factorized form. Since the EFIE operator is diagonal in that basis, we take advantage of the similarity relation developed in Chapter 2, to get a full representation of the HEFIE. The essential difficulty is, therefore, to find a representation of the phase conjugation operator in the basis of vector spherical harmonics.
With a representation of the phase conjugation operator (and its inverse) in the basis of the vectorial spherical harmonics and using the similarity relation between the EFIE and the HEFIE, we get an explicit representation of the HEFIE. Since these transformation matrices are essentially band-matrices, using the fact that the EFIE has a diagonal matrix representation, we obtain a band matrix representation of the HEFIE. This last representation gives us another point of view on some aspects of the HEFIE and the Helmholtz decomposition with edge finite element discretization.

Contents

Part I

Definition and mathematical analysis of new boundary integral equations

Chapter 1

A brief review of electromagnetism

Contents

The objective of this chapter is to present some general relations from electromagnetic field theory and, in particular, define electromagnetic scattering problems. First, from the Maxwell equations, in the formalism of differential forms, we describe how to get the Helmholtz equations that govern the behaviour of both the electric and the magnetic field in a homogeneous space. Then, we show how to represent the electric and magnetic fields in terms of their boundary values through the Lorentz relation and the elementary solution of the Helmholtz equation. Finally, we present the scattering problem and the principal integral equations used to solve it. The main results can be found in [5, 27, 28, 29, 30, 31]. We present a short overview of differential forms in the first section, more detailed material is provided in Appendix A.

1.1 A hitchhiker's guide to differential forms

The goal of this first section is to give a short overview of differential forms on $\mathbb{R}^3$ in order to set the notations and allow the reader unfamiliar with this formulation of electromagnetism to follow the developments carried out in this first part. We recommend the reading of [29, 27, 32, 33, 34] and Appendix A for a more complete overview.

. Motivations

Despite its centenary existence (E. Cartan, 1899) and its general adoption in fundamental theoretical physics (such as general relativity, quantum field theory, Hamiltonian dynamics, . . .),

the differential form formulation is still not well established in the world of research in electromagnetic modelling (see [35] for historic overview). Despite some interesting publications such [27] or [29], for example, the major part of the literature on electromagnetics is still formulated in vector calculus.

In fact, the algebra and calculus of differential forms, due to its convenience, compactness, and many other qualities, is ideally suited to the study of electromagnetics. The calculus of differential forms, which has been applied to EM theory by Deschamps [27], Lindell [28], Bossavit [36], Warnick [29, 37, 38, 39] and other authors [40, 41, 42, 43], make main results and equations in EM theory more concise than the usual vector analysis presentations. For example, the differential forms provide a simple, compact and elegant formulation for the Maxwell and Helmholtz equations using only two operators: the exterior derivative operator $\mathbf{d}$ and the Hodge star operator $\star$ while vectorial formulation requires the use of the gradient, the curl and the divergence.

The calculus of differential forms offers both algebraic and geometrical advantages over vector analysis. With differential forms, vector identities and theorems are reduced to simpler algebraic properties and manipulations are often more transparent and less tedious than they would be in vector analysis (see [29] or [44, Chapter 4]). In particular, the behaviour under coordinate changes of differential forms is as simple as with scalar functions because, in a certain way, the reference frame makes part of the definition of the differential form. Differential forms also let field quantities and the laws they obey to be manipulated and visualised in a more intuitive manner. In addition, there is a simple correspondence between the formalism of differential forms and classical vector calculus.

. Space and coordinate charts

Let $\mathbb{E}^3$, be the Euclidean space of dimension 3, with a canonical coordinate chart $\mathbb{R}^3$. We use the coordinate triples to identify points and write for a $p \in \mathbb{E}^3$ the coordinate triple in the canonical chart as $(p^1, p^2, p^3) \in \mathbb{R}^3$. For the chosen chart, the specific element $(0, 0, 0)$ is used as the coordinates of a reference point and we will refer to it both as $0 \in \mathbb{R}^3$ and as $0 \in \mathbb{E}^3$. As a three-dimensional linear manifold, $\mathbb{E}^3$ is isomorphic to each of its tangent spaces $T_p\mathbb{E}^3$, where p is any point in $\mathbb{E}^3$. Let $\{e_i\}_{i\in[\![1;3]\!]}$ be a basis of the particular tangent space $T_0\mathbb{E}^3$, we can then define the isomorphism $\xi \in T_0\mathbb{E}^3 \mapsto p_\xi \in \mathbb{E}^3$ by identifying the components of a vector in $T_0\mathbb{E}^3$ with the coordinates of a point $p \in \mathbb{E}^3$, i.e., the "coordinates"of p_ξ in the canonical chart are given by $p^k_\xi = \xi^k$ for $k \in [\![1; 3]\!]$ the components of ξ the basis of $T_0\mathbb{E}^3$. We also write $\xi_p \in T_0\mathbb{E}^3$ with $\xi^k_p = p^k$ for the inverse of this isomorphism.

For each of the tangent spaces, we can define the dual vector space as a space of linear forms on the tangent spaces. These are called the co-tangent spaces and we write $T^*\mathbb{E}^3$.

We can introduce a different chart, say C, on $\mathbb{E}^3$ which associates other coordinate triples with the points. As an example, we elaborate a chart of the so-called spherical coordinates. In spherical coordinates each point gets a triple of coordinates which we write as (r, ϑ, φ). The chart transition mapping is defined by expressing the canonical coordinates as functions of the new ones.

$$\begin{aligned} & C = \mathbb{R}_+ \times (0, \pi) \times [0, 2\pi), \\ \mu : \quad & C \to \mathbb{R}^3, \\ & (r, \vartheta, \varphi) \mapsto (x, y, z), \end{aligned}$$

where we used the shorthand notation

$$\begin{aligned} x &= r\sin(\vartheta)\cos(\varphi), \\ y &= r\sin(\vartheta)\sin(\varphi), \\ z &= r\cos(\vartheta). \end{aligned}$$

Note, that, strictly speaking this chart alone does not cover the whole Euclidean space. We should not have said that each point in $\mathbb{E}^3$ gets a new coordinate triple, in fact the points with canonical coordinates $(0, 0, x^3)$ are not covered because there is no canonical way to complete the chart continuously because the choice of φ is ambiguous for these points.

The Euclidean space $\mathbb{E}^3$ is a metric manifold and it includes in its definition a metric on its tangent vector spaces. This metric determines the way angles between directions are measured and sizes are associated with subsets (lengths of curves, areas of surfaces, volumes of full subsets, etc). On a Euclidean manifold, the tangent spaces have a scalar product defined by this metric. A metric is a symmetric positive bilinear form g,

$$\begin{aligned} g: \ T_p\mathbb{E}^3 \times T_p\mathbb{E}^3 &\to \mathbb{R}^+, \\ (u, v) &\mapsto g(u, v) = \sum_{i,j=1}^{3} g_{ij} u^i v^j. \end{aligned}$$

This metric induces a metric in the co-tangent spaces

$$\begin{aligned} g^*: \ T_p^*\mathbb{E}^3 \times T_p^*\mathbb{E}^3 &\to \mathbb{R}^+, \\ (u, v) &\mapsto g^*(u, v) = \sum_{i,j=1}^{3} g^{ij} u_i v_j, \end{aligned}$$

where the coefficients g_{ij} and g^{ij} constitute two square matrices which are the inverses of each other, such that $\sum_k g_{ik} g^{kj} = \delta_i^j$.

The distinction between a given manifold, on the one hand, and charts on the manifold, on the other hand, is made in order to be able to define intrinsic objects on the manifold by means of constraints on the transformations of their representations under chart transitions. Tangent vectors in $T_p\mathbb{E}^3$ are supposed to be intrinsic, i.e., they should be usable for representing the growth rate of functions on the manifold. These growth rates, with a direction and an amplitude, are required to have a chart independent interpretation. The metric is another example of an intrinsic object intricately related to the objective meaning of tangent vectors.

In the canonical chart $\mathbb{R}^3$ on $\mathbb{E}^3$, the metric has, by definition, the coefficients

$$g_{ij} = \delta_{ij},$$

so the matrix representation is the 3×3 unit matrix. A change of charts on $\mathbb{E}^3$ must be such that the scalar products of vectors in any $T_p\mathbb{E}^3$ remain invariant.

The metric can be used to define an isomorphism between a tangent space $T_p\mathbb{E}^3$ and its co-tangent space $T_p^*\mathbb{E}^3$ by "transposition"

$$\begin{aligned} \flat: \ T_p\mathbb{E}^3 &\to T_p^*\mathbb{E}^3, \\ u &\mapsto u^\flat = g(u, \cdot) = \sum_i g_{ij} u^i a^j \\ \sharp: \ T_p^*\mathbb{E}^3 &\to T_p\mathbb{E}^3, \\ \alpha &\mapsto \alpha^\sharp = g^*(\alpha, \cdot) = \sum_i g^{ij} \alpha_i e_j. \end{aligned}$$

In short, for a tangent vector u, the metric transpose has coefficients

$$(u^\flat)_k = \sum_i u^i g_{ik},$$

for a co-tangent vector α the metric transpose has coefficients

$$(\alpha^\sharp)^k = \sum_i \alpha_i g^{ik}.$$

These notations are inspired by the musical interpretation of the word transposition and the convention to write vector coefficients with upper indices and co-vector coefficients with lower indices. As a musical $\flat$ indicates a note's lower alteration and $\sharp$ a note's higher alteration, these transpositions are also called the musical isomorphisms. As the vector or co-vector nature of an object should be defined before it is used, one could also write X^t for the metric transpose irrespective of whether X is a tangent vector or a tangent cotangent vector.

. The space of differential forms

Let x^i be the so-called i-th coordinate function:

$$\begin{aligned} x^i : \quad & \mathbb{E}^n \to \mathbb{R}, \\ & p \mapsto x^i(p) \end{aligned}$$

in the canonical chart. We also use the shorthand notation $p^k = x^k(p)$. Following developments made in Sections A.2–A.7, we know that an admissible basis for the cotangent spaces $T_p^*\mathbb{E}^3$, the space of linear forms on $T_p\mathbb{E}^3$ (or the space of 1-forms), is the set $\{dx^k\}_{k\in[\![1;3]\!]}$ where dx^k is the differential of the function x^k. Therefore, every 1-form α can be written as

$$\alpha = \sum_{i=1}^{n} \alpha_i dx^i, \tag{1.1}$$

where the α_i are real functions. If the functions α_i are differentiable, α is called a differential form of degree 1.

The 1-forms constitute, in each point p, a linear space of dimension 3, noted $\Lambda_p^1\mathbb{E}^3$ or just Λ_p^1 if no confusion is possible. We introduce the space of p-forms by means of the exterior product "$\wedge$", as elements of a vector space Λ^p, with dimension $\binom{n}{p}$. Λ^p is defined as

$$\Lambda^p = \bigwedge^p \Lambda^1 \tag{1.2}$$

such that each p-form, ω, can be written in a generic way as:

$$\omega = \sum_{\substack{m_1,\ldots,m_p=1 \\ m_1<\ldots<m_p}}^{n} \omega_{m_1,\ldots,m_p} dx^{m_1} \wedge \ldots \wedge dx^{m_p}. \tag{1.3}$$

The coefficients with the special constraint on the indices are referred to as the essential coefficients of the p-form. This notation looks a little tedious, but in the concrete computations one mostly manipulates the object ω or a few auxiliary objects which define its constituents. Anyway, on $\mathbb{E}^3$, even the completely explicit representation is rather simple (see Example 1.1).

Example 1.1 : **Differential forms on $\mathbb{E}^3$ in the canonical chart**

The 0-forms are simply defined by the scalar-valued functions on $\mathbb{R}^3$. The 1-form α, defined by

$$\alpha = \alpha_1\, dx^1 + \alpha_2\, dx^2 + \alpha_3\, dx^3 \tag{1.4}$$

has three coefficients. It can be transposed into a tangent vector of $T\mathbb{E}^3$ through the isomorphisms $\sharp$. A 2-form ω defined by

$$\omega = \omega_1\, dx^2 \wedge dx^3 + \omega_2\, dx^3 \wedge dx^2 + \omega_3\, dx^1 \wedge dx^2 \tag{1.5}$$

has also three coefficients. However, it is not the transpose of a tangent vector. Finally, a 3-form γ is defined by

$$\gamma = \gamma_{123}\, dx^1 \wedge dx^2 \wedge dx^3 \tag{1.6}$$

and has only one essential coefficient but it is not the same object as a scalar function. □

This example shows that differential forms of different degrees can have the same number of essential coefficients, but are truly different objects. The Hodge star operator gives the relation between such forms (see [27, Section III.b] and [32, Section 2.7]).

. The Hodge star operator

In this paragraph, we define the Hodge star operator $\star$. It is a linear, bijective, mapping from Λ^p to Λ^{n-p}. In a general context, this application depends on a metric and a choice of orientation on the concerning space. In the context of an space such $\mathbb{E}^3$, we use the standard metric

$$g^* = \begin{pmatrix} 1 & 0 & 0 \\ 0 & 1 & 0 \\ 0 & 0 & 1 \end{pmatrix}$$

and the standard orientation. A general expression of this operator is given in Appendix A.6, here, we focus on its application in $\mathbb{E}^3$ (see Example 1.2).

Example 1.2 : **The Hodge star in $\mathbb{E}^3$**

Let consider the chart $\mathbb{R}^3$, with coordinate functions (x, y, z), and the basis (dx, dy, dz) for the co-tangent space. We have:

$$\begin{aligned} \star 1 &= dx \wedge dy \wedge dz, & \star\, dx \wedge dy \wedge dz &= 1, \\ \star\, dx &= dy \wedge dz, & \star(dy \wedge dz) &= dx, \\ \star\, dy &= dz \wedge dx, & \star(dz \wedge dx) &= dy, \\ \star\, dz &= dx \wedge dy, & \star(dx \wedge dy) &= dz. \end{aligned}$$

□

This example shows that in the canonical chart on $\mathbb{E}^3$ the Hodge star operator is its own inverse.

. The exterior derivative and co-differential operators

We now introduce the exterior derivative and the co-differential operator, written $\mathbf{d}$ and $\boldsymbol{\delta} = \star^{-1}\, \mathbf{d}\, \star$, respectively. We can focus here on $\mathbf{d}$ in $\mathbb{R}^3$, the properties of $\boldsymbol{\delta}$ can easily be deduced using those of $\star$ and $\mathbf{d}$.

Example 1.3 : **The exterior derivative in $\mathbb{R}^3$**

We begin with the action of $\mathbf{d}$ on a function f:

$$\mathbf{d}\, f = \frac{\partial f}{\partial x} dx + \frac{\partial f}{\partial y} dy + \frac{\partial f}{\partial z} dz. \tag{1.7}$$

We note that this definition can be related to the one of the gradient in an space ∇f. The exterior derivative of a 1-form, i.e., $\alpha = \alpha_x\ dx + \alpha_y\ dy + \alpha_z\ dz$, can be expanded as:

$$\mathbf{d}\,\alpha = \left(\frac{\partial \alpha_z}{\partial y} - \frac{\partial \alpha_y}{\partial z}\right) dy \wedge dz + \left(\frac{\partial \alpha_x}{\partial z} - \frac{\partial \alpha_z}{\partial x}\right) dz \wedge dx + \left(\frac{\partial \alpha_y}{\partial x} - \frac{\partial \alpha_x}{\partial y}\right) dx \wedge dy. \tag{1.8}$$

We see that it is similar to the expression of a curl in a vectorial calculus $\nabla \times \omega$. Finally, for a *2-form* $\omega = \omega_x\ dy \wedge dz + \omega_y\ dz \wedge dx + \omega_z\ dx \wedge dy$, we have:

$$\mathbf{d}\,\omega = \left(\frac{\partial \omega_x}{\partial x} + \frac{\partial \omega_y}{\partial y} + \frac{\partial \omega_z}{\partial z}\right) dx \wedge dy \wedge dz. \tag{1.9}$$

In this last formulation, we can recognize the expression of the divergence operator, $\nabla \cdot B$, but the three components of ω are not comparable to a metric transpose of a vector. □

. Link with the conventional vectorial calculus

We add here some relations to make a link between the conventional vector calculus and the differential form calculus. To summarize, we can make a link between them through almost a dozen of relation well chosen allowing us to pass from a vectorial state to differential state (see Figure 1.1). We suppose here that we work with $M = \mathbb{R}^3$ with its conventional system of coordinates $\mathbf{x}$ (and its three coordinate functions $\{x^i\}_{i\in[\![1;3]\!]}$). We also give to TM and $T^*M = \Lambda^1(M)$ the conventional metric.

We denote by $\flat$ and $\sharp$ two musical isomorphisms (see Definition A.19) and by $\cdot^\tau$ the "identity function" allowing us to see an object of $\Lambda^0(M)$ as an element of $C^\infty(M, \mathbb{R})$. With this notation, we have

$$\begin{array}{llll}
\forall f \in C^\infty & \operatorname{grad}(f) = (\mathbf{d}(f^\tau))^\sharp, & \forall \beta \in \Lambda^0(M) & \mathbf{d}\,\beta = (\operatorname{grad}(\beta^\tau))^\flat, \\
\forall v \in TM & \operatorname{div}(v) = (\delta(v^\flat))^\tau, & \forall \alpha \in \Lambda^1(M) & \boldsymbol{\delta}\,\alpha = (\operatorname{div}(\alpha^\sharp))^\tau, \\
\forall v \in TM & \overrightarrow{\operatorname{rot}}(v) = (\star(\mathbf{d}(v^\flat)))^\sharp, & \forall \alpha \in \Lambda^1(M) & \star\,\mathbf{d}\,\alpha = (\overrightarrow{\operatorname{rot}}(\alpha^\sharp))^\flat, \\
\forall \omega \in \Lambda^2(M) & \mathbf{d}\,\omega = \star((\operatorname{div}((\star\omega)^\sharp))^\tau), & & \\
\forall \gamma \in \Lambda^3(M) & \boldsymbol{\delta}\,\gamma = \star((\operatorname{grad}((\star\gamma)^\tau))^\flat), & \forall \omega \in \Lambda^2(M) & \boldsymbol{\delta}\,\omega = (\overrightarrow{\operatorname{rot}}((\star\omega)^\sharp))^\flat.
\end{array}$$

Example 1.4 : The Gauss Law

As an example, let us consider the Gauss Law. Let $H \in \Lambda^1$ denote the magnetic field intensity, $\mu \in \Lambda^0$ the permeability and $\rho^m \in \Lambda^3$ the magnetic charge density (see Table 1.1 for notations). The Gauss law states:

$$\mathbf{d} \star (\mu H) = \frac{\rho^m}{\mu_0}. \tag{1.10}$$

In detail, we have

$$\begin{aligned} \mu H &= \mu H_x dx + \mu H_y dy + \mu H_z dz, \\ \star(\mu H) &= \mu H_x dy \wedge dz + \mu H_y dz \wedge dx + \mu H_z dx \wedge dy, \\ \mathbf{d} \star (\mu H) &= (\partial_x(\mu H_x) + \partial_y(\mu H_y) + \partial_z(\mu H_z))\, dx \wedge dy \wedge dz = \frac{\rho^m_{xyz}}{\mu_0} dx \wedge dy \wedge dz, \end{aligned}$$

i.e.,

$$\partial_x(\mu E_x) + \partial_y(\mu E_y) + \partial_z(\mu E_z) = \frac{\rho^m_{xyz}}{\mu_0}. \tag{1.11}$$

Here, we find the more standard calculus form

$$\mathrm{div}(\mu H^\flat) = \frac{(\star \rho_m)^\tau}{\mu_0}. \tag{1.12}$$

□

Example 1.5 : The Lenz-Faraday equation

As another example, let us consider the Lenz-Faraday equation. Let $E \in \Lambda^1$ denote the electric field intensity, $H \in \Lambda^1$ the magnetic field intensity and $m \in \Lambda^2$ the magnetic current density. The Lenz-Faraday equation holds:

$$\mu_0 \partial_t \star H + \mathbf{d}\, E = -m. \tag{1.13}$$

We have:

$$\begin{aligned} \star H &= H_x dy \wedge dz + H_y dz \wedge dx + H_z dx \wedge dy, \\ \partial_t \star H &= \partial_t H_x dy \wedge dz + \partial_t H_y dz \wedge dx + \partial_t H_z dx \wedge dy, \\ \mathbf{d}\, E &= (\partial_y E_z - \partial_z E_y)\, dy \wedge dz + (\partial_z E_x - \partial_x E_z)\, dy \wedge dz + (\partial_x E_y - \partial_y E_x)\, dy \wedge dz, \\ m &= m_x dy \wedge dz + m_y dz \wedge dx + m_z dx \wedge dy, \end{aligned}$$

which gives:

$$\mu \partial_t \star H + \mathbf{d}\, E = -m \Longleftrightarrow \begin{cases} \varepsilon \partial_t H_x - (\partial_y E_z - \partial_z E_y) &= -m_x, \\ \varepsilon \partial_t H_y - (\partial_z E_x - \partial_x E_z) &= -m_y, \\ \varepsilon \partial_t H_z - (\partial_x E_y - \partial_y E_x) &= -m_z. \end{cases}$$

Here, we find the more standard calculus form

$$\mu_0 \partial_t H + \overrightarrow{\mathrm{rot}}(E^\flat)^\tau = - \star m. \tag{1.14}$$

□

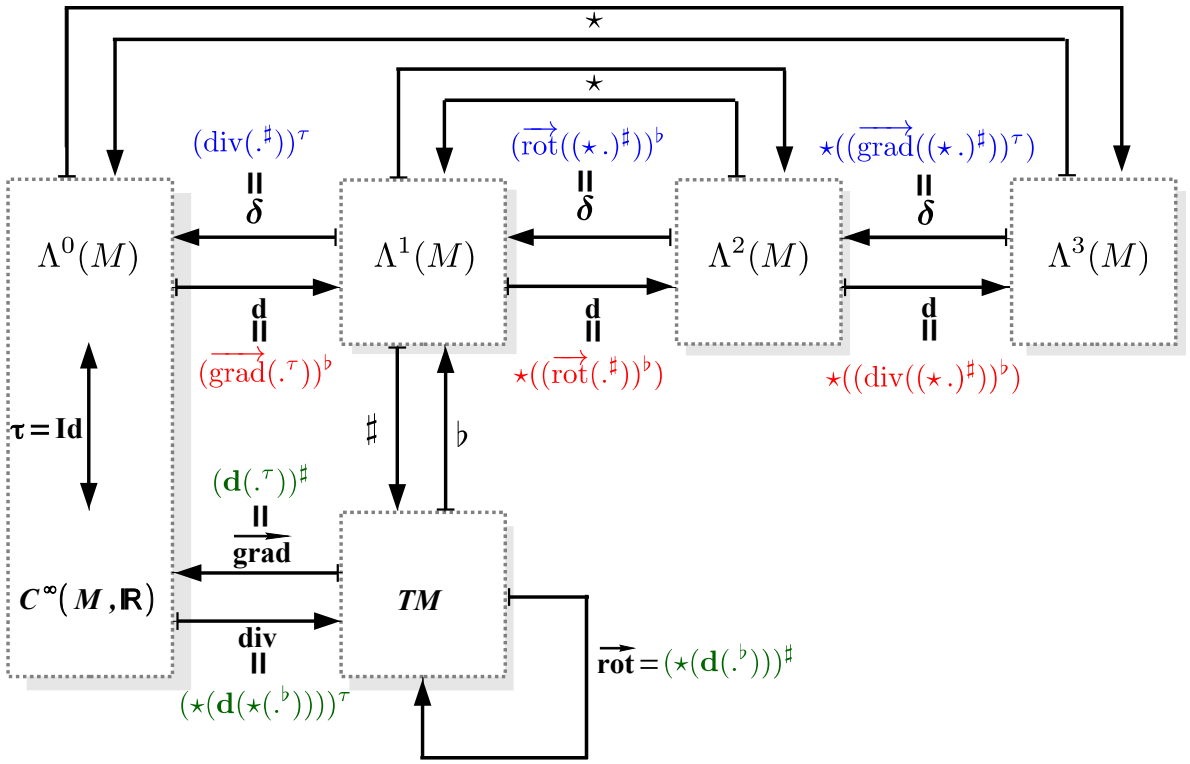

Figure 1.1 – Link between the different spaces involved in vector calculus and differential form calculus.

. Change of variables/coordinates - Pull-back, Integration

Differential forms are particularly well behaved under change of variables. This is essentially because their expressions include the differentials of the functions $x = (x^1, ..., x^n)$. Let the coordinates x be given in terms of new coordinates $u = (u^1, ..., u^m)$ through a set of n functions $x^i = f^i(u^1, ..., u^m)$ which define the mapping

$$\begin{aligned} f: \ U \subset \mathbb{R}^m &\to \mathbb{R}^n, \\ u &\mapsto f(u) \end{aligned} \tag{1.15}$$

and let

$$\alpha = \sum_J a_J(x) dx^J \tag{1.16}$$

be a p-form. Here J is a multi-index and $\mathbf{d}\, x^J = dx^J \equiv dx^{J_1} \wedge \dots dx^{J_p}$.

The change of variables from x to u in α is called the pull-back of α with f and is written as $f^*\alpha$. The pull-back of differential forms is a generalisation of the function composition and is done by substituting $f^i(u)$ for x^i, both in the coefficient functions a_J and in the differentials. The pull-back of a basis form dx^i is computed as

$$\mathbf{d}\, f^i(u) = \sum_j \frac{\partial f^i}{\partial u^j} du^j. \tag{1.17}$$

The products in (1.16) are then simplified according to the rules of exterior algebra.

Note that the above expressions include the case where the mapping f defines a chart on a lower dimensional manifold embedded in $\mathbb{E}^3$. The pull-back operation applied to differential forms on the embedding space restricts these forms implicitly to the embedded manifold.

Example 1.6 :

As a first example, consider the electric field one-form in $\mathbb{R}^2$

$$E = X(x,y)dx + Y(x,y)dy \tag{1.18}$$

and "new variables"(ρ,θ) related to (x,y) by

$$f : (\rho,\theta) \to (x,y) = (\rho\cos(\theta), \rho\sin(\theta)). \tag{1.19}$$

Then

$$(dx,dy) = (\cos(\theta)d\rho - \rho\sin(\theta)d\theta \ , \ \sin(\theta)d\rho + \rho\cos(\theta)d\theta). \tag{1.20}$$

Substituting (1.19) in (1.18) and simplifying gives

$$f^*E = R(\rho,\theta)d\rho + \Theta(\rho,\theta)d\theta \tag{1.21}$$

with

$$\begin{aligned} R(\rho,\theta) &= X^{'}(\rho,\theta)\cos(\theta) + Y^{'}(\rho,\theta)\sin(\theta), \\ \Theta(\rho,\theta) &= -X^{'}(\rho,\theta)\sin(\theta) + Y^{'}(\rho,\theta)\cos(\theta), \\ X^{'} &= f^*X = X\circ f, \\ Y^{'} &= f^*Y = Y\circ f. \end{aligned}$$

□

Example 1.7 :

As a second example, consider the electric field represented by a 1-form in the canonical chart $\mathbb{R}^3$

$$E = E_x(x,y,z)dx + E_y(x,y,z)dy + E_z(x,y,z)dz. \tag{1.22}$$

We define a curve in $\mathbb{E}^3$ by introducing a curvilinear coordinate $\theta \in (0,\pi)$ and the mapping

$$f : \ \theta \mapsto (a\cos(\theta), a\sin(\theta), 0) \in \mathbb{R}^3. \tag{1.23}$$

Then

$$\begin{aligned} f^*dx &= -a\sin(\theta)d\theta, \\ f^*dy &= a\cos(\theta), \\ f^*dz &= 0. \end{aligned}$$

Substituting (1.23) in (1.22) and simplifying gives

$$f^*E = E_x(f(\theta))a\left(\cos(\theta) - \sin(\theta)\right)d\theta. \tag{1.24}$$

□

This example shows the implicit restriction of a field in $\mathbb{R}^3$ to the tangential component.

The following properties of the pull-back can also be verified:

$$f^*(\alpha+\beta) = f^*\alpha + f^*\beta, \tag{1.25}$$
$$f^*(\alpha\beta) = (f^*\alpha)(f^*\beta), \tag{1.26}$$
$$f^*(\mathbf{d}\,\alpha) = \mathbf{d}(f^*\alpha), \tag{1.27}$$
$$(f\circ g)^* = g^*\circ f^*. \tag{1.28}$$

An important application of the pull-back concerns the computation of integrals over a d-dimensional manifold M (curve, surface or three-dimensional sub-domain) embedded in $\mathbb{E}^3$. The integral over M of a differential form ω defined on $\mathbb{E}^3$ can be computed in local charts

$$\tau : U \subset \mathbb{R}^d \to V \subset M \subset \mathbb{E}^3 \tag{1.29}$$

and equals the integral of $\tau^*\omega$ over M.

Take, for instance, a surface $M \subset \mathbb{E}^3$ represented in the canonical chart by $M \subset \mathbb{R}^3$. In general, the surface can only be defined locally by a parameterization, i.e., by a mapping from an open set $U \in \mathbb{R}^2$ to $V \subset M$:

$$f : U \ni (u^1, u^2) = u \mapsto (f^1(u), f^2(u), f^3(u)). \tag{1.30}$$

Consider an electric current distribution defined on the canonical chart by a 2-form

$$J = J_{23}dx^2\wedge dx^3 + J_{31}dx^3\wedge dx^1 + J_{12}dx^1\wedge dx^2$$

where the coefficient J_{23}, J_{31} and J_{12} are functions of the coordinates (x^1, x^2, x^3). The total current, I, flowing through (traversing) the surface M can be computed as the integral

$$I = \int_M J.$$

Using the local parameterization f, we get for the current I_V flowing through $V \subset M$,

$$\begin{aligned} I_V &= \int_{u\in U} f^*J, \\ &= \int_{u\in U} \sum_{i,j} J_{ij}(f(u)) f^*(dx^i\wedge dx^j) \end{aligned}$$

where

$$f^*dx^i\wedge dx^j = \sum_{n,m} (\partial_m f^i)(u)(\partial_n f^j) du^m\wedge du^n.$$

If we have covered the complete surface M with charts $f_i : U_i \to V_i \subset M$ such that $M = \cup_i V_i$ and $V_i \cap V_j = \emptyset$ for $i \neq j$, the total current is given by

$$\begin{aligned} I &= \int_M J, \\ &= \sum_i \int_{U_i} (f_i^*J) - \sum_{i,j} \int_{U_i\cap U_j} (f_i^*J) \end{aligned}$$

This example shows that the pull-back of differential forms handles the Jacobian by definition. Of course, the computations have not really changed, but the calculus of differential forms gives a cleaner formulation than vector calculus.

1.2 Fundamental equations of electromagnetism

This second section presents the Maxwell equations in the formalism of the differential forms. The main idea is to provide all the necessary material to set the electromagnetic wave equation for both electric and magnetic fields. To ensure complete understanding and easier reading, we begin with some notations summarized in the Table 1.1.

Quantity	Form	Degree	Other information
Speed of light in vacuum	c	constant	$c = 299792458\ m.s^{-1}$
Permeability of free space	μ_0	constant	$\mu_0 = 4\pi.10^{-7} m.kg.s^{-2}$
Permittivity of free space	ε_0	constant	$\varepsilon_0 = 1/(\mu_0 c^2)$
Permeability	μ	*0-form*	$\mu = \mu_r.\mu_0$
Permittivity	ε	*0-form*	$\varepsilon = \varepsilon_r.\varepsilon_0$
Electrical conductivity	σ	*0-form*	$\sigma \geq 0$
Electric Field intensity	E	*1-form*	
Magnetic Field Intensity	H	*1-form*	
Electric Current Density	j	*2-form*	
Magnetic Current Density	m	*2-form*	(theoretical only)
Electric Flux Density	D	*2-form*	$D = \varepsilon \star E$
Magnetic Flux Density	B	*2-form*	$B = \mu \star H$
Electric Charge Density	ρ	*3-form*	
Magnetic Charge Density	ρ_m	*3-form*	

Table 1.1 – The differential forms that represent fields and sources

In the rest of this document (i.e., in all the subsequent chapters), we will consider a homogeneous isotropic linear medium. Note also that from a physical point of view, there are no magnetic currents nor charges. It is an artificial construction that can simplify specific modelling issues and also provides an esthetic symmetry in some equations.

1.2.1 The Maxwell equations

Now that we have properly defined the various quantities involved, we can introduce Maxwell's equations in differential forms. See [28, 29, 45, 46].

Properties 1.8 : **Gauss, Lenz-Faraday, Maxwell-Ampère and conservation laws**

$$\mathbf{d} \star (\mu H) = \rho_m/\mu_0 \qquad \text{the Gauss law,} \tag{1.31}$$
$$\mathbf{d} \star (\varepsilon E) = \rho/\varepsilon_0 \qquad \text{the Gauss law,} \tag{1.32}$$

$$\mu \partial_t \star H + \mathbf{d}\, E = -m \qquad \text{the Lenz-Faraday equation,} \tag{1.33}$$
$$\varepsilon \partial_t \star E - \mathbf{d}\, H = -j \qquad \text{the Maxwell-Ampère law,} \tag{1.34}$$

$$\partial_t \rho + \mathbf{d}\, j = 0 \qquad \text{the charge conservation laws,} \tag{1.35}$$
$$\partial_t \rho_m + \mathbf{d}\, j_m = 0 \qquad \text{the charge conservation laws.} \tag{1.36}$$

□

Proof 1.9 :

In order to illustrate the previous properties, we develop here, componentwise, the Gauss law and the Maxwell-Ampère law.

- The Gauss law:

$$\begin{aligned} E &= E_x dx + E_y dy + E_z dz, \\ \varepsilon E &= \varepsilon E_x dx + \varepsilon E_y dy + \varepsilon E_z dz, \\ \star(\varepsilon E) &= \varepsilon E_x dy \wedge dz + \varepsilon E_y dz \wedge dx + \varepsilon E_z dx \wedge dy, \\ \mathbf{d} \star(\varepsilon E) &= (\partial_x(\varepsilon E_x) + \partial_y(\varepsilon E_y) + \partial_z(\varepsilon E_z))\, dx \wedge dy \wedge dz = \frac{\rho_{xyz}}{\varepsilon_0} dx \wedge dy \wedge dz, \end{aligned}$$

  i.e., $\partial_x(\varepsilon E_x) + \partial_y(\varepsilon E_y) + \partial_z(\varepsilon E_z) = \frac{\rho_{xyz}}{\varepsilon_0}$.

- The Maxwell-Ampère law:

$$\begin{aligned} E &= E_x dx + E_y dy + E_z dz, \\ \star E &= E_x dy \wedge dz + E_y dz \wedge dx + E_z dx \wedge dy, \\ \partial_t \star E &= \partial_t E_x dy \wedge dz + \partial_t E_y dz \wedge dx + \partial_t E_z dx \wedge dy, \\ H &= H_x dx + H_y dy + H_z dz, \\ \mathbf{d}\, H &= (\partial_y H_z - \partial_z H_y)\, dy \wedge dz + (\partial_z H_x - \partial_x H_z)\, dy \wedge dz + (\partial_x H_y - \partial_y H_x)\, dy \wedge dz, \\ j &= j_x dy \wedge dz + j_y dz \wedge dx + j_z dx \wedge dy, \end{aligned}$$

  which gives:

$$\varepsilon \partial_t \star E - \mathbf{d}\, H = -j \Longleftrightarrow \begin{cases} \varepsilon \partial_t E_x - (\partial_y H_z - \partial_z H_y) &= -j_x, \\ \varepsilon \partial_t E_y - (\partial_z H_x - \partial_x H_z) &= -j_y, \\ \varepsilon \partial_t E_z - (\partial_x H_y - \partial_y H_x) &= -j_z. \end{cases}$$

⊠

We now restrict our considerations to time harmonic fields and use complex phasors to describe these fields, both E and H can then be written as follows:

$$E(x,t) = \mathrm{Re}\left(\widehat{E}(x) e^{-i\omega t}\right), \tag{1.37}$$

$$H(x,t) = \mathrm{Re}\left(\widehat{H}(x) e^{-i\omega t}\right), \tag{1.38}$$

where $\widehat{E}$ and $\widehat{H}$ are respectively the phasors of the electric and magnetic fields, with

$$\mathbf{d}\, \widehat{E} - i\omega\mu \star \widehat{H} = -\widehat{m}, \tag{1.39}$$

$$\mathbf{d}\, \widehat{H} + i\omega\varepsilon \star \widehat{E} = \widehat{j}\,. \tag{1.40}$$

Then, if we introduce the wave number κ ($\kappa = \omega/c$) and the vacuum impedance, Z, defined by

$$Z = \sqrt{\frac{\mu_0}{\varepsilon_0}}$$

and the following equalities

$$\omega\mu_0 = \omega\sqrt{\varepsilon_0.\mu_0}.\sqrt{\frac{\mu_0}{\varepsilon_0}} = \kappa Z,$$
$$\omega\varepsilon_0 = \omega\sqrt{\varepsilon_0.\mu_0}.\sqrt{\frac{\varepsilon_0}{\mu_0}} = \kappa Z^{-1},$$

we get:

$$\mathbf{d}\,\widehat{E} - i\mu_r\kappa Z \star \widehat{H} = -\widehat{m}, \tag{1.41}$$
$$\mathbf{d}\,\widehat{H} + i\varepsilon_r\kappa Z^{-1} \star \widehat{E} = \widehat{j}\,. \tag{1.42}$$

1.2.2 Electromagnetic continuity and boundary conditions

Consider the configuration presented in Figure 1.2. Let Ω_1 and Ω_2 be two subdomains in $\mathbb{R}^3$ representing media with two different dielectric characteristics (ε_1, μ_1 and ε_2, μ_2). Let Σ denote the interface, i.e., a closed or an open surface in $\mathbb{R}^3$, between the two media. Let M denote a subset of $\mathbb{R}^2$ and τ a continuous and continuously differentiable function from $M \subset \mathbb{R}^2$ to $\mathbb{R}^3$ giving a local parameterization of the interface Σ. Then, the generalized electromagnetic boundary conditions can be described at the interface Σ through the formula:

$$\begin{aligned}
\tau^*\left(E^{(1)} - E^{(2)}\right) &= -\bar{\star} m_S,\\
\tau^*\left(H^{(1)} - H^{(2)}\right) &= \bar{\star}\, j_S,\\
\tau^*\left(D^{(1)} - D^{(2)}\right) &= \rho,\\
\tau^*\left(B^{(1)} - B^{(2)}\right) &= \rho_m,
\end{aligned} \tag{1.43}$$

where $E^{(j)}$ and $H^{(j)}$ denote the fields in the domain Ω_j, $D = \varepsilon_0 \star E$ and $B = \mu_0 \star H$, j_S (m_S) denote the *1-form* surface electric (respectively magnetic) current, $\bar{\star}$ the Hodge star operator on Σ -the equivalent of $\star$, but restricted to the two dimensional manifold- and τ^* denotes the pull-back of τ.

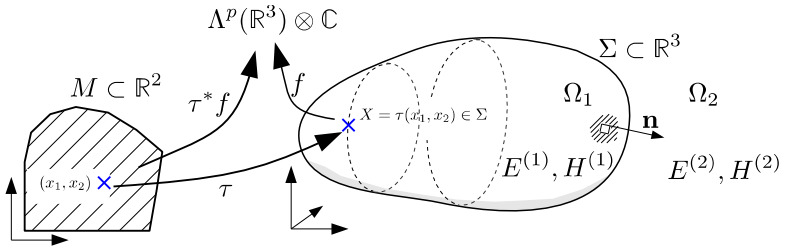

Figure 1.2 – Interface between two dielectric media.

In scattering theory, metallic obstacles at frequencies above a few MHz are considered as Perfectly Electric Conducting (PEC), i.e., with an infinite conductivity:

$$\sigma = +\infty\,. \tag{1.44}$$

The resulting surface current density $\bar{\star}\tau^*(H)$ is believed to be equivalent to the actual current penetrating into the body in only a very thin layer. Then, to satisfy the Maxwell's equations, the electromagnetic field must vanish on the boundary of PEC bodies. Under these conditions, if Ω_1 denotes the PEC body and Ω_2 the dielectric exterior medium, the transmission condition

becomes:

$$\begin{aligned}\tau^*(E^{(1)} - E^{(2)}) &= 0,\\ \tau^*(H^{(1)} - H^{(2)}) &= \bar{\star}\, j_S,\\ \tau^*(D^{(1)} - D^{(2)}) &= \rho,\\ \tau^*(B^{(1)} - B^{(2)}) &= 0\,.\end{aligned} \tag{1.45}$$

Furthermore, considering an unbounded exterior domain, the fields $\{E, H\}$ of (1.41) and equation (1.42) are subject to the outgoing radiation condition which can take two equivalent forms:

$$\lim_{\|x\|\to\infty} (E - Z \star dr \wedge H) = o(\|x\|^{-1}), \tag{1.46}$$

$$\lim_{\|x\|\to\infty} (H - Y \star dr \wedge E) = o(\|x\|^{-1}), \tag{1.47}$$

uniformly on $dr = x^t/\|x\|$ where $Z = (\mu_0/\varepsilon_0)^{1/2} = Y^{-1}$.
With the partial differential equations (1.41)-(1.42), the continuity condition (1.43) and the outgoing radiation condition (1.46) or (1.47), we have formulated the basis of electromagnetic field theory.

1.3 Free space representation

We assume now that ε and μ are constant and symbols $\ll\hat{}\gg$ on phasors are omitted. We also assume that $\mu_r = \varepsilon_r = 1$. The objectives of this section is to define the Helmholtz equation for both electric and magnetic fields in free space and find its elementary solution (see [28, 47]).

1.3.1 The Maxwell equations with constant coefficients

First, we can eliminate one of the two fields E or H and get a second order equation for the remaining field. We start with the "frequency domain" Maxwell equations. If we apply the operator $\mathbf{d}\star$ to both equations (1.39) and (1.40), we have

$$\mathbf{d}\star\mathbf{d}\,E - i\kappa Z\,\mathbf{d}\,H = -\,\mathbf{d}\star m, \tag{1.48}$$

$$\mathbf{d}\star\mathbf{d}\,H + i\kappa Z^{-1}\,\mathbf{d}\,E = \mathbf{d}\star j, \tag{1.49}$$

i.e.,

$$\begin{aligned}\mathbf{d}\,H &= \frac{1}{i\kappa Z}\left(\mathbf{d}\star\mathbf{d}\,E + \mathbf{d}\star m\right),\\ \mathbf{d}\,E &= \frac{1}{i\kappa Z^{-1}}\left(\mathbf{d}\star m - \mathbf{d}\star\mathbf{d}\,H\right).\end{aligned}$$

Thus, re-injecting these last two equalities into the Maxwell equations, the electric field E satisfies:

$$\frac{1}{i\kappa Z}\left(\mathbf{d}\star\mathbf{d}\,E + \mathbf{d}\star m\right) + i\kappa Z^{-1}\star E = j \tag{1.50}$$

and the magnetic field:

$$\frac{1}{i\kappa Z^{-1}}\left(\mathbf{d}\star j - \mathbf{d}\star\mathbf{d}\,H\right) - i\kappa Z\star H = -m \tag{1.51}$$

or again

Proposition 1.10 :

$$\mathbf{d}\star(\mathbf{d}\,E) - \kappa^2 \star E = i\kappa Z j - \mathbf{d}\star(m)\,, \tag{1.52}$$
$$\mathbf{d}\star(\mathbf{d}\,H) - \kappa^2 \star H = i\kappa Z^{-1} m + \mathbf{d}\star(j)\,. \tag{1.53}$$

□

Applying the operator $\mathbf{d}$, we obtain

$$\begin{aligned}
\mathbf{d}\,\mathbf{d}\star\mathbf{d}\,E - \kappa^2\,\mathbf{d}\star E &= i\kappa Z\,\mathbf{d}\,j - \mathbf{d}\,\mathbf{d}\star m,\\
-\kappa^2\,\mathbf{d}\star E &= i\kappa Z\,\mathbf{d}\,j,\\
\mathbf{d}\star E &= -i\kappa Z\left(\frac{1}{\kappa^2}\,\mathbf{d}\,j\right).
\end{aligned} \tag{1.54}$$

Now if we use the following equality

$$\Delta = \mathbf{d}\,\boldsymbol{\delta} - \boldsymbol{\delta}\,\mathbf{d} = \mathbf{d}\star\mathbf{d}\star - \star\mathbf{d}\star\mathbf{d}, \tag{1.55}$$

we have

$$\begin{aligned}
\mathbf{d}\star\mathbf{d}\,E - \kappa^2 \star E &= i\kappa Z j - \mathbf{d}\star m,\\
\star\,\mathbf{d}\star\mathbf{d}\,E - \kappa^2 E &= i\kappa Z \star j - \boldsymbol{\delta}\,m,\\
-\Delta E + \mathbf{d}\star\ \underbrace{\mathbf{d}\star E}_{\text{cf. equation (1.54)}}\ - \kappa^2 E &= i\kappa Z \star j - \boldsymbol{\delta}\,m,\\
-\Delta E - ikZ\left(\frac{1}{\kappa^2}\right)\mathbf{d}\star\mathbf{d}\,j - \kappa^2 E &= i\kappa Z \star j - \boldsymbol{\delta}\,m,\\
-\Delta E - \kappa^2 E &= i\kappa Z\left(\frac{1}{\kappa^2}\,\mathbf{d}\star\mathbf{d}\,j + \star j\right) - \boldsymbol{\delta}\,m\,.
\end{aligned}$$

Proposition 1.11 : **Helmholtz's equation for the electric field**

E satisfies

$$-\left(\Delta + \kappa^2\right) E = T \quad \text{in } \mathbb{R}^3 \tag{1.56}$$

with

$$\Delta = \mathbf{d}\,\boldsymbol{\delta} - \boldsymbol{\delta}\,\mathbf{d} \quad \text{and} \quad T = i\kappa Z\left(\frac{1}{\kappa^2}\,\mathbf{d}\star\mathbf{d}\,j + \star j\right) - \boldsymbol{\delta}\,m\,. \tag{1.57}$$

□

In the same way, we can work on the magnetic field H. Starting from

$$\mathbf{d}\star\mathbf{d}\,H - \kappa^2 \star H = i\kappa Z^{-1} m + \mathbf{d}\star j,$$

we successively have

$$\begin{aligned}
\mathbf{d}\star\mathbf{d}\,H - \kappa^2 \star H &= i\kappa Z^{-1} m + \mathbf{d}\star j,\\
\mathbf{d}\,\mathbf{d}\star\mathbf{d}\,H = -\kappa^2\,\mathbf{d}\star H &= i\kappa Z^{-1}\,\mathbf{d}\,m + \mathbf{d}\,\mathbf{d}\star j,\\
\mathbf{d}\star H &= i\kappa Z^{-1}\left(\frac{1}{\kappa^2}\,\mathbf{d}\,m\right).
\end{aligned}$$

Moreover, we have

$$\begin{aligned}
\star\,\mathbf{d}\star\mathbf{d}\,H &= -\Delta H + \mathbf{d}\star\mathbf{d}\star H,\\
&= -\Delta H - i\kappa Z^{-1}\left(\frac{1}{\kappa^2}\,\mathbf{d}\star\mathbf{d}\,m\right).
\end{aligned}$$

Therefore, we get

$$-\Delta H - \kappa^2 H = i\kappa Z^{-1}\left(\frac{1}{\kappa^2}\,\mathbf{d}\star\mathbf{d}\,m + \star m\right) + \boldsymbol{\delta}\, j\,.$$

Proposition 1.12 : **Helmholtz's equation for the magnetic field**

H satisfies

$$-\left(\Delta + \kappa^2\right) H = S \quad \text{in } \mathbb{R}^3 \tag{1.58}$$

with

$$\Delta = \mathbf{d}\,\boldsymbol{\delta} - \boldsymbol{\delta}\,\mathbf{d} \quad \text{and} \quad S = i\kappa Z^{-1}\left(\frac{1}{\kappa^2}\,\mathbf{d}\star\mathbf{d}\,m + \star m\right) - \boldsymbol{\delta}\, j\,. \tag{1.59}$$

□

1.3.2 Integral representations

In this section, after setting up the two problems associated with the free-space propagation for both electric and magnetic fields, we propose a solution for both of them. In order to get these solutions, we proceed in three steps. First, we define the solution of the homogeneous problem, then we define elementary solutions, called Green's states that contribute to give, in a third step, expressions for general solutions of the Helmholtz equations (see [48] for references). In order to solve them, we consider the associated problem

$$-(\Delta + \kappa^2)\mathbf{G}(x,y) = \delta_{x-y} I \quad \text{on } \mathbb{R}^3 \tag{1.60}$$

where δ denotes the Dirac function and I the unit $1\otimes 1$-*form*

$$I = \sum_{i=1}^{3} dx^i \otimes dy^i \tag{1.61}$$

and $\mathbf{G}$ is the $1\otimes 1$-*form* solution, also called Green function, defined by

$$\mathbf{G}(x,y) = \sum_{i=1}^{3} G(x,y)dx^i \otimes dy^i = \sum_{i=1}^{3} \frac{e^{i\kappa|x-y|}}{4\pi|x-y|} dx^i \otimes dy^i\,. \tag{1.62}$$

With this elementary solution, we find a solution of the general problem. But, for the moment, we assume that solutions of Maxwell's problem exist.

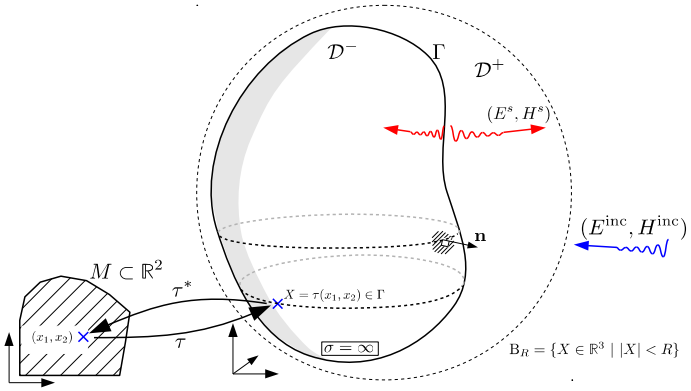

Figure 1.3 – Representation of the different fields and considered domains.

Consider the situation presented in Figure 1.3. Let $\mathcal{D}^-$ be an open bounded subset of $\mathbb{R}^3$ centered at the origin. Let Γ be its boundary, M a subset of $\mathbb{R}^2$ and τ be a continuous and

continuously differentiable function from $M \subset \mathbb{R}^2$ to $\mathbb{R}^3$, giving a parameterization of the surface Γ. Suppose moreover that $\overline{\mathcal{D}^-} = \mathcal{D}^- \cup \Gamma$ is a C^k smooth submanifold with boundary such that Stokes' theorem applies, i.e.,

$$\forall \omega \in \Lambda^2(\mathbb{R}^3),\ \int_{\mathcal{D}^-} d\omega = \int_{\Gamma} \tau^*(\omega)\,. \tag{1.63}$$

We then define B_R the sphere described by

$$B_R = \Big\{ x \in \mathbb{R}^3 \mid |x| < R \Big\}$$

and denote by $\mathcal{D}^+$ the intersection of the complement of $\mathcal{D}^- \cup \Gamma$ and B_R, and by $\mathbf{n}$, the outward pointing normal on Γ. We suppose throughout that $\mathcal{D}^+$ is a connected domain. such $\mathcal{D}^+ \subset B_R$, for $R > R_0$.
In $\mathcal{D}^+$ or $\mathcal{D}^-$, we consider two solutions of Maxwell's equations, labelled a and b, with possibly different constitutive parameters. From the Stokes theorem, we have:

$$\begin{aligned}\int_{\partial D} (E^a \wedge H^b - E^b \wedge H^a) = i\omega \int_D (\mu^b - \mu^a)(\star H^a \wedge H^b) - (\varepsilon^b - \varepsilon^a)(E^a \wedge \star E^b) \\ + \int_D (m^b \wedge H^a - m^a \wedge H^b) + (j^b \wedge E^a - j^a \wedge E^b)\,.\end{aligned} \tag{1.64}$$

This last integral relation is useful to derive the boundary integral representations of the solutions in the different domains $\mathcal{D}^+$ or $\mathcal{D}^-$. In order to describe them, we can define one of the states appearing in the Lorentz relations, for example $\{E^a, H^a\}$, as a suitable singular function called the Green's state.

Definition 1.13 : Green's states

1. The electric Green's state:
   $\{E^e_{G,i}, H^e_{G,i}\}$ with $E^e_{G,i} = \eta^{-1}\,\boldsymbol{\delta}\,\mathbf{d}(\phi dy^i)$ and $H^e_{G,i} = \boldsymbol{\delta}(\phi \star dy^i)$, is called the i-th electric Green's state ($i \in \{1,2,3\}$).

2. The magnetic Green's state:
   $\{E^m_{G,i}, H^m_{G,i}\}$ with $E^m_{G,i} = \boldsymbol{\delta}(\phi \star dy^i)$ and $H^e_{G,i} = \zeta^{-1}\,\boldsymbol{\delta}\,\mathbf{d}(\phi dy^i)$, is called the i-th magnetic Green's state ($i \in \{1,2,3\}$).

where $\phi \in C^\infty(\Lambda^0(\mathbb{R}^3 - \{0\}))$ is defined by

$$\phi(y) = \frac{\exp(ik\|y\|)}{4\pi\|y\|} \tag{1.65}$$

and satisfies $\Delta\phi + \eta\zeta\phi = 0$ in $\mathbb{R}^3 - \{0\}$ with $\eta = -i\omega\varepsilon$ and $\zeta = i\omega\mu$. □

Proposition 1.14 :

1. $\{E^e_{G,i}, H^e_{G,i}\}$ satisfies the homogeneous Maxwell equations in $\mathbb{R}^3 - \{0\}$ and the outgoing radiation condition.

2. $\{E^m_{G,i}, H^m_{G,i}\}$ also satisfies the homogeneous Maxwell equations.

□

We are now ready to derive the boundary integral representations.

Proposition 1.15 :

1. Let $\mathcal{D}^- \subset \mathbb{R}^3$ be a bounded domain and $\{E, H\}$ be a C^∞-smooth solution of the homogeneous Maxwell equations in D with constant constitutive parameters. Then

$$\forall x \in \mathcal{D}^-,\ E(x) = \int_\Gamma \tau^*(\Gamma_x^{ee} \wedge H - E \wedge \Gamma_x^{me}), \tag{1.66}$$

$$\forall x \in \mathcal{D}^-,\ H(x) = \int_\Gamma \tau^*(\Gamma_x^{em} \wedge H - E \wedge \Gamma_x^{mm}) \tag{1.67}$$

where

$$\Gamma_x^{ee}(y) = \Gamma^{ee}(x,y) = \sum_{i=1}^{3} E_{G,i}^e(y-x) \otimes dx^i, \tag{1.68}$$

$$\Gamma_x^{me}(y) = \Gamma^{me}(x,y) = \sum_{i=1}^{3} H_{G,i}^e(y-x) \otimes dx^i, \tag{1.69}$$

$$\Gamma_x^{em}(y) = \Gamma^{em}(x,y) = \sum_{i=1}^{3} E_{G,i}^m(y-x) \otimes dx^i, \tag{1.70}$$

$$\Gamma_x^{mm}(y) = \Gamma^{mm}(x,y) = \sum_{i=1}^{3} H_{G,i}^m(y-x) \otimes dx^i\,. \tag{1.71}$$

2. Let $\mathcal{D}^+ \subset \mathbb{R}^3$ be an exterior domain with piecewise smooth internal boundary and $\{E, H\}$ a C^∞ solution of the Maxwell equations that satisfies the outgoing radiation condition. Then we have the following integral representations with the same definition of Γ:

$$\forall x \in \mathcal{D}^-,\ E(x) = \int_\Gamma \tau^*(\Gamma_x^{ee} \wedge H - E \wedge \Gamma_x^{me}), \tag{1.72}$$

$$\forall x \in \mathcal{D}^-,\ H(x) = \int_\Gamma \tau^*(\Gamma_x^{em} \wedge H - E \wedge \Gamma_x^{mm}). \tag{1.73}$$

□

From now, we consider the exterior domain $\mathcal{D}^+$ with constant parameters ε and μ and a solution $\{E, H\}$ of the homogeneous Maxwell equations which satisfies the outgoing radiation condition. From Proposition 1.15, we know that E^s and H^s can be expressed through the boundary limits, $m_s = \star\tau^* E$ and $j_s = \star\tau^* H$, through

$$E^s = A^{ee} j_s + A^{me} m_s, \tag{1.74}$$

$$H^s = A^{em} j_s + A^{mm} m_s \tag{1.75}$$

with

$$(A^{ee})u)(x) := \int_\Gamma \tau^*(\Gamma_x^{ee}) \wedge \star u,$$

$$(A^{em})u)(x) := \int_\Gamma \tau^*(\Gamma_x^{em}) \wedge \star u,$$

$$(A^{me})u)(x) := \int_\Gamma \tau^*(\Gamma_x^{me}) \wedge \star u,$$

$$(A^{mm})u)(x) := \int_\Gamma \tau^*(\Gamma_x^{mm}) \wedge \star u\,.$$

Working on these four operators A^{ee}, A^{me}, A^{em} and A^{mm}, we can go a little further. For this, we introduce three new operators $\mathcal{A}$, Φ and $\mathcal{B}$ defined as

$$\begin{aligned}
\forall j \in \Lambda^1(\Gamma), \quad \forall x \in \mathcal{D}^+, \quad \mathcal{A}[j](x) &= \sum_{i=1}^{3} A_i[j]dx^i = \int_{y\in\Gamma} \tau^*(\mathbf{G}(x,y)) \wedge \star j(y), \\
\forall j \in \Lambda^1(\Gamma), \quad \forall x \in \mathcal{D}^+, \quad \mathcal{B}[j](x) &= \sum_{i=1}^{3} B_i[j]dx^i = \int_{y\in\Gamma} \tau^*(\star\,\mathbf{d}\,\mathbf{G}(x,y)) \wedge \star j(y), \\
\forall f \in \Lambda^0(\Gamma), \quad \forall x \in \mathcal{D}^+, \quad \Phi[f](x) &= \int_{y\in\Gamma} \tau^*(G(x,y)) \wedge \star f(y)
\end{aligned} \tag{1.76}$$

such that the following proposition holds:

Proposition 1.16 :

1. $\forall j \in \Lambda^1(\Gamma),\ \boldsymbol{\delta}\,\mathcal{A}[j] = -\Phi[\boldsymbol{\delta}\, j]$,
2. $\forall f \in \Lambda^0(\Gamma),\ \mathbf{d}\,\Phi[f] = -\mathcal{A}[\mathbf{d}\, f]$.

□

Proof 1.17 :

$$\begin{aligned}
\boldsymbol{\delta}\,\mathcal{A}[j] &= \boldsymbol{\delta}\left(\sum_{i=1}^{3} A_i[j]dx^i\right) \\
&= \sum_{i=1}^{3} \partial_{x_i} A_i[j] \\
&= \sum_{i=1}^{3} \partial_{x_i} \int_{y\in\partial\Omega} \tau^*(G(x,y)dy^i) \wedge \star j(y) \\
&= \int_{y\in\partial\Omega} \tau^*\left(\sum_{i=1}^{3} \partial_{x_i} G(x,y)dy^i\right) \wedge \star j(y) \\
&= \int_{y\in\partial\Omega} \tau^*\left(\sum_{i=1}^{3} -\partial_{y_i} G(x,y)dy^i\right) \wedge \star j(y) \\
&= \int_{y\in\partial\Omega} \tau^*\left(-\mathbf{d}\,G(x,y)\right) \wedge \star j(y) \\
&= -\int_{y\in\partial\Omega} \tau^*(G(x,y)) \wedge \star\boldsymbol{\delta}\, j(y) \\
&= -\Phi[\boldsymbol{\delta}\, j]\,.
\end{aligned}$$

$$\begin{aligned}
A[df] &= \int_{y\in\partial\Omega} \tau^*(\mathbf{G}(x,y)) \wedge \star\,\mathbf{d}\, f(y) \\
&= \int_{y\in\partial\Omega} \tau^*(\boldsymbol{\delta}\,\mathbf{G}(x,y)) \wedge \star f(y) \\
&= \int_{y\in\partial\Omega} \tau^*\left(\sum_{i=1}^{3} \frac{\partial}{\partial y^i} G(x,y)dx^i\right) \wedge \star f(y) \\
&= \sum_{i=1}^{3} \left(\int_{y\in\partial\Omega} \tau^*\left(\frac{\partial}{\partial y^i} G(x,y)\right) \wedge \star f(y)\right) dx^i \\
&= \sum_{i=1}^{3} \left(\int_{y\in\partial\Omega} \tau^*\left(-\frac{\partial}{\partial x^i} G(x,y)\right) \wedge \star f(y)\right) dx^i \\
&= -\sum_{i=1}^{3} \frac{\partial}{\partial x^i} \left(\int_{y\in\partial\Omega} \tau^*\left(G(x,y)\right) \wedge \star f(y)\right) dx^i \\
&= -\sum_{i=1}^{3} \frac{\partial}{\partial x^i} \Phi[f]dx^i \\
&= -\,\mathbf{d}\,\Phi[f]
\end{aligned}$$

⊠

From the definition, using the previous proposition, A^{ee}, A^{me}, A^{em} and A^{mm} can then be expressed through these new operators.

Proposition 1.18 :

With respect to the previous notations, we have:

1. $\forall j \in \Lambda^1(\Gamma),\ A^{ee} j = \eta^{-1}\, \mathbf{d}\, \boldsymbol{\delta}\, \mathcal{A}[j] + \zeta \mathcal{A}[j]$,
2. $\forall m \in \Lambda^1(\Gamma),\ A^{me} m = \mathcal{B}[m]$,
3. $\forall j \in \Lambda^1(\Gamma),\ A^{em} j = \mathcal{B}[j]$,
4. $\forall m \in \Lambda^1(\Gamma),\ A^{ee} j = \zeta^{-1}\, \mathbf{d}\, \boldsymbol{\delta}\, \mathcal{A}[j] + \eta \mathcal{A}[j]$.

□

Finally, using these last notations, we obtain a solution of the Helmholtz equation for both the electric and the magnetic fields.

Proposition 1.19 : **Electric field in free space**

The electric field E satisfies the following equation

$$E = i\kappa Z \left(\frac{1}{\kappa^2}\, \mathbf{d}\, \boldsymbol{\delta}\, \mathcal{A}[j_s] + \mathcal{A}[j_s] \right) + \mathcal{B}[m_s] \tag{1.77}$$

with

$$\mathcal{A}[j](x) = \int_{y \in \Gamma} \tau^*(\mathbf{G}(x,y)) \wedge \star\, j(y)$$

and

$$\mathcal{B}[j](x) = \int_{y \in \Gamma} \tau^*(\star\, \mathbf{d}\, \mathbf{G}(x,y)) \wedge \star\, j(y)\,.$$

□

In the same way, we get the same expression for the magnetic field H.

Proposition 1.20 : **Magnetic field in free space**

The magnetic field H satisfies the following equation

$$H = i\kappa Z^{-1} \left(\frac{1}{\kappa^2}\, \mathbf{d}\, \boldsymbol{\delta}\, \mathcal{A}[m_s] + \mathcal{A}[m_s] \right) - \mathcal{B}[j_s] \tag{1.78}$$

with

$$\mathcal{A}[j](x) = \int_{y \in \Gamma} \tau^*(\mathbf{G}(x,y)) \wedge \star\, j(y)$$

and

$$\mathcal{B}[j](x) = \int_{y \in \Gamma} \tau^*(\star\, \mathbf{d}\, \mathbf{G}(x,y)) \wedge \star\, j(y)\,.$$

□

1.4 Surface integral equations and scattering problems

In this section, we present the essential ingredients necessary to characterize and solve electromagnetic scattering problems. For this, we notably recall the definition of a plane wave and of the Radar Cross Section. We then present the main integral equations used for solving the scattering problems.

1.4.1 Plane waves, far fields and Radar Cross Section

. Plane waves

Far away from all sources, every electromagnetic field locally has the structure of a plane wave, i.e., as a particular solution of the Maxwell equations without sources. This approximation is frequently used in radar detection problems and notably in the definition of the Radar Cross Section. Plane waves are particular solutions of the Maxwell system such that

$$E(x) = E_0 e^{-i\kappa\vartheta(x)}\mathbf{p}_E \quad \text{and} \quad H(x) = H_0 e^{-i\kappa\vartheta(x)}\mathbf{p}_H \tag{1.79}$$

where the *1-form* ϑ is defined through a direction of propagation θ (a unit vector) as

$$\begin{array}{rccc} \vartheta & : & T\mathbb{R}^3 & \to & \mathbb{R}, \\ & & x = (x^1, x^2, x^3) & \mapsto & \sum_{i=1}^3 \theta^i x^i, \end{array} \tag{1.80}$$

and where κ is the wave number, $\mathbf{p}_E$ and $\mathbf{p}_H$ respectively the electric and the magnetic polarisation. To ensure that E and H are solutions of the Maxwell system, the amplitudes of the fields, $\mathbf{p}_E$, $\mathbf{p}_H$ and the propagation direction θ must satisfy the following relations:

$$\left\{ \begin{array}{rcl} \vartheta \wedge E_0\mathbf{p}_E &=& ZH_0\mathbf{p}_H, \\ H_0\mathbf{p}_H \wedge \vartheta &=& Z^{-1}E_0\mathbf{p}_E\,. \end{array} \right. \tag{1.81}$$

. Far fields and Radar Cross Section

In some practical situations, the value of the electromagnetic fields far away from the sources can be required. In such cases, the *far field*, an asymptotic first order approximation, is used, notably in scattering and Radar Cross Section problems. In fact, when the observation point x is located very far away from the source ($\kappa r \gg 1$, with $r = \text{dist}(\text{source}, x)$), by considering the right-hand side of the equation (1.77), a first order approximation in $1/r$, can be made to greatly simplify the computation. This simplification gives to the electromagnetic field, locally, the same behaviour as a plane wave.

Mathematically, the electromagnetic field radiated by a source j_S with a compact support Γ contained in a sphere of diameter R_0 and centered on the origin allows an asymptotic expansion in $1/r \to 0$. As we just wrote, the first term is called the *far field* approximation. Let $\theta = (\nu, \phi)$ be orthogonal coordinates on the sphere centered of radius R and $\tau_R : S_R^2 \to \mathbb{R}^3$ the map of the sphere into $\mathbb{R}^3$, then

$$(\tau_R^* E)(\theta) = \sum_{p=1}^{2} e_p(\theta)\frac{\exp(ikR)}{4\pi R}d\theta_p + \mathscr{O}\left(\frac{1}{R^2}\right), \tag{1.82}$$

$$(\tau_R^* H)(\theta) = \sum_{p=1}^{2} Y_0 e_p(\theta)\frac{\exp(ikR)}{4\pi R}\bar{\star}(d\theta_p) + \mathscr{O}\left(\frac{1}{R^2}\right) \tag{1.83}$$

with

$$e_p(\theta) = \int_{x\in\Gamma}\sum_{q=1}^{2}\exp(-ik\vartheta(x))\gamma_{p,q}dx_q \wedge j_S(x) \tag{1.84}$$

where $d\theta_1 = d\nu$ and $d\theta_2 = d\phi$ are the elements of the spherical base, $\bar{\star}$ has the same meaning as $\star$, but on the reduced basis $(d\theta_1, d\theta_2)$, and γ is the metric tensor on the cotangent space with $\tau_R^*(\sum_{q=1}^2 \gamma_{pq}dx_q) = d\theta_p$.
Considering a plane incident wave E^i on an obstacle contained in D with a propagation direction

θ_i and electric polarization $\mathbf{p}_E$, the bistatic Radar Cross Section (RCS) observed in the direction θ_s can be defined as:

$$\sigma(\theta_s, \theta_i) = \frac{\|E^s(\theta_s)\|^2}{\|E^i(\theta_i)\|^2}\,. \tag{1.85}$$

1.4.2 The three principal integral equations

In the previous section, we have presented the principal equations required to describe both electric and magnetic fields in free space. In this subsection, we consider the scattering problem of a plane wave incident on a perfectly electric conducting object and present the main integral equations used to solve it.

From a general point of view, scattering and Radar Cross Section problems are radiation problems where the local surface current j_S is induced by an other external current or field. To formalize this problem, suppose that we have currents that generate an incident field $\{E^{\text{inc}}, H^{\text{inc}}\}$ in a homogeneous region characterized by parameters ε and μ. If we introduce a conducting object Ω into this region, an induced surface current j_S is created as well as a scattered field $\{E^s, H^s\}$. The objective in most applications is to obtain this scattered field. The key idea in scattering theory is to parameterize the scattered field by the induced surface currents and find these currents as the solution of a boundary integral equation.

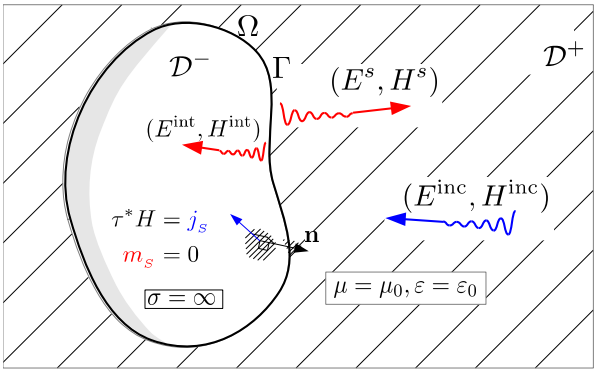

Figure 1.4 – The considered configuration.

. Solution principle

In this section, we assume that the obstacle Ω is perfectly conducting, i.e. $\sigma = \infty$ and $m_S = 0$, and that the domain is delimited by a boundary $\Gamma = \partial\Omega$ immersed in a vacuum space ($\varepsilon_r = 1, \mu_r = 1$), as described in Figure 1.4. The obstacle is illuminated by an incident wave $\{E^{\text{inc}}, H^{\text{inc}}\}$ and the fields $\{E, H\} = \{E^S + E^{\text{inc}}, H^S + H^{\text{inc}}\}$ satisfies the following boundary value problem which consists of the Maxwell system and a radiation condition:

$$\left\{\begin{array}{rcll} \mathbf{d}\, E - i\kappa Z \star H &=& 0 & \text{in } \mathcal{D}, \\ \mathbf{d}\, H + i\kappa Z^{-1} \star E &=& 0 & \text{in } \mathcal{D}, \\ \lim\limits_{r\to+\infty} r(E^S - Z \star H^S \wedge dr) &=& 0, & \end{array}\right. \tag{1.86}$$

We admit in the next developments that this problem has a unique solution.
There are several formulations for a solution by integral equations. The one we present here is based on a formulation where the unknowns are the physical currents:

$$\tau^*(H^+) = \star\, j_S \quad \text{and} \quad \tau^*(E^+) = \star\, m_S\,. \tag{1.87}$$

This corresponds to a representation of the field E and H through the Stratton-Chu formula. The key idea here is to cancel the internal field based on the following theorem.

Theorem 1.21 :

Let $\{E^{\text{inc}}, H^{\text{inc}}\}$ be a plane wave and j_S and m_S two distributions on Γ. Set

$$\left\{\begin{array}{lcl} \forall x \in \mathcal{D}^+, \quad E(x) & = & E^{\text{inc}}(x) + i\kappa Z \left(\frac{1}{\kappa^2}\,\mathbf{d}\,\boldsymbol{\delta}\,\mathcal{A}[j_S] + \mathcal{A}[j_S]\right) + \mathcal{B}[m_S](x), \\ \forall x \in \mathcal{D}^+, \quad H(x) & = & H^{\text{inc}}(x) + i\kappa Z^{-1} \left(\frac{1}{\kappa^2}\,\mathbf{d}\,\boldsymbol{\delta}\,\mathcal{A}[m_S] + \mathcal{A}[m_S]\right) - \mathcal{B}[j_S](x) \end{array}\right. \tag{1.88}$$

and

$$\left\{\begin{array}{lcl} \forall x \in \mathcal{D}^-, \quad E^{\text{int}}(x) & = & E^{\text{inc}}(x) + i\kappa Z \left(\frac{1}{\kappa^2}\,\mathbf{d}\,\boldsymbol{\delta}\,\mathcal{A}[j_S] + \mathcal{A}[j_S]\right) + \mathcal{B}[m_S](x), \\ \forall x \in \mathcal{D}^-, \quad H^{\text{int}}(x) & = & H^{\text{inc}}(x) + i\kappa Z^{-1} \left(\frac{1}{\kappa^2}\,\mathbf{d}\,\boldsymbol{\delta}\,\mathcal{A}[m_S] + \mathcal{A}[m_S]\right) - \mathcal{B}[j_S](x), \end{array}\right. \tag{1.89}$$

the electromagnetic field obtained by summing the incident wave and the field created by these currents respectively in $\mathcal{D}^+$ and in the internal domain $\mathcal{D}^-$. Then E, H, j_S and m_S are linked by the relation (1.87) if and only if $\forall x \in \mathcal{D}^-$,

$$\left\{\begin{array}{lcl} E^{\text{int}}(x) & = & 0, \\ H^{\text{int}}(x) & = & 0\,. \end{array}\right. \tag{1.90}$$

□

In the context of our problem, we chose the obstacle to be perfectly conducting. Therefore $m_S = 0$. For this, we have to ensure the condition (1.90) in order to obtain an integral representation of the field in $\mathcal{D}^+$ using j_S:

$$\left\{\begin{array}{lcl} \forall x \in \mathcal{D}^+, \quad E(x) & = & E^{\text{inc}}(x) + i\kappa Z \left(\frac{1}{\kappa^2}\,\mathbf{d}\,\boldsymbol{\delta}\,\mathcal{A}[j_S] + \mathcal{A}[j_S]\right), \\ \forall x \in \mathcal{D}^+, \quad H(x) & = & H^{\text{inc}}(x) - \mathcal{B}[j_S](x)\,. \end{array}\right. \tag{1.91}$$

Theorem 1.22 :

Let τ^*_+ and τ^*_- denote respectively the exterior and the interior limit of τ^*. $A[j_S]$ is continuous through Γ, i.e.,

$$\tau^*_\pm \left(A[j_S](x) + \frac{1}{\kappa^2}\,\mathbf{d}\,\boldsymbol{\delta}\,A[j_S](x)\right) = \tau^* \left(A[j_S](x) + \frac{1}{\kappa^2}\,\mathbf{d}\,\boldsymbol{\delta}\,A[j_S](x)\right)$$

but not $B[j_S]$ which satisfies

$$\tau^*_\pm \left(\mathcal{B}[j_S]\right) = \pm\frac{1}{2} \star j_S(x) + \mathcal{B}^+[J_s](x)$$

with

$$\forall x \in \Gamma,\ \mathcal{B}^+[j_S](x) = \int_{y \in (\Gamma - \delta\Gamma)} \tau^* \left(\star\,\mathbf{d}\,\mathbf{G}(x,y)\right) \wedge j(y)$$

where $\delta\Gamma$ is a very small region of Γ located around x. □

As E^{int} and H^{int} are solutions of the Maxwell problem in $\mathcal{D}^-$

$$\left\{ \begin{array}{rcll} \mathbf{d}\, E^{\text{int}} - i\kappa Z \star H^{\text{int}} & = & 0 & \text{in } \mathcal{D}^-, \\ \mathbf{d}\, H^{\text{int}} + i\kappa Z^{-1} \star E^{\text{int}} & = & 0 & \text{in } \mathcal{D}^-, \end{array} \right. \tag{1.92}$$

we show that, in order to get the condition (1.90), it is enough to cancel the traces. Therefore, we have for E:

$$\forall x \in \Gamma,\ -\tau^*(E^{\text{inc}}) = i\kappa Z \tau^* \left(\frac{1}{\kappa^2}\, \mathbf{d}\, \boldsymbol{\delta}\, \mathcal{A}[j_S] + \mathcal{A}[j_S] \right), \tag{1.93}$$

and for H:

$$\begin{aligned} \forall x \in \Gamma,\ \tau_+^*(H(x)) &= \tau_+^*(H^{\text{inc}}) - \tau_+^*(\mathcal{B}[j_S](x)), \\ \star\, j_s &= \tau_+^*(H^{\text{inc}}) - \frac{1}{2} \star j_S(x) - \tau^*(\mathcal{B}^+[j_S](x)), \\ \tau^*(H^{\text{inc}}) &= \frac{1}{2} \star j_S(x) + \tau^*(\mathcal{B}^+[j_S])(x). \end{aligned} \tag{1.94}$$

. Electric Field Integral Equation (EFIE)

The Electric Field Integral Equation, referred to as EFIE, is an universal equation valid for open and closed surfaces. Denoting j_S the unknown surface current, the EFIE is given by the Equation (1.93) as follows:

$$\forall x \in \Gamma,\ i\kappa Z \tau^* \left(\frac{1}{\kappa^2}\, \mathbf{d}\, \boldsymbol{\delta}\, \mathcal{A}[j_S] + \mathcal{A}[j_S] \right) = -\tau^*(E^{\text{inc}}) \tag{1.95}$$

or in the equivalent form

$$\forall x \in \Gamma,\ \tau^* \left(\zeta \mathcal{A}[j_S] + \frac{1}{\eta}\, \mathbf{d}\, \boldsymbol{\delta}\, \mathcal{A}[j_S] \right) = -\tau^*(E^{\text{inc}}) \tag{1.96}$$

with $\zeta = i\omega\mu$ and $\eta = -i\omega\varepsilon$. This last problem is always well-posed except for a countable set of exceptional values κ^E corresponding to internal resonance frequencies of $\mathcal{D}^-$ (solution of homogeneous Dirichlet problems in $\mathcal{D}^-$).

. Magnetic Field Integral Equation (MFIE)

The Magnetic Field Integral Equation, referred to as MFIE, is an equation only valid for closed surfaces. Denoting j_S the unknown surface current, the MFIE can be obtained from the Equation (1.94) and is as follows:

$$\forall x \in \Gamma,\ \frac{1}{2} j_S(x) + \star\, \tau^* \left(\mathcal{B}^+[j_S](x) \right) = \star\, \tau^*(H^{\text{inc}}). \tag{1.97}$$

Once again, this problem is well-posed except for a countable set of exceptional values κ^H (solution of homogeneous Neumann problems in $\mathcal{D}^-$).

. Combined Equation (CFIE)

Finally, we present the combined field equation named CFIE. It is an equation well-posed for any value of κ with better conditioning than the EFIE. This equation can be presented as a linear combination of the EFIE and the MFIE by:

$$\text{CFIE} = \alpha \text{EFIE} + (1 - \alpha) Z\ \text{MFIE} \tag{1.98}$$

where α is a real parameter such that $0 < \alpha < 1$. Generally, the value $\alpha = 1/5$ gives a good conditioning.

Chapter 2

Adaptation of the Electric and Magnetic Field Integral Equations (EFIE-MFIE) to plane wave scattering

Contents

In the previous chapter, we have introduced the scattering problem and set the main equations used in order to solve it. In this chapter, we study the problem from the mathematical point of view and provide a well-suited set of function spaces which will allow us to study the existence and uniqueness of a solution of the scattering problem. First, we define the function spaces for the analysis of the conventional EFIE and MFIE. Then, we present Herberthson's modified versions of the EFIE and the MFIE. These new formulations adapt the conventional integral equations to a given incident plane-wave by multiplying the kernel distribution (Green function) by a phase function specific for this incident plane wave. The fundamental unknown of the new integral equations is a pseudo current distribution which, at high frequencies, is less oscillating than the actual boundary values of the scattered field. It appears that the new integral equations can be studied in the same function spaces as the original integral equations. We present some theoretical results on the Hodge-Helmholtz decomposition and detail the way

we handle Herberthson's equations. Finally, we prove the existence and the uniqueness of a solution to the specific formulation proposed by Herberthson, namely the HEFIE.

2.1 Function spaces and variational formulations

In the previous chapter, we presented the Electric Field Integral Equation (EFIE) and the Magnetic Field Integral Equation (MFIE), the main equations used to solve the scattering problems. Until now, we assumed that all our operations were valid if we had enough regularity for the distributions involved in the calculations.
The first objective of this section is to provide a sufficient functional background for justifying the construction of both the EFIE and the MFIE. The second objective is to give enough material to derive the modified versions proposed by Herberthson and to study the involved operators.

2.1.1 Function spaces and unique solution of boundary value problems

. The considered problem

To begin, we define some notations that are used in all of this chapter. Let $\mathcal{D}^-$ be an open bounded subset of $\mathbb{R}^3$ centered at the origin. Let Γ be its boundary, M a subset of $\mathbb{R}^2$ and τ a continuous and continuously differentiable mapping from $M \subset \mathbb{R}^2$ to $\mathbb{R}^3$ giving a local parameterization of Γ. Suppose moreover that $\bar{\mathcal{D}}^- = \mathcal{D}^- \cup \Gamma$ with a C^k smooth boundary. We denote by $\mathcal{D}^+$ the complement of $\mathcal{D}^- \cup \Gamma$ and by $\mathbf{n}$ the outward pointing normal on Γ. To finish, we suppose throughout that $\mathcal{D}^+$ is a connected domain to ensure the uniqueness of the exterior solution. We also define B_R the sphere described by

$$B_R = \Big\{ x \in \mathbb{R}^3 \text{ such that } |x| < R \Big\}$$

with $\mathcal{D}^- \subset B_R$, for $R > R_0$. The configuration is summarized in Figure 2.1.
Then, we consider the following scattering problem. Let Γ denote the surface of the perfectly electric conducting (PEC) scatterer, $\{E^{\text{inc}}, H^{\text{inc}}\}$ an incident plane wave illuminating Γ described by a wave number κ, a direction of propagation θ and a electric/magnetic polarisation $\{\mathbf{p}_E, \mathbf{p}_H\}$ such as $\theta \wedge \mathbf{p}_E = Z\mathbf{p}_H$ and

$$\forall y \in \mathbb{R}^3, \; E^{\text{inc}}(y) = \psi(y)\mathbf{p}_E = e^{-i\kappa\vartheta(y)}\mathbf{p}_E, \tag{2.1}$$

$$H^{\text{inc}}(y) = \psi(y)\mathbf{p}_H = e^{-i\kappa\vartheta(y)}\mathbf{p}_H \tag{2.2}$$

where the linear function ϑ is defined through the direction of propagation $\vartheta \; : x \in \mathbb{R}^3 \mapsto \sum_i \theta^i x^i$.

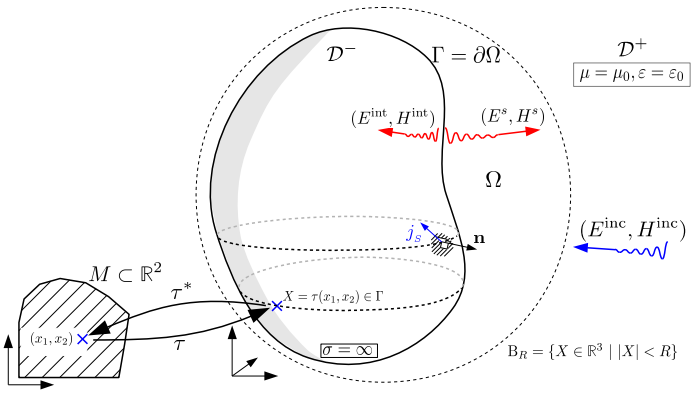

Figure 2.1 – The considered configuration.

For any open region $\Omega \subset \mathbb{R}^3$, we define the free space time-harmonic Maxwell equations without sources for the electromagnetic field $\{E, H\}$ as

$$\mathbf{d}\, E = +i\omega\mu \star H, \tag{2.3}$$
$$\mathbf{d}\, H = -i\omega\varepsilon \star E, \tag{2.4}$$

where $\mu > 0$ denotes the magnetic permeability, $\varepsilon > 0$ the electric permittivity and $\omega > 0$ the pulsation, respecting the two relations $i\omega\mu = i\kappa Z$ and $i\omega\varepsilon = i\kappa/Z$ where κ is the wave number and Z the vacuum impedance.

. Functional spaces

Before describing more precisely the different operators used to formulate the problem, we set some functional space notations. For any open domain Ω in $\mathbb{R}^3$, we use the notation

$$\mathrm{H}^0_{\boldsymbol{\delta}}(\Omega) = \left\{ u \in \Lambda^1 \mathrm{L}^2(\Omega) \mid \boldsymbol{\delta}\, u \in \Lambda^0 \mathrm{L}^2(\Omega) \right\} \tag{2.5}$$

to describe the set of *1-forms* with coefficients in $\mathrm{L}^2(\Omega)$ where $\mathrm{L}^2(\Omega)$ denotes the space of square summable fields. On Γ, the usual Sobolev spaces of regularity order s of *1-forms* are denoted $\mathrm{H}^s(\Gamma)$ and the corresponding norm is written

$$u \mapsto |u|_s. \tag{2.6}$$

On Γ, we introduce the Hilbert spaces $\mathrm{H}^s_{\boldsymbol{\delta}}(\Gamma)$

$$\mathrm{H}^s_{\boldsymbol{\delta}}(\Gamma) = \left\{ u \in \Lambda^1 \mathrm{H}^s(\Gamma) \mid \boldsymbol{\delta}\, u \in \Lambda^0 \mathrm{H}^s(\Gamma) \right\} \tag{2.7}$$

and equip them with the norms

$$u \mapsto \|u\|_s \ : \ \|u\|_s^2 = |u|_s^2 + |\,\boldsymbol{\delta}\, u|_s^2. \tag{2.8}$$

The exterior derivative and the spaces $\mathrm{H}^s_{\mathbf{d}}(\Gamma)$ are defined in a similar way:

$$\mathrm{H}^s_{\mathbf{d}}(\Gamma) = \left\{ u \in \Lambda^1 \mathrm{H}^s(\Gamma) \mid \mathbf{d}\, u \in \Lambda^2 \mathrm{H}^s \right\}. \tag{2.9}$$

Note that $u \mapsto \star\, u$ induces isomorphisms from $\mathrm{H}^s_{\mathbf{d}}(\Gamma)$ into $\mathrm{H}^s_{\boldsymbol{\delta}}(\Gamma)$ and from $\mathrm{H}^s_{\boldsymbol{\delta}}(\Gamma)$ into $\mathrm{H}^s_{\mathbf{d}}(\Gamma)$. Recall that we have the pull-back operators

$$\tau^*_{|_{\mathcal{D}^-}} : \qquad \mathrm{H}^0_{\mathbf{d}}(\mathcal{D}^-) \to \mathrm{H}^{-1/2}_{\mathbf{d}}(\Gamma), \tag{2.10}$$
$$v \mapsto v_{\mathrm{T}} = \tau^*(v) \tag{2.11}$$

and for arbitrary large enough $R > 0$ (with $B_R = \{x \in \mathbb{R}^3 \mid |x| < R\}$)

$$\tau^*_{|_{\mathcal{D}^+}} : \qquad \mathrm{H}^0_{\mathbf{d}}(\mathcal{D}^+ \cap B_R) \to \mathrm{H}^{-1/2}_{\mathbf{d}}(\Gamma), \tag{2.12}$$
$$v \mapsto v_{\mathrm{T}} = \tau^*(v)\,. \tag{2.13}$$

For simplicity, we denote by $\mathrm{H}^0_{\mathbf{d},\mathrm{loc}}(\mathcal{D}^+)$ the space of *1-forms* in $\mathcal{D}^+$ whose restrictions are in $\mathrm{H}^0_{\mathbf{d}}(\mathcal{D}^+ \cap B_R)$ for all $R > 0$.

. Existence and uniqueness

We consider here an electromagnetic field $\{E, H\}$ solution of the Maxwell equations. The idea is to search $\{E, H\}$ in $\mathrm{H}^0_{\mathbf{d},\mathrm{loc}}(\mathcal{D}^+)$ or $\mathrm{H}^0_{\mathbf{d}}(\mathcal{D}^-)$. The Silver-Müller radiation condition at infinity for an electromagnetic field $\{E, H\} \in \mathrm{H}^0_{\mathbf{d},\mathrm{loc}}(\mathcal{D}^+)^2$ reads

$$\lim_{r\to\infty} r(E - Z \star dr \wedge H) = o(1), \tag{2.14}$$

$$\lim_{r\to\infty} r(H - Y \star dr \wedge E) = o(1) \tag{2.15}$$

with $r = \|x\|$. For exterior problems, we have the existence and uniqueness result ([49]-[50, Theorem 5.4.6, p.220]):

Theorem 2.1 :

For all $\kappa > 0$, all $v \in \mathrm{H}^{-1/2}_{\mathbf{d}}(\Gamma)$, there is a unique $\{E, H\} \in \mathrm{H}^0_{\mathbf{d},\mathrm{loc}}(\mathcal{D}^+)^2$ solving the Maxwell equation in $\mathcal{D}^+$, satisfying the Silver-Müller radiation condition, and such that $\tau^*(E) = v$. The corresponding solution operator is continuous. □

For interior problems, we have the following theorem:

Theorem 2.2 :

There is a unique real positive strictly increasing and unbounded sequence (κ_n) such that setting $\mathbb{K} = \{\kappa_n \mid n \in \mathbb{N}\}$, we have

- for all $\kappa \notin \mathbb{K}$, for all $v \in \mathrm{H}^{-1/2}_{\mathbf{d}}(\Gamma)$, there is a unique $\{E, H\} \in \mathrm{H}^0_{\mathbf{d}}(\mathcal{D}^-)^2$ solving the Maxwell equations in $\mathcal{D}^-$ and such that $\tau^*(E) = v$.
- For all $\kappa \in \mathbb{K}$, the space of solutions $\{E, H\} \in \mathrm{H}^0_{\mathbf{d}}(\mathcal{D}^-)^2$ to Maxwell's equations in $\mathcal{D}^-$, such that $\tau^*(E) = 0$, is a non-trivial finite dimensional space.

The elements of $\mathbb{K}$ are called internal resonance wave-numbers. □

2.1.2 Variational formulation of boundary integral equations

Let $\mathbf{G}$ be the Green function, the $1 \otimes 1$-*form* solution of (1.60), defined by

$$\mathbf{G}(x, y) = \sum_{i=1}^{3} G(x, y) dx^i \otimes dy^i = \sum_{i=1}^{3} \frac{e^{i\kappa|x-y|}}{4\pi|x - y|} dx^i \otimes dy^i \,. \tag{2.16}$$

Let $\mathcal{A}$ be the *1-form* potential defined in Chapter 1 which maps any sufficiently smooth *1-form* over Γ into a field in $\mathcal{D}^{\pm}$ defined away from Γ by

$$\mathcal{A}[u](x) = \int_\Gamma \tau^*(\mathbf{G}(x, y)) \wedge \star\, u(y), \tag{2.17}$$

its associated operators Φ which works on *0-forms* over Γ

$$\Phi[f](x) = \int_\Gamma \tau^*(G(x, y)) \wedge \star\, f(y) \tag{2.18}$$

and the potential $\mathcal{B}$ which also works on *1-forms*

$$\mathcal{B}[u](x) = \int_\Gamma \tau^*(\star\, \mathbf{d}\, \mathbf{G}(x, y)) \wedge \star\, u(y) \,. \tag{2.19}$$

With these notations, we have the following theorem.

Theorem 2.3 : **[49, Theorem 2.3, p.185], [50, Theorem 5.5.1, p.234]**

Suppose $\{E, H\}$ is a field whose restrictions to $\mathcal{D}^-$ and $\mathcal{D}^+$ are respectively in $\mathrm{H}^0_{\mathbf{d}}(\mathcal{D}^-)^2$ and $\mathrm{H}^0_{\mathbf{d},\mathrm{loc}}(\mathcal{D}^+)^2$ and solve the Maxwell equations (2.3) and (2.4) for a given wave-number κ. Suppose also that it satisfies the Silver-Müller radiation condition. Define the electric and magnetic currents j_s and m_s on Γ by the jump formula

$$\begin{aligned} \tau^*\left(H_{|_{\mathcal{D}^+}} - H_{|_{\mathcal{D}^-}}\right) &= \star\, j_s, \\ \tau^*\left(E_{|_{\mathcal{D}^-}} - E_{|_{\mathcal{D}^+}}\right) &= \star\, m_s, \end{aligned} \tag{2.20}$$

then in $\mathcal{D}^-$ and $\mathcal{D}^+$, we have

$$E = \frac{1}{\eta}\,\mathbf{d}\,\boldsymbol{\delta}\,\mathcal{A}[j_s] + \zeta\mathcal{A}[j_s] + \mathcal{B}[m_s], \tag{2.21}$$

$$H = \frac{1}{\zeta}\,\mathbf{d}\,\boldsymbol{\delta}\,\mathcal{A}[m_s] + \eta\mathcal{A}[m_s] - \mathcal{B}[j_s]. \tag{2.22}$$

□

After setting the problem, we can detail more precisely the different operators involved in the formulation of the problem.

Corollary 2.4 :

Since $\{E, H\}$ belongs to $\mathrm{H}^0_{d,\mathrm{loc}}(\mathcal{D}^\pm)$, $\tau^* : \mathrm{H}^0_{d,\mathrm{loc}}(\mathcal{D}^\pm) \to \mathrm{H}^{-1/2}_{\mathbf{d}}(\Gamma)$ and $\star : \mathrm{H}^{-1/2}_{\mathbf{d}}(\Gamma) \to \mathrm{H}^{-1/2}_{\boldsymbol{\delta}}(\Gamma)$ are continuous, the electric and the magnetic currents j_s and m_s belong to $\mathrm{H}^{-1/2}_{\boldsymbol{\delta}}(\Gamma)$. □

Proposition 2.5 : **See [51, Chapter 2]**

$$\begin{aligned} \tfrac{1}{\eta}\,\mathbf{d}\,\boldsymbol{\delta}\,\mathcal{A} + \zeta\mathcal{A} \;&:\; \mathrm{H}^{-1/2}_{\boldsymbol{\delta}}(\Gamma) \;\longrightarrow\; \mathrm{H}^0_{\mathbf{d},\mathrm{loc}}(\mathcal{D}^+), \\ \mathcal{B} \;&:\; \mathrm{H}^{-1/2}_{\boldsymbol{\delta}}(\Gamma) \;\longrightarrow\; \mathrm{H}^0_{\mathbf{d},\mathrm{loc}}(\mathcal{D}^+). \end{aligned} \tag{2.23}$$

□

Definition 2.6 :

For $\kappa \neq 0$, we define the Electric Field Integral operator for PEC surface ($m_s = 0$) by

$$\begin{aligned} \mathcal{E} \qquad \mathrm{H}^{-1/2}_{\boldsymbol{\delta}}(\Gamma) &\longrightarrow \mathrm{H}^{-1/2}_{\mathbf{d}}(\Gamma), \\ u &\longmapsto \tau^*\left(\zeta\mathcal{A}[u] - \frac{1}{\eta}\,\mathbf{d}\,\boldsymbol{\delta}\,\mathcal{A}[u]\right). \end{aligned} \tag{2.24}$$

In the same way, we define the Magnetic Field Integral operator:

$$\begin{aligned} \mathcal{M} \qquad \mathrm{H}^{-1/2}_{\boldsymbol{\delta}}(\Gamma) &\longrightarrow \mathrm{H}^{-1/2}_{\mathbf{d}}(\Gamma), \\ u &\longmapsto \star\,\frac{1}{2}u + \tau^*(\mathcal{B}^+[u])\,. \end{aligned} \tag{2.25}$$

□

. Variational formulation and discretization for PEC surface

To simplify the notations, we introduce

$$(u, v) \in \Lambda^1(\Gamma) \times \Lambda^1(\Gamma) \mapsto \langle u\ ;\ v\rangle = \int_\Gamma u \wedge \star v. \tag{2.26}$$

This allows us to write a variational formulation of the EFIE as: for a given $v \in \mathrm{H}_{\mathbf{d}}^{-1/2}(\Gamma)$ find

$$u \in \mathrm{H}_{\boldsymbol{\delta}}^{-1/2}(\Gamma) \;\text{ such that }\; \forall u' \in \mathrm{H}_{\boldsymbol{\delta}}^{-1/2}(\Gamma),\; \langle \mathcal{E}[u] \;;\; u' \rangle = \langle v \;;\; u' \rangle \,. \tag{2.27}$$

In a scattering problem, v is given by $v = -\tau^*(E^{\mathrm{inc}})$. In the same way, we obtain a variational formulation of the MFIE: for a given $v \in \mathrm{H}_{\mathbf{d}}^{-1/2}(\Gamma)$, find $u \in \mathrm{H}_{\boldsymbol{\delta}}^{-1/2}(\Gamma)$ such that

$$\forall u' \in \mathrm{H}_{\boldsymbol{\delta}}^{-1/2}(\Gamma),\; \langle \mathcal{M}[u] \;;\; u' \rangle = \langle v \;;\; u' \rangle \,. \tag{2.28}$$

In a scattering problem, we have $v = \star\tau^*(H^{\mathrm{inc}})$.

2.2 Herberthson's modification of the boundary integral equations by phase conjugation and previous work

In this section, we present Herberthson's work on the EFIE and on the MFIE, notably the modified version he proposed for both of them. Most of the development can be found in [24], [25] or [26]. For the sake of coherence, we only modified some notations and voluntary choose to keep the same formalism used by Herberthson in his publications.
We still consider here an electromagnetic scattering problem on a PEC surface Γ, but we add a supplementary constraint on the shape of the surface supposing that Γ is homeomorphic to the sphere, i.e., Γ is a surface with a genus 0. This allows to use the Helmholtz decomposition, in both the EFIE and the MFIE, to find a new formulation in terms of scalar functions. We conclude this section with a short discussion on the link that can be made with previous work, notably of Zhou [16].

2.2.1 Herberthson's work

. Introduction

To set the notations, we assume that in the frequency domain an incoming plane wave illuminating a surface Γ centered at the origin is given by $\mathbf{E}^{\mathrm{inc}}(\mathbf{r}) = E_0 e^{i\mathbf{k}\cdot\mathbf{r}}\hat{\mathbf{x}}$. The associated corresponding magnetic field is $\mathbf{H}^{\mathrm{inc}}(\mathbf{r}) = H_0 e^{i\mathbf{k}\cdot\mathbf{r}}\hat{\mathbf{y}}$ where $\mathbf{k} = \kappa\hat{\mathbf{z}}$. To finish, $\mathbf{J}$ denotes the surface current. With these notations, the EFIE reads

$$\forall r \in \Gamma,\; -E_0 e^{-ikz}\hat{\mathbf{x}} \,\hat{=}\, (\zeta\mathbf{I} + \frac{1}{\eta}\nabla\nabla\cdot) \int_\Gamma G(r,r')\,\mathbf{J}(r')d\Gamma'. \tag{2.29}$$

Here G is the Green function defined earlier $G(r,r') = \frac{e^{ik|r-r'|}}{4\pi|r-r'|}$, and where $\hat{=}$ means tangential equality on Γ. Under the same assumptions, the MFIE reads

$$\forall r \in \Gamma,\; H_0 e^{-ikz}\hat{\mathbf{y}} \,\hat{=}\, -\frac{1}{2}\,\mathbf{n}\times\mathbf{J}(r) + \int_\Gamma \nabla' G(r,r') \times \mathbf{J}(r')d\Gamma', \tag{2.30}$$

where $\mathbf{n}$ is the normal vector to Γ at r. All integrals are taken in the Cauchy principal value sense. Note that this formulation of the MFIE is quite different from ours and leads to slightly different properties as we will show later. From this, the CFIE can be obtained through a linear combination of (2.29) and (2.30)

$$\mathrm{CFIE} = \alpha\mathrm{EFIE} + (1-\alpha)\mathrm{MFIE} \tag{2.31}$$

with $\alpha \in]0;1[$.

. Reformulation using potentials

The first key idea of the Herberthson reformulation is to observe that the left-hand side (LHS) of (2.29) and (2.30) can be naturally viewed as covector fields (or *1-forms*). Since both equations involve tangential equality at each $r \in \Gamma$, these covectors lie in $T_p^*\Gamma$ the cotangent space at $p = p(r) \in \Gamma$. The current $\mathbf{J}$ is also a covector field on Γ.

The second element introduced by Herberthson is the Hodge decomposition. Assuming for simplicity that the closed surface Γ is homeomorphic to a sphere, he proposed to use the Hodge decomposition theorem that asserts that every covector field ω can be decomposed as the sum of a gradient and a cogradient. More precisely, every *1-form* ω can be described with three constituents

$$\omega = \mathbf{d}\,\Phi + \beta + \boldsymbol{\delta}\,\psi \tag{2.32}$$

where Φ is a scalar (or a *0-form*), β is an harmonic *1-form* and ψ is a *2-form*. However, since the scattering surface is homeomorphic to a sphere, we can benefit from an interesting simplification. Indeed with such a surface, there are no non-trivial harmonic *1-forms* and the harmonic β denoted here vanishes over the surface. Thus, with $\Psi = \star\,\psi$ such that Ψ is a scalar function, we have

$$\omega = \mathbf{d}\,\Phi + \boldsymbol{\delta} \star \Psi \;\cong\; \nabla_s\Phi + n \times \nabla_s\Psi, \tag{2.33}$$

which means that every tangential field ω on Γ can be expressed through two scalar potentials Φ and Ψ (see for example Figure 2.2).

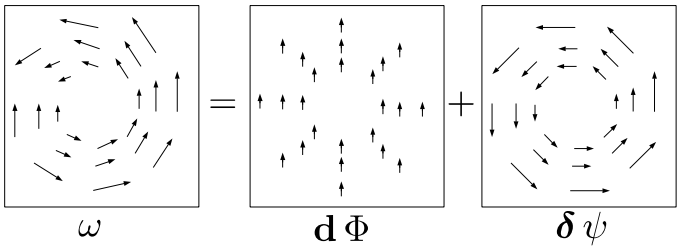

Figure 2.2 – Illustration of the Hodge decomposition.

Next, Herberthson highlighted the fact that the left-hand side (LHS) of (2.29) and (2.30) can be turned into exact gradients of a scalar function, $-E_0\hat{\mathbf{x}} = \nabla(-E_0 x)$ and $H_0\hat{\mathbf{y}} = \nabla(H_0 y)$, respectively, by multiplying both sides of the equations with the conjugate of the phase function of the incident plane wave, e^{ikz}. Hence, multiplying (2.29) and (2.30) with e^{ikz}, he introduced the following functions

$$h(r, r') = G(r, r')e^{ik(z-z')}, \quad \hat{\mathbf{J}}(r') = e^{ikz'}\,\mathbf{J}(r') \tag{2.34}$$

and the following new equations for the EFIE and the MFIE:

$$\forall r \in \Gamma,\; -E_0\hat{\mathbf{x}} \mathrel{\hat{=}} (\zeta\mathbf{I} + \frac{1}{\eta}\nabla\nabla\cdot) \int_\Gamma G(r, r')e^{-ikz'}\hat{\mathbf{J}}(r')d\Gamma', \tag{2.35}$$

$$\forall r \in \Gamma,\; H_0\hat{\mathbf{y}} \mathrel{\hat{=}} -\frac{1}{2}\,\mathbf{n} \times \hat{\mathbf{J}}(r) + \int_\Gamma \nabla' G(r, r')e^{-ikz'} \times \hat{\mathbf{J}}(r')d\Gamma', \tag{2.36}$$

which leads to the following variational forms

$$\begin{aligned}
\int_\Gamma -E_0\hat{\mathbf{x}}\cdot\mathbf{J}' &= \zeta \iint_{\Gamma\times\Gamma} h(r, r')\hat{\mathbf{J}}(r')\cdot\mathbf{J}'(r)d\Gamma d\Gamma + \frac{1}{\eta}\iint_{\Gamma\times\Gamma} G(r, r')\nabla_s(e^{ikz}\hat{\mathbf{J}}(r))\cdot\nabla_s(e^{-ikz}\,\mathbf{J}'(r))d\Gamma' d\Gamma, \\
\int_\Gamma H_0\hat{\mathbf{x}}\cdot\mathbf{J}' &= -\frac{1}{2}\int_\Gamma \hat{\mathbf{J}}(r')\cdot\mathbf{J}'(r)d\Gamma + \iint_{\Gamma\times\Gamma} e^{ik(z-z')}\,\mathbf{J}'(r)\cdot(\nabla' G(r, r') \times \hat{\mathbf{J}}(r'))d\Gamma' d\Gamma\,.
\end{aligned}$$

Since $E_0\hat{\mathbf{x}}$ (and also $H_0\hat{\mathbf{x}}$) is an exact *1-form*, we have

$$\int_\Gamma E_0\hat{\mathbf{x}}\cdot\mathbf{J}' = \int_\Gamma \nabla_s x^i\cdot\mathbf{J}' = -\int_\Gamma x^i(\nabla\cdot\mathbf{J}'). \tag{2.37}$$

Therefore, if $\mathbf{J}'$ belongs to Ker(div), the left-hand side vanishes. In this way, Herberthson reduces (2.35) and (2.36) to equations for two scalar potentials Φ and Ψ. The resulting equation for the EFIE is given in [24] and will not be repeated here. To summarize, using the decomposition $\hat{\mathbf{J}} = \mathbf{d}\,\Phi + \boldsymbol{\delta}\star\Psi$, working directly on the discretization of the scalar potentials Φ and Ψ and giving them n degrees of freedom each, we obtain a $2n\times 2n$ system of equations, that we can write as

$$\begin{pmatrix} H^{\Phi\Phi} & H^{\Phi\Psi} \\ H^{\Psi\Phi} & H^{\Psi\Psi} \end{pmatrix} \begin{pmatrix} [\Phi]_{n\times 1} \\ [\Psi]_{n\times 1} \end{pmatrix} = \begin{pmatrix} v_\Phi \\ 0 \end{pmatrix}. \tag{2.38}$$

In terms of functional sub-spaces, the Helmholtz theorem decomposes the current into potential ($\widehat{\mathbf{J}}_d = \nabla_s\Phi$) and solenoidal ($\widehat{\mathbf{J}}_s = \mathbf{n}\times\nabla_s\Psi$) currents. This decomposition appears interesting in the case we consider the RCS coefficient in the forward direction $\sigma(\theta^i,\theta^i)$. From the definition given in Section 1.4.1, we have:

$$\begin{aligned} \sigma(\theta^i,\theta^i) &= \|E^\infty(\theta^i,\theta^i)\|^2, \\ E^\infty(\theta^i,\theta^i) &= \int_\Gamma (\underbrace{\exp(-ik\vartheta^s)}_{\bar{\psi}}\underbrace{\hat{\mathbf{x}}}_{\nabla_s x^i})\cdot\mathbf{J}, \\ &= \int_\Gamma \left(\nabla_s x^i\right)\cdot\bar{\psi}\,\mathbf{J} = \int_\Gamma \left(-x^i\nabla\cdot(\bar{\psi}\,\mathbf{J})\right). \end{aligned}$$

Therefore, it appears that only the potential part of the pseudo-current $\widehat{\mathbf{J}}_d$ has an impact on this forward scattering coefficient. The last point, but not the least, highlighted by Herberthson, is that the replacement of $\mathbf{J}$ by $\hat{\mathbf{J}}$ may lead to a sparser sampling and consequently reduces the numerical computation. In fact, the oscillations of the surface current are induced by the oscillations of the incident plane wave. Therefore, the pseudo current $\hat{\mathbf{J}} = \bar{\psi}\,\mathbf{J}$, which is described as the physical current multiplied with the conjugate phase, may then resemble a more slowly varying "envelop" and may hence be sampled more sparsely (see Figure 2.3). For high frequencies, this could substantially reduce the numerical problem.

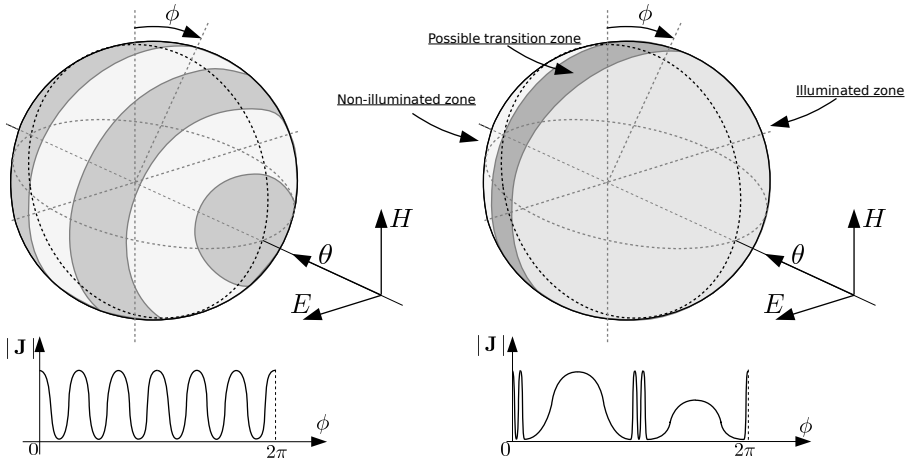

Figure 2.3 – Symbolic representation of oscillations for both the physical current (on the left) and the pseudo-current (on the right).

2.2.2 Links with previous work and implications

. Discussion of Herberhtson's work

At the end of this short presentation of Herberthson's work, three points have to be discussed in order to prepare the following developments.
The first concerns the ≪regularity≫ of the pseudo-current. By multiplying the physical current by the conjugate phase of the plane wave, we get a pseudo-current with less oscillations than the physical current (except for some possible specific areas). This new pseudo-current should allow an important reduction of the number of degrees of freedom in the discretization of the equations (independently of the Hodge decomposition). This ≪regularity≫ will be studied in terms of reduction of the number of degrees of freedom in Chapter 5.

The second point is the choice of the Hodge decomposition. Indeed, in his presentation, Herberthson assumed that the treated surface is homeomorphic to a sphere (i.e., a surface with a genus 0). This restriction is interesting from a practical point of view, since it leads to a much simpler formulation with only two components by deleting the harmonic component. However, when the surface is not genus 0, this harmonic component is non-zero and must be considered. Therefore, we need to consider another form of decomposition if we want to describe $\hat{\mathbf{J}}$ as the sum of two components belonging to two orthogonal subspaces.
The last point is the implementation with the potentials Ψ and Φ. A priori, there is no restriction or problem to deal with these potentials and it appears quite natural to do it regarding the proposed decomposition. However, as we have chosen to formulate it in a slightly different form to treat more complex objects, where the harmonic component has to be expressed, we wish to deal with vector quantities on the surface (more precisely with *1-forms* over Γ). If we treat surfaces that are homeomorphic to a sphere, the two methods remain strictly equivalent.

. Previous developments

The two integral equations (2.35) and (2.36) are close to what has emerged in previous works presented in the literature. In particular those carried out by T. Abboud, J.-C. Nédélec and B. Zhou [16, 17, 18], A. De la Bourdonnaye and M. Tolentino [19, 20] or A. Bachelot, E. Darrigrand and K. Mer-Nkonga [21, 22, 23] who proposed various variations around an acceleration method based on estimations of the phase or discretization of the phase of the unknown current $\mathbf{J}$.
Early work of T. Abboud, J.-C. Nédélec and B. Zhou, was based on a scattering configuration with a regular and convex bounded surface $\Gamma \subset \mathbb{R}^3$ illuminated by a plane wave $\mathbf{E}^{\text{inc}}$ as described above. As explained in [16], the major difficulty of the high-frequency problems comes from the approximation of the phase of the physical current $\mathbf{J}$. To make an analogy, to properly approach a sinusoidal function over a period, it is necessary to have a minimum of control points or evaluation points. The same rule applies to the physical current which has also the form of an oscillating function over the scattering surface. Considering an incident plane wave, the idea consists in finding a solution $\mathbf{J}$ in the form

$$\mathbf{J}(x) = \tilde{\mathbf{J}}(k, x)e^{ik\phi(x)} \tag{2.39}$$

where $\tilde{\mathbf{J}}$ and ϕ are two unknowns describing respectively the modulus and the phase of the physical current. In agreement with an asymptotic expansion, valid on a convex object, it is possible to give at any point a first approximation of the phase in the form:

$$\phi(x) = ik\phi_0(x) + k^{1/3}\phi_1(x) = ik\theta\cdot\mathbf{x} + k^{1/3}\phi_1(x). \tag{2.40}$$

In the illuminated zone, see Figure 2.3, the physical current takes the following expression:

$$\mathbf{J}(x) = \tilde{\mathbf{J}}(k, x)e^{ik\phi_0(x)}, \tag{2.41}$$

oscillating in the same way as the incident wave, whereas in the transition zone or in the non-illuminated zone, the asymptotic expansion gives us:

$$\mathbf{J}(x) = \tilde{\mathbf{J}}(k, x)e^{ik\phi_0(x)+k^{1/3}\phi_1(x)}. \tag{2.42}$$

Considering these different expressions for the phase, Zhou proposes to approach the phase of the current by the phase of the incident wave on Γ arguing that, even if, by the fact, we commit an error in the transition and non-illuminated areas, the modulus decreases exponentially. If we write that

$$\mathbf{J} = e^{ik\phi_0(x)}\hat{\mathbf{J}}(x), \tag{2.43}$$

with ϕ_0 the phase of the incident wave, as we have already mentioned, the new function $\hat{\mathbf{J}}$ appears less oscillating insofar as we have already isolated the more oscillating part of the current phase.
From there, Zhou proposes to couple this approximation with the method of integral equations to reduce the number of degrees of freedom necessary to obtain the physical current. However, the price to pay for a coarse mesh is, from a numerical point of view, to treat more precisely the remaining oscillating integrals involved in the computation of the Galerkin matrix. To deal with it, he build a technical system of a double mesh, called micro-local discretization, requiring a certain programming effort with a coarse mesh to represent the current and a fine mesh to calculate correctly the integrals.
The main difference from Herberthson's work is the fact that in Abboud-Nédélec-Zhou's work, the phase is not strictly introduced in the EFIE operator. Indeed, they preserve the kernel distribution of the EFIE operator and introduce new approximation spaces. To simplify, the proposed idea consists in taking test functions of the form $x \mapsto e^{ik\theta\cdot\mathbf{x}}\mathbf{J}_k(x)$, where $\mathbf{J}_k$ is an conventional edge function. Finally, an estimate of the error between the solution of the continuous and discrete problems is obtained as function of the maximum edge length of the mesh (or of the two meshes if any) and the frequency (see [16, Chapter 1]). Based on this error estimate, an asymptotic relaxing on the required number of degrees of freedom on the coarse mesh can be expected.
His conclusion is that for the Maxwell equations this method, which requires an important programming effort, provides a significant improvement over the classical method in terms of number of degrees of freedom and also in terms of computation time for a convex object.
In the thesis of E. Darrigrand [21] the above ideas are further developed. This work provides a detailed study of a combination of the fast multipole method, the method introduced by Zhou and the integral formulation of B. Després [23].

. Discussion

As we have already mentioned earlier, the first difference between the works of Zhou-Darrigrand and those of Herberthson are "philosophical". In Zhou's work, the initial idea was to try to estimate and approximate the phase of the physical current as well as possible and to represent the physical current as a slowly varying modulation of this phase function. As such, he evokes the possibility of taking more complex phase functions to approximate this quantity better and better. Herberthson chose to eliminate the phase function of the incident plane wave from the right-hand side and exploit all possible relations to obtain a new particular matrix system (2.38) for two slowly varying scalar functions.

The second difference, which in our opinion is the most interesting, is the choice the different authors made concerning how to handle the phase. In the work of Zhou-Darrigrand, the discretization of the conventional equations is done with modified test functions, while Herberthson chose to modify the integral operator itself and use conventional test functions.
This difference seems to us very important insofar as it brings some developments that in the case where one uses exponential test functions are not clearly transparent. First, by introducing a new operator similar (in the mathematical sense of the term) to the conventional operator, it allows us, besides answering the questions of existence and uniqueness of a solution. Then by working on this new operator $\mathcal{H}$ and exploiting its relation with the conventional operator $\mathcal{E}$, we have been able to highlight the existence of a perturbation such as:

$$\mathcal{E} + \mathcal{K} = \mathcal{H}. \tag{2.44}$$

This perturbation operator, $\mathcal{K}$, appears to be quite simple to implement, as far as it does not contain any new singular terms, it lends itself well enough to a fast deployment from already existing codes as we show in Chapter 3 (this also allows us to use every tools already available for the reduction of computation times: multipoles, H-matrices, ...). We were also able to clearly demonstrate that this operator $\mathcal{K}$ needs less numerical effort than the conventional operator $\mathcal{E}$ and that the latter is well-suited to a model reduction.

Finally, if Herberthson's formulation through two scalar potentials brings some constraints on the scattering surface, the generalization that we proposed in this chapter, does not impose any topological genus. We also note that, in this decomposition, only K depends on the incident wave's direction and needs to be recalculated for each new direction of incidence.

2.3 Weak formulation of the modified equations

In the first section of this chapter, we set up the functional background for the EFIE and the MFIE, defined the different function spaces that describe the different operators involved, but also the spaces in which the solutions live. We recall step by step the construction of modified versions of the EFIE and the MFIE proposed by Herberthson, that we respectively call the HEFIE and HMFIE. Then we present the Hodge decomposition and some other related decompositions to give the final systems obtained before discretization.

2.3.1 Variational formulation of the modified integral equations

First, we recall the problem. Let Γ denote the surface of an open or closed perfectly electric conducting (PEC) scatterer with normal unit $\mathbf{n}$, $\mathbf{E}^{\text{inc}}$ an incident plane wave illuminating Γ, parameterized by a wave number κ, a direction of propagation θ and an electric polarisation $\mathbf{p}_E$ such that $\forall y \in \mathbb{R}^3$, $\mathbf{E}^{\text{inc}}(y) = \psi(y)\mathbf{p}_E = e^{-i\kappa\vartheta(y)}\mathbf{p}_E$. Let $\mathbf{J}$ be the induced surface current distribution on Γ.

. The Herberthson Electric Field Integral Equation

First, as we wrote earlier, with these notations, the EFIE (Electric Field Integral Equation) reads

$$\forall x \in \Gamma,\ \tau^*\left(\zeta\mathcal{A}[\mathbf{J}] + \frac{1}{\eta}\,\mathbf{d}\,\boldsymbol{\delta}\,\mathcal{A}[\mathbf{J}]\right) = -\tau^*(E^{\text{inc}}) \tag{2.45}$$

where $\zeta = i\omega\mu$ and $\eta = -i\omega\varepsilon$ and $\mathcal{A}$ denotes the single layer potential defined by

$$\mathcal{A}[j](x) = \int_{y\in\Gamma} \tau^*(\mathbf{G}(x,y)) \wedge \star\, j(y) \tag{2.46}$$

with $\mathbf{G}$ the $1 \otimes 1$-*form* solution, also called Green's function, defined by

$$\mathbf{G}(x,y) = \sum_{i=1}^{3} G(x,y) dx^i \otimes dy^i = \sum_{i=1}^{3} \frac{e^{i\kappa|x-y|}}{4\pi|x-y|} dx^i \otimes dy^i \,. \tag{2.47}$$

This equation leads to the following variational problem:

$$\begin{cases} \text{Find } \mathbf{J} \in \mathrm{H}_{\boldsymbol{\delta}}^{-1/2}(\Gamma), \text{ such as } \forall\, \mathbf{J}' \in \mathrm{H}_{\boldsymbol{\delta}}^{-1/2}(\Gamma), \\ \langle \mathcal{E}[\mathbf{J}] \,;\, \mathbf{J}' \rangle = \zeta \displaystyle\int_\Gamma \tau^* \left(\mathcal{A}[\mathbf{J}]\right) \wedge \star\, \mathbf{J}' + \frac{1}{\eta} \int_\Gamma \tau^* \left(\Phi[\boldsymbol{\delta}\, \mathbf{J}]\right) \wedge \star\, \boldsymbol{\delta}\, \mathbf{J}' = - \int_\Gamma \tau^*(\mathbf{E}^{\mathrm{inc}}) \wedge \star\, \mathbf{J}' \,. \end{cases} \tag{2.48}$$

Starting from the conventional EFIE problem, the first step is to multiply the left and the right-hand side by the conjugate phase $\bar{\psi}$ in order to get on the right-hand side only a constant *1-form*, $\mathbf{p}_E$,

$$\forall x \in \Gamma,\ \tau^* \left(\bar{\psi}(x) \zeta \mathcal{A}[\mathbf{J}] + \frac{1}{\eta} \bar{\psi}(x)\, \mathbf{d}\, \boldsymbol{\delta}\, \mathcal{A}[\mathbf{J}] \right) = -\tau^*(\bar{\psi}(x) E^{\mathrm{inc}}) = -\tau^*(\mathbf{p}_E) \,. \tag{2.49}$$

The second step is to introduce a pseudo-current,

$$\hat{\mathbf{J}} = \bar{\psi}\, \mathbf{J}, \tag{2.50}$$

to obtain the HEFIE:

$$\forall x \in \Gamma,\ \tau^* \left(\bar{\psi}(x) \zeta \mathcal{A}[\psi \hat{\mathbf{J}}] + \frac{1}{\eta} \bar{\psi}(x)\, \mathbf{d}\, \boldsymbol{\delta}\, \mathcal{A}[\psi \hat{\mathbf{J}}] \right) = -\tau^*(\bar{\psi}(x) E^{\mathrm{inc}}) = -\tau^*(\mathbf{p}_E) \,. \tag{2.51}$$

This last equation leads to the following variational problem:

$$\begin{cases} \text{Find } \hat{\mathbf{J}} \in \mathrm{H}_{\boldsymbol{\delta}}^{-1/2}(\Gamma), \text{ such as } \forall\, \mathbf{J}' \in \mathrm{H}_{\boldsymbol{\delta}}^{-1/2}(\Gamma), \\ \langle \mathcal{H}[\hat{\mathbf{J}}] \,;\, \mathbf{J}' \rangle = \zeta \displaystyle\int_\Gamma \tau^* \left(\mathcal{A}[\psi \hat{\mathbf{J}}] \right) \wedge \star\, \psi\, \mathbf{J}' + \frac{1}{\eta} \int_\Gamma \tau^* \left(\Phi[\boldsymbol{\delta}(\psi \hat{\mathbf{J}})] \right) \wedge \star\, \boldsymbol{\delta}(\psi\, \mathbf{J}') = - \int_\Gamma \tau^*(\mathbf{p}_E) \wedge \star\, \mathbf{J}' \end{cases} \tag{2.52}$$

where

$$\begin{aligned} \mathcal{H} : \qquad \mathrm{H}_{\boldsymbol{\delta}}^{-1/2}(\Gamma) &\longrightarrow \mathrm{H}_{\mathbf{d}}^{-1/2}(\Gamma), \\ v &\longmapsto \tau^* \left[\bar{\psi} \zeta \mathcal{A}[\psi v] - \frac{1}{\eta} \bar{\psi}\, \mathbf{d}\, \boldsymbol{\delta}\, \mathcal{A}[\psi v] \right]. \end{aligned} \tag{2.53}$$

It is important to note that the multiplication by $\bar{\psi}$ or ψ does not change the nature of the functions involved. Therefore, $\hat{\mathbf{J}}$ and $\mathbf{J}'$ lives in $\mathrm{H}_{\boldsymbol{\delta}}^{-1/2}(\Gamma)$ even if in this formulation, the pseudo-current $\hat{\mathbf{J}}$ computed does not represent the physical current distribution induced by the incident plane wave, but a pseudo-current potentially less oscillating.

. The Herberthson Magnetic Field Integral Equation

In the same way, we can make a link between the conventional MFIE and the HMFIE. Suppose that $\mathbf{p}_H = Y_0 \theta \wedge \mathbf{p}_E$ such as $\forall y \in \mathbb{R}^3$, $\mathbf{H}^{\mathrm{inc}}(y) = \psi(y) \mathbf{p}_H = e^{-i\kappa\theta \cdot y} \mathbf{p}_H$. With these notations, the MFIE reads

$$\forall x \in \Gamma,\ \frac{1}{2}\, \mathbf{J}(x) + \star\, \tau^* \left(\mathcal{B}[\mathbf{J}](x) \right) = \star\, \tau^*(H^{\mathrm{inc}}) \tag{2.54}$$

where $\mathcal{B}$ is described by

$$\mathcal{B}[j](x) = \int_{y\in\Gamma} \tau^*(\star\,\mathbf{d}\,\mathbf{G}(x,y)) \wedge \star\, j(y)\,. \tag{2.55}$$

This first equation leads to the following variational problem:

$$\begin{cases} \text{Find } \mathbf{J} \in \mathrm{H}_{\boldsymbol{\delta}}^{-1/2}(\Gamma), \forall\, \mathbf{J}' \in \mathrm{H}_{\boldsymbol{\delta}}^{-1/2}(\Gamma), \\ \langle \mathcal{M}[\mathbf{J}]\ ;\ \mathbf{J}'\,\rangle = \dfrac{1}{2}\displaystyle\int_\Gamma \mathbf{J} \wedge \star\mathbf{J}' + \int_\Gamma \star\tau^*(\mathcal{B}^+[\mathbf{J}) \wedge \star\mathbf{J}' = \int_\Gamma \star\tau^*(\mathbf{H}^{\mathrm{inc}}) \wedge \star\mathbf{J}' \end{cases} \tag{2.56}$$

Starting from the conventional MFIE problem, the first step is once again to multiply the left and the right-hand side by the conjugate phase $\bar{\psi}$ in order to get on the right-hand side only a constant *1-form*

$$\frac{1}{2}\bar{\psi}(x)\,\mathbf{J}(x) + \bar{\psi}(x) \star \tau^*\left(\mathcal{B}[\mathbf{J}](x)\right) = \star\tau^*(\bar{\psi}H^{\mathrm{inc}})(x) = \star\tau^*(\mathbf{p}_H)\,. \tag{2.57}$$

Then the second step is to introduce the pseudo-current,

$$\hat{\mathbf{J}} = \bar{\psi}\,\mathbf{J}, \tag{2.58}$$

to obtain the HMFIE:

$$\forall x \in \Gamma,\ \frac{1}{2}\hat{\mathbf{J}}(x) + \bar{\psi}(x) \star \tau^*\left(\mathcal{B}[\psi\hat{\mathbf{J}}](x)\right) = \star\tau^*(\mathbf{p}_H)\,. \tag{2.59}$$

This last equation leads to the following variational problem:

$$\begin{cases} \text{Find } \hat{\mathbf{J}} \in \mathrm{L}^2(\Gamma),\ \text{such as } \forall\, \mathbf{J}' \in \mathrm{L}^2(\Gamma), \\ \dfrac{1}{2}\displaystyle\int_\Gamma \hat{\mathbf{J}} \wedge \star\mathbf{J}' + \int_\Gamma \bar{\psi} \star \tau^*(\mathcal{B}[\psi\hat{\mathbf{J}}) \wedge \star\mathbf{J}' = \int_\Gamma \star\tau^*(\mathbf{p}_H) \wedge \star\mathbf{J}'\,. \end{cases} \tag{2.60}$$

In this last expression, we can observe that our formulation is slightly different from the Herberthson's one presented earlier. Notably, we do not have the same right-hand side and that will lead to different properties.

2.3.2 The Helmholtz, Hodge and Helmholtz-Hodge decomposition

In this section, we address the choice of the decomposition. In his work, Herberthson proposed to break down the current into two components

$$\hat{\mathbf{J}} = \mathbf{d}\,\Phi + \boldsymbol{\delta} \star \Psi \tag{2.61}$$

using a Hodge decomposition where the harmonic components vanish due to specific restriction of the surface (a surface homeomorphic to a sphere, i.e., with genus equal to 0). In our work, we choose to present this decomposition in another form which takes into account the harmonic *1-form* in order to deal with any surface topology.

The Helmholtz-Hodge Decomposition of vector fields is one of the fundamental theorems in many domains (not only in electromagnetism). It gives a description of a vector field in terms of its divergence-free and rotational-free components. Since various domains or applications can be considered, this decomposition can take different forms and admits different equivalent descriptions. Depending of the applications, researchers or domains, different names have been used: Helmholtz, Hodge, Helmholtz-Hodge or Hodge-Helmholtz. Basically, this decomposition

defines generally two or three different components (see Figure 2.4) and the motivation to choose a name is sometimes subjective. For a more complete overview of the subject see [52], we give below a short highlight of all of them.

Let $\Lambda^k(\mathscr{M})$ denote the space of smooth weakly differentiable *k-forms* on the manifold $\mathscr{M}$ and $\mathscr{H}$ the spaces of harmonic *k-forms* such that:

$$\mathscr{H}^k(\mathscr{M}) = \left\{\alpha \in \Lambda^k(\mathscr{M}) \mid \mathbf{d}\,\alpha = 0,\ \boldsymbol{\delta}\,\alpha = 0\right\}. \tag{2.62}$$

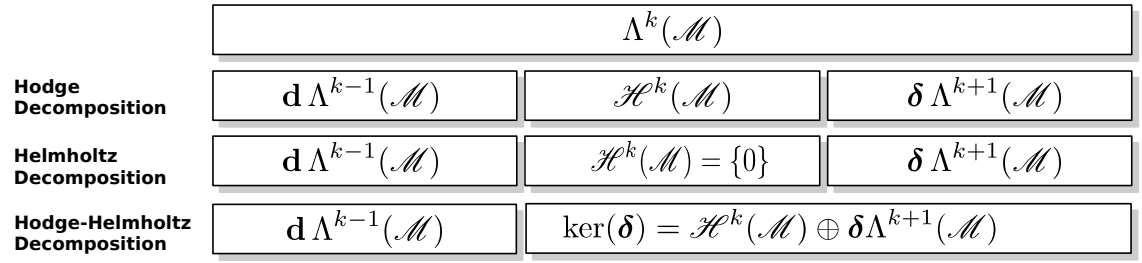

Figure 2.4 – The Hodge-Helmholtz Decomposition.

Theorem 2.7 : **The Hodge-Helmholtz Decomposition, see [52, Section 3]**

Let $\mathscr{M}$ be a compact, boundary-less, oriented Riemannian manifold. Then the space of differential *k-forms* on $\mathscr{M}$, $\Lambda^k(\mathscr{M})$ can be decomposed as a direct sum of the exterior derivative of a *k-1 form*, the codifferential of a *k+1 form* and a harmonic *k form*. The three components are mutually L^2-orthogonal and thus are uniquely determined

$$\Lambda^k = \mathbf{d}\,\Lambda^{k-1} \oplus \boldsymbol{\delta}\,\Lambda^{k+1} \oplus \mathscr{H}^k. \tag{2.63}$$

- The Hodge Decomposition:
  if $\omega \in \Lambda^k(\mathscr{M})$, then ω can be decomposed as

  $$\omega = \mathbf{d}\,\alpha + \boldsymbol{\delta}\,\beta + \gamma \tag{2.64}$$

  such that $\alpha \in \Lambda^{k-1}(\mathscr{M})$, $\beta \in \Lambda^{k+1}(\mathscr{M})$, $\gamma \in \Lambda^k(\mathscr{M})$. Furthermore, $\mathbf{d}\,\alpha$, $\boldsymbol{\delta}\,\beta$ and γ are mutually L^2-orthogonal and thus are uniquely determined.

- The Helmholtz Decomposition:
  if $\omega \in \Lambda^k(\mathscr{M})$, then ω can be expressed as:

  $$\omega = \mathbf{d}\,\Phi + \boldsymbol{\delta}\,\psi \tag{2.65}$$

  where by definition $\Phi \in \Lambda^{k-1}(\mathscr{M})$ and $\psi \in \Lambda^{k+1}(\mathscr{M})$ ($\mathbf{d}\,\mathbf{d}\,\Phi = 0$ and $\boldsymbol{\delta}\,\boldsymbol{\delta}\,\psi = 0$).

- The Hodge-Helmholtz Decomposition:
  if $\omega \in \Lambda^k(\mathscr{M})$, then ω can be uniquely decomposed in the form

  $$\omega = \mathbf{d}\,\alpha + \beta \tag{2.66}$$

  where α is a *0-form*, the *1-form* β belongs to the kernel of $\boldsymbol{\delta}$ and is tangential to the boundary along $\partial\Omega$.

□

This theorem gives the spirit of the decomposition: find two functions $\mathbf{J}^D$ and $\mathbf{J}^S$ belonging respectively to $\mathrm{Im}(\mathbf{d})$ and $\mathrm{Ker}(\boldsymbol{\delta})$. More precisely, looking for a solution in $\mathrm{H}_{\boldsymbol{\delta}}^{-1/2}(\Gamma)$, we have the following theorem:

Theorem 2.8 : **Hodge Decomposition of $\mathrm{H}_{\boldsymbol{\delta}}^{-1/2}(\Gamma)$, see [53, Theo. 2.2]-[54, Sect. 5]**

The space $\mathrm{H}_{\boldsymbol{\delta}}^{-1/2}(\Gamma)$ has the direct decomposition

$$\mathrm{H}_{\boldsymbol{\delta}}^{-1/2}(\Gamma) := \mathbf{d}\,\mathrm{H}_{\Delta}^{-1/2}(\Gamma) \oplus (\mathrm{H}_{\boldsymbol{\delta}}^{-1/2}(\Gamma) \cap \mathrm{Ker}(\boldsymbol{\delta})) \tag{2.67}$$

where

$$\mathrm{H}_{\Delta}^{s}(\Gamma) = \left\{ u \in \Lambda^0\mathrm{H}^{s+3/2}(\Gamma) \mid \Delta u \in \Lambda^0\mathrm{H}^{s}(\Gamma) \right\}. \tag{2.68}$$

Moreover, when restricted to $\mathrm{L}^2(\Gamma) \cap \mathrm{H}_{\boldsymbol{\delta}}^{-1/2}(\Gamma)$, the decomposition is $\mathrm{L}^2(\Gamma)$-orthogonal. □

Finally, we can apply the Hodge-Helmholtz decomposition to our current

$$\hat{\mathbf{J}} = \mathbf{J}^D + \mathbf{J}^S, \tag{2.69}$$

looking a divergent part $\mathbf{J}^D$ in $\mathbf{d}\,\mathrm{H}_{\Delta}^{-1/2}(\Gamma)$ and a solenoidal part $\mathbf{J}^S$ in $\mathrm{H}_{\boldsymbol{\delta}}^{-1/2}(\Gamma) \cap \mathrm{Ker}(\boldsymbol{\delta})$. Unlike Herberthson, we choose to work with *1-forms* rather than *0-forms*. Now, the idea will be to integrate this decomposition in the variational problems (HEFIE and HMFIE) in order to get a 2×2 system.

. The HEFIE and the Hodge-Helmholtz decomposition

We begin with the HEFIE and the following variational problem:

$$\begin{cases} \text{Find } \hat{\mathbf{J}} \in \mathrm{H}_{\boldsymbol{\delta}}^{-1/2}(\Gamma), \quad \text{such that } \forall\, \mathbf{J}^{'} \in \mathrm{H}_{\boldsymbol{\delta}}^{-1/2}(\Gamma), \\ \langle \mathcal{H}[\hat{\mathbf{J}}] \,;\, \mathbf{J}^{'} \rangle = \zeta \displaystyle\int_{\Gamma} \tau^* \left(\mathcal{A}[\psi \hat{\mathbf{J}}] \right) \wedge \star\, \psi\, \mathbf{J}^{'} + \frac{1}{\eta} \int_{\Gamma} \tau^* \left(\Phi[\boldsymbol{\delta}(\psi \hat{\mathbf{J}})] \right) \wedge \star\, \boldsymbol{\delta}(\psi\, \mathbf{J}^{'}) = - \displaystyle\int_{\Gamma} \tau^*(\mathbf{p}_E) \wedge \star\, \mathbf{J}^{'}. \end{cases} \tag{2.70}$$

The first step is to remark that the right-hand side has a particular form. Indeed, we have the inner product of $\mathbf{J}^{'}$ against an exact *1-form* $\mathbf{p}_E$ (means that there exists a *0-form* e^i such that $\mathbf{p}_E = \mathbf{d}\, e^i$) . Therefore, we have:

$$\langle \tau^* \mathbf{p}_E \,;\, \mathbf{J}^{'} \rangle = \int_{\Gamma} \tau^*(\mathbf{p}_E) \wedge \star \mathbf{J}^{'} = \int_{\Gamma} \tau^*(\mathbf{d}\, e^i) \wedge \star \mathbf{J}^{'} = - \int_{\Gamma} \tau^*(e^i) \wedge \star\, \boldsymbol{\delta}\, \mathbf{J}^{'} = -\langle \tau^* e^i \,;\, \boldsymbol{\delta}\, \mathbf{J}^{'} \rangle. \tag{2.71}$$

If $\mathbf{J}^{'}$ belongs to $\mathrm{H}_{\boldsymbol{\delta}}^{-1/2}(\Gamma) \cap \mathrm{Ker}(\boldsymbol{\delta})$, it is then obvious that the right-hand side vanishes. The second step is then to decompose both $\hat{\mathbf{J}}$ and $\mathbf{J}^{'}$ into a divergent and a solenoidal part in order to benefit from the properties of the right-hand side. Finally, this new variational problem leads to a new linear system

$$\begin{pmatrix} H^{DD} & H^{DS} \\ H^{SD} & H^{SS} \end{pmatrix} \begin{pmatrix} J^D \\ J^S \end{pmatrix} = \begin{pmatrix} C^D \\ 0 \end{pmatrix}$$

where $\begin{pmatrix} H^{DD} & H^{DS} \\ H^{SD} & H^{SS} \end{pmatrix} = \begin{pmatrix} \langle \mathcal{H}[J^D] \,;\, J^D \rangle & \langle \mathcal{H}[J^D] \,;\, J^S \rangle \\ \langle \mathcal{H}[J^S] \,;\, J^D \rangle & \langle \mathcal{H}[J^S] \,;\, J^S \rangle \end{pmatrix}$ and $C^D = -\langle E_0\, \tau^*(e^i) \,;\, \boldsymbol{\delta}\, J^D \rangle$.

. The HMFIE and Hodge-Helmholtz decomposition

We can do the same manipulations on the HMFIE. Starting from the variational problem

$$\begin{cases} \text{Find } \hat{\mathbf{J}} \in \mathrm{H}_{\boldsymbol{\delta}}^{-1/2}(\Gamma), \text{ such that } \forall\, \mathbf{J}^{'} \in \mathrm{H}_{\boldsymbol{\delta}}^{-1/2}(\Gamma), \\ \dfrac{1}{2}\displaystyle\int_{\Gamma} \hat{\mathbf{J}} \wedge \star\, \mathbf{J}^{'} + \int_{\Gamma} \bar{\psi} \star \tau^{*}(\mathcal{B}^{+}[\psi\hat{\mathbf{J}}) \wedge \star\, \mathbf{J}^{'} = \int_{\Gamma} \star\, \tau^{*}(\mathbf{p}_{H}) \wedge \star\, \mathbf{J}^{'} \end{cases} \tag{2.72}$$

the first step is once again to make that the right-hand side has a particular form. Indeed, we have a *0-form* h^i such that $\mathbf{p}_{H} = \mathbf{d}\, h^i$ and hence:

$$\langle \star\, \tau^{*}(\mathbf{p}_{H}) \;;\; \mathbf{J}^{'} \rangle = \int_{\Gamma} \star\, \tau^{*}(\mathbf{p}_{H}) \wedge \star\, \mathbf{J}^{'} = \int_{\Gamma} \star\, \tau^{*}(\mathbf{d}\, h^i) \wedge \star\, \mathbf{J}^{'} = \int_{\Gamma} \tau^{*}(h^i) \wedge \mathbf{d}\, \mathbf{J}^{'} = -\langle \tau^{*} h^i \;;\; \mathbf{d}\, \mathbf{J}^{'} \rangle. \tag{2.73}$$

Therefore, this time, if $\mathbf{J}^{'}$ belongs to $\mathbf{d}\, \mathrm{H}_{\Delta}^{-1/2}(\Gamma)$ the right-hand side vanishes. The second step is then to decompose both $\hat{\mathbf{J}}$ and $\mathbf{J}^{'}$ into a divergent and a solenoidal part in order to benefit from the properties of the right-hand side. In the end, the variational problem gives the following linear system

$$\begin{pmatrix} H_m^{DD} & H_m^{DS} \\ H_m^{SD} & H_m^{SS} \end{pmatrix} \begin{pmatrix} J^D \\ J^S \end{pmatrix} = \begin{pmatrix} 0 \\ V^S \end{pmatrix}$$

where $\begin{pmatrix} H_m^{DD} & H_m^{DS} \\ H_m^{SD} & H_m^{SS} \end{pmatrix} = \begin{pmatrix} \langle \mathcal{M}[\psi J^D] \;;\; \bar{\psi} J^D \rangle & \langle \mathcal{M}[\psi J^D] \;;\; \bar{\psi} J^S \rangle \\ \langle \mathcal{M}[\psi J^S] \;;\; \bar{\psi} J^D \rangle & \langle \mathcal{M}[\psi J^S] \;;\; \bar{\psi} J^S \rangle \end{pmatrix}$ and $V^S = -\langle \tau^{*} h^i \;;\; \mathbf{d}\, J^S \rangle$.

2.4 Existence and uniqueness of the solution

In this section, we give all the different elements necessary to prove the existence and the uniqueness of a solution to the specific formulation proposed by Herberthson, namely the HEFIE. Firstly, we show the similarity between the conventional EFIE and the HEFIE. Then, we present a formulation to represent the HEFIE operator as the sum of the EFIE operator and a perturbation.

2.4.1 Algebraic equivalence between conventional and modified equations

First, let us define the similarity or equivalence between the equation proposed by Herberthson (2.52) and the conventional EFIE (2.48). To do this, we give a description of the two operators $\mathcal{E}$ and $\mathcal{H}$ which define respectively the EFIE and the HEFIE:

$$\begin{aligned} \mathcal{E}: \quad & \mathrm{H}_{\boldsymbol{\delta}}^{-1/2}(\partial\Omega) \longrightarrow \mathrm{H}_{\mathbf{d}}^{-1/2}(\partial\Omega), \\ & u \longmapsto \tau^{*}\left[\zeta \mathcal{A}[u] - \frac{1}{\eta}\, \mathbf{d}\, \boldsymbol{\delta}\, \mathcal{A}[u]\right], \end{aligned} \tag{2.74}$$

$$\begin{aligned} \mathcal{H}: \quad & \mathrm{H}_{\boldsymbol{\delta}}^{-1/2}(\partial\Omega) \longrightarrow \mathrm{H}_{\mathbf{d}}^{-1/2}(\partial\Omega), \\ & v \longmapsto \tau^{*}\left[\bar{\psi}\zeta \mathcal{A}[\psi v] - \frac{1}{\eta}\bar{\psi}\, \mathbf{d}\, \boldsymbol{\delta}\, \mathcal{A}[\psi v]\right], \end{aligned} \tag{2.75}$$

where $\zeta = i\omega\mu_0$, $\eta = i\omega\varepsilon_0$ and where $\mathrm{H}_{\boldsymbol{\delta}}^{-1/2}(\partial\Omega)$ and $\mathrm{H}_{\mathbf{d}}^{-1/2}(\partial\Omega)$ are two spaces of distributions on $\partial\Omega$ defined as:

$$\mathrm{H}_{\boldsymbol{\delta}}^{s}(\partial\Omega) = \{u \in \mathrm{H}^{s}(\partial\Omega) |\, \boldsymbol{\delta}\, u \in \mathrm{H}^{s}(\partial\Omega)\}, \tag{2.76}$$

$$\mathrm{H}_{\mathbf{d}}^{s}(\partial\Omega) = \{u \in \mathrm{H}^{s}(\partial\Omega) |\, \mathbf{d}\, u \in \mathrm{H}^{s}(\partial\Omega)\}. \tag{2.77}$$

With these notations, the conventional EFIE (2.48) reads

$$\mathcal{E}j = -\tau^* E^i, \tag{2.78}$$

whereas the Herberthson modified EFIE (2.52) can be written as:

$$\mathcal{H}\hat{j} = -\tau^* \left(\bar{\psi} E^i\right). \tag{2.79}$$

Then, we introduce the operator Ψ

$$\begin{aligned} \Psi : \qquad & \mathrm{H}^s(\partial\Omega) \longrightarrow \mathrm{H}^s(\partial\Omega), \\ & h \longmapsto \Psi h = \psi h, \end{aligned} \tag{2.80}$$

where ψ is the $\partial\Omega$-trace of the analytic phase function on $\mathbb{R}^3$:

$$\psi = \tau^*(e^{i\kappa\vartheta}) \ : \ x \in \mathbb{R}^3 \mapsto e^{i\kappa\vartheta(x)} \tag{2.81}$$

and its conjugate and inverse

$$\begin{aligned} \Psi^{-1} : \qquad & \mathrm{H}^s(\partial\Omega) \longrightarrow \mathrm{H}^s(\partial\Omega), \\ & f \longmapsto \Psi^{-1} f = \bar{\psi} f \,. \end{aligned} \tag{2.82}$$

With these notations, the system (2.79) can easily be re-written as:

$$\mathcal{H}v = \Psi^{-1}\mathcal{E}(\Psi v) = -\tau^* \left(\bar{\psi} E^i\right). \tag{2.83}$$

Therefore, if we note that Ψ is a homeomorphism on any $\mathrm{H}^s(\partial\Omega)$ (since ψ is an invertible C^∞ application and that its inverse is also C^∞), we can conclude that the two systems are algebraically equivalent. Obviously, the same relation can also be established between the MFIE and the HMFIE. To illustrate the equivalence between the EFIE and the HEFIE, we quickly give some direct consequences in terms of null-spaces and solutions.

. Null-spaces

First, we begin with the link between the kernels of the EFIE and the HEFIE. Let $g \in \mathrm{Ker}(\mathcal{E})$, we have:

$$\mathcal{E}g = \tau^* \left[\zeta \mathcal{A}[g] - \frac{1}{\eta}\, \mathbf{d}\, \boldsymbol{\delta}\, \mathcal{A}[g]\right] = 0. \tag{2.84}$$

We can easily prove that $\Psi^{-1}g \in \mathrm{Ker}(\mathcal{H})$. Indeed, since $\mathcal{H} = \Psi^{-1}\mathcal{E}\Psi$, we can write:

$$\mathcal{H}(\Psi^{-1}g) = \Psi^{-1}\mathcal{E}(\Psi\Psi^{-1}g) = \Psi^{-1}\mathcal{E}g = \Psi^{-1}0_{\mathbf{H}} = 0_{\mathbf{H}}. \tag{2.85}$$

Now, if $h \in \mathrm{Ker}(\mathcal{H})$, we can show that $\Psi h \in \mathrm{Ker}(\mathcal{E})$:

$$\mathcal{E}(\Psi h) = \Psi\Psi^{-1}\mathcal{E}(\Psi h) = \Psi\mathcal{H}h = \Psi 0_{\mathbf{H}} = 0_{\mathbf{H}}. \tag{2.86}$$

Finally, we have the two following properties:

$$\begin{cases} g \in \mathrm{Ker}(\mathcal{E}) & \Longrightarrow \quad \Psi^{-1}g \in \mathrm{Ker}(\mathcal{H}), \\ h \in \mathrm{Ker}(\mathcal{H}) & \Longrightarrow \quad \Psi h \in \mathrm{Ker}(\mathcal{E}). \end{cases} \tag{2.87}$$

. Solutions

Now if we are interested in the link between solutions of the EFIE and the HEFIE, we also have equivalence results. Let j be a solution of the EFIE problem (2.78), i.e.,

$$\mathcal{E}j = \tau^* \left[\zeta \mathcal{A}[j] - \frac{1}{\eta} \mathbf{d}\, \boldsymbol{\delta}\, \mathcal{A}[j] \right] = -\tau^* E^i. \tag{2.88}$$

We easily prove that $\Psi^{-1}j$ is a solution of the HEFIE (2.79):

$$\mathcal{H}(\Psi^{-1}j) = \Psi^{-1}\mathcal{E}(\Psi\Psi^{-1}j) = \Psi^{-1}\mathcal{E}j = \Psi^{-1}\left(-\tau^* E^i\right) = -\tau^*\left(\Psi E^i\right) = -\tau^*(\bar{\psi}E^i). \tag{2.89}$$

We also have the converse, if $\hat{j}$ is a solution of the HEFIE, then $\Psi\hat{j}$ is solution of the EFIE:

$$\mathcal{E}(\Psi\hat{j}) = \Psi\Psi^{-1}\mathcal{E}(\Psi\hat{j}) = \Psi\mathcal{H}\hat{j} = \Psi\left(-\tau^*\left(\Psi^{-1}E^i\right)\right) = -\tau^*\left(\Psi\Psi^{-1}E^i\right) = -\tau^*\left(E^i\right). \tag{2.90}$$

This shows that the HEFIE has a solution if and only if the corresponding EFIE has a solution and these solutions are unique.

2.4.2 The HEFIE as perturbation of the EFIE

. Analysis of the perturbation

Let us begin by describing the operator HEFIE, denoted by $\mathcal{H}$, as the sum of the conventional EFIE operator $\mathcal{E}$ and a perturbation term, denoted by $\mathcal{K}$, through

$$\mathcal{H} = \mathcal{E} + \mathcal{K} \tag{2.91}$$

with

$$\begin{aligned} \mathcal{K} \qquad & \mathrm{H}_{\boldsymbol{\delta}}^{-1/2}(\partial\Omega) \longrightarrow \mathrm{H}_{\mathbf{d}}^{-1/2+s}(\partial\Omega), \\ & u \longmapsto \tau^*\left[\bar{\psi}\zeta\mathcal{A}[\psi u] - \zeta\mathcal{A}[\psi u] - \frac{1}{\eta}\bar{\psi}\,\mathbf{d}\,\boldsymbol{\delta}\,\mathcal{A}[\psi u] + \frac{1}{\eta}\,\mathbf{d}\,\boldsymbol{\delta}\,\mathcal{A}[u]\right] \end{aligned} \tag{2.92}$$

where s has to be determined. Because of the continuity of the operators Ψ and Ψ^{-1} we have $s \geq 0$. To facilitate the description of $\mathcal{K}$, we introduce the operator $\mathbf{A} = \tau^*(\mathcal{A})$ and write this operator as the sum of $\mathcal{K}_1$ and $\mathcal{K}_2$:

$$\mathcal{K} = \zeta\mathcal{K}_1 - \frac{1}{\eta}\mathcal{K}_2 \tag{2.93}$$

with

$$\begin{aligned} \mathcal{K}_1 j &= \bar{\psi}\mathbf{A}[\psi j] - \mathbf{A}[j], \\ \mathcal{K}_2 j &= \bar{\psi}\,\mathbf{d}\,\boldsymbol{\delta}\,\mathbf{A}[\psi j] - \mathbf{d}\,\boldsymbol{\delta}\,\mathbf{A}[j]\,. \end{aligned}$$

In fact, this decomposition also shows a good way to implement the HEFIE as we will see later (see Chapter 3).

. Structure of $\mathcal{K}_2$

Let u and v in $\mathrm{H}_{\boldsymbol{\delta}}^{-1/2}(\partial\Omega)$, we have:

$$\begin{aligned} \langle \mathcal{K}_2(u)\ ;\ v\rangle &= \langle \bar{\psi}\,\mathbf{d}\,\boldsymbol{\delta}\,\mathbf{A}[\psi u] - \mathbf{d}\,\boldsymbol{\delta}\,\mathbf{A}[u]\ ;\ v\rangle, \\ &= \langle \bar{\psi}\,\mathbf{d}\,\boldsymbol{\delta}\,\mathbf{A}[\psi u]\ ;\ v\rangle - \langle\, \mathbf{d}\,\boldsymbol{\delta}\,\mathbf{A}[u]\ ;\ v\rangle, \\ &= \langle\, \mathbf{d}\,\boldsymbol{\delta}\,\mathbf{A}[\psi u]\ ;\ \bar{\psi}v\rangle - \langle\, \mathbf{d}\,\boldsymbol{\delta}\,\mathcal{A}[u]\ ;\ v\rangle, \\ &= \langle\, \boldsymbol{\delta}\,\mathbf{A}[\psi u]\ ;\ \boldsymbol{\delta}(\bar{\psi}v)\rangle - \langle\, \boldsymbol{\delta}\,\mathbf{A}[u]\ ;\ \boldsymbol{\delta}\,v\rangle. \end{aligned} \tag{2.94}$$

The idea now is to commute the operators $\boldsymbol{\delta}$ and $\mathbf{A}$, which is possible with the operator Φ introduced in the Chapter 1 since $\boldsymbol{\delta}\,\mathcal{A}[j] = -\Phi[\boldsymbol{\delta}\,j]$. We then introduce $\tau^*(\Phi) = \boldsymbol{\Phi}$. Using this new operator $\boldsymbol{\Phi}$ in the latter equality (2.94), we write

$$-\langle \mathcal{K}_2(u)\ ;\ v\rangle = \langle \boldsymbol{\Phi}[\boldsymbol{\delta}(\psi u)]\ ;\ \boldsymbol{\delta}(\bar{\psi}v)\rangle - \langle \boldsymbol{\Phi}[\boldsymbol{\delta}\,u]\ ;\ \boldsymbol{\delta}\,v\rangle. \tag{2.95}$$

Moreover, the two factors $\boldsymbol{\delta}(\psi u)$ and $\boldsymbol{\delta}(\bar{\psi}v)$ can be expanded as follows:

$$\boldsymbol{\delta}(\bar{\psi}v) = \star(\mathbf{d}\,\bar{\psi}\wedge\star v) + \bar{\psi}\wedge\boldsymbol{\delta}\,v = v \lrcorner \mathbf{d}\,\bar{\psi} + \bar{\psi}\,\boldsymbol{\delta}\,v \tag{2.96}$$

with $a \lrcorner b = \star(b\wedge\star a)$. Therefore, we have

$$\begin{aligned}
-\langle \mathcal{K}_2 u\ ;\ v\rangle &= \langle \boldsymbol{\Phi}\left[u \lrcorner \mathbf{d}\,\psi + \psi\,\boldsymbol{\delta}\,u\right]\ ;\ \boldsymbol{\delta}(\bar{\psi}v)\rangle - \langle \boldsymbol{\Phi}[\boldsymbol{\delta}\,u]\ ;\ \boldsymbol{\delta}\,v\rangle, && (2.97)\\
&= \langle \boldsymbol{\Phi}\left[u \lrcorner \mathbf{d}\,\psi\right] + \boldsymbol{\Phi}\left[\psi\,\boldsymbol{\delta}\,u\right]\ ;\ \boldsymbol{\delta}(\bar{\psi}v)\rangle - \langle \boldsymbol{\Phi}[\boldsymbol{\delta}\,u]\ ;\ \boldsymbol{\delta}\,v\rangle, && (2.98)\\
&= \langle \boldsymbol{\Phi}\left[u \lrcorner \mathbf{d}\,\psi\right] + \boldsymbol{\Phi}\left[\psi\,\boldsymbol{\delta}\,u\right]\ ;\ v \lrcorner \mathbf{d}\,\psi + \bar{\psi}\,\boldsymbol{\delta}\,v\rangle - \langle \boldsymbol{\Phi}[\boldsymbol{\delta}\,u]\ ;\ \boldsymbol{\delta}\,v\rangle, && (2.99)
\end{aligned}$$

which finally gives us five terms:

$$\begin{aligned}
-\langle \mathcal{K}_2 u\ ;\ v\rangle = &\langle \boldsymbol{\Phi}[\psi\,\boldsymbol{\delta}\,u]\ ;\ \bar{\psi}\,\boldsymbol{\delta}\,v\rangle && (2.100)\\
&- \langle \boldsymbol{\Phi}[\boldsymbol{\delta}\,u]\ ;\ \boldsymbol{\delta}\,v\rangle && (2.101)\\
&+ \langle \boldsymbol{\Phi}[u \lrcorner \mathbf{d}\,\psi]\ ;\ v \lrcorner \mathbf{d}\,\bar{\psi}\rangle && (2.102)\\
&+ \langle \boldsymbol{\Phi}[u \lrcorner \mathbf{d}\,\psi]\ ;\ \bar{\psi}\,\boldsymbol{\delta}\,v\rangle && (2.103)\\
&+ \langle \boldsymbol{\Phi}[\psi\,\boldsymbol{\delta}\,u]\ ;\ v \lrcorner \mathbf{d}\,\bar{\psi}\rangle\,. && (2.104)
\end{aligned}$$

. Regularity of the new kernel $G(\psi\bar{\psi}-1)$

We can also go a little further and detail the difference of the terms (2.100) and (2.101), i.e., study the regularity of

$$\langle \boldsymbol{\Phi}[\psi\,\boldsymbol{\delta}\,u]\ ;\ \bar{\psi}\,\boldsymbol{\delta}\,v\rangle - \langle \Phi(\boldsymbol{\delta}\,u)\ ;\ \boldsymbol{\delta}\,v\rangle. \tag{2.105}$$

We have

$$\begin{aligned}
\Phi[\psi\,\boldsymbol{\delta}\,u] &= \int_{y\in\partial\Omega} \tau^*(G(x,y))\wedge(\psi(y)\,\boldsymbol{\delta}\,u(y))\,,\\
(2.100)-(2.101) &= \int_{x\in\partial\Omega}\left(\int_{y\in\partial\Omega}\tau^*(G(x,y))\wedge(\psi(y)\,\boldsymbol{\delta}\,u_n(y))\right)\wedge\left(\bar{\psi}(x)\,\boldsymbol{\delta}\,v(x)\right)\\
&\quad - \int_{x\in\partial\Omega}\left(\int_{y\in\partial\Omega}\tau^*(G(x,y))\wedge\boldsymbol{\delta}\,u_n(y)\right)\wedge\boldsymbol{\delta}\,v(x),\\
&= \int_{x\in\partial\Omega}\left(\int_{y\in\partial\Omega}\tau^*(G(x,y)(\bar{\psi}(x)\psi(y)-1))\wedge\boldsymbol{\delta}\,u_n(y)\right)\wedge\boldsymbol{\delta}\,v(x).
\end{aligned}$$

First, we note that for x fixed, if $y\notin\chi_\epsilon^\Gamma(x)$ ($\chi_\epsilon^\Gamma(x) = \{y\in\Gamma | d(x,y)<\epsilon\}$), i.e., if y is not in the neighbourhood of x, the term under the integral sign is well defined and the function regular enough for the integral to be bounded. Remains the asymptotic behaviour of $G(x,y)(\bar{\psi}(x)\psi(y)-1)$ when $y\to x$.
We have:

$$\psi(y)\bar{\psi(x)} = e^{i\kappa\theta\cdot(x-y)} = 1+\kappa\theta\cdot(x-y) + \underset{y\to x}{o}(\|x-y\|) \tag{2.106}$$

hence

$$\frac{e^{i\kappa\|x-y\|}}{4\pi\|x-y\|}\Big(\psi(y)\bar{\psi}(x)-1\Big)=\frac{e^{i\kappa\|x-y\|}}{4\pi\|x-y\|}\left(\kappa\theta\cdot(x-y)+\underset{y\to x}{o}(\|x-y\|)\right). \tag{2.107}$$

Otherwise, since

$$\exists c \ \text{ such that } \ |\theta\cdot(x-y)|\leq c\|x-y\|, \tag{2.108}$$

we can conclude that the limit of $\frac{e^{i\kappa\|x-y\|}}{4\pi\|x-y\|}\Big(\psi(y)\bar{\psi}(x)-1\Big)$, when y tends to x, is bounded and that this part of the operator $\mathcal{K}_2$ is more regular than the conventional $\mathbf{d}\,\boldsymbol{\delta}\,\mathbf{A}$. As to the remaining terms, a regularity analysis of the kernel distributions does not allow to conclude that $\mathcal{K}$ is a compact operator.

Part II

Numerical implementation and exploration of the different solution method

Chapter 3

Numerical Implementation

Contents

In this chapter, we consider the practical implementation of the integral equation introduced by M. Herberthson, the HEFIE, which adapts the Electric Field Integral Equation (EFIE). The aim is to give all the elements needed to build the Galerkin problem as presented in the Chapter 2, that leads to the linear system:

$$HJ = C \Longleftrightarrow \begin{pmatrix} H^{DD} & H^{DS} \\ H^{SD} & H^{SS} \end{pmatrix} \begin{pmatrix} J^D \\ J^S \end{pmatrix} = \begin{pmatrix} C^D \\ 0 \end{pmatrix}. \tag{3.1}$$

First, we consider the practical implementation of the HEFIE in an edge finite element space. The originality of this implementation is to take advantage of the gained experience on the EFIE, in terms of implementation and finite element code, and focus not on the HEFIE itself, but on the perturbation $\mathcal{K}_e$ with respect to the EFIE. This approach introduces a new matrix K_e that represents the perturbation on edge finite elements. It also allows us to get the Galerkin matrix $\tilde{H}$, representing the HEFIE on edge finite elements, through the relation

$$\tilde{H} = E + K_e \tag{3.2}$$

where E is the Galerkin matrix of the EFIE.
In a second step, we present the implementation of the Helmholtz decomposition on edge finite element functions. The goal is to move the system from the initial HEFIE on edge finite elements

$$\tilde{H}\tilde{J} = \tilde{C} \tag{3.3}$$

into the one above (C.22) which splits the current distribution into the part belonging to $\mathrm{Im}(\mathbf{d})$ and the one to $\mathrm{Ker}(\boldsymbol{\delta})$, and highlight a right-hand side with a lot of null-terms. For this, we summarize various elements necessary for constructing this decomposition and introduce a new matrix D_H that allows us to obtain the desired system through the formula

$$H = D_H \tilde{H} D_H^{-1} = D_H (E + K_e) D_H^{-1} \,. \tag{3.4}$$

A general overview of the methodology and notations can be found in Figure 3.1. Finally, in the same spirit as the HEFIE, we end this chapter presenting a possible implementation of the HMFIE and the HCFIE.

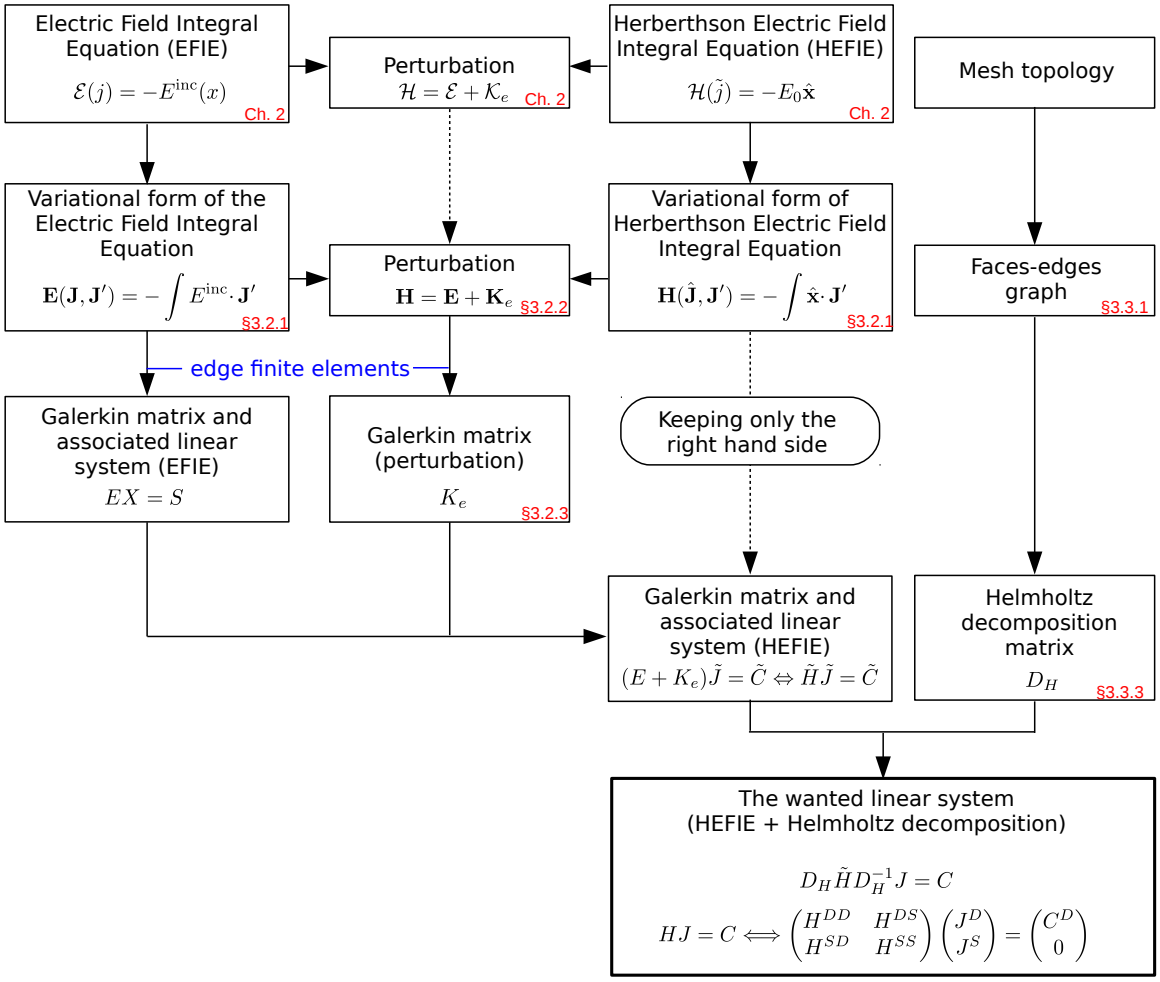

Figure 3.1 – General overview of the method.

3.1 Setting up the HEFIE with edge finite elements

We are interested in the numerical solution of the Herberthson equation, the HEFIE, and more particularly in the development of an edge finite element discretisation. In this section, we present how to compute the Galerkin matrix $\tilde{H}$ associated with the operator $\mathcal{H}$ starting from the Galerkin matrix E of the conventional EFIE. To do this, we will rely on a relationship already given (2.91) where the operator $\mathcal{H}$ is represented as the sum of the conventional EFIE operator $\mathcal{E}$ and a perturbation $\mathcal{K}_e$

$$\mathcal{H} = \mathcal{E} + \mathcal{K}_e \,. \tag{3.5}$$

The main idea is to focus on $\mathcal{K}_e$ and on its discretisation in an edge finite element space. This choice is motivated on two facts.

First, as the EFIE is already a well documented equation, all the information we need on the HEFIE can be obtained from the conventional EFIE (see e.g., Chapter 2). The detailed computations to get the Galerkin matrix of the edge element discretisation of the EFIE is amply described in the literature (see e.g., [7, 55, 56]), and therefore we do not need to develop the details of this part if we chose to set up the HEFIE Galerkin matrix on this functions space. Secondly, in the perturbation part, we can take advantage of a regularisation of the Green's kernel G due to the multiplier $\bar{\psi}_x\psi_y - 1$. Thus, the perturbation part is well-suited for numerical integrations such as Gauss integration.

This section is divided into three parts. First, we present the different variational formulations of both conventional EFIE and HEFIE, exceptionally in vector form. Then we detail how to describe the form associated with the variational perturbation $\mathbf{K}$ and we give in a third time the details of a possible implementation. At the end of this section, we have all necessary elements for an edge finite element discretisation of the Herberthson equation.

3.1.1 Two equivalent problems : EFIE vs HEFIE

We begin with a short overview of two equivalent problems, the conventional EFIE and the HEFIE.

. Electric Field Integral Equation

Let Γ denote the surface of an open or closed perfectly electric conducting (PEC) scatterer with normal unit $\mathbf{n}$, $\mathbf{E}^{\text{inc}}$ an incident plane wave illuminating Γ, described with a wave number κ, a direction of propagation θ and an electric polarisation $\mathbf{p}_E$ such as $\forall y \in \mathbb{R}^3$, $\mathbf{E}^{\text{inc}}(y) = \psi(y)\mathbf{p}_E = e^{-i\kappa\theta\cdot y}\mathbf{p}_E$, and let $\mathbf{J}$ be the induced surface current distribution on Γ. In this notation, the EFIE (Electric Field Integral Equation) reads

$$\mathbf{tr}\left[\left(\zeta\,\mathbf{I}_{\text{d}} - \frac{1}{\eta}\,\nabla\,\nabla\cdot\right)\mathcal{A}[\mathbf{J}](x)\right] = -\mathbf{tr}(\mathbf{E}^{\text{inc}}(x)) \tag{3.6}$$

where $\zeta = i\omega\mu_0$, $\eta = i\omega\epsilon_0$ and $\mathcal{A}$ denotes the single layer potential defined by

$$\mathcal{A}[j](x) = \int_\Gamma G(x,y)j(y)d\Gamma \tag{3.7}$$

where G is the free-space Green function. This first equation leads to the following variational problem:

$$\begin{cases} \text{Find } \mathbf{J} \in H_{\text{div}}^{-1/2}(\Gamma), \text{ such that } \forall\,\mathbf{J}' \in H_{\text{div}}^{-1/2}(\Gamma), \\ \displaystyle\iint_{\Gamma\times\Gamma} G_{x,y}\left(\zeta\,\mathbf{J}_y\cdot\mathbf{J}'_x - \frac{1}{\eta}\,\nabla_{\text{s}}\cdot\mathbf{J}_y\,\nabla_{\text{s}}\cdot\mathbf{J}'_x\right)dydx = -\displaystyle\int_\Gamma \mathbf{E}^{\text{inc}}\cdot\mathbf{J}'\,d\Gamma\,. \end{cases} \tag{3.8}$$

In further developments, we will use the notation $\mathbf{E}$ to described the bilinear form of this variational problem:

$$\mathbf{E}(\mathbf{J},\mathbf{J}') = \iint_{\Gamma\times\Gamma} G_{x,y}\left(\zeta\,\mathbf{J}_y\cdot\mathbf{J}'_x - \frac{1}{\eta}\,\nabla_{\text{s}}\cdot\mathbf{J}_y\,\nabla_{\text{s}}\cdot\mathbf{J}'_x\right)dydx\,. \tag{3.9}$$

. The Herberthson Electric Field Integral Equation

Starting from the conventional EFIE problem,

$$\mathbf{tr}\left[\left(\zeta\,\mathbf{I}_{\mathrm{d}}-\frac{1}{\eta}\,\nabla\,\nabla\cdot\right)\mathcal{A}[\mathbf{J}](x)\right]=-\mathbf{tr}(\mathbf{E}^{\mathrm{inc}}(x)), \tag{3.10}$$

the first step is to multiply the left and the right-hand side by the conjugate phase $\bar{\psi}$ in order to get on the right-hand side only a constant vector $\mathbf{p}_E$ (formally a *1-form*)

$$\mathbf{tr}\left[\bar{\psi}(x)\left(\zeta\,\mathbf{I}_{\mathrm{d}}-\frac{1}{\eta}\,\nabla\,\nabla\cdot\right)\mathcal{A}[\mathbf{J}](x))\right]=-\mathbf{tr}(\bar{\psi}(x)\mathbf{E}^{\mathrm{inc}}(x))=-\mathbf{tr}(\mathbf{p}_E)\,. \tag{3.11}$$

The second step is to highlight a pseudo-current,

$$\hat{\mathbf{J}}=\bar{\psi}\,\mathbf{J}, \tag{3.12}$$

to obtain the HEFIE:

$$\forall\,\mathbf{x}\in\Gamma,\ \mathbf{tr}\left[\bar{\psi}\left(\zeta\,\mathbf{I}_{\mathrm{d}}-\frac{1}{\eta}\,\nabla\,\nabla\cdot\right)\mathcal{A}[\psi\hat{\mathbf{J}}](x)\right]=-\mathbf{tr}(\mathbf{p}_E)\,. \tag{3.13}$$

This last equation leads to the following variational problem:

$$\begin{cases}\text{Find } \hat{\mathbf{J}}\in H_{\mathrm{div}}^{-1/2}(\Gamma),\ \text{such that } \forall\,\mathbf{J}^{'}\in H_{\mathrm{div}}^{-1/2}(\Gamma) \text{ and } \mathbf{E}^{\mathrm{inc}}=\psi\mathbf{p}_E,\\[2ex] \displaystyle\iint_{\Gamma\times\Gamma} G_{x,y}\left(\zeta(\psi_y\hat{\mathbf{J}}_y)\cdot(\bar{\psi}_x\,\mathbf{J}^{'}_x)-\frac{1}{\eta}\,\nabla_{\mathrm{s}}\cdot(\psi_y\hat{\mathbf{J}}_y)\,\nabla_{\mathrm{s}}\cdot(\bar{\psi}_x\,\mathbf{J}^{'}_x)\right)dydx=-\int_{\Gamma}\mathbf{p}_E\cdot\mathbf{J}^{'}\,d\Gamma\,.\end{cases} \tag{3.14}$$

In this last formulation, the pseudo-current $\hat{\mathbf{J}}$ computed does not represent the physical current distribution induced by the incident plane wave, but the pseudo-current. Note also, that $\mathbf{J}$, $\hat{\mathbf{J}}$ and $\mathbf{J}^{'}$ belong in the same subspace $H_{\mathrm{div}}^{-1/2}(\Gamma)$. For the purpose of the following developments, we introduce:

$$\mathbf{H}(\hat{\mathbf{J}},\mathbf{J}^{'})=\iint_{\Gamma\times\Gamma} G_{x,y}\left(\zeta(\psi_y\hat{\mathbf{J}}_y)\cdot(\bar{\psi}_x\,\mathbf{J}^{'}_x)-\frac{1}{\eta}\,\nabla_{\mathrm{s}}\cdot(\psi_y\hat{\mathbf{J}}_y)\,\nabla_{\mathrm{s}}\cdot(\bar{\psi}_x\,\mathbf{J}^{'}_x)\right)dydx\,. \tag{3.15}$$

3.1.2 Highlighting the perturbation

After describing the two problems, the conventional EFIE and the HEFIE, the idea is to take advantage of the fact that HEFIE can be seen as a perturbation of the EFIE. Insofar as the EFIE is already well documented in the literature (e.g., [7] or [56]) and since there are already effective implementations, we are only interested in the perturbation part.
So, the first step is to highlight the perturbation, i.e., the associated variational operator $\mathbf{K}_e$. We start from the equation (2.91) giving us the perturbation term $\mathbf{K}_e=\mathbf{H}-\mathbf{E}$

$$\mathbf{K}_e(\mathbf{J},\mathbf{J}')=\iint G_{x,y}\left[\zeta\bar{\psi}_x\,\mathbf{J}'_x\cdot\psi_y\,\mathbf{J}_y-\zeta\,\mathbf{J}'_x\cdot\mathbf{J}_y-\frac{1}{\eta}\underbrace{\nabla_{\mathrm{s}}\cdot(\bar{\psi}_x\,\mathbf{J}'_x)\,\nabla_{\mathrm{s}}\cdot(\psi_y\,\mathbf{J}_y)}_{(I_3)}+\frac{1}{\eta}\,\nabla_{\mathrm{s}}\cdot\mathbf{J}'_x\,\nabla_{\mathrm{s}}\cdot\mathbf{J}_y\right]dxdy\,. \tag{3.16}$$

If we now develop the third term of this sum, we get:

$$I_3 = \iint G_{x,y} \left(\nabla_{\mathrm{s}} \cdot (\bar{\psi}_x \, \mathbf{J}'_x) \right) \nabla_{\mathrm{s}} \cdot (\psi_y \, \mathbf{J}_y) \Big) \,, \tag{3.17}$$

$$= \int \Big(\nabla_{\mathrm{s}} \, \bar{\psi}_x \cdot \mathbf{J}'_x + \bar{\psi}_x \, \nabla_{\mathrm{s}} \cdot \mathbf{J}'_x \Big) \left(\int G_{x,y} \left(\nabla_{\mathrm{s}} \, \psi_y \cdot \mathbf{J}_y + \psi_y \, \nabla_{\mathrm{s}} \cdot \mathbf{J}_y \right) dy \right) dx, \tag{3.18}$$

$$\begin{aligned} = & \int \nabla_{\mathrm{s}} \, \bar{\psi}_x \cdot \mathbf{J}'_x \int G_{x,y} \, \nabla_{\mathrm{s}} \, \psi_y \cdot \mathbf{J}_y \, dydx + \int \nabla_{\mathrm{s}} \, \bar{\psi}_x \cdot \mathbf{J}'_x \int G_{x,y} \psi_y \, \nabla_{\mathrm{s}} \cdot \mathbf{J}_y \, dydx \\ & + \int \bar{\psi}_x \, \nabla_{\mathrm{s}} \cdot \mathbf{J}'_x \int G_{x,y} \, \nabla_{\mathrm{s}} \, \psi_y \cdot \mathbf{J}_y \, dydx + \int \bar{\psi}_x \, \nabla_{\mathrm{s}} \cdot \mathbf{J}'_x \int G_{x,y} \psi_y \, \nabla_{\mathrm{s}} \cdot \mathbf{J}_y \, dydx \end{aligned} \tag{3.19}$$

and developing $\nabla_{\mathrm{s}} \, \theta$, it then results in:

$$\begin{aligned} I_3 = & \kappa^2 \int \mathbf{J}'_x \left[\theta^T \theta \right] \int G_{x,y} \bar{\psi}_x \psi_y \, \mathbf{J}_y \, dydx + i\kappa \int \mathbf{J}'_x \cdot \theta \int G_{x,y} \bar{\psi}_x \psi_y \, \nabla_{\mathrm{s}} \cdot \mathbf{J}_y \, dydx \\ & - i\kappa \int \nabla_{\mathrm{s}} \cdot \mathbf{J}'_x \int G_{x,y} \bar{\psi}_x \psi_y \theta \cdot \mathbf{J}_y \, dydx + \int \nabla_{\mathrm{s}} \cdot \mathbf{J}'_x \int G_{x,y} \bar{\psi}_x \psi_y \, \nabla_{\mathrm{s}} \cdot \mathbf{J}_y \, dydx \,. \end{aligned} \tag{3.20}$$

Thus, we get the following formulation for the perturbation:

$$\mathbf{K}_e(\mathbf{J}, \mathbf{J}') = \mathbf{H}(\mathbf{J}, \mathbf{J}') - \mathbf{E}(\mathbf{J}, \mathbf{J}'), \tag{3.21}$$

$$\begin{aligned} = & \quad \zeta \iint G_{x,y} \left(\bar{\psi}_x \psi_y - 1 \right) \mathbf{J}'_x \cdot \mathbf{J}_y \, dxdy \\ & - \frac{1}{\eta} \iint G_{x,y} \left(\bar{\psi}_x \psi_y - 1 \right) \nabla_{\mathrm{s}} \cdot \mathbf{J}'_x \, \nabla_{\mathrm{s}} \cdot \mathbf{J}_y \, dxdy \\ & - \frac{\kappa^2}{\eta} \iint \mathbf{J}'_x \left[G_{x,y} \bar{\psi}_x \psi_y \theta^T \theta \right] \mathbf{J}_y \, dxdy \\ & + \frac{i\kappa}{\eta} \int \theta \cdot \mathbf{J}'_x \int G_{x,y} \bar{\psi} \psi \, \nabla_{\mathrm{s}} \cdot \mathbf{J}_y \, dydx - \frac{i\kappa}{\eta} \int \nabla_{\mathrm{s}} \cdot \mathbf{J}'_x \int G_{x,y} \bar{\psi}_x \psi_y \theta \cdot \mathbf{J}_y \, dydx, \\ = & \, \zeta A(\mathbf{J}, \mathbf{J}') - \frac{1}{\eta} \Phi(\mathbf{J}, \mathbf{J}') - \frac{\kappa^2}{\eta} B(\mathbf{J}, \mathbf{J}') + \frac{i\kappa}{\eta} R(\mathbf{J}, \mathbf{J}') \,. \end{aligned} \tag{3.22}$$

3.1.3 Integrals involved in the perturbation computation

We can now study the discretization with edge elements, which brings the variational equation to a linear system:

$$\tilde{H} \tilde{J} = (E + K_e) \tilde{J} = \tilde{C} \,. \tag{3.23}$$

The construction of the right-hand side is straightforward, since we only need to integrate edge finite functions against a constant vector. The assembly of the matrix K_e can be achieved in the same manner than the matrix E (cf. [7]) by decomposing the double integral over $\Gamma \times \Gamma$ in a double sum over the triangles of the mesh.

We have four elementary operators A, Φ, B and R, each with its own characteristics. The objective of this part is to outline the important points to consider for the development of an edge finite elements code. Basically, we have to numerically compute integrals over two triangles with either the kernel $G(x,y)\bar{\psi}(x)\psi(y)$ or $G(x,y)(\bar{\psi}(x)\psi(y) - 1)$ where ψ is the phase of the incident wave and G the conventional Green function. The main trick is to break down these two kernels into a regular and a singular part that we eventually treat with an analytical expression. Thereafter, we assume that the surface $\partial\Omega$ is meshed with a set of triangles. Edge finite element functions are considered as test functions $\mathbf{J}$. For a complete description of these functions, see [56].

Whatever the elementary operator (A, Φ, B and R), integrals may be broken down in two

successive integrals:

$$\int_{T_1}\int_{T_2}\{...\}\,dT_1(x)dT_2(y) = \int_{T_1} F^{T_2}(x)dT_1(x) \tag{3.24}$$

with

$$F^{T_2}(x) = \int_{T_2}(x)\,\{...\}\,dT_2(y)\,. \tag{3.25}$$

The external integral (3.24) over T_1 can always be evaluated numerically, whereas the internal integral (3.25) over T_2 can be evaluated numerically only if T_1 and T_2 are distinct.

. The operators A and Φ

The integral involved in A and Φ are regular enough to be evaluated numerically since they present no real singularities. This regularity can be shown regarding the kernel's limit for $y \to x$. Indeed, we have

$$\lim_{y\to x} G(x,y)\left(\bar{\psi}(x)\psi(y) - 1\right) = 0 \tag{3.26}$$

which implies that we can numerically compute the internal integrals of A and Φ (with Gaussian integration) by applying a specific treatment to the kernel

$$G(x,y)\left(\bar{\psi(x)}\psi(y) - 1\right) \tag{3.27}$$

which takes account that limit.

. The operator B

For the elementary operator B, we have:

$$F_B^{T_1}(x) = \int_{T_2} G(x,y)\bar{\psi}(x)\psi(y)\,\mathbf{J}(y)dy\,. \tag{3.28}$$

The trick is to break down this integral into three terms:

$$\begin{aligned}
F_B^{T_1}(x) &= \int_{T_2} G(x,y)\bar{\psi}(x)\psi(y)\,\mathbf{J}(y)dy, && (3.29)\\
&= \int_{T_2} \frac{e^{i\kappa|x-y|}}{|x-y|}\bar{\psi}(x)\psi(y)\,\mathbf{J}(y)dy, && (3.30)\\
&= \int_{T_2} \frac{e^{i\kappa|x-y|}-1}{|x-y|}\bar{\psi}(x)\psi(y)\,\mathbf{J}(y)dy + \int_{T_2}\frac{\bar{\psi}(x)\psi(y)}{|x-y|}\,\mathbf{J}(y)dy, && (3.31)\\
&= \int_{T_2} \frac{e^{i\kappa|x-y|}-1}{|x-y|}\bar{\psi}(x)\psi(y)\,\mathbf{J}(y)dy + \int_{T_2}\frac{\bar{\psi}(x)\psi(y)-1}{|x-y|}\,\mathbf{J}(y)dy + \int_{T_2}\frac{\mathbf{J}(y)}{|x-y|}dy\,. && (3.32)
\end{aligned}$$

The first two integrals are regular enough to be evaluated numerically with a Gauss integration method, taking in consideration the two following limits:

$$\lim_{y\to x}\frac{e^{i\kappa|x-y|}-1}{|x-y|}\bar{\psi}(x)\psi(y) = i\kappa \quad\text{and}\quad \lim_{y\to x}\frac{\bar{\psi}(x)\psi(y)-1}{|x-y|} = 0\,. \tag{3.33}$$

Remains the last one which should be handled analytically. However, it is an integral already appearing in the computation of conventional EFIE discretisations (see [7, Chapter 2, Section 2.2.2]).

. The operator R

The last operator R is not complicated. There are two different integrals

$$\begin{aligned} I_1 &= F_{C,1}^{T_1}(x), \\ &= \int_{T_2} G(x,y)\bar{\psi}(x)\psi(y)\,\nabla_{\mathrm{s}}\cdot\mathbf{J}(y)dy \quad \text{and} \quad I_2 = F_{C,2}^{T_1}(x) = \int_{T_2} G(x,y)\bar{\psi}(x)\psi(y)\,\mathbf{J}(y)dy\,. \end{aligned} \tag{3.34}$$

Note that, if we use edge functions, $\nabla_{\mathrm{s}}\cdot\mathbf{J}(y) = \frac{1}{|T_2|}$ which quickly simplifies the calculation:

$$I_1 = \frac{1}{|T|}\int_T G(x,y)\bar{\psi}(x)\psi(y)dy, \tag{3.35}$$

$$= \frac{1}{|T|}\int_T \frac{e^{i\kappa|x-y|}-1}{|x-y|}\bar{\psi}(x)\psi(y)dy + \frac{1}{|T|}\int_T \frac{\bar{\psi}(x)\psi(y)-1}{|x-y|}dy + \frac{1}{|T|}\int_T \frac{1}{|x-y|}dy\,. \tag{3.36}$$

The first two parts are quite easy (see limits (3.33)). The third involves the Newton potential

$$\int_T \frac{1}{|x-y|}dy \tag{3.37}$$

which is an integral already treated in the calculation of conventional EFIE discretisations (see [7, Chapter 2, Section 2.2.1]). The second integral I_2 is already present in the integral needed for the discretisation of the operator B.

3.2 Setting up the Helmholtz decomposition with edge finite elements

In the previous section, we described how to implement the Herberthson equation (C.22) with edge finite elements as in the discretisation of the conventional EFIE. More precisely how to get the Galerkin matrix $\tilde{H}$, associated with the operator $\mathcal{H}$, from the Galerkin matrix E of the EFIE problem through the formula

$$\tilde{H} = E + K_e\,. \tag{3.38}$$

The latter leads to a linear system which is not exactly the one we are looking for (cf. (C.22)). Indeed it is possible to go further by noting that the right-hand side of the equation (3.13) has a particular form, it is a gradient, and thus, integrated against a function belonging to the null-space of the divergence, this right-hand side cancel out. Hence the idea is to apply the Helmholtz decomposition on the current distribution $\hat{\mathbf{J}}$

$$\bar{\psi}\,\mathbf{J} = \hat{\mathbf{J}} = \hat{\mathbf{J}}^D + \hat{\mathbf{J}}^S \quad \text{with} \quad \hat{\mathbf{J}}^D \in \mathrm{Ker}(\mathbf{d}) \quad \text{and} \quad \hat{\mathbf{J}}^S \in \mathrm{Ker}(\boldsymbol{\delta}) \tag{3.39}$$

in order to get for at least on a part a "zero right-hand side" (C.22). The main objective of this section is to present the Helmholtz decomposition on edge finite elements and explain what we do in practice to get the system (C.22). As the Helmholtz decomposition is already well described in the literature (cf. [57, 58, 59, 60]), we focus on the principal elements useful for the understanding. This section is divided in three parts:

- first we show how to set up divergence free functions, the "loop functions", on the basis of edge finite element functions,
- then we investigate how to construct these loop functions

- and finally we explain the remaining methodology to implement the Helmholtz decomposition.

In the end, this decomposition takes the form of an equivalence transformation, with a sparse matrix D_H, a very simple matrix, giving the expected matrix H

$$H = \begin{pmatrix} H^{DD} & H^{DS} \\ H^{SD} & H^{SS} \end{pmatrix} \simeq D_H(E+K)D_H^{-1} \tag{3.40}$$

and the associated linear system

$$\begin{pmatrix} H^{DD} & H^{DS} \\ H^{SD} & H^{SS} \end{pmatrix} \begin{pmatrix} J^D \\ J^S \end{pmatrix} = \begin{pmatrix} C^D \\ 0 \end{pmatrix} \tag{3.41}$$

where $J^D \in \mathrm{Im}(\mathbf{d})$ part and $J^S \in \mathrm{Ker}(\boldsymbol{\delta})$.

3.2.1 How to see the Helmholtz decomposition as a linear constraint

In the previous section, we showed how to implement the Herberthson equation using edge finite elements. In order to get the expected system (C.22), we need to set up the Helmholtz decomposition on these function spaces.
Let $\mathcal{T}$ be a triangulation of the surface $\partial\Omega$, with v vertices, e edges and f faces. Let J_i be the edge function associated with the i^{th} edge (see Figure 3.2), we can describe every current J defined on the surface by:

$$J(x) = \sum_{i=1}^{e} \lambda_i J_i(x) \tag{3.42}$$

with

$$\begin{cases} J_{i,T_1}(y) = \dfrac{+1}{2|T_1|}(y-A), \\ \\ J_{i,T_2}(y) = \dfrac{+1}{2|T_2|}(y-C) \end{cases} \tag{3.43}$$

and

$$\nabla\cdot J_i(r) = \begin{cases} \dfrac{+1}{|T_1|} \quad \text{sur} \quad T_1, \\ \\ \dfrac{-1}{|T_2|} \quad \text{sur} \quad T_2. \end{cases} \tag{3.44}$$

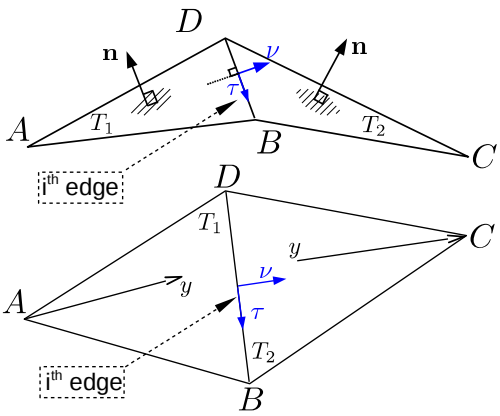

Figure 3.2 – Representation of one basis function on two triangles.

From the Helmholtz decomposition theorem, every current J can also be broken down into two terms J^S and J^D:

$$\begin{aligned} J &= J^S + J^D, \\ \text{with} \quad J^D &\in \mathrm{Im}(\mathbf{d}), \\ J^S &\in \mathrm{Ker}(\boldsymbol{\delta}). \end{aligned} \tag{3.45}$$

In the previous section, we showed how to build the Gakerkin matrix associated to the HEFIE in edge finite elements. This choice is notably justified by the fact that these are basic functions commonly used in the discretization of integral equations EFIE/MFIE/CFIE since they generate a conforming approximation space in $H_{\mathrm{div}}^{-1/2}(\Gamma)$, the functional space in which we search our current $\mathbf{J}$ (and our pseudo-current $\hat{\mathbf{J}}$).

As we require the compliance with the condition (3.45) on each cell of the triangulation, we have to build functions belonging to the kernel of the divergence with a linear combination of well chosen edge functions. The construction of loop functions starts here.

. First approach

In order to build such linear combinations, the first idea could be to set the constraint for each cell and summarized them as an algebraic problem. Indeed, each desired linear combination can be related to the kernel of a constraint matrix M of size $(f-1)\times e$. Let $f = \sum \alpha_i J_i$ be one of such linear combinations. On each cell, f can be described as a weighted sum of three edge functions J_i respecting $\boldsymbol{\delta}\, f = \sum \alpha_i\, \boldsymbol{\delta}\, J_i = 0$. By imposing the same type of constraint on each triangle of the mesh, it fully characterizes the prototype of one of these linear combinations. From a matrix point of view, these constraints can be summarized in a linear system:

$$MA = 0 \Longleftrightarrow \begin{bmatrix} \boldsymbol{\delta}\, J_{1|C_1} & \boldsymbol{\delta}\, J_{2|C_1} & \dots & \boldsymbol{\delta}\, J_{\tilde{E}-1|C_1} & \boldsymbol{\delta}\, J_{\tilde{E}|C_1} \\ \dots & & & & \\ \dots & & & & \\ \boldsymbol{\delta}\, J_{1|C_{F-1}} & \boldsymbol{\delta}\, J_{2|C_{F-1}} & \dots & \boldsymbol{\delta}\, J_{\tilde{E}-1|C_{F-1}} & \boldsymbol{\delta}\, J_{\tilde{E}|C_{F-1}} \end{bmatrix} \begin{bmatrix} \alpha_1 \\ \alpha_2 \\ \dots \\ \alpha_{\tilde{E}-1} \\ \alpha_{\tilde{E}} \end{bmatrix} = \begin{bmatrix} 0 \\ 0 \\ \dots \\ 0 \\ 0 \end{bmatrix} \tag{3.46}$$

where $J_{i|C_k}$ denotes the restriction of the edge function J_i on the k^{th} cell of the mesh, $\tilde{E}$ the number of internal edges and F the number of cells. That is the foundation of the first idea. We could go further by noting that since on each row of the matrix M, there are only three coefficients with $\pm 1/|T_C|$ for values, the system can be reduced and its coefficients belong to the set $\{+1, -1\}$. But this is not the solution we adopt here.

. Second approach: cycles in the face-edge graph

In order to build linear combination belonging to the null-space of the divergence, it is also possible to have a topological approach. Noting that the current flow, described by the edge function i (cf. Equation (3.43)) is normalized across the edge, it is quite easy to link function belonging the divergence's kernel to cycles in the face-edge graph. That is why we build loop functions from a topological study of the mesh.
To each independent cycle C of the face-edge graph, we will associate a loop function J_C belonging to the divergence's kernel. By imposing a normalized flow α on each edge e_i of the cycle C, and taking the appropriate linear combination of functions, see Figure 3.3, carried by the

edges of the cycle C as

$$\forall \alpha,\ \exists \{\lambda_i\}_{i=1..\mathrm{card}(C)},\ \forall e_i \in C,\ \lambda_i \int_{e_i} J_i^C.\nu = \alpha \quad J_C = \sum_{i=1}^{\mathrm{card}(C)} \lambda_i J_i, \tag{3.47}$$

we can ensure that $J_C \in \mathrm{Ker}(\boldsymbol{\delta})$.

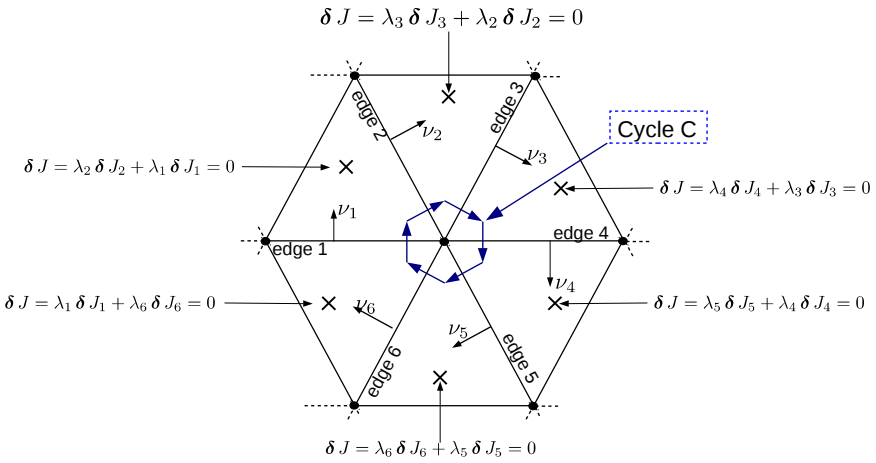

Figure 3.3 – Representation of a cycle and conditions to satisfy to obtain the wanted linear combination.

Further, we note that if the edge functions are as described earlier, then the coefficients $\{\lambda_i\}$ of the linear combination are trivial and belong to the set $\{-1, +1\}$, since the flow through an edge is ± 1. Finally, the only thing that matters is the orientation of the edge in the cycle and in the triangulation. So, in order to get the right combination, we need to work through the edges in one clearly defined direction and pay attention to the orientation chosen in the code. We can also remark that this topological construction gives particular solutions of the problem (3.46).

3.2.2 Topological solution of the constraint problem

Then, comes the question of how to identify these cycles. To answer, we need to recall some notions about graph theory and spanning trees (see [61, 62, 63, 64]).
Let $\mathcal{T}$ be a triangulation of the surface $\partial\Omega$, with v vertices, e edges and f faces. We define the Euler characteristic as a topological invariant of the surface defined as $\chi_{Euler} = v - e + f$, constant giving the genus g of the object studied, see Figure 3.4 for examples, via the relationship $\chi_{Euler} = 2 - 2g$.

Let $\mathcal{G}$ be the face-edge graph associated with the triangulation. If $\mathcal{G}$ is a graph containing f faces and if it is connected (which means that the object Ω is in one piece), then there is at least one $(f-1)$-connected minimum spanning tree, mean by this that we can connect all the faces of the object with $f-1$ well selected edges (see Figure 3.5).

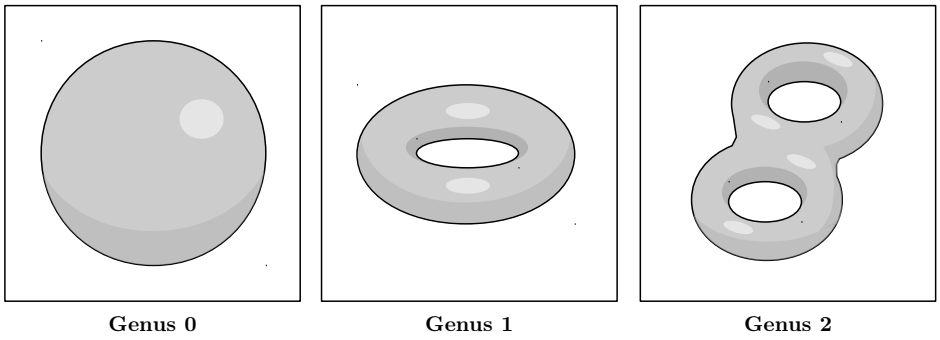

Figure 3.4 – Genus of different objects - from the left to the right : a sphere, a torus and a double torus.

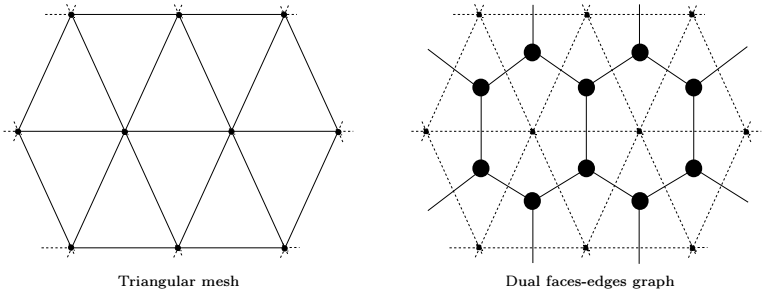

Figure 3.5 – Duality between triangular mesh and face-edge graph.

Let $\mathcal{G}_m$ be one of these spanning tree (it is not the only one a priori). If the existence of this graph is proved (typically by building it), any additional edges inexorably close an unique path through the spanning tree $\mathcal{G}_m$ and thus, generates a cycle. Let $\tilde{e}$ be the number of edges of $\mathcal{G}$ ($\tilde{e} \leq e$, $\tilde{e}$ could be defined as the number of internal edges of $\mathcal{T}$, or the number of edges not belonging to the closure of $\partial\Omega$) then there are $\tilde{e} - (f - 1)$ edges closing the cycles.
Thereby we exhibit a method to identify our loop functions which is valid for any kind of surface (whatever the genus is). Identifying edges closing the graph, we can build independent cycles. So, the method could be summarised as follow:

1. build the dual face-edge graph,
2. choose a spanning tree,
3. for every edge not included in the spanning tree, join its end points by a path through the tree to identify edges contained in the cycle,
4. choose the coefficients $\{\lambda_i\}$ corresponding to a chosen cycle orientation.

The last point to address is related to the number of unknowns. Indeed, if we want to keep the same number of unknowns $\tilde{e}$, we need to substitute some edge functions by loop functions. The question is, which one to replace? In this context, the answer is obvious. Indeed, if we replace every function associated with an edge closing the graph by the created loop function, it retains the same number of unknowns and does not degenerate our basis. It is the subsequently chosen solution.
To conclude, we illustrate the process by handling two simple examples explicitly, a two-dimensional finite plane surface and a cube, and show a spanning tree and the associated loop functions for each example.

. First example : a 2D finite plane surface

In this first example, we consider a 2D finite plane surface. From the triangular mesh, we define

- the number of vertices : $v = 9$,
- the number of faces $f = 8$,
- the number of edges $e = 16$,
- the number of internal edges $\tilde{e} = 8$ and
- the Euler characteristic $\chi_{Euler} = 1$.

If we consider this mesh for a computation, we have:

- the number of unknowns $N = 8$,
- the number of edge functions to keep $d = 7$,
- the number of loop functions $s = 1$.

The different steps and a loop function are represented in Figure 3.6.

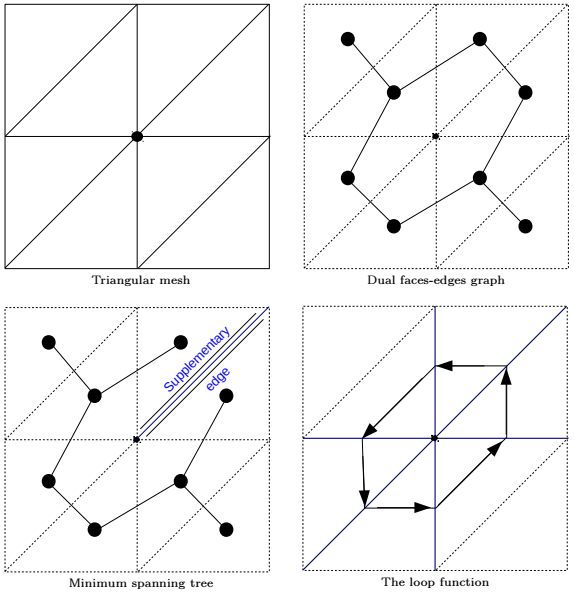

Figure 3.6 – Identification and construction of loop function on a 2D finite plane mesh.

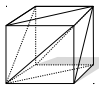

Figure 3.7 – The considered mesh.

. Second example : a cube

In this example, we consider a cube (Figure 3.7). From the triangular mesh, we define

- the number of vertices : $v = 18$,
- the number of faces $f = 12$,
- the number of edges $e = 18$,
- the number of internal edges $\tilde{e} = 18$ and
- the Euler characteristic $\chi_{Euler} = 2$.

If we consider this mesh for a computation, we have:

- the number of unknown $N = 18$,
- the number of edge functions to keep $d = 11$,
- the number of loop functions $s = 7$.

The different steps and a complete set of loop functions are represented in Figure 3.8

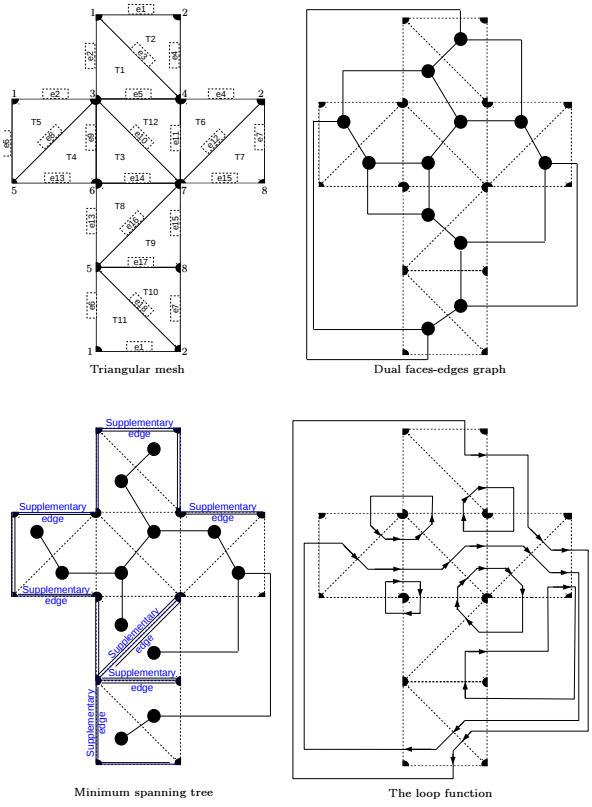

Figure 3.8 – Identification and construction of loop functions on a cube.

. About the construction of the cycles

In this document, we have chosen to present the identification of the loop functions by means of the construction of a spanning tree on the face-edge graph. However, this is not the only one possibility. Indeed, depending on the genus of objects, other methods could be considered. In [57, 65, 66], for example, authors present the possibility to build loop functions around the internal nodes of the mesh for 0-genus objects or 2D finite plane surface like the one we present above, but that will not work for surface with a higher genus (e.g., a torus).
Another important point is the choice of the spanning tree. Indeed, we can use different heuristics: Depth First Search, Breadth First Search, domain decomposition, ..., that will not necessarily give the same spanning three and thus the same loop functions. This potentially leaves some degree of freedom for the implementation and representation of the solenoidal currents. We also need to keep in mind that any linear combinations of loop functions remains a cycle function.

. The relative length of J^D and J^S

The last thing we want to address in this subsection is related to the dimensions of J^D and J^S in regard to the global dimension of the problem. For simplicity, assume that ∂D has genus equal to 0, which means that ∂D is a surface homologous to a sphere, and supports a consistent triangular mesh. Under these conditions, all the edges are internal and the system has a dimension e. We wrote that we had to maintain $f-1$ edges and construct $e-(f-1)$ loop functions. The legitimate question is what proportion this represents. To answer this question, it is possible to show that

$$\lim_{\substack{V\to+\infty \\ v\in\mathbb{N}^+}} \frac{f-1}{e} = \frac{2}{3}\,. \tag{3.48}$$

using the fact that in this configuration $3f = 2e$. From this limit, we can grant that, with the finest meshes, we keep two-thirds of the total dimensions in $\mathrm{Im}(\mathbf{d})$ and one-thirds in $\mathrm{Ker}(\boldsymbol{\delta})$.

3.2.3 Cycles and matrix representation of the Helmholtz decomposition

So far, we have described how to implement the Helmholtz decomposition in a space of edge finite elements. This involves a topological study of the mesh, the modeling of cycles in the face-edge graph and the construction of loop functions.
In practice, we went to another step by suggesting a formulation outsourcing this decomposition. It is possible to separate the Helmholtz decomposition from the computation of the Galerkin matrix. Insofar as the Helmholtz decomposition resulted in the creation of loop functions, which are linear combinations of edge functions, it seems reasonable to represent the decomposition as a change of basis matrix D_H.
One idea is to directly translate these linear combinations into a matrix D, obtain a matrix $\hat{H} = D\tilde{H}D^{-1}$ and get the associated linear system. The problem is that in this way, one looses the identification of the two parts J^D and J^S.
A good solution is to initially identify and collect basis functions with a degree of freedom (DoF) on an edge in the spanning tree in one group and the ones with a DoF on the co-tree in another group. From a matrix point of view, it is a re-ordering of the Galerkin matrix coefficients, which can be formalized with permutation matrix P. Secondly, we can apply the appropriate basis change in order to get the loop functions, basis change formalized with a matrix D_H.
Furthermore, if edge functions are properly normalized (see previous subsections) and care was

taken to create independent cycles, then the latter matrix take the following form:

$$D_H = \begin{pmatrix} \mathbf{I}_d & 0 \\ S & \mathbf{I}_s \end{pmatrix} \tag{3.49}$$

where $\mathbf{I}_d$ is the identity matrix of size $(f-1)\times(f-1)$, $\mathbf{I}_s$ of size $(\tilde{e}-(f-1))\times(\tilde{e}-(f-1))$ and S a sparse matrix (see Figure 3.9)

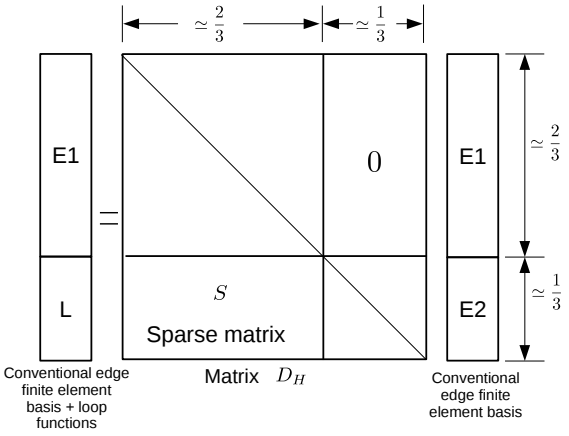

Figure 3.9 – The considered matrix D_H link between the conventional edge function and Helmholtz decomposition.

To make appear the unit sub-diagonal matrix $\mathbf{I}_s$, it may be necessary to change the orientation of some cycles (which results in a simple multiplication by -1 of the concerned line). In this form, the inverse matrix is explicit:

$$D_H^{-1} = \begin{pmatrix} \mathbf{I}_d & 0 \\ -S & \mathbf{I}_s \end{pmatrix}. \tag{3.50}$$

Finally, we get the wanted matrix H through the relation:

$$H = D_H P \tilde{H} P^T D_H^{-1} \tag{3.51}$$

and the associated linear system

$$HJ = C \Longleftrightarrow \begin{pmatrix} H^{DD} & H^{DS} \\ H^{SD} & H^{SS} \end{pmatrix} \begin{pmatrix} J^D \\ J^S \end{pmatrix} = \begin{pmatrix} C^D \\ 0 \end{pmatrix} \tag{3.52}$$

where $J^D \in \mathrm{Im}(\mathbf{d})$ and $J^S \in \mathrm{Ker}(\boldsymbol{\delta})$.

3.3 Setting up the HMFIE

3.3.1 Two equivalent problems : MFIE vs HMFIE

We begin with a short overview of two equivalent problems, the conventional MFIE and the HMFIE.

. Magnetic Field Integral Equation

Let once again Γ denote the surface of closed perfectly electric conducting (PEC) scatterer with normal unit $\mathbf{n}$, $\mathbf{H}^{\text{inc}}$ an incident plane wave illuminating Γ, described with a wave number κ, a direction of propagation θ and a polarisation $\mathbf{p}_H = Y_0\theta \wedge \mathbf{p}_E$ such as $\forall y \in \mathbb{R}^3$, $\mathbf{H}^{\text{inc}}(y) = \psi(y)\mathbf{p}_H = e^{-i\kappa\theta\cdot y}\mathbf{p}_H$, and let $\mathbf{J}$ be the induced surface current distribution on Γ. In this notation, the MFIE (Magnetic Field Integral Equation) reads

$$\forall\, \mathbf{x} \in \Gamma,\ \mathbf{tr}\left[\frac{1}{2}\,\mathbf{J}(x) + \mathbf{n}\times\mathcal{B}[\mathbf{J}](x)\right] = \mathbf{tr}\left[\mathbf{n}\times\mathbf{H}^{\text{inc}}(x)\right] \tag{3.53}$$

where, for this section, $\mathcal{B}$ is described by

$$\mathcal{B}[j](x) = \int_\Gamma \nabla_y G(x,y)\times j(y)d\Gamma \tag{3.54}$$

where G is the free-space Green function. This first equation leads to the following variational problem:

$$\begin{cases} \text{Find } \mathbf{J} \in L^2_{\text{T}}(\Gamma,\mathbb{C}^3),\ \text{such that } \forall\, \mathbf{J}^{'} \in L^2_{\text{T}}(\Gamma,\mathbb{C}^3), \\ \dfrac{1}{2}\displaystyle\int_\Gamma \mathbf{J}^{'}(x)\cdot\mathbf{J}(x)d\Gamma_x + \iint_{\Gamma\times\Gamma} \mathbf{J}^{'}_x\cdot\left(\mathbf{n}_x\wedge\left(\nabla_y G_{x,y}\wedge\mathbf{J}_y\right)\right)d\Gamma_x d\Gamma_y = \displaystyle\int_\Gamma \mathbf{n}\wedge\mathbf{H}^{\text{inc}}\cdot\mathbf{J}^{'}\,d\Gamma\,. \end{cases} \tag{3.55}$$

In further developments, we use the notation $\mathbf{M}$ to described the left-hand side operator of this variational problem:

$$\mathbf{M}(\mathbf{J},\mathbf{J}^{'}) = \frac{1}{2}\int_\Gamma \mathbf{J}^{'}(x)\cdot\mathbf{J}(x)d\Gamma_x + \int_\Gamma\int_\Gamma \mathbf{J}^{'}(x)\cdot\left(\mathbf{n}(x)\wedge\left(\nabla_y G(x,y)\wedge\mathbf{J}(y)\right)\right)d\Gamma_x d\Gamma_y\,. \tag{3.56}$$

. The Herberthson Magnetic Field Integral Equation

Starting from the conventional MFIE problem,

$$\mathbf{tr}\left[\frac{1}{2}\,\mathbf{J}(x) + \mathbf{n}\times\mathcal{B}[\mathbf{J}](x)\right] = \mathbf{tr}\left[\mathbf{n}\times\mathbf{H}^{\text{inc}}(x)\right], \tag{3.57}$$

the first step is to multiply the left and the right-hand side by the conjugate phase $\bar{\psi}$ in order to get on the right-hand side only a constant vector $\mathbf{p}_H$ (formally a *1-form*)

$$\bar{\psi}(x)\left(\frac{1}{2}\,\mathbf{J}(x) + \mathbf{n}\times\mathcal{B}[\mathbf{J}](x)\right) = \bar{\psi}\,\mathbf{n}\times\mathbf{H}^{\text{inc}}(x) = \mathbf{n}\times\mathbf{p}_H\,. \tag{3.58}$$

Therefore, the second step is to highlight a pseudo-current

$$\hat{\mathbf{J}} = \bar{\psi}\,\mathbf{J} \tag{3.59}$$

to obtain the HMFIE:

$$\forall \mathbf{x} \in \Gamma,\ \mathbf{tr}\left[\frac{1}{2}\hat{\mathbf{J}}(x) + \bar{\psi}(x)\,\mathbf{n} \times \mathcal{B}[\psi\hat{\mathbf{J}}](x)\right] = \mathbf{tr}\left[\mathbf{n} \times \mathbf{H}^{\text{inc}}(x)\right] = \mathbf{tr}\left[\mathbf{n} \times \mathbf{p}_H\right]. \tag{3.60}$$

This last equation leads to the following variational problem:

$$\begin{cases} \text{Find } \hat{\mathbf{J}} \in L^2_{\mathrm{T}}(\Gamma, \mathbb{C}^3),\ \text{such that } \forall\, \mathbf{J}^{'} \in L^2_{\mathrm{T}}(\Gamma, \mathbb{C}^3), \\ \dfrac{1}{2}\displaystyle\int_\Gamma \mathbf{J}^{'}_x \cdot \hat{\mathbf{J}}_x d\Gamma_x + \iint\limits_{\Gamma\times\Gamma} \bar{\psi}_x\, \mathbf{J}^{'}_x \cdot \left(\mathbf{n}_x \wedge \left(\nabla_y G_{x,y} \wedge \psi_y \hat{\mathbf{J}}_y\right)\right) d\Gamma_x d\Gamma_y = \displaystyle\int_\Gamma \mathbf{n} \wedge \mathbf{p}_H \cdot \mathbf{J}^{'}\, d\Gamma\,. \end{cases} \tag{3.61}$$

In this last formulation, once again, the pseudo-current $\hat{\mathbf{J}}$ computed is not the physical current induced by the incident plane wave. For the purpose of the next developments, we introduce :

$$\mathbf{H}_m(\hat{\mathbf{J}}, \mathbf{J}^{'}) = \frac{1}{2}\int_\Gamma \mathbf{J}^{'}_x \cdot \hat{\mathbf{J}}_x d\Gamma_x + \int_\Gamma \int_\Gamma \bar{\psi}_x\, \mathbf{J}^{'}_x \cdot \left(\mathbf{n}_x \wedge \left(\nabla_y G_{x,y} \wedge \psi_y \hat{\mathbf{J}}_y\right)\right) d\Gamma_x d\Gamma_y\,. \tag{3.62}$$

3.3.2 Highlighting and computing the perturbation

After describing the two problems, the conventional MFIE and the HMFIE, we repeat the same procedure as for the HEFIE: taking advantage of the fact that HMFIE can be seen as a perturbation of the MFIE. Once again, the MFIE is documented in the literature (e.g., [7] or [56]) and since it has effective implementations, we are interested only in the perturbation part.

So, the first step is to highlight the perturbation, i.e., the associated variational operator $\mathbf{K}_m$ in order to describe it on the basis of edge finite elements. We start from the formula giving us the perturbation term $\mathbf{K}_m = \mathbf{H}_m - \mathbf{M}$

$$\mathbf{K}_m(\mathbf{J}, \mathbf{J}') = \iint\limits_{\Gamma\times\Gamma} \left(\bar{\psi}(x)\psi(y) - 1\right) \mathbf{J}^{'}(x) \cdot (\mathbf{n}(x) \wedge (\nabla_y G(x,y) \wedge \mathbf{J}(y)))\, dxdy\,. \tag{3.63}$$

At this point, we note that the perturbation of the MFIE $\mathbf{K}_m$ is radically simpler than the perturbation of the EFIE $\mathbf{K}_e$ since we have only one elementary operator quite easy to implement. Once again, integrals may be broken down in two successive integrals:

$$\int_{T_1}\int_{T_2} \{...\}\, dT_1(x) dT_2(y) = \int_{T_1} F^{T_2}(x) dT_1(x) \tag{3.64}$$

with

$$F^{T_2}(x) = \int_{T_2} (x)\, \{...\}\, dT_2(y), \tag{3.65}$$

but, in this case, unlike the HEFIE, both the external (3.64) and the internal (3.65) integrals can be evaluated numerically because in the case $T_1 = T_2$, we have

$$-\nabla_y G(x,y) = \nabla_x G(x,y) = e^{i\kappa|x-y|}\frac{x-y}{|x-y|^2}\left(i\kappa - \frac{1}{|x-y|}\right)\ , \tag{3.66}$$

the collinearity of $\mathbf{n}(x)$ and $\nabla_y G(x,y) \wedge \mathbf{J}(y)$ implies

$$\forall (x,y) \in T,\ \mathbf{n}(x) \wedge (\nabla_y G(x,y) \wedge \mathbf{J}(y)) = 0\,. \tag{3.67}$$

3.3.3 Linear systems

With the above relations, we obtain the linear system

$$\tilde{H}_m \tilde{J} = \tilde{V} \Longleftrightarrow (M + K_m)\tilde{J} = \tilde{V}\,. \tag{3.68}$$

Here, we can apply once again the Helmholtz decomposition in the same way as the HEFIE and build a new linear system

$$H_m J = V \Longleftrightarrow D_H(M + K_m)D_H^{-1} J = D_H \tilde{V} \Longleftrightarrow \begin{pmatrix} H_m^{DD} & H_m^{DS} \\ H_m^{SD} & H_m^{SS} \end{pmatrix} \begin{pmatrix} J^D \\ J^S \end{pmatrix} = \begin{pmatrix} 0 \\ V^S \end{pmatrix}. \tag{3.69}$$

As we wrote earlier (see Chapter 2), both EFIE/HEFIE equations (and MFIE/HMFIE) are similar and are well-posed for all κ unless forbidden values. In this context, the CFIE was introduced to avoid these exceptional values and ensure the existence and uniqueness of a solution at any frequency.

In the same way that the CFIE was defined, we set

$$\text{HCFIE} = \alpha\text{HEFIE} + (1-\alpha)\text{HMFIE} \tag{3.70}$$

which give in matrix form:

$$H_c = \alpha H + (1-\alpha) Z_0 H_m \tag{3.71}$$

or

$$H_c J = W \Longleftrightarrow D_H \left(\alpha \tilde{H} + (1-\alpha)\tilde{H}_m\right) D_H^{-1} J = \alpha C + (1-\alpha)V. \tag{3.72}$$

Concluding remarks

In this chapter, we have presented the practical implementation of the various integral equations proposed by Herberthson, namely the HEFIE (Section 3.1), the HMFIE and the HCFIE (Section 3.3). First, we gave all the necessary elements required to build the Galerkin problem on the edge finite element basis. Our approach led us to develop for each equation the Galerkin matrix of the perturbations K_e and K_m for respectively the HEFIE and the HMFIE (see Chapter 2 for mathematical justifications) in order to benefit from the gained experience on the conventional integral equations and obtain the discretization of the Herberthson equations through the relations

$$\tilde{H} = E + K_e \text{ and } \tilde{H}_m = M + K_m \tag{3.73}$$

where E and M are the Galerkin matrix of respectively the EFIE and the MFIE and H et H_m those of the HEFIE and the HMFIE. As we showed the implementation of these perturbations is simple and requires only either numerical integrations or evaluation of singular integral for which analytical expressions exist and implementation present in the computation of the conventional Galerkin matrix (see [7]).

In a second step, we have presented the establishment of the Helmholtz decomposition (Section 3.2). We detailed how to build a set of functions belonging to $\text{Ker}(\boldsymbol{\delta})$ from edge finite element basis and the construction of a minimum spanning tree on the face-edge graph (Figures 3.3, 3.6 and 3.8). This method led us to formulate the Helmholtz decomposition through a change of basis and a matrix D_H (Figure 3.9).

Finally, we get the desired system (C.22) through the relation:

$$H = D_H \tilde{H} D_H^{-1}. \tag{3.74}$$

Chapter 4

Computational analysis of the solution of the linear systems for two scattering configurations

Contents

In the previous chapter, we detailed the implementation of Herberthson's version of the EFIE, MFIE and CFIE, notably by describing the construction of the associated Galerkin matrix and the establishment of the Helmholtz decomposition on the edge finite element basis. The objective of this chapter is to establish some properties of those Galerkin matrices and present some elements concerning the solution of the associated linear systems. For this, we consider two examples of the scattering of a plane wave by a conducting body.

First, we begin this chapter with a description of the two different conducting bodies, a sphere and an airplane (a 737 Boeing), and give for each example the polarisation of the plane wave considered. Then, we introduce the solver we use in our application, namely the Generalized Minimum Residual Method (GMRES) iterative solver, and recall its main characteristic elements.

In order to choose an appropriate solution method, it quickly appears necessary to look at the interaction between divergent and solenoidal currents, which are reflected in the norms of some

blocks of the matrices. To observe these interactions, we focus on simple cases: the diffraction of a plane wave on a perfectly conducting sphere and on a perfectly conducting airplane over a range of frequencies.
Through this study, we attempt to highlight the performance of the HEFIE and the HMFIE and identify the situations where the new formulation will be the best suited one (in terms of structures, frequencies, ...). Then, we look at the solution of the linear systems and especially at possible preconditioners for the new linear systems. Therefore, to evaluate the benefit of our solution methods, we begin with an analysis of the additional costs generated by the construction of the HEFIE from the EFIE (and, by the way, of the HMFIE from the MFIE). Choosing the Krylov iterative solver GMRES as a reference, we translate these costs into an equivalent minimal number of GMRES iterations to gain in order to say that Herberthson's version are competitive. We then proposed various preconditioners based on our previous studies and experience and compare for the two chosen configurations the number of GMRES iterations required to solve the system in order to judge on the interest of both the HEFIE/HMFIE and our preconditioners.

4.1 Definition of the configurations: a sphere and an airplane

. The objects considered

In this chapter, we consider two perfectly conducting objects. The first is a sphere with radius $a = 1m$, meshed with 1.200 edges, 402 points, 800 faces, mesh adapted to the chosen range of frequencies, submitted to an incident plane wave $\{E^{\text{inc}}(x), H^{\text{inc}}(x)\} = \{e^{i\kappa\theta\cdot x}\mathbf{p}_E\ ,\ e^{i\kappa\theta\cdot x}\mathbf{p}_H\}$ with $\theta = (0,0,1)$, $\mathbf{p}_E = (1,0,0)$ and $\mathbf{p}_H = Y_0\theta\wedge\mathbf{p}_E$. In this case, the object and the problem is invariant by rotation.
The second object considered is the mesh of a Boeing 737 with 2.568 edges, 858 points and 1.712 faces, mesh well adapted to the chosen range of frequencies. The principal characteristics are given in Figure C.3. In the numerical applications, we consider an incident wave $\{E^{\text{inc}}(x), H^{\text{inc}}(x)\} = \{e^{i\kappa\theta\cdot x}\mathbf{p}_E\ ,\ e^{i\kappa\theta\cdot x}\mathbf{p}_H\}$ with $\theta = \left(-\sqrt{2}/2, \sqrt{2}/2, 0\right)$ and $\mathbf{p}_E = \left(\sqrt{2}/2, \sqrt{2}/2, 0\right)$.

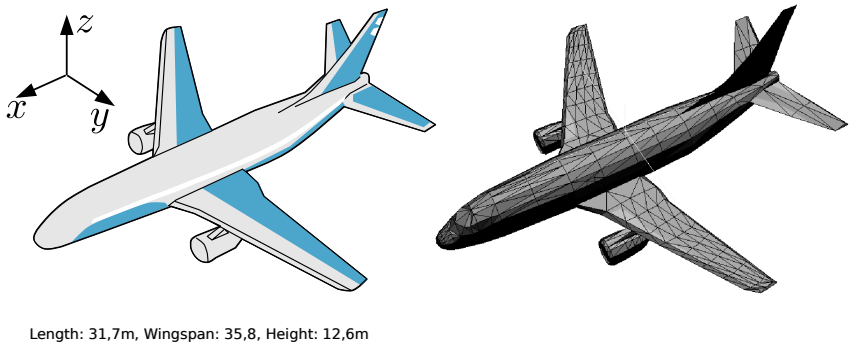

Figure 4.1 – The considered airplane and its mesh.

. The considered systems

In this chapter we considered Herberthson's version of the three conventional boundary integral equations and their associated linear systems. To set the notations, we recall here the considered problems.

The HEFIE:

$$D_H P \tilde{H}_e P^T D_H^{-1} J = H_e J = \begin{pmatrix} H_e^{DD} & H_e^{DS} \\ H_e^{SD} & H_e^{SS} \end{pmatrix} \begin{pmatrix} J^D \\ J^S \end{pmatrix} = \begin{pmatrix} C^D \\ 0 \end{pmatrix} = C. \tag{4.1}$$

The HMFIE:

$$D_H P \tilde{H}_m P^T D_H^{-1} J = H_m J = \begin{pmatrix} H_m^{DD} & H_m^{DS} \\ H_m^{SD} & H_m^{SS} \end{pmatrix} \begin{pmatrix} J^D \\ J^S \end{pmatrix} = \begin{pmatrix} 0 \\ V^S \end{pmatrix} = V. \tag{4.2}$$

The HCFIE:

$$D_H \left(\alpha \tilde{H} + (1-\alpha) \tilde{H}_m \right) D_H^{-1} J = H_c J = W = \alpha C + (1-\alpha) V \tag{4.3}$$

with $\alpha = 0.2$ and

$$H_c = \begin{pmatrix} H_c^{DD} & H_c^{DS} \\ H_c^{SD} & H_c^{SS} \end{pmatrix}. \tag{4.4}$$

4.2 Solution methods

4.2.1 General considerations

In the previous chapter, we have shown that the discretization of the integral equations leads to a dense linear system

$$HJ = C \tag{4.5}$$

with $H \in \mathcal{M}_{N\times N}(\mathbb{C})$, $J \in \mathbb{C}^N$ and $C \in \mathbb{C}^N$ where N is the number of unknowns of the problem. Basically, there exist two families of methods for the solution of a such system.

- First, there is the family of direct methods (LU, Cholesky, ...) that consist of a factorization of the matrix H. These methods are usual very precise since the exact solution of the linear system is computed up to rounding errors. In addition, once the factorization performed, it can be used to compute the solution associated with different right-hand sides (for example the two polarisations of an incident plane wave). However direct methods are in general extremely costly. The cost of the factorization grows as $O(N^3)$ which means that they are not used when the number of unknowns becomes large.

- Secondly, there is the family of iterative methods that seek the solution step by step by calculating a matrix-vector product in each iteration. Generally, each solution x must meet the following criterion

  $$\|HJ - C\| \leq \varepsilon \tag{4.6}$$

  where $\varepsilon \in \mathbb{R}$ is a parameter to control the accuracy of the solution. The main asset of the iterative methods, compared to direct methods, is that the cost of each iteration is of the order $O(N^2)$. However, iterative solvers are very sensitive to the conditioning of the matrix H. The consequence is that the solver can be very long to converge or converges not at all. Furthermore, the number of iterations needed to find a solution is not predictable, adding some additional difficulties in the sense that we cannot know whether the method will converge quickly or not before having tried.

4.2.2 The GMRES solver

To solve our linear systems, we shall use the Generalized Minimum Residual Method (GMRES) iterative solver. This is probably the most widely used method in boundary integral equations. It was formulated by Y. Saad [6] and for the sake of completeness, we choose to recall the principle elements. A complete description can be found in [6].

In this short section, we consider a linear system to solve, namely the system $Ax = b$, system with a size N. The GMRES is a so-called projective iterative method based on the construction of a Krylov space. Let $r^n = b - Ax^n$ denote the residue where x^n is the approximate solution at the iteration n of the method. The idea of the GMRES method is to build a basis of a Krylov subspace, namely the space $\mathscr{K}_n(A, r_0)$, and to seek a solution x^n into this subspace. Therefore, at each iteration the vector x^n can be written as follows:

$$x^n = x^0 + \sum_{k=1}^{n-1} \lambda_k A^k r_0. \tag{4.7}$$

If V_n is an orthonormal basis of the Krylov space $\mathscr{K}_n(A, r_0)$ built incrementally, because the sequence of subspaces are embedded (i.e., $\mathscr{K}_{n-1}(A, r_0) \subset \mathscr{K}_n(A, r_0)$), then any vector x of $\mathscr{K}_n(A, r_0)$ can be written as:

$$x = x^0 + V_n y \tag{4.8}$$

where y is a vector of size n. The idea then is to present y as the solution of a minimization problem, more precisely the minimization of the residue. For this, we introduce the following function J to minimize:

$$J(y) = \|b - Ax\|_2 = \|b - A(x^0 + V_n y)\|_2, \tag{4.9}$$

where

$$\begin{aligned} b - Ax &= b - A(x^0 + V_n y), \\ &= r_0 - AV_n y. \end{aligned} \tag{4.10}$$

In addition, the Arnoldi method used to build the orthonormal basis V_n leads to a relation between AV_n and the basis at the next iteration V_{n+1}. We have:

$$AV_n = V_{n+1} H_n \tag{4.11}$$

where $H_n \in \mathscr{M}_{n+1,n}$ is an upper Hessenberg matrix. Noting that r_0 is collinear to the first vector of V_{n+1} (namely the vector $r_0 = \beta v_1$), we can write that

$$\begin{aligned} b - Ax &= r_0 - AV_n y, \\ &= r_0 - V_{n+1} H_n y, \\ &= \beta v_1 - V_{n+1} H_n y, \\ &= V_{n+1}(\beta v_1 - H_n y). \end{aligned} \tag{4.12}$$

Thus, as the columns of the matrix V_{n+1} constitute an orthonormal basis, they are mutually orthogonal and normalized. Hence, we can write that y is the minimum of the following function:

$$J(y) = \|b - Ax\|_2 = \|b - A(x^0 + V_n y)\|_2 = \|\beta v_1 - H_n y\|_2. \tag{4.13}$$

Therefore, at each iteration the vector x^n, an approximate solution to the linear system, will be given by the following equality:

$$x_n = x_0 + V_n y_n \quad \text{with} \quad y_n = \operatorname{argmin}_y \|\beta v_1 - H_n y\|. \tag{4.14}$$

Without introducing the minimization strategies, the vector solution y_n will be easy to compute as it only requires the solution of a small least squares problem of size $(n+1) \times n$ where n aims to be small if the problem is not too ill-conditioned.
Since at each iteration the method requires the evaluation of a matrix-vector product, its cost is in $O(2N_{iter}N^2)$ where N_{iter} is the number of iterations required to attain a residual error $\varepsilon = \|\beta_1 v_1 - H_n y_n\|$.

4.3 Numerical properties of the operators

4.3.1 Norm estimates

. Motivations

Once the linear systems obtained, we aim to design a solution that promotes obtaining $J = (J^D, J^S)$. Due to the particular shape of the system matrices, i.e., the natural 2×2 block structure and where the right-hand side vanishes on a complete subspace

$$\begin{pmatrix} H_e^{DD} & H_e^{DS} \\ H_e^{SD} & H_e^{SS} \end{pmatrix} \begin{pmatrix} J^D \\ J^S \end{pmatrix} = \begin{pmatrix} C^D \\ 0 \end{pmatrix} \quad \text{or} \quad \begin{pmatrix} H_m^{DD} & H_m^{DS} \\ H_m^{SD} & H_m^{SS} \end{pmatrix} \begin{pmatrix} J^D \\ J^S \end{pmatrix} = \begin{pmatrix} 0 \\ V^S \end{pmatrix}, \tag{4.15}$$

we want to study the possibility to use a solution method based on the Schur complement system either

$$S_e J^D = \left(H_e^{DD} - H_e^{DS} (H_e^{SS})^{-1} H_e^{SD} \right) J^D = C^D \tag{4.16}$$

or

$$S_m J^S = \left(H_m^{DD} - H_m^{DS} (H_m^{SS})^{-1} H_m^{SD} \right) J^S = V^S. \tag{4.17}$$

As we wrote in Chapter 2, the Helmholtz theorem allows us to break down the current into a potential $\mathbf{J}^d$ and solenoidal $\mathbf{J}^s$ currents. This one appears interesting in the case we consider the RCS in the forward direction $\sigma(\theta^i, \theta^i)$ since only the potential part of the pseudo-current $\widehat{\mathbf{J}}^d$ contributes to this particular RCS coefficient.
If we do not present this as the main asset of the Herberthson formulation, we have, at least at the beginning of our study explored the possibility to get only the potential part of the current. For this, in regard to the particular shape of the matrix, we investigate different methods to promote the convergence of a GMRES method into this subspace. That was one of our initial argument to analyse the norms (and the spectrum) of the operator (or more exactly of each block of the matrix).
Independently of the nature of $\mathbf{J}^d$ which happens to be the contributive part of this particular coefficient (and the original purpose of our work), our ability to get quickly $\mathbf{J}^d$ or not had another interest. Typically, if we could find a method that gave really quickly a good estimation of $\mathbf{J}^d$ (typically by solving a system of size $2N/3$ or $N/6$ with the macro-elements approach presented in Chapter 5), we would certainly have a RCS coefficient, but we would also have and above all the solution of the global system by solving a smaller subsystem (of size $N/3$ or $N/12$ if we use the macro-element approach).
In the manuscript, we do not detail this approach on how to promote the convergence on $\mathbf{J}^d$. We only motivate how $\mathbf{J}^d$ could be useful to us and what the approach by Schur's complement would gave.

To study this possibility, it is interesting in a first approach to look at the norms of the different blocks of these two matrices. In an extreme case, if the norm of the extra-diagonal

blocks H^{DS} and H^{SD} appears to be equal to zero or to be very small compared the norm of the diagonal blocks H^{DD} and H^{DS}, the solution of an approximate reduced system like

$$\begin{pmatrix} H_e^{DD} & 0 \\ 0 & H_e^{SS} \end{pmatrix} \begin{pmatrix} J^D \\ J^S \end{pmatrix} = \begin{pmatrix} C^D \\ 0 \end{pmatrix} \quad \text{or} \quad \begin{pmatrix} H_m^{DD} & 0 \\ 0 & H_m^{SS} \end{pmatrix} \begin{pmatrix} J^D \\ J^S \end{pmatrix} = \begin{pmatrix} 0 \\ V^S \end{pmatrix} \tag{4.18}$$

could offer a first estimation for the solution vector J. In the same way, if the norm of the product $H^{DS}(H^{SS})^{-1}H^{SD}$ is small enough in regard to the norm of the block H^{DD}, a good preconditioner to the Schur complement (for example the inverse of H^{DD}) could give a fast solution for J^D (or J^S for the HMFIE Schur complement).

Therefore, in order to choose an appropriate solution method, it appears necessary to look at the spectral norms of the various blocks of the matrix that reflect the interactions between divergent and solenoidal currents. To recall, the spectral norm of a matrix A is the largest singular value of A, i.e., the square root of the largest eigenvalue of the matrix A^*A. To observe these norms, we have chosen to focus on simple cases: the diffraction of a plane wave on a perfectly conducting sphere and on a perfectly conducting airplane over a range of frequencies. Through this study, we attempt to highlight the performance of the HEFIE and the HMFIE, but also identify the situations where the new formulations can be the best suited (in terms of structures, frequencies, ...) and provide an adapted solution method for the linear systems.

. The sphere

The results for the sphere, presented in Figures 4.2, 4.3 and 4.4, show some interesting properties.
Let us begin with the norm of the HEFIE blocks. In Figure 4.2, we show the norm of each of the four blocks $(H^{DD}, H^{DS}, H^{SD}, H^{SS})$ as a function of the frequency of the illuminating wave. Firstly, we note that at the lowest frequencies ($f < 5.10^7$Hz), the norms of the upper blocks of the matrix H^{DD} and H^{DS} decrease linearly on a logarithmic scale whereas the norms of the lower blocks H^{SD} and H^{SS} remain nearly constant. For higher frequencies, when the wavelength is smaller than the radius of the sphere, the norm of the block H^{SS} slowly increases. Globally, since for the highest frequencies the norms of the blocks H^{DD}, H^{SD} and H^{SS} have the same order of magnitude, we observe that the divergent and the solenoidal part of currents are strongly coupled.
Now, if we are looking at the norm of the HMFIE blocks presented in Figure 4.3, we can observe that the dynamic is significantly different. Indeed, we observe that the norms of each block remains constant for the lowest frequencies and slowly increase when the wavelength becomes smaller than the radius of the sphere. Furthermore, since the ratio of the norms of each blocks still unchanged, we observe the same coupling between divergent and solenoidal current on all the range of frequencies considered.
Finally, we can see that the norms of the blocks of the HCFIE matrix are quite similar to those of the HEFIE. We observe the same decreasing of the upper blocks and nearly the same coupling for the divergent and the solenoidal part.

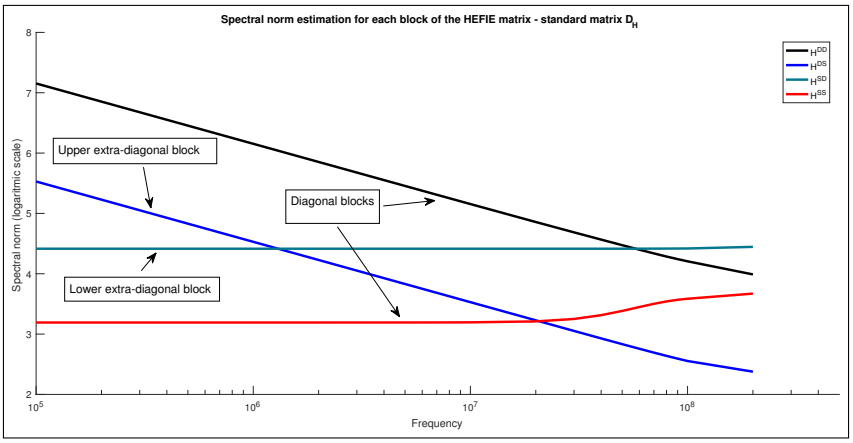

Figure 4.2 – Spectral norm estimation for each block of H_e (HEFIE) on a range of frequencies for the SPHERE (logarithmic scale).

.

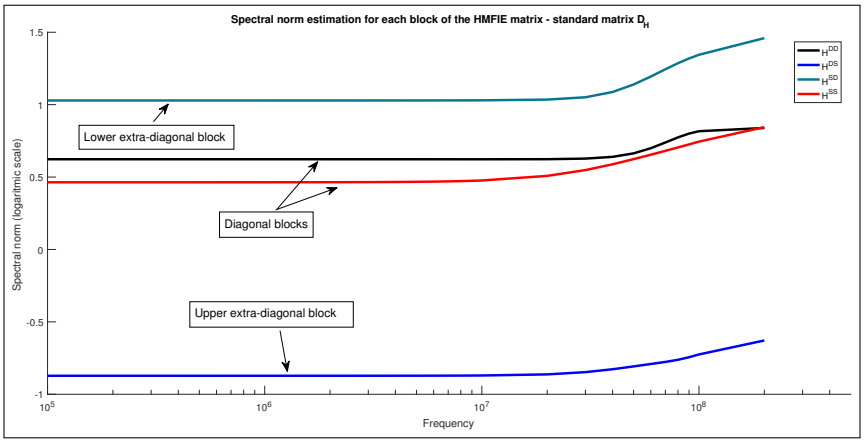

Figure 4.3 – Spectral norm estimation for each block of H_m (HMFIE) on a range of frequencies for the SPHERE (logarithmic scale).

.

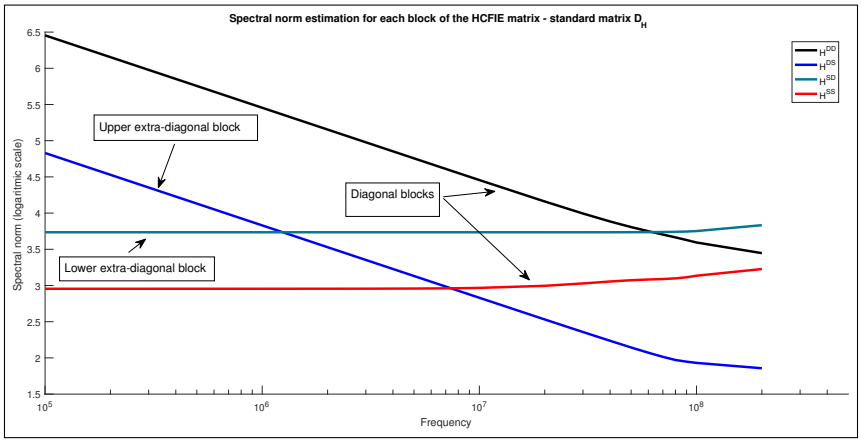

Figure 4.4 – Spectral norm estimation for each block of H_c (HCFIE) on a range of frequencies for the SPHERE (logarithmic scale).

.

. The airplane

Similar results for the airplane are presented in Figures 4.5, 4.6 and 4.7. Globally we have a slightly different situation than we had with the sphere.
Indeed, if we look at the norms of the different blocks of the HEFIE for the airplane in Figure 4.5, we can observe that every norm decreases with the frequency and not only the first row blocks. We can also observe that the ratio between the different norms of the blocks is constant in frequency. Furthermore, we can note that the coupling is stronger than for the sphere, since the norm of the lower extra-diagonal block that represent the interaction between divergent and solenoidal current is higher than the norm of the diagonal blocks. We also remark that the norm of the upper extra-diagonal block is slightly lower than the other ones.
Now if we observe the norms of the different blocks of the HMFIE matrix in Figure 4.6, we can remark that, as for the sphere, the norm remains constant over the range of frequencies. We also have the same distribution for the norms, meaning by this that the norm of the lower extra-diagonal blocks is higher than the norm of the diagonal block and much higher than the norm of the upper extra-diagonal block. Once again the coupling of divergent and solenoidal currents is strong.
To finish, we observe that, as for the sphere, the norms of the blocks of the HCFIE matrix are quite similar to those of the HEFIE.

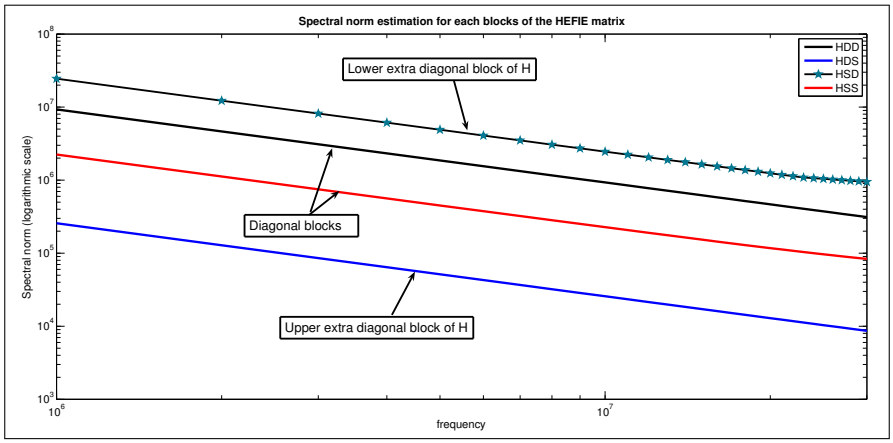

Figure 4.5 – Spectral norm estimation for each block of H_e (HEFIE) on a range of frequencies for the PLANE (logarithmic scale).

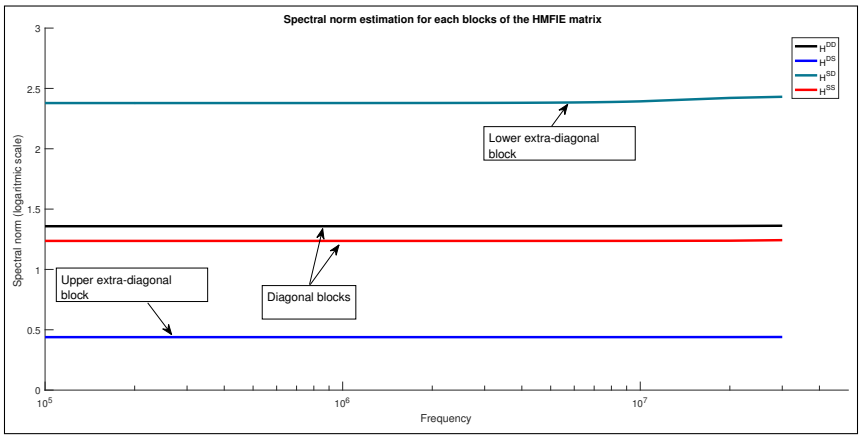

Figure 4.6 – Spectral norm estimation for each block of H_m (HMFIE) on a range of frequencies for the PLANE (logarithmic scale).

.

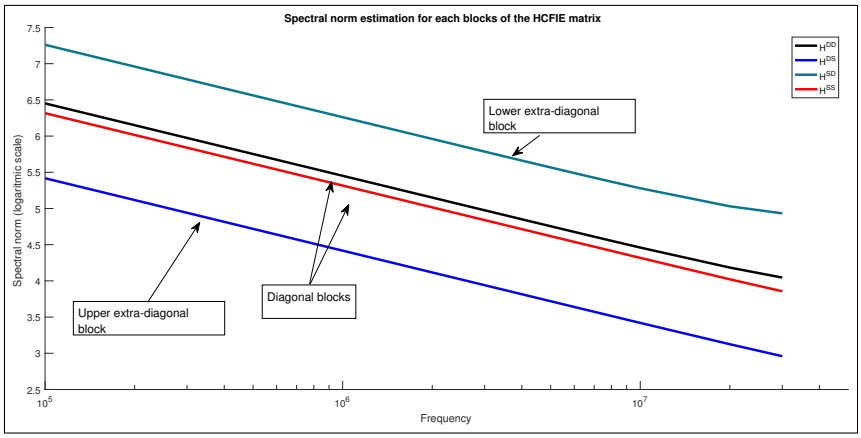

Figure 4.7 – Spectral norm estimation for each block of H_c (HCFIE) on a range of frequencies for the PLANE (logarithmic scale).

.

. Consequences

The conclusion of this study, is that through the norm of the different blocks of the matrix, we observe a strong coupling between the divergent and the solenoidal parts of the pseudo-current, which is clearly expressed by the large norm of the lower or upper extra-diagonal matrix blocks. This strong coupling is quite annoying since it does not allow us to use a reduced system or a Schur complement system to obtain a first estimation of the vector solution. In fact, if we try to solve the Schur complement system

$$S_e J^D = \left(H^{DD} - H^{DS}(H^{SS})^{-1}H^{SD}\right) J^D = C^D \tag{4.19}$$

with a Krylov method, such as GMRES, we observe that the method does not converge and nearly reaches the maximal number of iteration (even using the inverse of H^{DD} to precondition the system). Globally, it is not possible to neglect the interaction between the divergent and the solenoidal part of the pseudo-current.

4.3.2 The choice of cycles and its influence on norm estimates

The HEFIE, as the HMFIE and the HCFIE are defined using the Helmholtz decomposition of the space of pseudo-currents. In the previous chapter, we presented different way to construct the loop functions and formalized this decomposition. For different reasons, we chose a method based on the study of the face-edge graph of the mesh. We also noted that as soon as we get a first basis of loop functions, it was possible to get any other basis, since the linear combination of two loop functions is still a loop function.
In this section, we want to show that the choice of loop functions can have an impact on the norm of the different blocks of the Galerkin matrix.
Let us consider a 2×2 block matrix $\tilde{H}$, representing a generic Galerkin matrix, and a decomposition matrix D_H of the following form:

$$\tilde{H} = \begin{pmatrix} \tilde{H}_{11} & \tilde{H}_{12} \\ \tilde{H}_{21} & \tilde{H}_{22} \end{pmatrix}, \tag{4.20}$$

$$D_H = \begin{pmatrix} \mathbf{I}_\mathrm{d} & 0 \\ C & D \end{pmatrix} \quad \text{and} \quad D_H^{-1} = \begin{pmatrix} \mathbf{I}_\mathrm{d} & 0 \\ -D^{-1}C & D^{-1} \end{pmatrix}. \tag{4.21}$$

The product of $D_H \tilde{H} D_H^{-1}$ gives:

$$D_H \tilde{H} D_H^{-1} = \begin{pmatrix} \tilde{H}_{11} - \tilde{H}_{12} D^{-1} C & \tilde{H}_{12} D^{-1} \\ C\tilde{H}_{11} + D\tilde{H}_{21} - (C\tilde{H}_{12} + D\tilde{H}_{22}) D^{-1} C & (C\tilde{H}_{12} + D\tilde{H}_{22}) D^{-1} \end{pmatrix}. \tag{4.22}$$

In the particular case where D is the identity matrix, the product gives:

$$D_H \tilde{H} D_H^{-1} = \begin{pmatrix} \tilde{H}_{11} - \tilde{H}_{12} C & \tilde{H}_{12} \\ C\tilde{H}_{11} + \tilde{H}_{21} - (C\tilde{H}_{12} + \tilde{H}_{22}) C & (C\tilde{H}_{12} + \tilde{H}_{22}) \end{pmatrix}. \tag{4.23}$$

These explicit representations show the role of C and D in the various blocks. To illustrate the influence of the choice of the loop functions, we compare three methods to build the loop functions and the decomposition matrix. Starting from the one we presented in the previous chapter, we call "standard", and with which we obtained results in the previous sub-section, we can build two other decomposition matrices.

- The first can be built through an orthogonalization of the loop functions. Typically, we re-use the standard cycles and we orthogonalize them to make an independent basis. This can be easily done by using a modified Gram-Schmidt orthogonalization method (GSM) on the sub-matrix $[S \ \mathbf{I}_\mathrm{d}]$, i.e., on the last lines of the matrix D_H represented in Figure 3.9. The result can be related to the matrix we could obtain after solving the system (3.46) presented as an alternative method.

- The second one can also be built on previously computed cycles. The idea is, this time, to reduce as much as possible the size of the cycles to only keep "elementary" cycles (around vertices to simplify). This procedure can also directly be performed using the coefficients of the decomposition matrix and looks like a Gram-Schmidt method working on $\mathbb{Z}^1 = \{-1, 0, +1\}$. We call this procedure GSZ in reference to it.

We are not going to give the full implementation of these two procedures, but we show what it looks like on a few cycles in Figure 4.8. Just note that these procedures have a strong effect on the matrix D_H. In the case of the GSM procedure, we have for D a lower triangular matrix and an almost full matrix for C. In the case of the GSZ procedure, we have two really sparse matrices for D and C. For these two cases, the inverse is no longer trivial to compute and requires more attention. To illustrate this, we present in Figure 4.9 the shape of the three decomposition matrices for the mesh of the sphere: the standard, the GSM and the GSZ matrix.

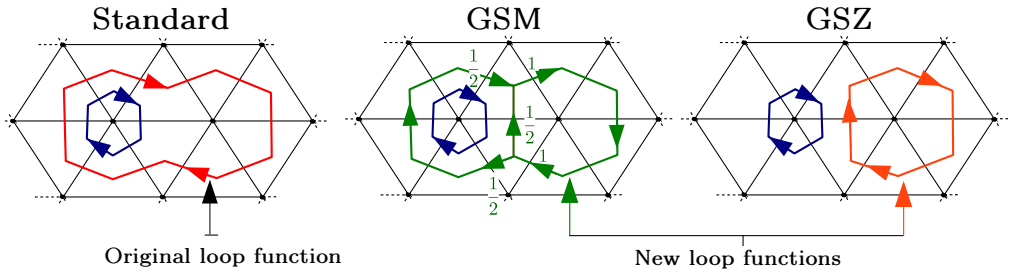

Figure 4.8 – Visualization of the new loop functions considered with the GSM and the GSZ algorithm.

.

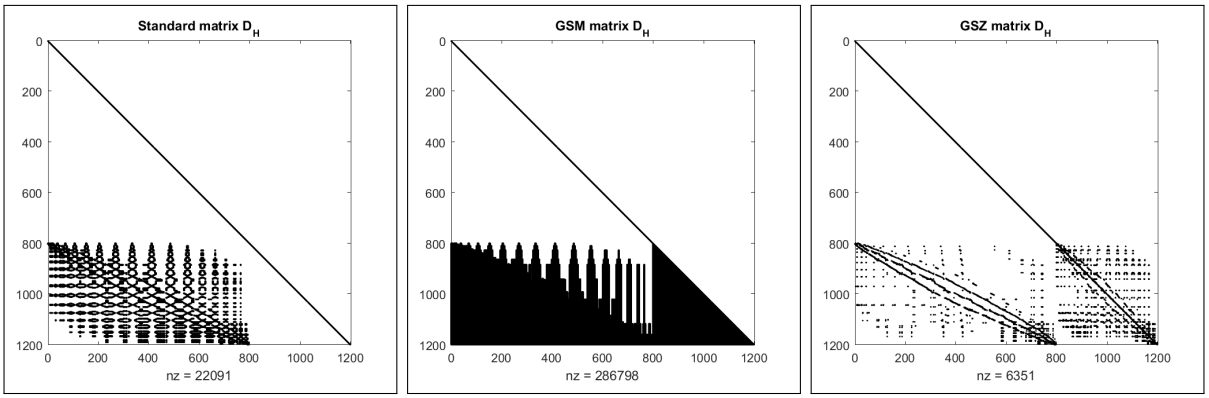

Figure 4.9 – Representation of the non-zero coefficient of the different matrix D_H considered for the sphere mesh. From the left to the right : the standard D_H matrix, the GSM D_H matrix and the GSZ D_H matrix. For each matrix, the number of non-zero coefficients is indicated.

. The norms with the GSM and GSZ decomposition matrices

To finish, we present the norms of the different blocks of the matrices using either GSM or GSZ D_H matrix.
Let us begin with the GSM decomposition matrix. If we look at the norms of the different blocks presented in the Figures 4.10, 4.11 and 4.12, we can observe many differences with the standard decomposition matrix. First we can observe that with this decomposition matrix, the norms of the upper blocks are quite the same as the norm of the lower blocks, meaning that $\|H^{DD}\| \simeq \|H^{DS}\|$ and $\|H^{SD}\| \simeq \|H^{SS}\|$. We then remark that the norms of the upper blocks are always larger than the norms of the lower blocks. We also note that the ratio remains constant for the lowest frequencies whereas the ratio tends to decrease at the highest frequencies.
The effect of the GSZ matrix is simpler to describe. As we can see in Figures 4.13, 4.14 and 4.15, the behaviour of the GSZ D_H matrix is the same as the standard D_H matrix. Basically, the only thing that changes, is the ratio between the different norms. The dynamic still unchanged.

The concluding remark of this short study is that the choice of the loop function basis is important since it clearly has an impact on the norm of the final matrix and possibly leads to different solution methods. In cases where we are interested in only either J^D or J^S, we emphasize hat the choice of the loop functions can greatly modify the ratio between the norms of the diagonal and extra-diagonal blocks. Therefore, it is possible that a right choice of preconditioner and loop function construction leads to a system where the norm of the extra-diagonal blocks are weak enough to work on two separate sub-systems. Therefore, in the rest of this chapter, we continue to identify the components J^D and J^S to remind of this possibility.

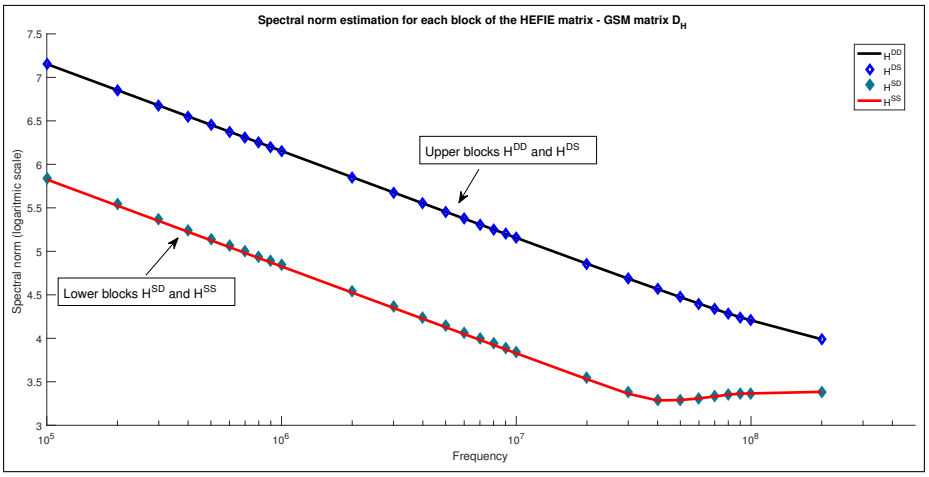

Figure 4.10 – Spectral norm estimation for each block of H_e (HEFIE) on a range of frequencies for the SPHERE using the GSM decomposition matrix (logarithmic scale).

.

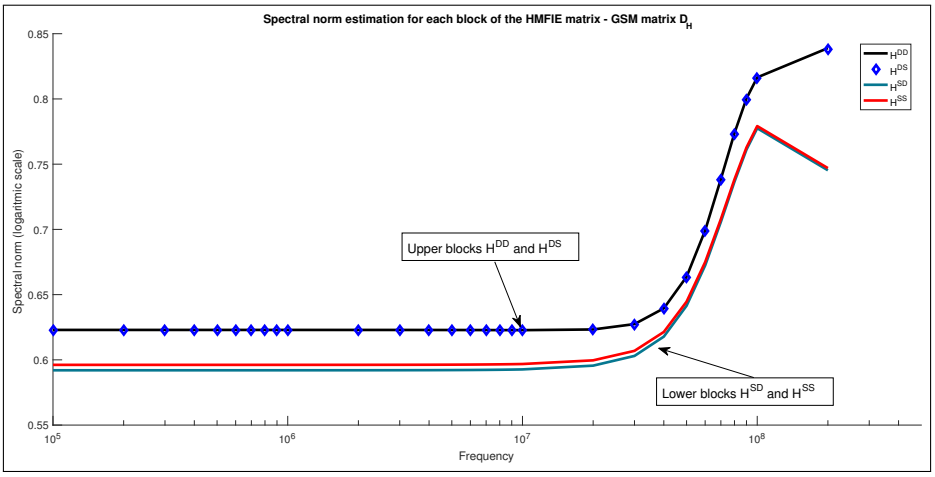

Figure 4.11 – Spectral norm estimation for each block of H_m (HMFIE) on a range of frequencies for the SPHERE using the GSM decomposition matrix (logarithmic scale).

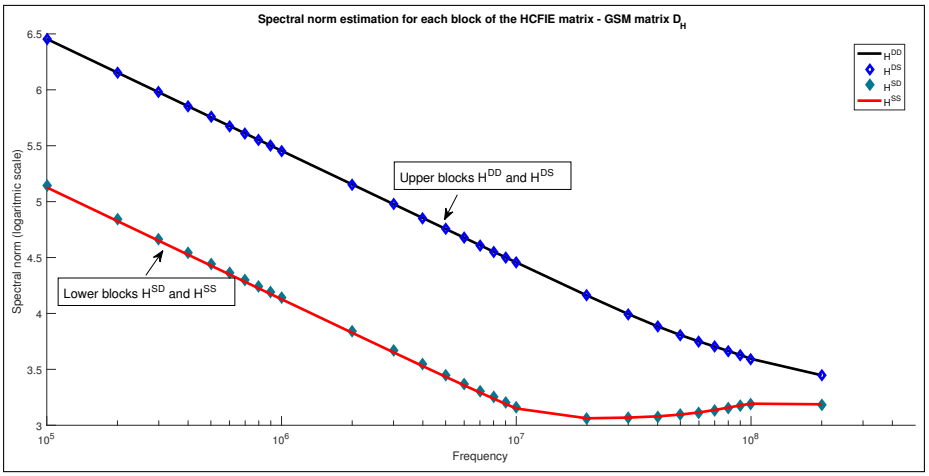

Figure 4.12 – Spectral norm estimation for each block of H_c (HCFIE) on a range of frequencies for the SPHERE using the GSM decomposition matrix (logarithmic scale).

.

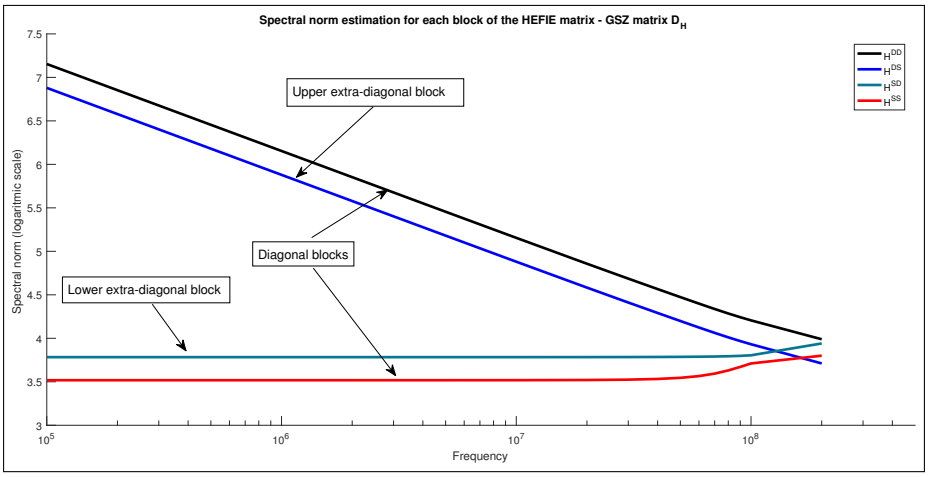

Figure 4.13 – Spectral norm estimation for each block of H_e (HEFIE) on a range of frequencies for the SPHERE using the GSZ decomposition matrix (logarithmic scale).

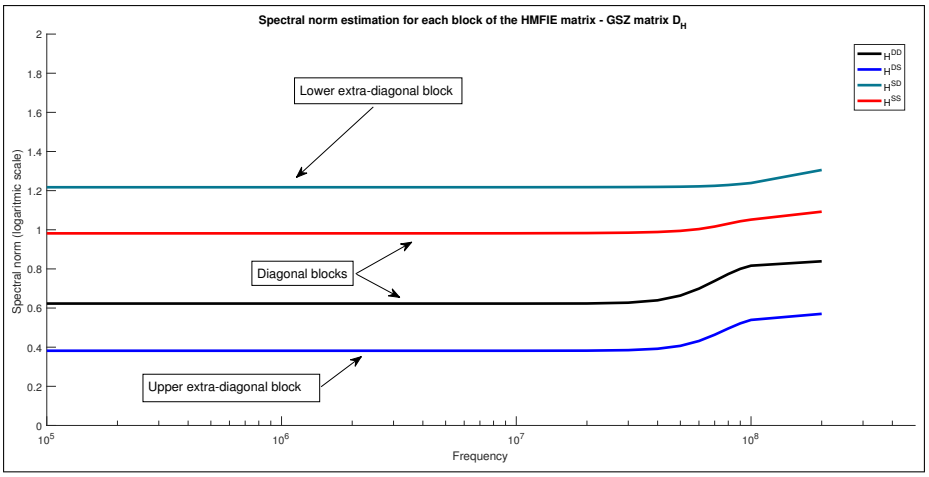

Figure 4.14 – Spectral norm estimation for each block of H_m (HMFIE) on a range of frequencies for the SPHERE using the GSZ decomposition matrix (logarithmic scale).

.

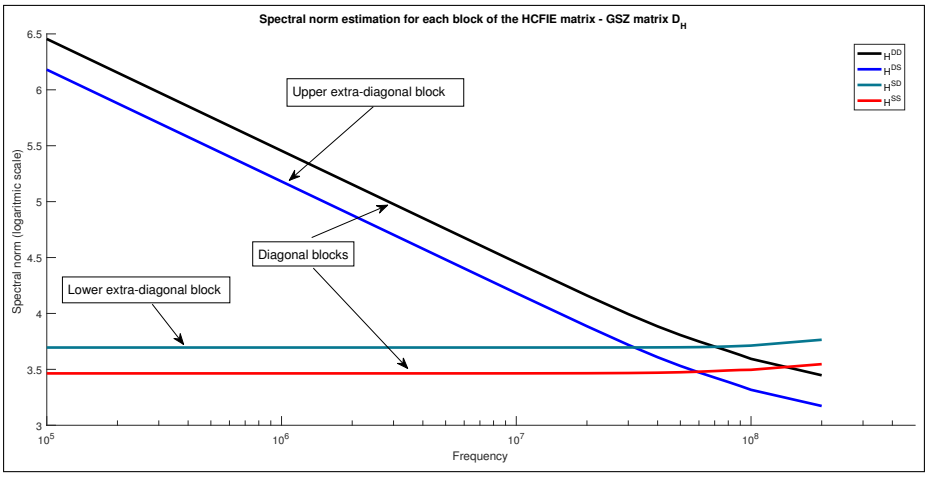

Figure 4.15 – Spectral norm estimation for each block of H_c (HCFIE) on a range of frequencies for the SPHERE using the GSZ decomposition matrix (logarithmic scale).

.

4.4 Computational cost and preconditioning

4.4.1 Computational cost

After detailing the computation of the matrix K (and, therefore, of the matrix $\tilde{H}$) in the previous chapter and before describing the preconditioners being able to facilitate the resolution, we analyse the computational costs of these different elements.

. Assembly cost of the matrix $K_e/\tilde{H}_e$

Let us begin with the computational cost of the matrix K or $\tilde{H}$ (a good implementation will not necessary make the choice of computing K separately from E). For this, suppose that we have a first implementation of the assembly of the matrix E on the basis of edge finite elements. This one requires, for each couple of function $\{\mathbf{J}, \mathbf{J}^{'}\}$, the evaluation of the following integrals:

$$\mathbf{E}(\mathbf{J}, \mathbf{J}^{'}) = \zeta \iint\limits_{\Gamma\times\Gamma} G_{x,y}\, \mathbf{J}^{'}_x \cdot \mathbf{J}_y \, dxy - \frac{1}{\eta} \iint\limits_{\Gamma\times\Gamma} G_{x,y}\, \nabla_{\mathrm{s}} \cdot \mathbf{J}^{'}_x \, \nabla_{\mathrm{s}} \cdot \mathbf{J}_y \, dxdy. \tag{4.24}$$

The assembly of the matrix E can then be achieved by decomposing the double integral over $\Gamma \times \Gamma$ into a double sum over the triangles of the mesh:

$$\mathbf{E}(\mathbf{J}, \mathbf{J}^{'}) = \sum_{T_1} \sum_{T_2} \zeta \iint\limits_{T_1\times T_2} G_{x,y}\, \mathbf{J}^{'}_x \cdot \mathbf{J}_y \, dxdy - \frac{1}{\eta} \iint\limits_{T_1\times T_2} G_{x,y}\, \nabla_{\mathrm{s}} \cdot \mathbf{J}^{'}_x \, \nabla_{\mathrm{s}} \cdot \mathbf{J}_y \, dxdy. \tag{4.25}$$

For T_1 distinct from T_2, the integrals can be achieved numerically by using a Gauss points integration method

$$T_1 \neq T_2,\ \mathbf{E}(\mathbf{J}, \mathbf{J}^{'}) = \sum_{T_1} \sum_{T_2} \sum_{x\in\mathscr{G}_{T_1}} \sum_{y\in\mathscr{G}_{T_2}} \zeta\omega_x\omega_y G_{x,y}\, \mathbf{J}^{'}_x \cdot \mathbf{J}_y - \frac{1}{\eta}\omega_x\omega_y G_{x,y}\, \nabla_{\mathrm{s}} \cdot \mathbf{J}^{'}_x \, \nabla_{\mathrm{s}} \cdot \mathbf{J}_y \tag{4.26}$$

where ω_x and ω_y denote the weight coefficients of the Gauss integration. Considering that the support of $\mathbf{J}$ and $\mathbf{J}^{'}$ is limited to two triangles, an implementation of the assembly of the EFIE matrix could look like the Algorithm 1 (the case $T_1 = T_2$ not included).

Algorithm 1 Assembly of the EFIE matrix

```
for T1 = 1..F do
    for T2 = 1..F, T1 ≠ T2 do
        for i = 1..3 do                          ▷ –Loop over the edge functions defined on T1–
            for j = 1..3 do                      ▷ –Loop over the edge functions defined on T2–
                A = 0,
                Φ = 0,
                for x ∈ G_T1 do                  ▷ –Loop over the Gauss points of T1–
                    A_x = 0,
                    for y ∈ G_T2 do              ▷ –Loop over the Gauss points of T2–
                        A_x += ω_y ω_x J_y G_{x,y},
                        Φ += ω_y ω_x G_{x,y},
                A += J'_x A_x,
            Pos_i := position of the function J'_i in the finite element space,
            Pos_j := position of the function J_j in the finite element space,
            E[Pos_i][Pos_j] += ζA − (1/η)Φ
```

Now if we want to implement the HEFIE, we have to compute for each couple of edge functions $\{\mathbf{J}, \mathbf{J}^{'}\}$ the following integrals:

$$\begin{aligned}\mathbf{H}(\mathbf{J},\mathbf{J}') = \quad & \zeta \iint G_{x,y}\bar{\psi}_x\psi_y\, \mathbf{J}'_x\cdot \mathbf{J}_y\, dxdy \\ & - \frac{1}{\eta}\iint G_{x,y}\bar{\psi}_x\psi_y\, \nabla_{\mathrm{s}}\cdot \mathbf{J}'_x\, \nabla_{\mathrm{s}}\cdot \mathbf{J}_y\, dxdy \\ & - \frac{\kappa^2}{\eta}\iint \mathbf{J}'_x \left[G_{x,y}\bar{\psi}_x\psi_y\theta^T\theta\right]\mathbf{J}_y\, dxdy \\ & + \frac{i\kappa}{\eta}\int \theta\cdot\mathbf{J}'_x \int G_{x,y}\bar{\psi}\psi\, \nabla_{\mathrm{s}}\cdot\mathbf{J}_y\, dydx - \frac{i\kappa}{\eta}\int \nabla_{\mathrm{s}}\cdot\mathbf{J}'_x \int G_{x,y}\bar{\psi}_x\psi_y\theta\cdot\mathbf{J}_y\, dydx, \\ = \zeta\bar{A}(\mathbf{J},\mathbf{J}') & - \frac{1}{\eta}\bar{\Phi}(\mathbf{J},\mathbf{J}') - \frac{\kappa^2}{\eta}B(\mathbf{J},\mathbf{J}') + \frac{i\kappa}{\eta}R(\mathbf{J},\mathbf{J}')\,.\end{aligned} \tag{4.27}$$

Algorithm 2 Assembly of the HEFIE matrix

for $T_1 = 1..F$ **do**
  for $T_2 = 1..F$, $T_1 \neq T_2$ **do**
    for $i = 1..3$ **do** ▷ –Loop over the edge functions defined on T_1–
      for $j = 1..3$ **do** ▷ –Loop over the edge functions defined on T_2–
        $\bar{A} = 0$,
        $\bar{\Phi} = 0$,
        $B = 0$,
        $R = 0$,
        for $x \in \mathscr{G}_{T_1}$ **do** ▷ –Loop over the Gauss points of T_1–
          $\bar{A}_x = 0$,
          $R_x = 0$,
          for $y \in \mathscr{G}_{T_2}$ **do** ▷ –Loop over the Gauss points of T_2–
            $G_{x,y} = G_{x,y}\bar{\psi}(x)\psi(y)$,
            $\mathrm{var}_1 = \omega_y\omega_x G_{x,y}$,
            $\bar{A}_x \mathrel{+}= \omega_y\omega_x\, \mathbf{J}_y\, G_{x,y}$,
            $\bar{\Phi} \mathrel{+}= \mathrm{var}_1$,
            $R_x \mathrel{+}= \mathrm{var}_1$,
          $\bar{A} \mathrel{+}= \mathbf{J}^{'}_x\, A_x$,
          $B \mathrel{+}= \mathbf{J}^{'}_x\, \theta^T\theta A_x$,
          $R \mathrel{+}= \theta\cdot\mathbf{J}^{'}_x\, R_x + \theta\cdot A_x$,
        Pos_i := position of the function $\mathbf{J}^{'}_i$ in the finite element space,
        Pos_j := position of the function $\mathbf{J}_j$ in the finite element space,
        $E[\mathrm{Pos}_i][\mathrm{Pos}_j] \mathrel{+}= \zeta\bar{A} - \frac{1}{\eta}\bar{\Phi} - \frac{\kappa^2}{\eta}B + \frac{i\kappa}{\eta}R$,

Globally, we find more or less the same terms in the calculation of the matrix E and $\tilde{H}$. In the following developments, we denote by complex operations the conventional elementary operations $(+, -, \times, /)$ between complex variables. We present here an upper bound for the additional costs, refinements and optimization tips that can easily be made.

- The first step is to replace the Green kernel $G_{x,y}$ by

$$G_{x,y}\bar{\psi}_x\psi_y = \frac{e^{i\kappa\|x-y\|+i\kappa\theta\cdot(x-y)}}{4\pi\|x-y\|}. \tag{4.28}$$

This operation (cf Algorithm 2, line 13), correctly implemented, can be achieved in 8 complex operations: 6 for the inner product, $\theta \cdot (x - y)$ and 1 for the addition of $\|x - y\|$ and $\theta \cdot (x - y)$.

- The second step is to get the partial sum for R_x (cf. Algorithm 2, line 18) already computed for the need of $\bar{\Phi}$. We only need 1 complex operation.

- The computation of B and R, lines 20 and 21, requires 13 complex operations each (two inner products and some additions/multiplications).

- To finish, the final summation, line 24, requires 8 more complex operations.

Finally, without considering the computation of the diagonal which has a linear cost, summing all the supplementary costs, i.e., the costs not already included by the assembly of the matrix E, we find that the assembly of the matrix $\tilde{H}$ requires $81N_G^2F^2 + 243N_GF^2 + 24F^2$ complex additional operations where N_G denotes the number of Gauss points used in the integration and F the number of faces of the mesh.
In our application and considering our own experiment, it appears that the integrals are regular enough to be computed with three Gauss points per triangle. However, in the Table 4.1, we present the additional cost as a function of the number of Gauss point considered.

N_G	Additional cost	
3	$\sim 1482F^2$	$\sim 659N^2$
7	$\sim 5694F^2$	$\sim 2531\ N^2$

Table 4.1 – Additional cost for the computation of the matrix $\tilde{H}_e$ (F: number of faces, N: number of internal edges, N_G: number of Gauss points considered).

We can compare these costs to a number of GMRES iterations, by noting that, for example, a computational cost of $659N^2$ corresponds to 330 GMRES iterations.

. Assembly cost of the matrix K_m/H_m

To conclude this subsection, we evaluate the additional cost of the computation of the HMFIE matrix. As we wrote in the previous chapter, the perturbation has only one term:

$$\mathbf{K}_m(\mathbf{J}, \mathbf{J}') = \iint_{\Gamma\times\Gamma} \left(\bar{\psi}(x)\psi(y) - 1\right) \mathbf{J}'(x) \cdot (\mathbf{n}(x) \wedge (\nabla_y G(x, y) \wedge \mathbf{J}(y)))\, dxdy\,. \tag{4.29}$$

Moreover, it appears that this perturbation is completely regular and that there is no diagonal term in the K_m matrix. Finally, when we move from the MFIE to the HMFIE, the implementation is quite easy since it is sufficient to integrate $\bar{\psi}_x\psi_y$ in the computation of the Green kernel. The additional cost is then $81N_G^2F^2$ (see Table 4.2).

N_G	Additional cost	
3	$\sim 729\ F^2$	$\sim 324\ N^2$
7	$\sim 3969\ F^2$	$\sim 1764\ N^2$

Table 4.2 – Additional cost for the computation of the matrix $\tilde{H}_m$ (F: number of faces, N: number of internal edges).

4.4.2 Preconditioning

After establishing the different linear systems from Herberthson's equations, we naturally address their solution. Globally, if the HMFIE and HCFIE systems are relatively easy to solve, meaning that their solution by GMRES requires only a small number of iterations, the HEFIE system appeared more difficult to solve.
In our idea to get a linear system easier to solve than the conventional EFIE system, we focused our efforts on finding an effective preconditioner for the HEFIE. Therefore, we have explored some conventional tracks. Many of them have been proved to be useless or ineffective. We will not show in this chapter all the method we tested, it would be long and tedious. So we decide to present some tracks considered and indicate which ones are promising and the ones that could be potentially interesting, but need further developments.

. Definition of a good preconditioner

Consider the linear system to solve:

$$Hx = b. \tag{4.30}$$

The convergence of iterative Krylov methods, like GMRES, mostly dependent on spectral properties of the matrix H, in particular the distribution of its eigenvalues that are generally not known. A widely used technique, relying on so-called preconditioning, consists of replacing the linear system to be solved by an equivalent system $HM^{-1}y = b$ with $y = Mx$ where the matrix M has to be chosen such that

- the HM^{-1} is "closer" to the identity matrix than H,
- linear systems involving M are easy to solve (without computing explicitly M^{-1}),
- the matrix M is easy to compute.

We call M a right preconditioner to the system. Left or left and right preconditioning are also possible, but will not be used in this chapter. A good preconditioner is a matrix M that respects the above criteria and that eventually leads to a quicker solution of the linear system.

. Global preconditioning

The first idea is the use of conventional preconditioners such as Jacobi, Gauss-Seidel, Successive Over Relaxation method (SOR) or Symmetric Successive Over Relaxation method (SSOR). Let H the matrix to precondition. Assume that H can be decomposed as $H = D - E - F$ where D, E and F are respectively diagonal, strictly lower and strictly upper triangular. We then define the following conventional preconditioners:

- **Jacobi**: $M = D$,
- **Gauss-Seidel**: $M = D - E$ or $M = D - F$,
- **SOR**: $M = D/\omega - E$ or $M = D/\omega - F$ where ω is a parameter such that $0 < \omega < 2$,
- **SSOR**: $M = (D/\omega - F)D^{-1}(D/\omega - E)$.

Basically, none of these preconditioners works. In fact, each of them either greatly increases the number of iterations or sets the problem in a such configuration that GMRES cannot converge. We also tested some strategies, such for example **Sparse Approximate Inverse** preconditioning (see [67]). It could lead to some good preconditioners, but further developments are still required to confirm it.

. Local preconditioning

Noting the ineffectiveness of the preconditioners described above, we proposed to explore other tracks. Therefore, we attempted to build preconditioners not from the matrix H, but from the matrix $\tilde{H}$. Indeed, if one has a preconditioner for $\tilde{H}$, it is relatively easy to construct a preconditioner for the matrix $H = D_H P \tilde{H} P^{-1} D_H^{-1}$ by formally multiplying it by $D_H P$ on the left and by $P^{-1} D_H^{-1}$ on the right. This idea revealed to be the good one in a number of cases as we shall see later.
Therefore, we have constructed various "local" preconditioners. The term local refers to the fact that this preconditioner are build from the Galerkin matrix of the integral equations (and by the fact are preconditioner to the Galerkin matrix, up to the multiplication by D_H/D_H^{-1}) and not on the matrix obtained after using the Helmholtz decomposition. Assume that $\tilde{H}_p = P\tilde{H}P^{-1}$ can be decomposed as $\tilde{H}_p = \tilde{D} - \tilde{E} - \tilde{F}$ where $\tilde{D}$, $\tilde{E}$ and $\tilde{F}$ are respectively diagonal, strictly lower and upper triangular, we investigate the different preconditioners:

- **Jacobi**: $M = D_H \tilde{D} D_H^{-1}$,
- **Gauss-Seidel** : $M = D_H \left(\tilde{D} - \tilde{E}\right) D_H^{-1}$ or $M = D_H \left(\tilde{D} - \tilde{F}\right) D_H^{-1}$,
- **SOR**: $M = D_H \left(\tilde{D}/\omega - \tilde{E}\right) D_H^{-1}$ or
  $M = D_H \left(\tilde{D}/\omega - \tilde{F}\right) D_H^{-1}$ where ω is a parameter such that $0 < \omega < 2$,
- **SSOR**: $M = D_H(\tilde{D}/\omega - \tilde{F})\tilde{D}^{-1}(\tilde{D}/\omega - \tilde{E})D_H^{-1}$.

In a first approach, it can be quite unnatural to work on $P\tilde{H}P^{-1}$ since we shall not assemble the matrix. But in a clever implementation, the re-ordering should be integrated as a pre-processing, i.e., before to compute the matrix $\tilde{H}$, making this one implicit. Without any assumptions, we can also consider that the matrix $\tilde{H}_p$ has the following form:

$$\tilde{H}_p = \begin{pmatrix} \tilde{H}_p^{11} & \tilde{H}_p^{12} \\ \tilde{H}_p^{21} & \tilde{H}_p^{22} \end{pmatrix} \tag{4.31}$$

where the size of each block corresponds to those of H. Therefore, we also propose to introduce two other less conventional preconditioners:

- **Inverse block**:
$$M = D_H \begin{pmatrix} \tilde{H}_p^{11} & 0 \\ 0 & \tilde{H}_p^{22} \end{pmatrix} D_H^{-1}, \tag{4.32}$$
- **Schur block**:
$$M = D_H \begin{pmatrix} \tilde{H}_p^{11} - \tilde{H}_p^{12}(\tilde{H}_p^{22})^{-1}\tilde{H}_p^{21} & 0 \\ 0 & \tilde{H}_p^{22} \end{pmatrix} D_H^{-1}. \tag{4.33}$$

The originality of these last two formulations is to introduce at each iteration a solution close to the full solution. In a further development, in regard to their costs, it will be necessary to use a fast and sparse approximation of them.

. Costs

Globally, we observe that these new preconditioners work better than their counterpart in the global approach. If the Gauss-Seidel, the SOR and the SSOR do not reduce the number of iterations required to get the solution, the tree others (Jacobi, Inverse blocks and Schur blocks) work pretty well in the sense that they reduce the number of iterations in GMRES. However, the number of GMRES iteration is not the only criterion to consider in order to asses the validity of a preconditioner, there is also the CPU cost.
Basically, the multiplication by the matrix D_H has a complexity in $O(nnz(D_H))$ complex floating point operation where $nnz(D_H)$ denotes the number of non zero elements of D_H. We note that the inverse matrix D_H^{-1} is also a sparse matrix when we consider the standard and the GSZ algorithm. For GSM matrix D_H, this assertion can be wrong. Then, if we want to use the preconditioner defined above, we have to consider that

$$HM^{-1} = \left(D_H \tilde{H} D_H^{-1}\right)\left(D_H \tilde{M} D_H^{-1}\right)^{-1} = D_H \tilde{H} \tilde{M}^{-1} D_H^{-1}\,. \tag{4.34}$$

Therefore, at each iteration, in addition to the cost of the kernel of the preconditioner, we have to consider only two sparse matrix-matrix multiplications. To summarize, we display in Table 4.3 the cost of one iteration for the three preconditioner that we have considered.

Table 4.3 – Cost of the different preconditioners at each iteration of GMRES

Preconditioner	Cost at each iteration	Description	Option
Jacobi	$O(N)$	Multiplication by a diagonal matrix and the multiplication by D_H and D_H^{-1}	
Block inverse	$\sim\ O(\frac{2}{9}N^3)$	Resolution of two linear system with respective sizes of (2/3)N and (1/3)N and the multiplication by D_H and D_H^{-1}	Use GMRES to solve the linear systems
Block Schur	$O(N^3)$	Resolution of two linear systems with respective size (2/3)N and (1/3)N, one containing an inverse matrix, and the multiplication by D_H and D_H^{-1}	Use GMRES to solve the linear systems

4.5 Solution of the linear systems

In this last section, we present results obtained in the context of the solution of the different linear systems, namely the HEFIE, the HMFIE and the HCFIE, for the sphere and the airplane. We also give some results to illustrate the influence of the choice of the cycles on the solution of the different systems for the case of the sphere.

4.5.1 The sphere

We begin with the case of the diffraction of a plane wave by a PEC sphere (see Section 4.1 for more details). We consider the three linear problems, i.e., the HEFIE, the HMFIE and the HCFIE and we look at the number of iterations required to obtain a solution with the GMRES solver.

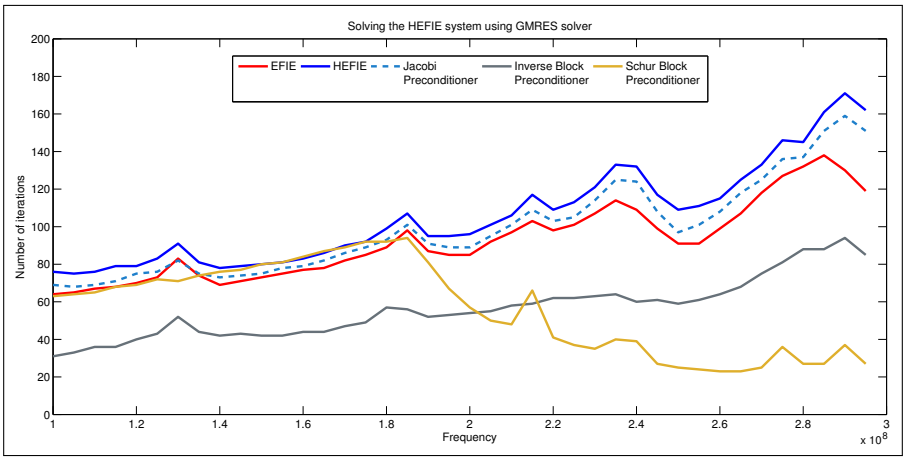

Figure 4.16 – Number of iterations required to attain a residual error of 10^{-4}, as function of the frequency for the EFIE system and the HEFIE system (preconditioned or not) for the SPHERE.

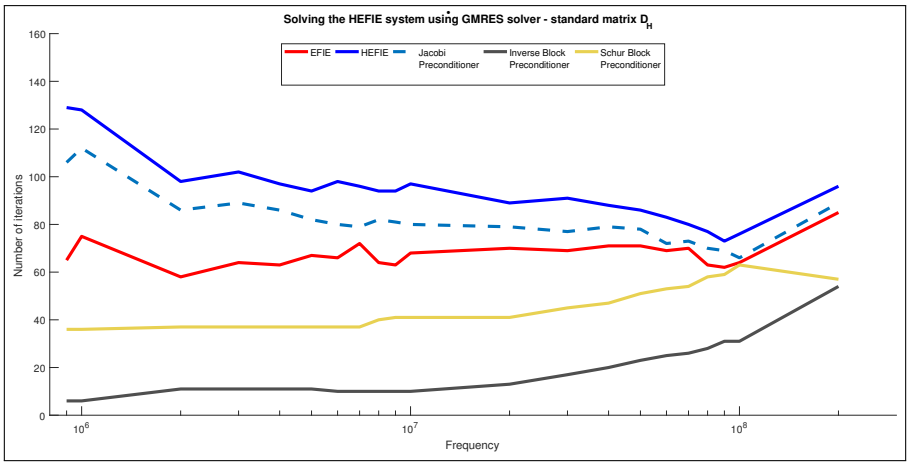

Figure 4.17 – Number of iterations required to attain a residual error of 10^{-4}, as function of the frequency for the EFIE system and the HEFIE system (preconditioned or not) for the SPHERE.

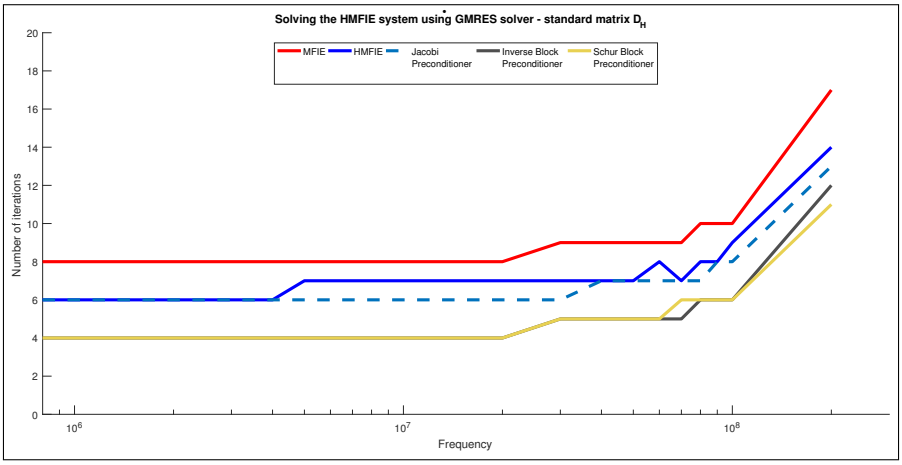

Figure 4.18 – Number of iterations required to attain a residual error of 10^{-4}, as function of the frequency for the MFIE system and the HMFIE system (preconditioned or not) for the SPHERE.

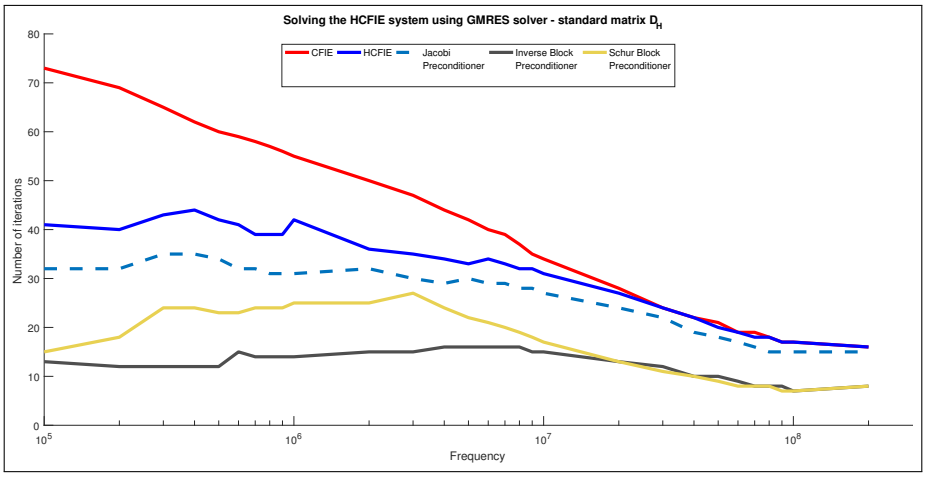

Figure 4.19 – Number of iterations required to attain a residual error of 10^{-4}, as function of the frequency for the CFIE system and the HCFIE system (preconditioned or not) for the SPHERE.

.

When we observe the different results, we note that in the case of the sphere, the EFIE and the HEFIE systems are quite similar in term of difficulties. Indeed, for both systems, see Figures 4.16 and 4.17, GMRES needs about the same number of iterations in order to reach the solution. It also turns out that the HEFIE is always a little more difficult to solve than the EFIE and that the Jacobi preconditioner is inefficient. The two other preconditioners, namely the Inverse Block and the Schur Block preconditioners, give an interesting result in term of number of iterations, but considering the additional costs they generate at each iteration, even using an iterative method for the solution of each sub-system, they do not constitute practicable preconditioners. When we look at the Figures 4.18 and 4.19, we observe the same thing. If the the two others systems, the MFIE/HMFIE and the CFIE/HCFIE, are clearly easier to solve, the Herberthson formulation does not bring any advantage in term of number of iterations. Furthermore, the three preconditioners give absolutely no advantage as they even do not significantly reduce the number of iterations.

4.5.2 The airplane

We continue with a larger geometry: the diffraction of a plane wave by a PEC airplane (see Section 4.1 for more details). Once again, we consider the three linear problems, i.e., the HEFIE, the HMFIE and the HCFIE and we look at the number of iterations required to obtain a solution with the GMRES solver.

When we observe the results presented in Figures 4.20, 4.21 and 4.22, we note that in that case, Herberthson's versions are easier to solve than their conventional counterpart. Notably, when we look at the number of iterations required to solve the HEFIE system, we observe that the HEFIE requires less iterations than the conventional EFIE, but also that the preconditioners described above have a huge beneficial impact on the number of iterations. If the Inverse and the Schur blocks remain costly, the Jacobi really improves the convergence for the HEFIE as for the HMFIE and the HCFIE. Moreover, if we sum up the different costs, it appears that obtaining the solution with the combination "HEFIE+Jacobi" costs a little less than with the EFIE.

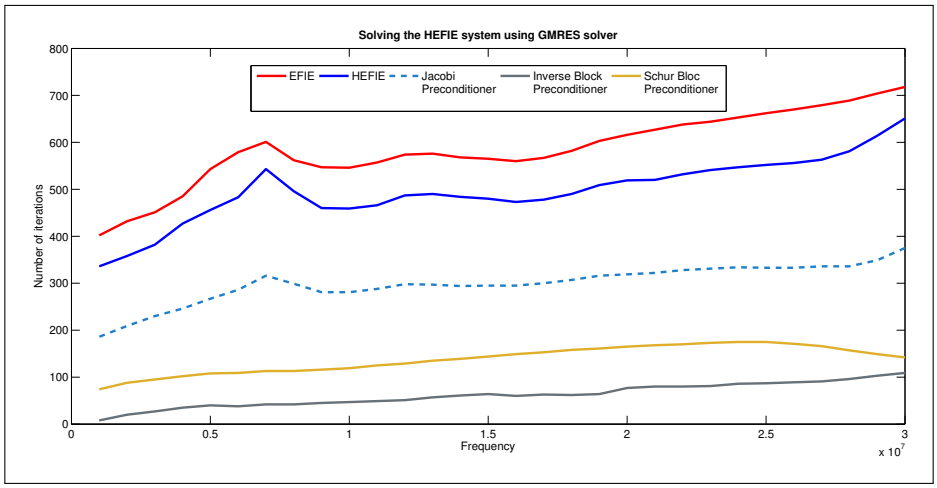

Figure 4.20 – Number of iterations required to attain a residual error of 10^{-4}, as function of the frequency for the EFIE system and the HEFIE system (preconditioned or not) for the PLANE.

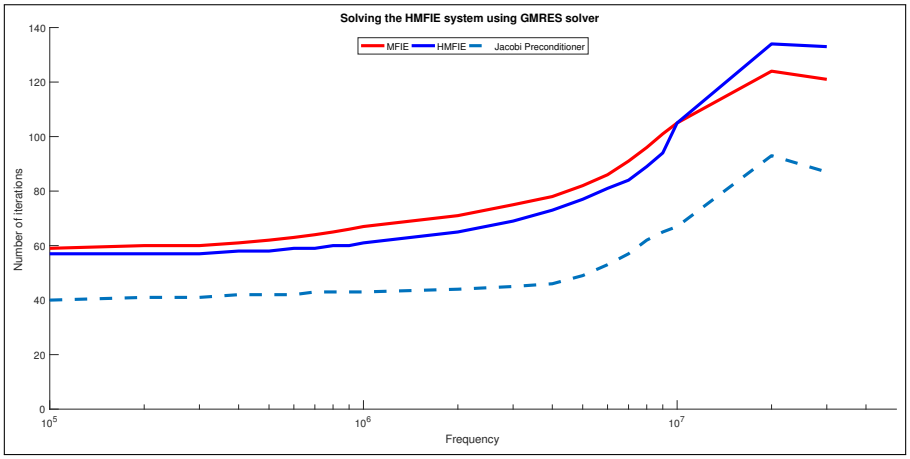

Figure 4.21 – Number of iterations required to attain a residual error of 10^{-4}, as function of the frequency for the MFIE system and the HMFIE system (preconditioned or not) for the PLANE.

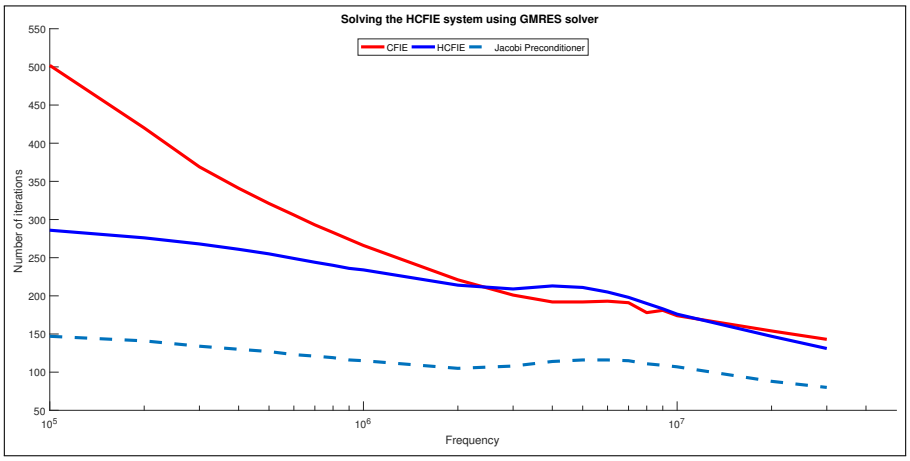

Figure 4.22 – Number of iterations required to attain a residual error of 10^{-4}, as function of the frequency for the CFIE system and the HCFIE system (preconditioned or not) for the PLANE.

.

4.5.3 Influence of the choice of the cycles

To complete this study, we want to present briefly the impact that the choice of the loop function basis can have on the solution. For this purpose, we give in Figures 4.23 and 4.24 the results obtained for HEFIE for the sphere. Basically, in regard to the figures below and our experiment, we observe only a very tiny influence on the considered preconditioners.
In fact, on this example, the impact of the choice of the loop function is not really as marked as it was on the norms of the operator. This could be explain by the fact that our solution methods are not very sensitive to the norms of the different blocks.

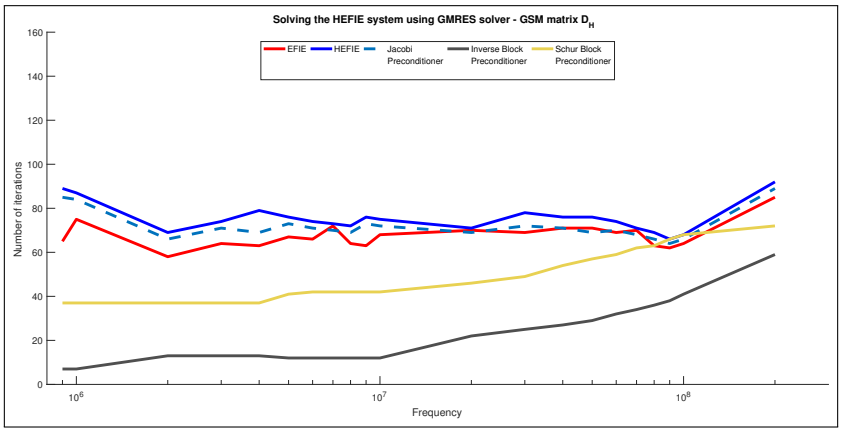

Figure 4.23 – Number of iterations required to attain a residual error of 10^{-4}, as function of the frequency for the EFIE system and the HEFIE system (preconditioned or not) for the SPHERE using the GSM method to build the loop functions.

.

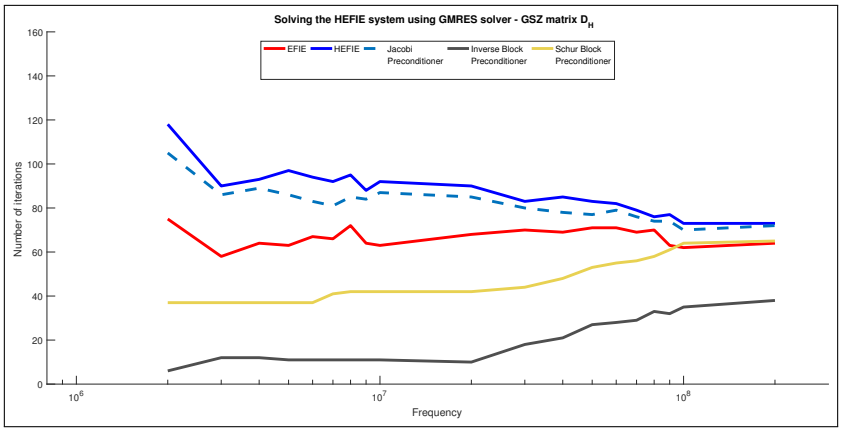

Figure 4.24 – Number of iterations required to attain a residual error of 10^{-4}, as function of the frequency for the EFIE system and the HEFIE system (preconditioned or not) for the SPHERE using the GSZ method to build the loop functions.

.

Concluding remarks

In this chapter, we wanted to establish some properties of the Galerkin matrices obtained from the Herberthson integral equations (the HEFIE, HMFIE and HCFIE) and highlight some elements on the solution of the associated linear systems.

First, considering the 2×2 blocks structure of the matrices and the shape of the right-hand sides, we study the norms of the different blocks of each matrix. The subsequent idea was to decide whether we could get either the divergent or the solenoidal part of the current using a Schur complement method. The non-possibility to use such a method was highlighted notably through the study of the interactions between divergent and solenoid parts of the current described by the norms of the different blocks of each matrix. Indeed, we observed a strong coupling between the divergent and the solenoidal parts of the pseudo-current, expressed by large norm of the extra-diagonal matrix blocks, that did not allow us to get either the divergent or the solenoidal part independently from the other.

Then, we considered various solution methods. To establish the background, we first detailed the additional costs imply by the construction of the Galerkin matrices in order to estimate the number of iterations to earn to balance the cost of the construction. These estimations are to be considered as a maximal costs and can pretend to be significantly reduced in future development using an acceleration or compression method like FMM [7] or ACA technique [10]. Then, we present the different preconditioners (and their costs) we built in order to facilitate the solution of the various linear systems.

To finish, we present results obtained for the different linear systems, the HEFIE as the HMFIE and the HCFIE, for the sphere and the airplane. We observed that in the case of the sphere, the various linear systems are quite similar in term of difficulties, i.e., for both systems GMRES need about the same number of iterations in order to reach the solution. It also turned out that the different preconditioners was inefficient in this configuration. Then, in the case of an airplane, we noted that the Herberthson versions were easier to solve than their conventional counterpart. We notably observed that the HEFIE requires less iterations than the EFIE and that the preconditioners described have a huge beneficial impact on the number of iterations. Summing up the different costs, it appears that the combination of the HEFIE and the developed Jacobi preconditioner cost a little less than the conventional EFIE and that the other preconditioners required to be approximated (with for example a sparse structure) to be costly efficient.

Chapter 5

Reduction of the number of degrees of freedom

Contents

In the previous chapters, we presented, the construction (Chapter 3) and the solution (Chapter 4) of the various linear systems arising from Herberthson's modified equations. Apart from the analysis of linear systems and their solution, we are interested in another important property provided by Herberthson's equations: the possibility to reduce the number of degrees of freedom required to get an accurate solution of the problem.
Considering the conventional equations and the diffraction of a plane wave with a frequency f_0, a good approximation of the surface current requires the edges of the mesh to have a maximum size, h, smaller than, say, $\lambda_0/7$. Therefore, working with a pseudo-current, it seems interesting to see whether the HEFIE suffers from the same constraint. First, to test this and illustrate some properties already noted by Zhou for his own formulation, we study the quality of the current obtained from the HEFIE with meshes conforming and non-conforming to this constraint. In order to get a good solution in terms of surface current, we show that it is necessary to work on a fine mesh. However, as the size of the associated linear system increases, it is useful to look for an alternative to the linear system obtained for a fine mesh. Therefore, our objective is to create a linear system with a size as small as possible that can give a good quality solution.
The idea is then to consider two meshes: a coarse mesh adapted for the representation of the pseudo-current but not necessarily conforming to the rule of $h < \lambda/7$ and a fine mesh conforming

to that constraint being twice finer than the coarse mesh. Noting that the interactions between local currents defined on the coarse mesh were poorly described, we propose to compute the Galerkin coefficients of the coarse mesh matrix by using the integration rules associated to the fine mesh. Therefore, by establishing a link between each edge function on the coarse mesh and the edge functions of the fine mesh as a well chosen linear combination, each coefficient of our coarsened or reduced Galerkin matrix can be seen as a linear combination of the coefficients of the matrix obtained for the fine mesh.
After building our reduced system for the EFIE and having validated its well behaviour by showing a good correspondence between the coarse system (matrices, right-hand side and solution) and the reduced system for lower frequencies and a better solution in terms of current and RCS for the highest frequencies (not as good as the EFIE on the fine mesh but better than the EFIE/HEFIE on the coarse mesh), we consider the reduced system for the HEFIE in terms of quality of the current solution, computational cost and number of GMRES iterations. Then in order to reduce the computational cost, we propose a new alternative reduced system by computing the perturbation part separately.
To finish, we present some perspectives about the treatment of multi-incidence scattering coefficients. With a conventional EFIE one can apply solution techniques for linear systems with multiple right-hand sides. As the HEFIE operator itself depends on the incidence direction, each new incidence direction changes the entire linear system. We show that the separate computation of the perturbation operator presents an interesting perspective and makes the HEFIE an interesting alternative even for multi-incidence computations.

5.1 Motivations and objectives

. Motivations

In Chapter 2, by presenting the equations proposed by Herberthson, we justified their existence and use, arguing that, since they were working on a pseudo-current, a priori less oscillating than the physical one, it would potentially lead to some systems easier to solve.

It appears from the results presented in Chapter 3 that the associated linear systems are not necessarily easier to solve than the conventional ones. Indeed, considering for example the sphere, we observed that for the same mesh, we needed a larger number of iterations in GMRES to solve the HEFIE system than the EFIE system. To overcome this difficulty, we built different preconditioners, considered different configurations and analysed the impact of the choice of loop functions. In this chapter, we decide to work on the mesh to improve the HEFIE solution.

Considering the conventional equations and the diffraction of a plane wave with a frequency f_0, we can show that to obtain a good approximation of the surface current, the edges of the mesh must have a length smaller than $\lambda_0/7$ (or $\lambda_0/10$ regarding the situations). As with the Herberthson integral equations, we are looking for a pseudo-current $\bar{\psi} j_S$, which is less oscillating than the physical current j_S, as we can see in Figures 5.1, 5.2 and 5.3, it seems interesting to study whether this constraint on the length of the edge can be released. In other words, we examine the possibility to get a current distribution as good as the solution obtained with the conventional method, but with a smaller number of degrees of freedom.

. Objectives

Therefore, the first objective of this chapter is to explore and make the most of this possibility. Specifically, if a maximum edge length ℓ is required to have good representation of the physical current j_S with the EFIE, we want to know whether a maximum edge length of 2ℓ allows for a

good approximation of $\bar{\psi} j_S$ (and hence of j_S) with the HEFIE.
For this purpose, in a first approach, we consider two meshes: a coarse mesh (with N edges) adapted for all the frequencies $f < f_0$ and a fine mesh (with $4N$ edges) adapted for all the range of frequencies considered (at least for $f \leq 2f_0$). On each mesh, we test both the EFIE and the HEFIE and compare the quality of the computed current. The underlying objective is to illustrate that, if the EFIE suffers of a mesh not adapted to the representation of the physical current and also of bad integration, the HEFIE only suffers of bad integrations when considering the coarse mesh.
We then introduce two other linear systems: a reduced EFIE system and a reduced HEFIE system, built from the fine mesh. We expect from this new HEFIE linear system to have all the good properties of both coarse and fine systems: the size of the coarse system and the quality of the fine one in term of solution. Finally, we propose a new formulation of this latter linear system in order to reduce the global computational cost and the part of H dependent of the incidence direction.

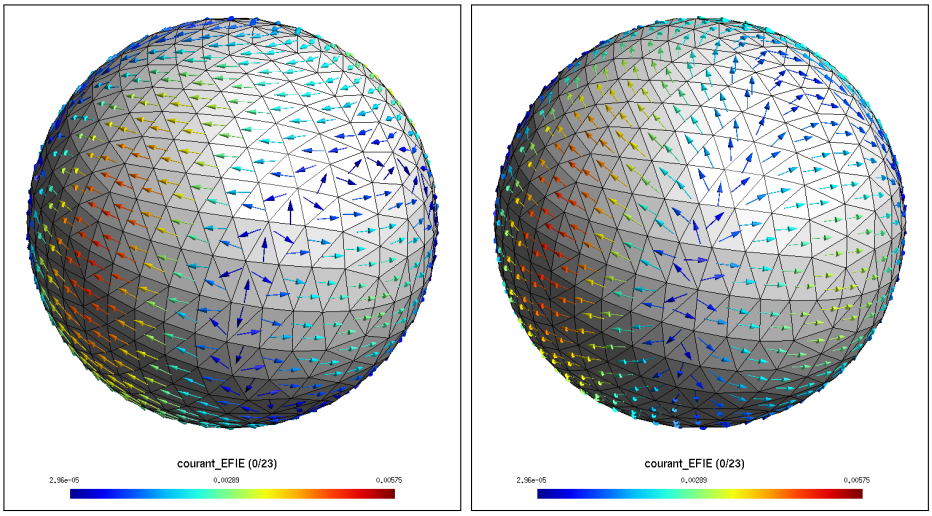

Figure 5.1 – Representation of the physical current on the sphere at 100MHz. (LEFT: illuminated face, RIGHT: non illuminated face)

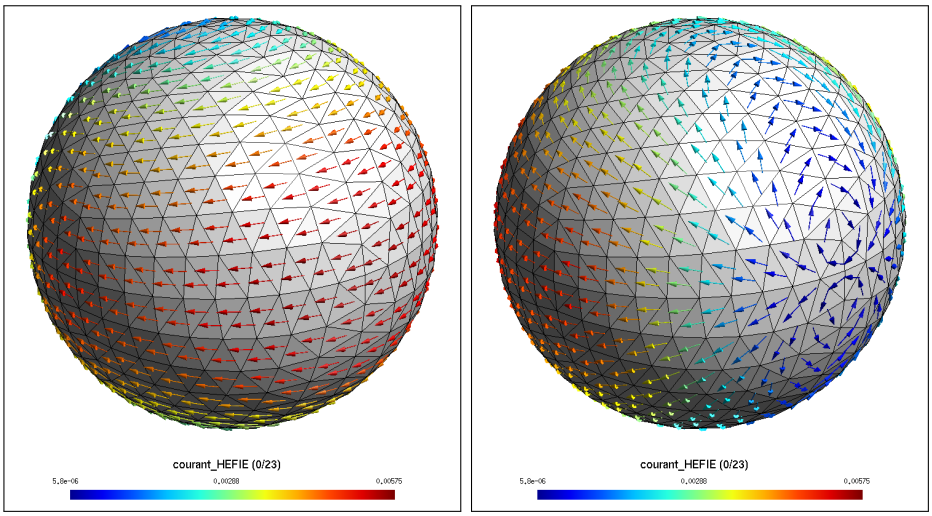

Figure 5.2 – Representation of the pseudo-current on the sphere at 100MHz. (LEFT: illuminated face, RIGHT: non illuminated face)

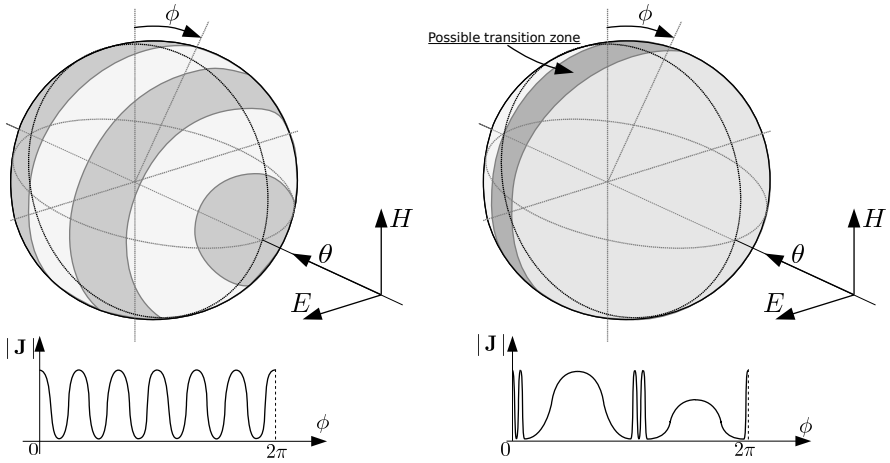

Figure 5.3 – Symbolic representation of oscillations for both the physical current (on the left) and the pseudo-current (on the right).

5.2 Frequency dependent limit on the mesh size for the HEFIE

In this subsection, our objective is to test the limits of the HEFIE and highlight the various constraints related to the mesh we must respect. For this, we consider the scattering problem of a plane wave by the sphere presented and detailed in Section 4.1.

5.2.1 Known limits for the EFIE

To begin, we consider two meshes: a coarse mesh and a fine mesh. Considering a scattering object and range of frequencies $[f_{\min}\ ;\ f_{\max}]$, we can encounter two configurations. Following the context.

- Either we have a definition of the geometry and a well-adapted fine mesh that respects the constraints imposed by the frequency range considered (as represented on the left in Figure 5.4),

- or we have only a coarse mesh corresponding coarsely to the geometry of the object that respects the imposed constraint only for frequencies lower than a frequency f_0 such $f_{\min} < f_0 < f_{\max}$ (as represented on the right in Figure 5.4).

Rigorously, to compute the current with the EFIE for a frequency larger than f_0, we have to work on the fine mesh. However, regarding the costs in terms of computational time and memory space, it would be interesting to work on the coarser mesh in order to work with a smaller linear system and thus reduce the cost.
The general idea is to make match and coexist these two meshes (without necessarily building them in practice) to benefit from the advantages of each of them. For practical reasons, in order to keep our study simple, we start with the coarse mesh from which we build the fine mesh. The reverse situation, i.e., build the coarse mesh from the fine mesh is also possible, but requires further developments and a more complex analysis of the mesh. In future developments, it should be the latter one that should be privileged.

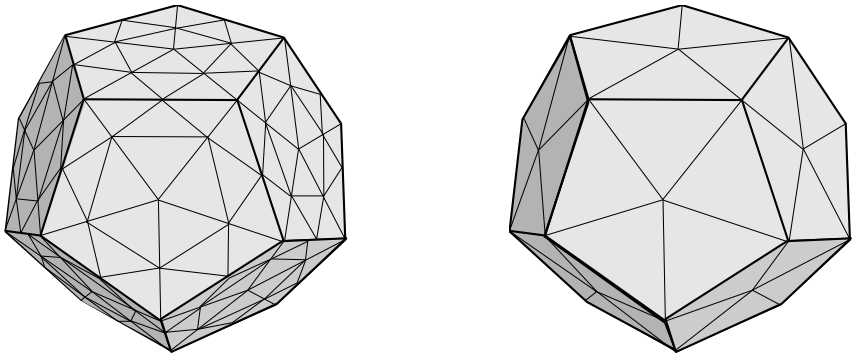

Figure 5.4 – On the left, the required mesh to work at $f > f_0$. On the right, the mesh on which we could expect to work with the HEFIE at $f > f_0$.

5.2.2 Example of a mesh refinement

The first step is then to build a refinement of the coarse mesh, which will be our fine mesh. For this, we chose a special method to refine the mesh. We decide to cut each triangle (or face) of the mesh into four small triangles. For practical reasons, we chose to split each edge into two equal parts by introducing a point in the middle of each edge of the coarse mesh as shown in Figure 5.5. Therefore, starting from a coarse mesh with e edges and f faces, we end up with a finer mesh with $4e$ edges and $4f$ faces (namely, $2e + 3f$ edges by building and taking into account that for the mesh of a genus-0 object $3f = 2e$, we obtain a total of $4e$ edges).

We chose this method for practical reasons. More precisely, we split every edge into two equal parts in order to represent every edge function on the coarse mesh as a very simple linear combination of edge functions on the fine mesh. Note that, in this chapter, we consider the polytope of the coarse mesh to define the true geometry. Latter in a second approach, we could consider other forms of refining and consider a projection method in order to fit the new points to the actual surface of the scattering object.

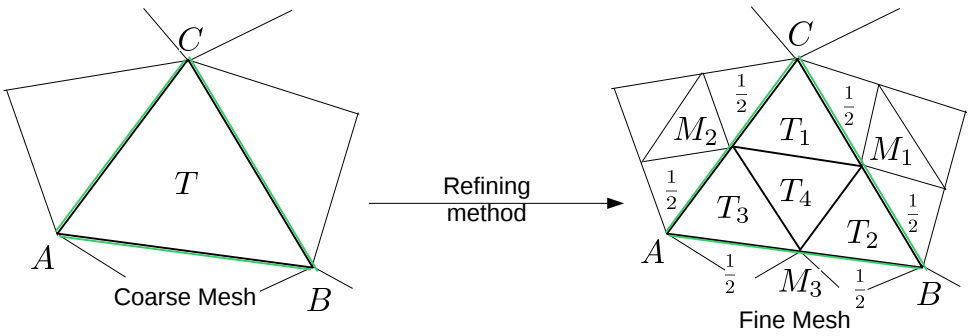

Figure 5.5 – Construction of the fine mesh.

5.2.3 The limits of the HEFIE

After creating the fine mesh, we can observe the quality of the surface current, solution of either the EFIE or the HEFIE on the coarse and the fine mesh. Basically, the idea is to see if the HEFIE must comply with the same constraint as the EFIE. In other words, we want to know if the rule of $\ell < \lambda/7$ (or $\ell < \lambda/10$) is still the same for the HEFIE than for the conventional EFIE. For this, we consider the sphere we used in Section 4.1 as our coarse mesh, mesh well adapted for all frequencies $f < f_0 = 1.6\ 10^8$Hz with a characteristic edge length lower than

$\lambda_0/10$, and look, for a range of frequencies, at the errors observed on the current and on the RCS coefficients.

. How we evaluate the errors

To evaluate these errors, we choose to evaluate the current at the centre of gravity of each face of the fine mesh, i.e., at four points for each face of the coarse mesh (see Figure 5.6). From the evaluation of the surface current, taking the EFIE solution on the fine mesh as reference, we compute a global relative error (in 2-norm) and report it in Figure 5.7. We also consider the errors on the RCS coefficients. For this, we evaluate the RCS coefficients in a large number of directions and report the relative error (in 2-norm) between the reference solution (obtained from the EFIE on the fine mesh) and the computed solution in Figure 5.8.

. Discussion

Looking at Figures 5.7 and 5.8, we observe that HEFIE is subject to the same constraint as the conventional EFIE. Indeed, we notice that for frequencies higher than $f_0 = 1.6\ 10^8$Hz, the error on the surface current increases significantly for both solutions obtained from the coarse mesh while the error remains low for the HEFIE solution obtained from the fine mesh. Therefore if we want to benefit of the regularity of the pseudo current to reduce the number of degrees of freedom, it seems necessary to work on a finer mesh or at least on the linear system built from it.

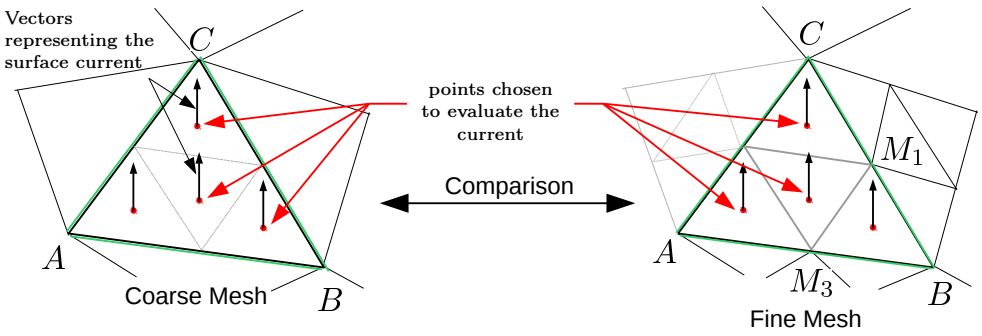

Figure 5.6 – Points chosen to evaluate the current on the coarse mesh and the fine mesh.

5.3 The macro-elements approach to order reduction

As seen above, the HEFIE suffers of the same constraints as the conventional EFIE, but for different reasons. For the EFIE, the coarse mesh presents two main defaults. First the mesh is not fine enough to correctly represent the oscillations of the physical current. Secondly, it does not allow for a correct integration of the Green function with the Gauss point method. The error we observe for the HEFIE can mainly be attributed to this last one. Indeed, if the mesh is adapted for the representation of the pseudo-current, the Green function still badly represented. In order to get a good solution in terms of surface current, it is necessary to work on a finer mesh. However, as the size of the associated linear system increases, it seems useful to look for an alternative to this linear system obtained from this mesh. The objective is to have a linear system with the same size as the one obtained from the coarse mesh and that would give the same solution quality than the fine system. The purpose of this section, and of this chapter as

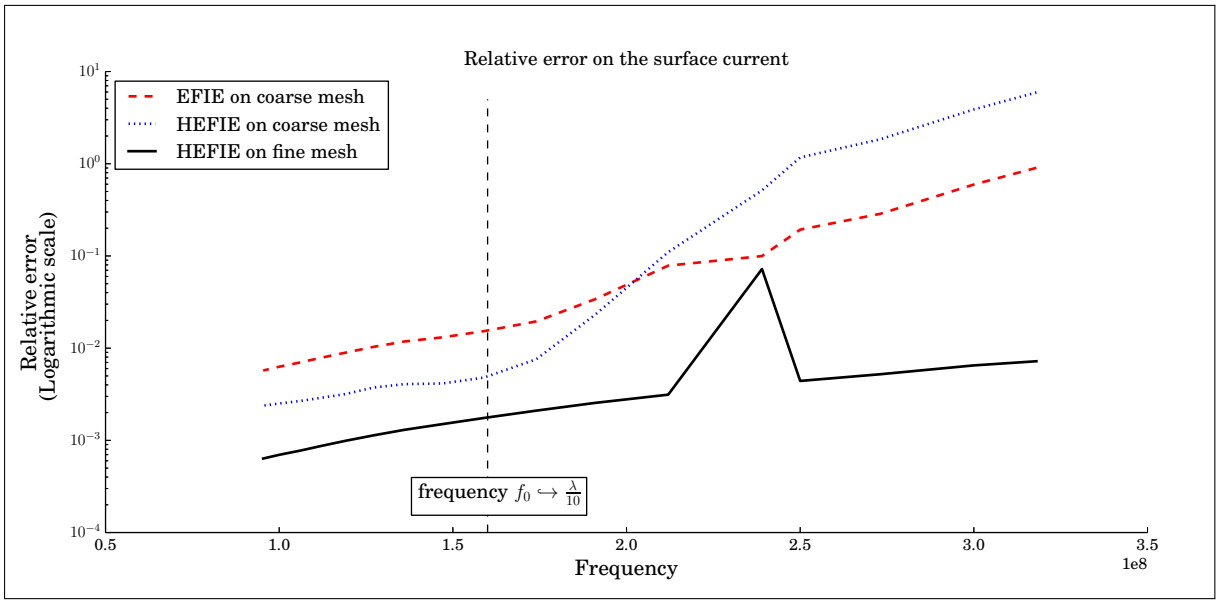

Figure 5.7 – Evolution of the relative error on the surface current for each system proposed (EFIE/HEFIE on the coarse mesh or on the fine mesh).

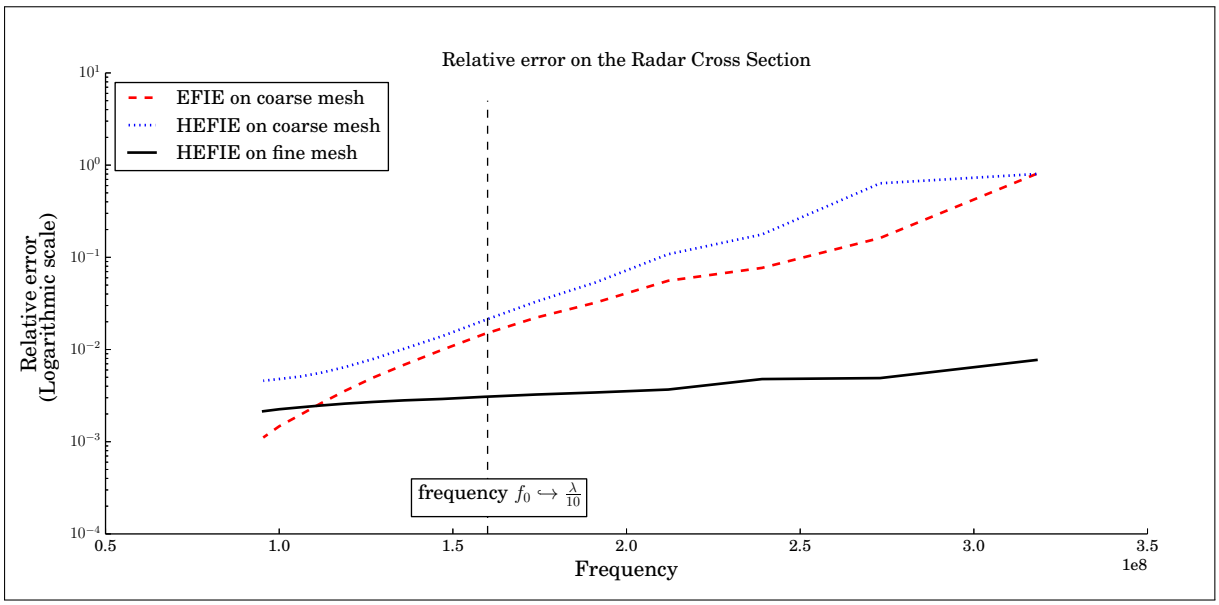

Figure 5.8 – Evolution of the relative error on the Radar Cross Section for each system proposed (EFIE/HEFIE on the coarse mesh or on the fine mesh).

a whole, is to design a linear system that meets both criteria.
The starting point is to note that the interactions between local currents defined on the coarse mesh are poorly described. A solution is to represent the Galerkin coefficients of the coarse matrix by using the integration rules associated with the fine mesh (see [16, 17, 18]). Therefore the idea is to make a link between each edge function on the coarse mesh and edge functions of the fine mesh through a well chosen linear combination. Basically, each coefficient of our coarsened or reduced matrix can be seen as a linear combination of the coefficients of the matrix obtained for the fine mesh (see [68, 69]).

5.3.1 Construction of the macro-elements

The first step is then to find this linear combination, i.e., to find how to represent an edge element on the coarse mesh with edge functions on the fine mesh. This is where the choice of the refinement method is critical. Consider a triangle $T = \{A, B, C\}$ on the coarse mesh and its refinement $\{M_1, M_2, M_3\}$ as drawn in Figure 5.5. We want to represent the macro-element (or edge function) J_{AB} carried by AB and defined by

$$\forall x \in T,\ J_{AB}(x) = \frac{1}{2|T|}(C - x) \quad \text{and} \quad \int_A^B J_{AB}(x) \cdot \nu_{AB} dx = 1, \tag{5.1}$$

as a linear combination of functions of the fine mesh. The objective is to find $\{\alpha, \beta, \gamma, \delta, \epsilon\}$ such that

$$\forall x \in T,\ J_{AB}(x) = \alpha J_{M_1M_2}(x) + \beta J_{M_2M_3}(x) + \gamma J_{M_1M_3}(x) + \delta J_{AM_3}(x) + \epsilon J_{M_3B}(x), \tag{5.2}$$

where J_{XY} is the edge function carried by the edge XY.

For the sake of simplicity, we give to each edge function an orientation toward the point C (see Figures 5.5 and 5.9 for the notations). We have three internal edges M_1M_2, M_2M_3 and M_1M_3 and six external ones: AM_3, M_3B, BM_1, M_1C, CM_2 and M_2A

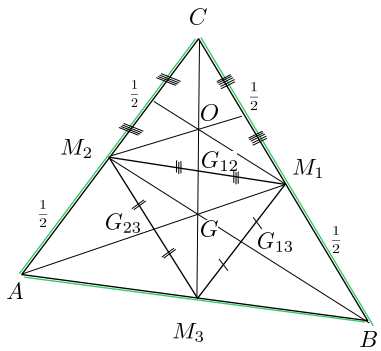

Figure 5.9 – Geometry of the problem.

First, we note that the contributions of the edge functions carried by AM_2, M_2C, CM_1 and M_1B to the macro-elements with degree of freedom on AB are necessarily zero. Indeed, since for $x \in AC$ or $x \in BC$ $J_{AB}(x)$ is tangent to the edges, i.e.,

$$\forall x \in AC,\ \exists c > 0,\ J_{AB}(x) = c\overrightarrow{AC} \ \text{ and } \ \forall x \in BC,\ \exists c > 0,\ J_{AB}(x) = \alpha\overrightarrow{BC}.$$

The edge functions carried by AM_2, M_2C, AC or BC give a distribution current toward B or A, thus their contribution are zero.

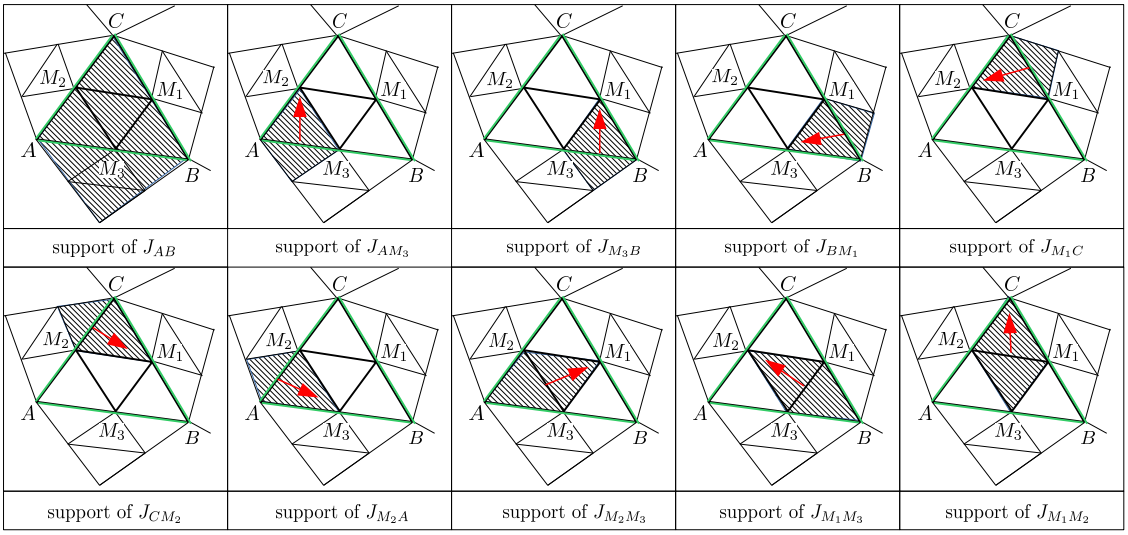

Figure 5.10 – Representation by shaded areas of the support of each edge function and their orientation by red arrows.

Therefore, the objective is to find the coefficient α, β, γ, δ and ϵ. We begin with δ and ϵ, the coefficients of respectively J_{AM_3} and J_{M_3B} (see Figure 5.10 for the support of each of them). Since the flow of J_{AB} through the edge AB is 1 and we have two small edges with the same length, to conserve the flow through AB, the contribution of these two "small" edge functions is necessarily $1/2$. This is the only edge functions able to define a non-zero flow through AB. Then, we have $\delta = \epsilon = 1/2$.
Then, we continue with the edge function carried by M_1M_2. Considering the triangle $T_1 = \{CM_2M_1\}$ (see Figure 5.10), the only edge function that contributes is $J_{M_1M_2}$. Therefore, if we take for example the point O, we can simply compare the areas of the triangles T and T_1 to find the required contribution. Indeed, in O, we have:

$$\frac{1}{2|T|}\overrightarrow{OC} = F_{AB}(O) = \alpha F_{M_1M_2}(O) = \frac{\alpha}{2|T_1|}\overrightarrow{OC}. \tag{5.3}$$

We deduce that $\alpha = 1/4$. Now if we consider the point G_{21}, the center of M_2M_1, we have three contributors: $J_{M_1M_2}$, $J_{M_2M_3}$ and $J_{M_1M_3}$. Thus, we have the following equality:

$$\begin{aligned} F_{AB}(G_{21}) &= \frac{1}{4}F_{M_1M_2}(G_{21}) + \beta F_{M_2M_3}(G_{21}) + \gamma F_{M_1M_3}(G_{21}), \\ \frac{1}{2|T|}\overrightarrow{G_{21}C} &= \frac{1}{8|T_1|}\overrightarrow{G_{21}C} + \beta\frac{1}{2|T_4|}\overrightarrow{G_{21}M_1} + \gamma\frac{1}{2|T_4|}\overrightarrow{G_{21}M_2}, \end{aligned}$$

i.e.,

$$\vec{0} = \beta\frac{1}{2|T_4|}\overrightarrow{G_{21}M_1} + \gamma\frac{1}{2|T_4|}\overrightarrow{G_{21}M_2} = \frac{\beta-\gamma}{2|T_4|}\overrightarrow{G_{21}M_1}. \tag{5.4}$$

We deduce that $\beta = \gamma$. To find the coefficient β, we can look at the current in G:

$$F_{AB}(G) = \frac{1}{4}F_{M_1M_2}(G) + \beta F_{M_2M_3}(G) + \beta F_{M_1M_3}(G), \tag{5.5}$$

$$\frac{1}{8|T_4|}\overrightarrow{GC} = \frac{1}{8|T_4|}\overrightarrow{M_3G} + \frac{\beta}{2|T_4|}\left(\overrightarrow{GM_1} + \overrightarrow{GM_2}\right), \tag{5.6}$$

$$\overrightarrow{GC} = \overrightarrow{M_3G} + 4\beta\left(\overrightarrow{GM_1} + \overrightarrow{GM_2}\right), \tag{5.7}$$

$$2\overrightarrow{M_3G} = \overrightarrow{M_3G} + 4\beta\overrightarrow{M_3G}, \tag{5.8}$$

$$\beta = \frac{1}{4}. \tag{5.9}$$

Finally, we obtain:

$$\forall x \in T,\ F_{AB}(x) = \frac{1}{4}F_{M_1M_2}(x) + \frac{1}{4}F_{M_2M_3}(x) + \frac{1}{4}F_{M_1M_3}(x) + \frac{1}{2}F_{AM_3}(x) + \frac{1}{2}F_{M_3B}(x). \tag{5.10}$$

A summary of all these developments can be found below in Figure 5.11.

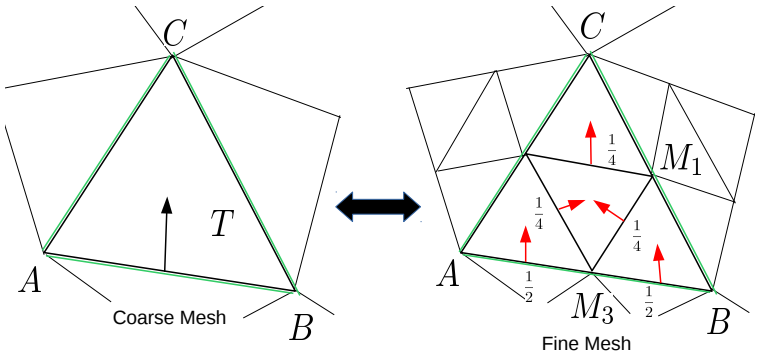

Figure 5.11 – Connection between edge functions defined on the coarse mesh and edge functions defined on the fine mesh

Therefore, we have a representation of any macro-elements defined on the coarse mesh, as a linear combination of eight edge elements defined on the fine mesh (two for each of the internal edges and two on the common edge). By extension, if we have a representation of the interactions between the current functions defined on the fine mesh, we can obtain a representation of the interactions between current functions defined on the coarse mesh through a simple linear combination. In practice this allows us, from an EFIE/HEFIE system built from the fine mesh to obtain a reduced system, with a smaller dimension, representing what should be an EFIE/HEFIE system computed for the coarse mesh.

In the examples below, we implement this coarsening (or reduction) with a restriction matrix R. In a future implementation, this projection must be integrated directly in the assembly of the matrix. Note that, from its definition, the matrix R, as we can see in Figure 5.12, is a sparse matrix with size $N \times 4N$ and only 8 coefficients on each row. The R matrix acts as a restriction from the five unknowns of the coarse ones, and R^T can be viewed as an interpolation going the other way around.
We define

$$E_{\text{RED}} = RE_{\text{FIN}}R^T \quad \text{and} \quad S_{\text{RED}} = RS_{\text{FIN}}, \tag{5.11}$$

$$H_{\text{RED}} = RH_{\text{FIN}}R^T \quad \text{and} \quad C_{\text{RED}} = RC_{\text{FIN}} \tag{5.12}$$

where E_{FIN} and H_{FIN} denote respectively the EFIE and HEFIE matrix built from the fine mesh and S_{FIN} and C_{FIN} their respective right-hand sides.

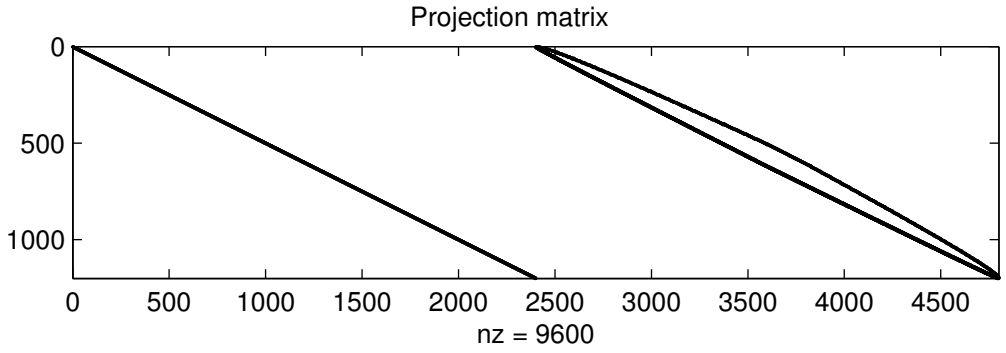

Figure 5.12 – The restriction (coarsening) matrix R for the sphere case defined in Section 4.1.

5.3.2 The EFIE reduced system

The first step before talking about the properties of the reduced HEFIE system is to validate the reduction method on the conventional EFIE system. To do this, we consider again the case of the sphere (see Section 4.1). First, we create the fine mesh, without projecting the new points on the sphere, and then we build the associated restriction matrix R. The idea then is to compare the three systems at our disposal (see Figure 5.13):

- the "coarse" system (COA): built directly from the coarse mesh,
- the "fine" system (FIN): built directly on the fine mesh and
- the "reduced" system (RED): built by coarsening/reduction from the fine system.

Then we observe the various objects at our disposal: the matrices E, the right-hand sides and the solutions of the different linear systems, but also the surface current and the Radar Cross Section.

In Figure 5.14, we display the relative error between the matrix, the right-hand side and the solution. We can observe that for "low frequencies", i.e., $f < 1.6\ 10^8$Hz (where the frequency f_0 corresponds to the maximum frequency we can consider with the coarse mesh), the coarse and reduced systems are very close to each other, in terms of both matrix, right-hand side and solution, since

$$\forall f < f_0,\ \frac{\|E_{\mathrm{COA}} - E_{\mathrm{RED}}\|_{INF}}{\|E_{\mathrm{COA}}\|_{INF}} \sim 10^{-2} \text{ and } \frac{\|S_{\mathrm{COA}} - S_{\mathrm{RED}}\|_2}{\|S_{\mathrm{COA}}\|_2} < 10^{-5}.$$

This suggests that we have properly built our projection (or coarsening) matrix R. For higher frequencies, we observe that the quantities associated with the coarse system move further away of the other two. Then, in Figure 5.15, the same thing is observed for the current: for "low" frequencies a fairly good correspondence is observed between the three computed currents, while for higher frequencies the current over the coarse system differs clearly from the other two, which results in different RCS figures as it can be seen in Figure 5.16. For higher frequencies ($f > f_0$), the relative error on the surface current begins to be important. We can explain this error by noting that if this new reduced system does not suffer of bad integrations, the mesh stills not adapted to the representation of the physical current.

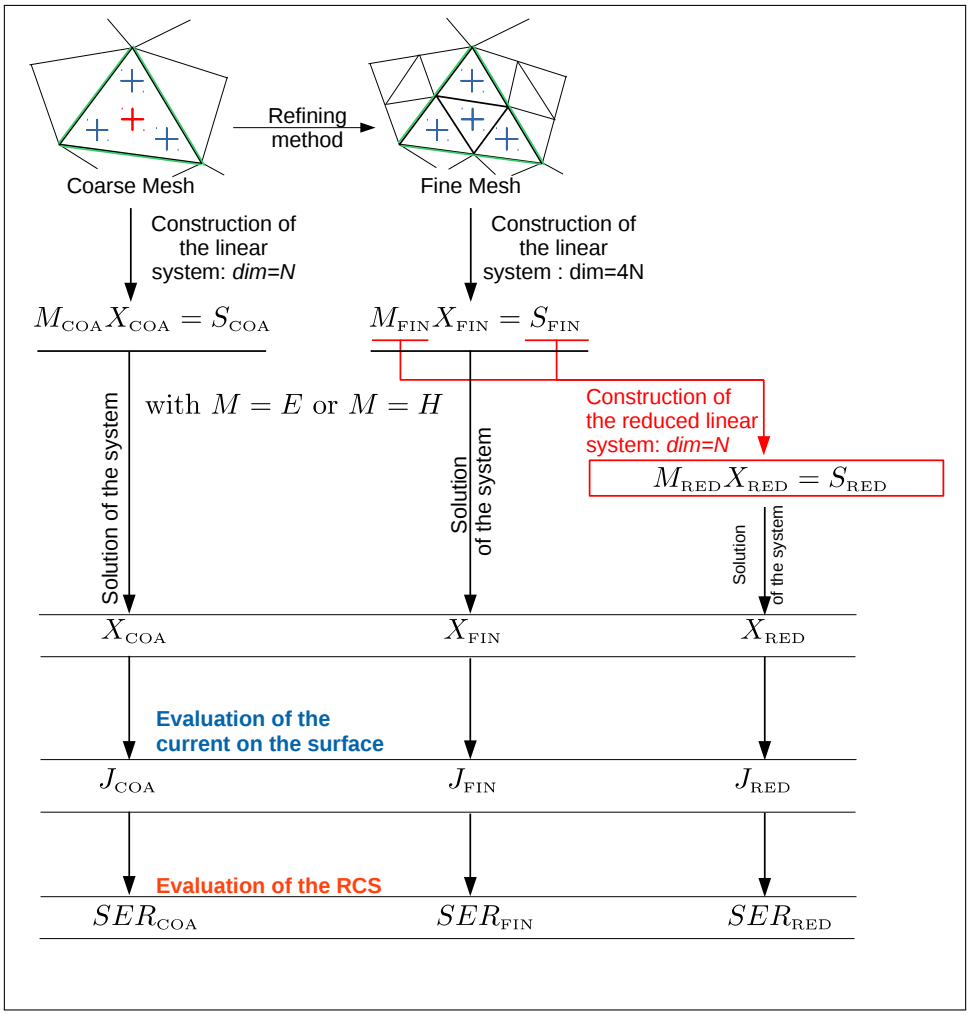

Figure 5.13 – Schematic view of the methodology: linear system and fields.

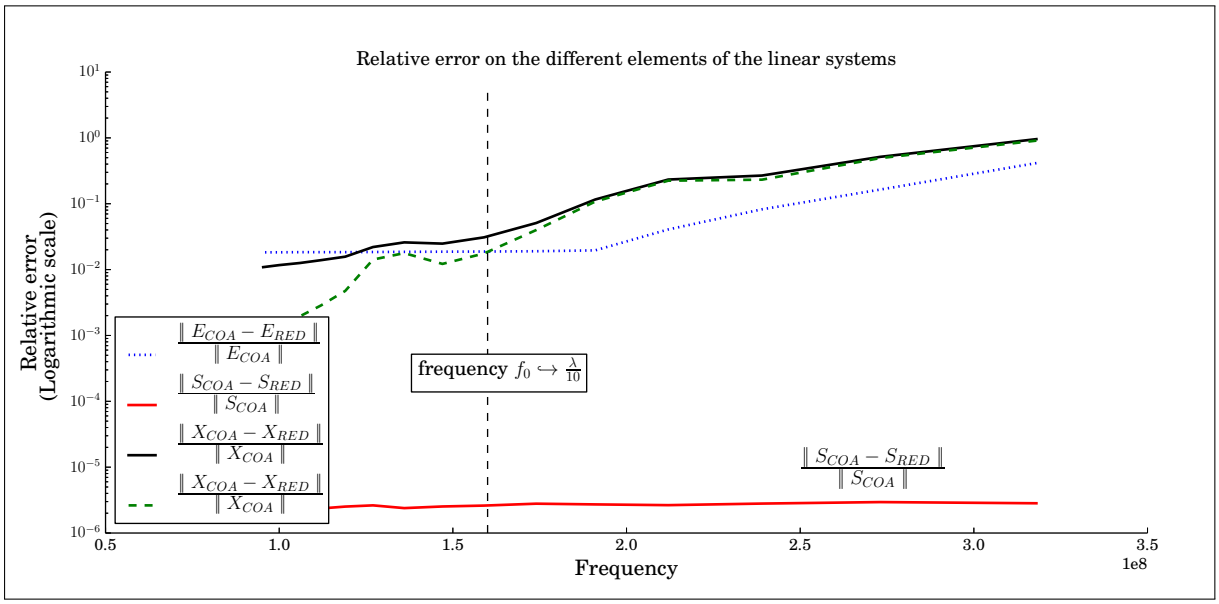

Figure 5.14 – Evolution of the relative error on the different element of the linear systems .

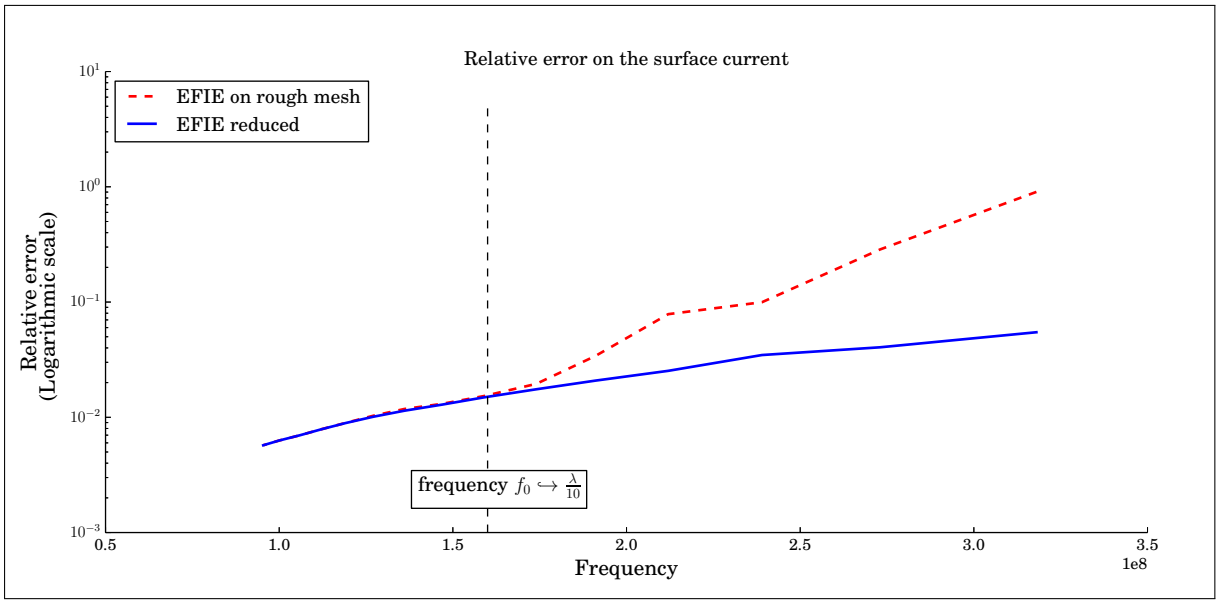

Figure 5.15 – Evolution of the relative error on the surface current for the EFIE built on the coarse mesh and the reduced EFIE.

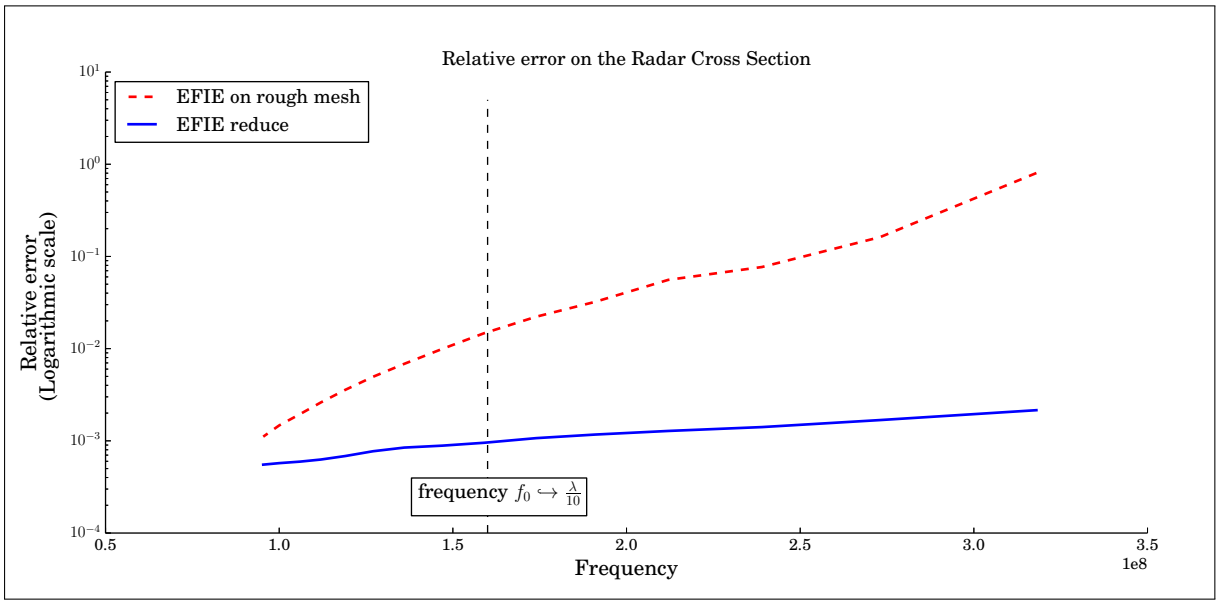

Figure 5.16 – Evolution of the relative error on the Radar Cross Section for the EFIE built on the coarse mesh and the reduced EFIE.

5.4 Construction of the reduced HEFIE system

After building our reduced system for the EFIE and having validated its good behaviour by showing

- a good correspondence between the coarse system (matrices, right-hand side and solution) and the reduced system for lower frequencies and
- a better solution in terms of current and RCS for the highest frequencies (not better than the EFIE on the fine mesh, but better than the EFIE/HEFIE on the coarse mesh),

we are now concerned with the reduced system for the HEFIE.

5.4.1 Validation of the reduced HEFIE systems

We consider once again the two meshes, the coarse one and the fine one, the associated projection matrix R as well as the six systems at our disposal:

- EFIE:
  - the coarse EFIE system: $E_{\text{COA}} X_{\text{COA}} = S_{\text{COA}}$,
  - the fine EFIE system: $E_{\text{FIN}} X_{\text{FIN}} = S_{\text{FIN}}$ and
  - the reduced EFIE system: $E_{\text{RED}} X_{\text{RED}} = S_{\text{RED}}$.
- HEFIE:
  - the coarse HEFIE system: $H_{\text{COA}} Y_{\text{COA}} = C_{\text{COA}}$,
  - the fine HEFIE system: $H_{\text{FIN}} Y_{\text{FIN}} = C_{\text{FIN}}$ and
  - the reduced HEFIE system: $H_{\text{RED}} Y_{\text{RED}} = C_{\text{RED}}$.

Now we look at the various quantities available. First, the linear system elements are observed, namely the matrix H, the right-hand side C and the solution Y of the system. We find the same characteristics as observed with the EFIE, where for low frequencies, the two systems (reduced and coarse) are equivalent whereas for the highest frequencies the two systems diverge from each another.

We then observe the different currents obtained. As we can note in Figure 5.17, the physical current obtained after solving the reduced system is much better than the current obtained with the coarse system. Indeed, we observe that over the entire frequency range the resulting current is comparable to the current obtained with EFIE/HEFIE fine system. Considering the results shown in Figure 5.18, one can also notice that the computation of the RCS is also much better, which is a direct consequence of the good quality obtained on the current.

Remark 5.1 :

We can observe a significant error on the surface current for $f \sim 2.4\ 10^8 Hz$. It appears that this frequency is close to one of the zeros of the 1st-order spherical Bessel function and therefore close to an internal resonance frequency for the sphere which could explain the error around this frequency. This is consistent with the fact that the RCS does not show a significant error at that frequency since an error on the internal problem does not radiate. □

Proposition 5.2 :

In first iteration, we built the reduced system by applying a projection matrix to the fine systems. It is also possible and recommended to build another reduced system for the HEFIE by using the perturbation matrix built from the coarse mesh as follow:

$$H_{\text{RED,alt}} = E_{\text{RED}} + K_{COA}.$$

It appears that for the case of the sphere, this reduced system has the same characteristics in terms of solution and quality as the one we presented above. However, it allows to reduce the part of H_{RED} dependent of the incident direction and also to reduce the associated computational cost. □

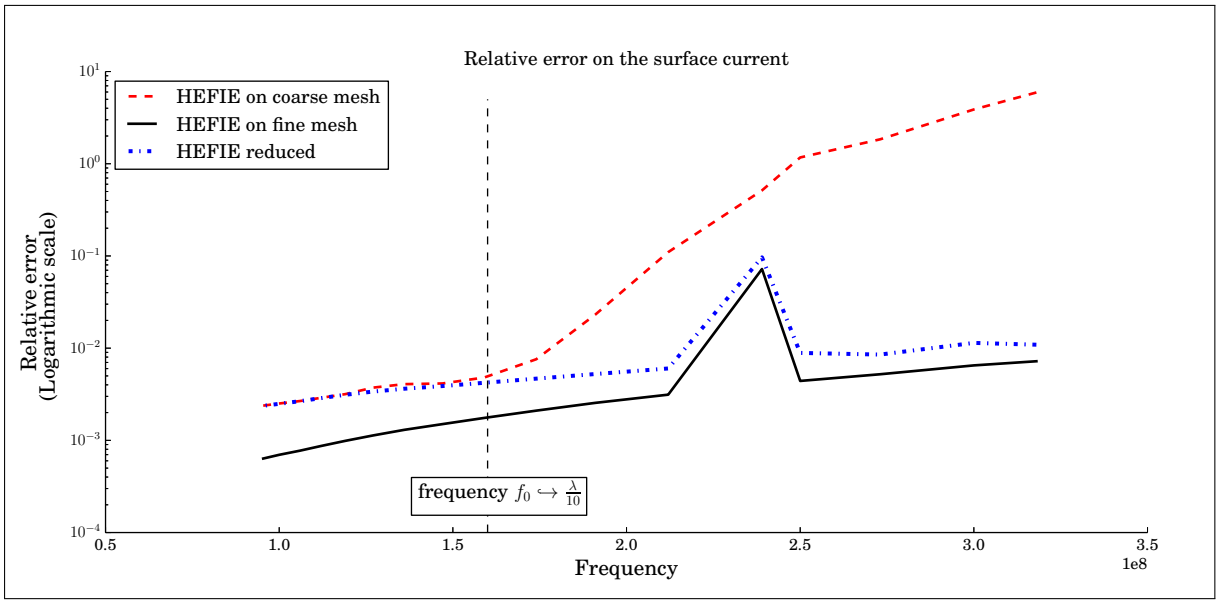

Figure 5.17 – Evolution of the relative error on the surface current for the HEFIE built on the coarse and the fine mesh and for the reduced HEFIE.

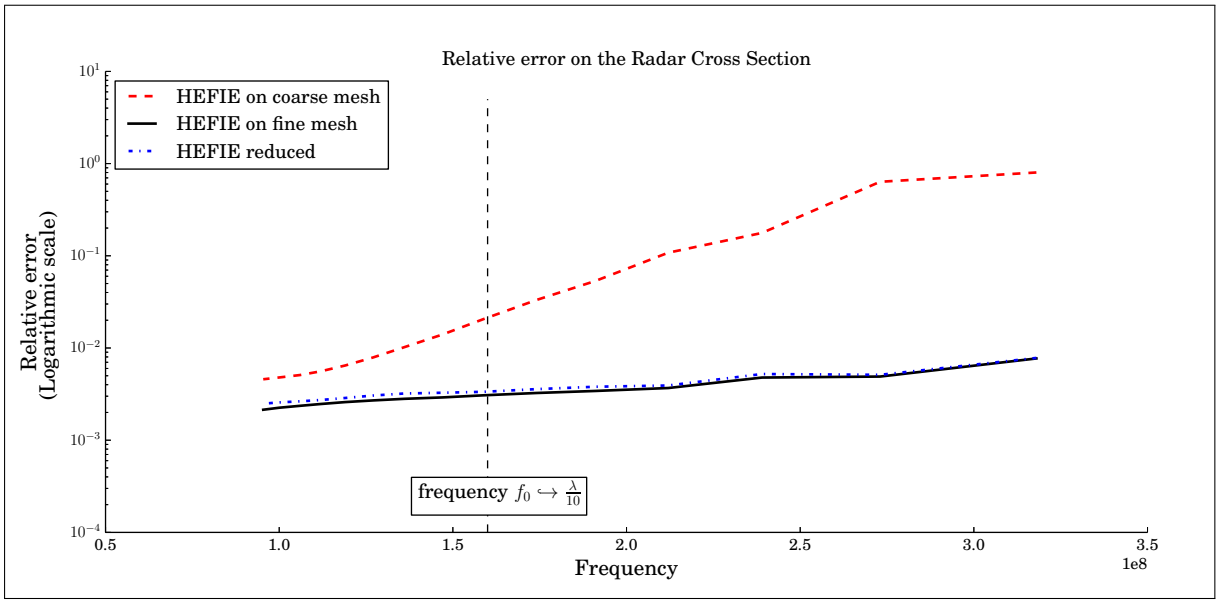

Figure 5.18 – Evolution of the relative error on the Radar Cross Section for the HEFIE built on the coarse and the fine mesh and for the reduced HEFIE.

5.4.2 Performance comparison of the various systems

After looking at the different errors, we wanted to compare the various linear systems using three criteria: the number of iterations needed to solve the linear system (see Figure 5.19), the quality of the resulting current (see Figure 5.20) and the computational cost (see Figure 5.21). In order to be as complete as possible, we add the curves corresponding to the alternative reduced system proposed in the Proposition 5.2.

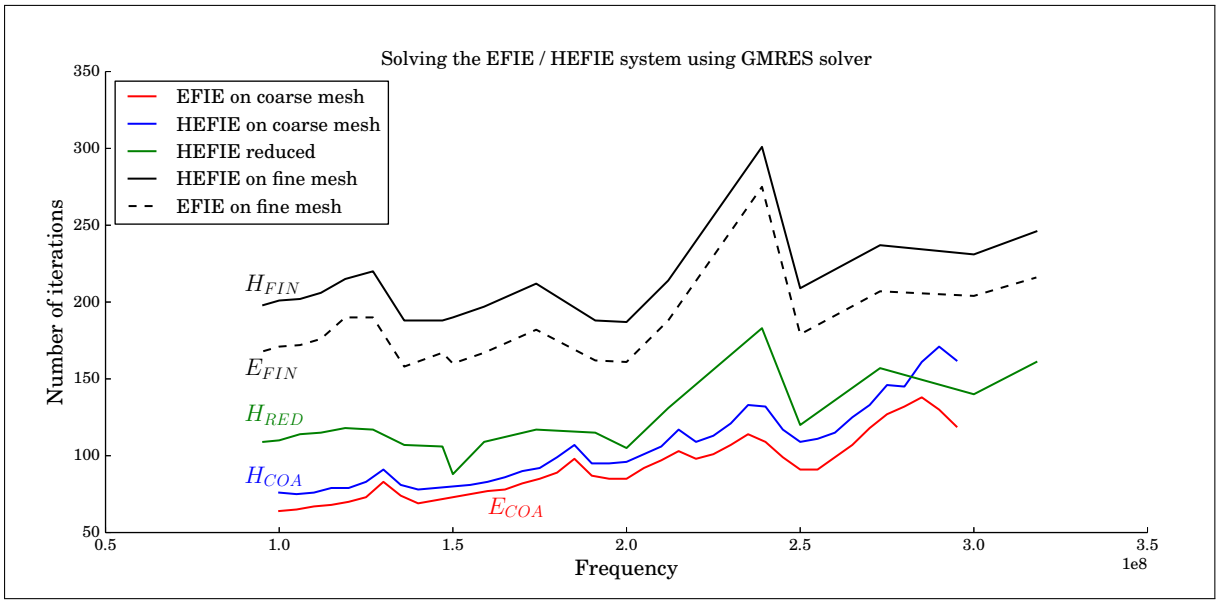

Figure 5.19 – Number of iterations required to attain a residual error of 10^{-4}, as function of the frequency for the various system (non preconditioned) for the SPHERE.

.

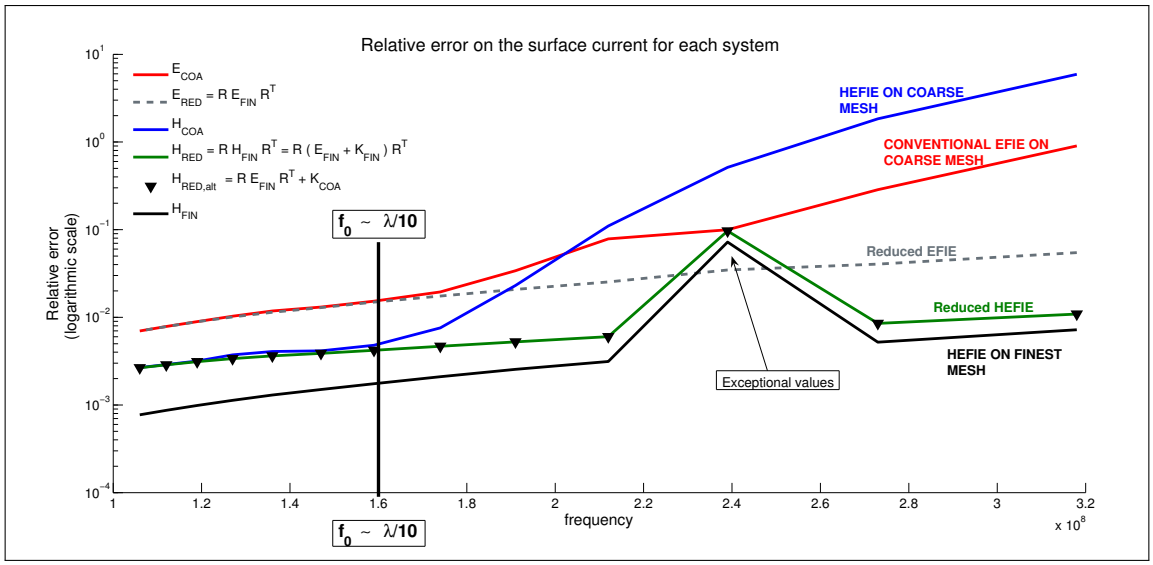

Figure 5.20 – Evolution of the relative error on the surface current for each system proposed (reduced, conventional on the coarse mesh or on the finest mesh).

We observe that through the fine and reduced (both original and alternative) HEFIE systems, we get a very good solution for the current (and hence for the RCS). We also note that each reduced system solution requires the same number of iterations as the systems built on the coarse mesh. Moreover, because of the smaller systems we are able both to have a good quality on the current solution and to ease the solution, in the sense that we work with matrices 16 times smaller and with systems easier to solve using an iterative solver. In that sense, we reached our objectives.

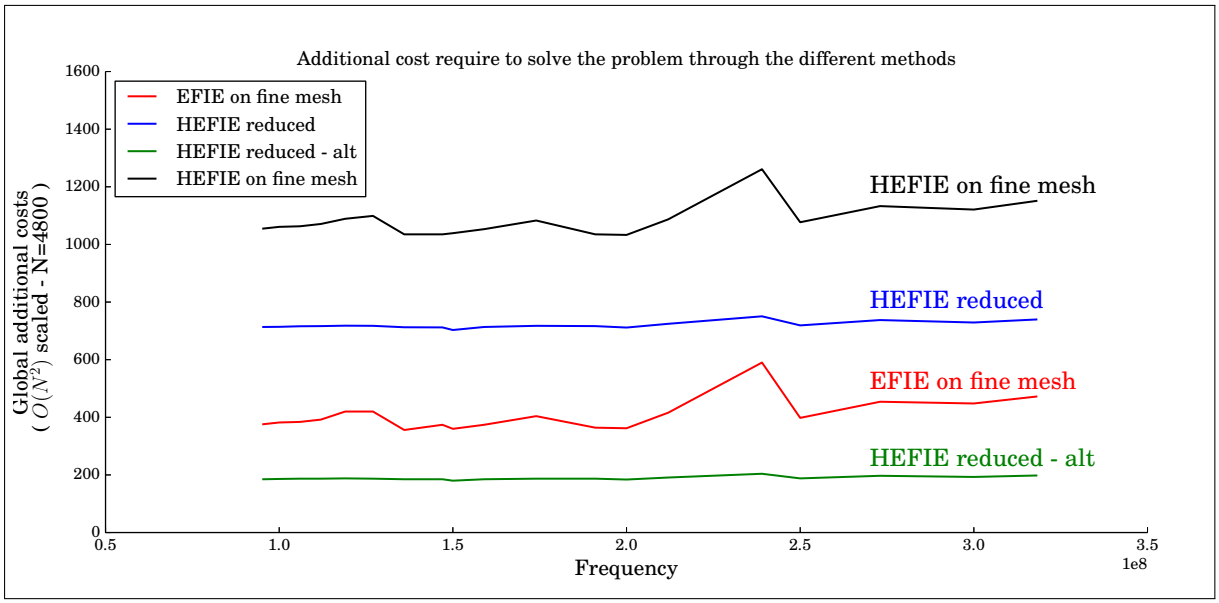

Figure 5.21 – Evaluation of the additional costs, i.e., without the computational cost of the matrix E_{FIN}, for the different methods to get the solution (additional costs = assembly of K (if required) + solution) .

However, for the special case of the sphere, if we look at the additional costs generated by the construction of the "fine" HEFIE systems (more precisely the system obtained for the fine mesh and the reduced system, and not the one presented in Proposition 5.2) and their solutions, it appears that the global cost is higher than with the EFIE systems. This can be explained firstly by the additional costs required by the computation of the matrix K and secondly by the fact that in the case of the sphere both fine systems (both EFIE and HEFIE) require the same number of GMRES iterations.

It may also be noted that the alternative reduced system presented in Proposition 5.2 is more advantageous than the EFIE in the sense that it costs less and gives a good solution. In this example, this is probably the best method. The cost difference between this one and the original reduced system is that we calculate the perturbation K directly on the coarse mesh.

The last point concerns the cost in terms of memory consumption. It turns out that the reduced systems have lower memory footprint than the EFIE and HEFIE systems, irrespective of whether we store the matrices H_{END} and R (the gain is given by the smaller number and the smaller size of the vector to be stored in GMRES) or we carry out directly the reduction during the assembly stage.

Finally, the conclusion drawn from the various tests studied in this chapter, is that the HEFIE is useful when the assembly cost of the perturbation matrix K is low compared to the cost of the resolution. Then it appears to be advantageous to use the reduced HEFIE system, with K computed on a coarse mesh. This allows to obtain a good solution at a lower computational cost than with the EFIE which always requires discretisation on a fine mesh (see Figure 5.21). However, these perspectives needs to be confirmed by a numerical study for larger size object and should also be compared when using acceleration techniques like FMM or H-Matrix. Obviously, the same strategy could be applied to the HMFIE (and the HCFIE).

Another advantage of computing K separately comes to the foreground in the context of multiple incidence scattering problems. This will be detailed in the following section.

5.5 Perspectives for multi-incidence scattering

In this section, we present some perspectives about the computation of multi-incidence scattering coefficients. Previously, we considered the essential problem for computing a generic plane wave scattering coefficient, i.e., to find the current distribution, induced by a single incident plane wave, on the boundary of a scattering obstacle. This problem was formulated as an electric field integral equation:

$$E_{\mathrm{FIN}} X = b.$$

If we want to handle a number of different incident waves, we should consider

$$\forall i \in [\![1; N_{RHS}]\!] \; E_{\mathrm{FIN}} X_i = b_i,$$

where b_i represents the RHS for a given direction of incidence and a given electric polarisation (orthogonal to that direction). In many cases of interest, N_{RHS} is a large number. With the EFIE, the problem is just a linear system with mutliple RHS's.

To recall, we give in Table 5.1 an evaluation of the assembly cost of the EFIE matrix as function of the number of degree of freedom in the discretised current distribution (this cost is derived from the algorithm 1).

N_G	Algorithmic cost	
3	$\sim 2600F^2$	$\sim 1150N^2$
7	$\sim 13.200F^2$	$\sim 5850\ N^2$

Table 5.1 – Algorithmic cost for the computation of the matrix $\tilde{E}$ (F: number of faces, N: number of internal edges, N_G: number of Gauss points considered).

To solve the integral equations, we consider three methods:

- the EFIE,
- the HEFIE reduced (either the one presented at the beginning of this chapter or the system proposed by Zhou [16]) for which we use symbols indexed by RED,
- the HEFIE reduced alternative (presented in Proposition 5.2) for which we use symbols indexed by RED, alt.

For each of them, we consider the principal computational characteristics: the assembly cost as function of the number of internal edges of the coarse mesh, N, the solution cost as function of N and of the number of iterations N^{iter} for a GMRES to obtain a residual error smaller than a given value. Rigorously, there is no reason to expect that $N_E^{iter} = N_{RED}^{iter}$ or $N_E^{iter} = N_{RED,alt}^{iter}$.

First, we present in Table 5.2, the different costs generated by the solution of the problem for a single incidence. We can see that if $H_{\mathrm{RED,alt}}$ (and H_{RED}) costs a little more to be build than E_{FIN}, it leads to the solution of a system with a smaller size and therefore to a lower total solution cost (assembly and solution included).

If we are interested in several directions of incidence, we see different behaviour (see Table C.3). Indeed, we note that the assembly cost of H_{RED} matrices is very important with respect to the other costs and that, consequently, this method is not adapted to the solution of

	Assembly cost	Solution cost	Total cost
E_{FIN}	$\simeq 18.400\ N^2$	$32N_E^{iter}N^2$	$(18.400 + 32N_E^{iter})N^2$
H_{RED}	$\simeq 27500\ N^2$	$2N_{RED}^{iter}N^2$	$(27.500 + 2N_{\text{RED}}^{iter})N^2$
$H_{\text{RED,alt}}$	$\simeq 19000\ N^2$	$2N_{RED,alt}^{iter}N^2$	$(19.000 + 2N_{RED,alt}^{iter})N^2$

Table 5.2 – Algorithmic cost of the assembly and the solution of the problem for each system and for one incidence direction (N: number of internal edges of the coarse mesh).

	Assembly cost	Solution cost	Total cost
E_{FIN}	$18.400\ N^2$	$180 \times 32N_E^{iter}N^2$	$(18.400 + 5760 * N_E^{iter})N^2$
H_{RED}	$(18.400 + 180 \times 9100)\ N^2$	$180 \times 2N_{RED}^{iter}N^2$	$(1.656.400 + 360 * N_{RED}^{iter})N^2$
$H_{\text{RED,alt}}^{+}$	$(18.400 + 180 \times 650)\ N^2$	$180 \times 2N_{RED,alt}^{iter}N^2$	$(135.400 + 360 * N_{RED,alt}^{iter})N^2$
$H_{\text{RED,alt}}^{*}$	$(18.400 + 180 \times 1300)\ N^2$	$180 \times 2N_{RED,alt}^{iter}N^2$	$(234.000 + 360 * N_{RED,alt}^{iter})N^2$

Table 5.3 – Algorithmic cost of the assembly and the solution of the problem for each system and for $N_{RHS} = 180$ incidence directions (N: number of internal edges of the coarse mesh). In this Table, N^{iter} must be interpreted as an average number of iterations required to attain a fixed residual error.

this kind of problems.

For $H_{\text{RED,alt}}$, we distinguish two options.

+ $H_{\text{RED,alt}}^{+}$
  The first one consists in assembling all the matrices K_{COA} at the same time as the E_{RED} matrix to reduce the construction costs at the expense of a storage cost becoming important (see Table 5.4).

* $H_{\text{RED,alt}}^{*}$
  The second option consists of assembling each of the K_{COA} matrices independently (each of them having an assembling cost $\sim 1300N^2$) and updating a matrix $H_{\text{RED,alt}}$ at each incidence.

In both cases, the assembly cost is higher than the assembly cost of E_{FIN}. However, we are led to solve smaller systems, potentially 16 times cheaper to solve (as we could expect $N_{RED,alt}^{iter} < N_E^{iter}$) . For alternative reduced systems and the EFIE, the resolution part becomes predominant when N^{iter} becomes large.

	Storage cost for 1 incidence	Storage cost for 180 incidences
E_{FIN}	$16N^2$	$16N^2$
H_{RED}	N^2	N^2
$H_{\text{RED,alt}}^{+}$	N^2	$\leq 17N^2$
$H_{\text{RED,alt}}^{*}$	N^2	$2N^2$

Table 5.4 – Storage cost for each system for 1 and 180 incidences directions (N: number of internal edges of the coarse mesh).

As an illustration, we draw the total cost for $N_{RHS} = 180$ in Figure 5.22 (summing the assembly and the solution costs) as a function of the average number of iterations required to attain a fixed residual error.
We note that there exist areas where one particular method can appear as the best suited.

Notably, when the average number of iterations is low, the assembly cost is the dominant part of the total cost. In that case, the EFIE is naturally advantageous. In the opposite case, when the average number of iteration is large, dealing with small systems gives the advantage to the reduced HEFIE systems. We summarize the assets and the drawback of each method in Table 5.5.

Method	Assembly cost	Solution cost	Storage cost
E_{FIN}	Low	High	High
H_{RED}	High	Low	Low
$H^{+}_{\text{RED,alt}}$	Moderate	Low	High
$H^{*}_{\text{RED,alt}}$	Moderate ($> H^{+}_{\text{RED,alt}}$)	Low	Low

Table 5.5 – Asset and drawback of each method proposed.

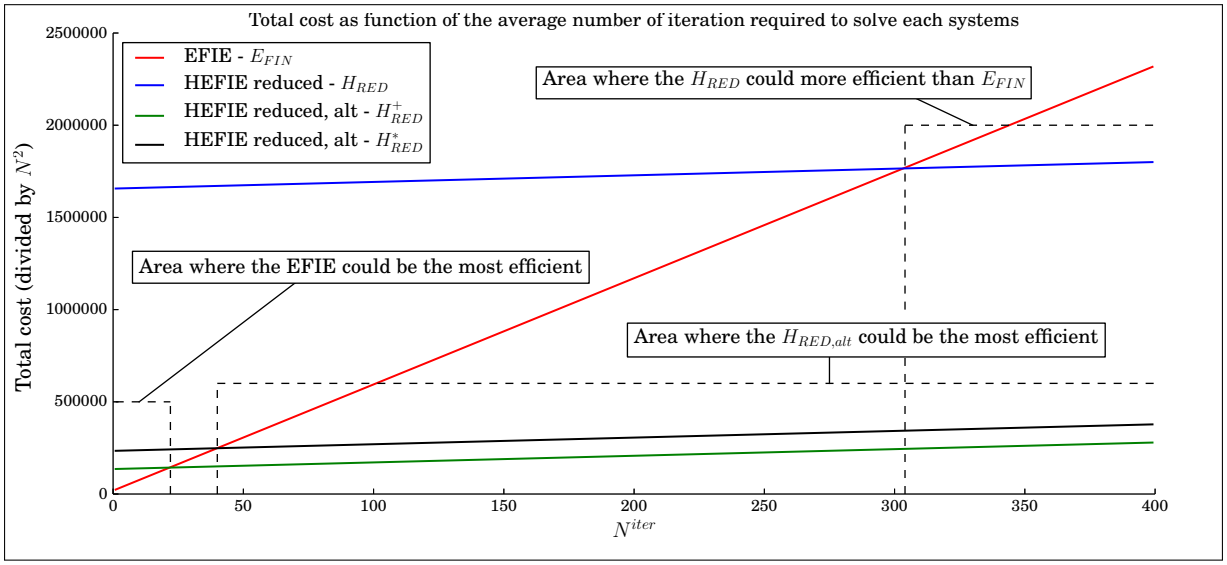

Figure 5.22 – Evolution of the total cost (summing the assembly and the solution costs) as function of the average number of iteration required to attain a fixed residual error.

To finish, the gap between the total cost of $H^{+}_{\text{RED,alt}}$ and $H^{*}_{\text{RED,alt}}$ grows with the number of incidence directions considered. In fact, more we consider incidence directions, more the assembly cost of $H^{*}_{\text{RED,alt}}$ is higher as regard to the assembly cost of $H^{+}_{\text{RED,alt}}$. The choice between the two options amounts to wondering which one we want to privilege (we can consider various implementation in between the two extreme ones presented here). However, no matter how many directions and which option we consider, the total cost of H_{RED} will always be higher than the cost of the two other reduced methods.

As we wrote previously, this section presents some strategies and ideas to deal with multi-incidence scattering, i.e., on how to proceed with multiple right-hand sides. We notably highlight that our HEFIE reduced alternative system have a great interest, compared to the HEFIE reduced (or the one proposed by Zhou), since its assembly cost is much lower. We also describe why our reduced systems (using either $H^{*}_{\text{RED,alt}}$ or $H^{*}_{\text{RED,alt}}$) could have an interest in regard to the EFIE/HEFIE: moderate assembly cost and low solution cost.

Concluding remarks

In this chapter, we studied a significant feature offered by Herberthson's equation: the possibility to reduce the number of degrees of freedom required to get an accurate solution of the problem. Considering the conventional equations and the diffraction of a plane wave with a frequency f_0, a good approximation of the surface current j_S requires the edges of the mesh to have a maximum size smaller than $\lambda_0/7$ (or $\lambda_0/10$). The first step was to demonstrate that the HEFIE was also subject to this constraint even if we work with the pseudo-current $\bar{\psi} j_S$ but for different reasons.
Therefore, noting the error made on the current with a not-conforming mesh was mainly due to a bad integration of the Green function, we proposed to derive a reduced system for the HEFIE, by building it from coefficients of a linear system obtained with a conforming mesh. For this, we considered two different meshes: a coarse mesh (not-conforming) and a fine mesh. The idea was to express each function carried by the edge of the coarse mesh (or macro-element) as a linear combination of edge functions carried by the fine mesh. Hence, introducing a restriction (or coarsening) matrix R, we formulate two new linear systems:

$$RH_{\text{FIN}}R^T J_{\text{RED}} = H_{\text{RED}} J_{\text{RED}} = C_{\text{RED}} = RC_{\text{FIN}} \quad \text{and} \quad (RE_{\text{FIN}}R^T + K_{\text{COA}})J_{\text{RED}} = C_{\text{RED}}$$

which have the same size as a system built on a coarse mesh (16 times smaller than the "fine" system) and the same quality in term of solution obtained after solution than the one obtained from a fine mesh.

Our idea may be compared to a local refinement [16, 21] of the mesh to calculate the oscillating integrals, there are however two points that distinguish the two ideas. First of all, the construction of the reduced systems in our method is a purely topological construction which will depend only of the chosen method of refinement. This has the great advantage of significantly reducing the size of the system for a low cost (which is fairly easy to integrate into the mesh refinement procedure). The second aspect is that here we were able to show that the perturbation part can be directly computed on the coarse mesh in order to minimize the costs. The counterpart is that here we work with a structure independent of the frequency since we use the same refinement procedure at any frequency. It is therefore not possible for us to check or take benefit from a greater reduction when the frequency increases. The error estimates formulated by Zhou-Darrigrand, by analogy to the Helmholtz 3D case, suggest that a greater ratio can be observed between the maximum size of the edges of the fine mesh and coarse when dealing with higher frequencies.

To finish, we validated our reduced method by testing it on the case of the sphere. We showed that this reduce system could lead to a faster solution than the conventional EFIE on a conforming mesh with at least the same quality for the current.

Part III

An analytical case : the perfectly conducting sphere

Chapter 6

Scattering of an electromagnetic plane wave by a sphere

Contents

In this chapter, we study Herberthson's version of the EFIE for the special case of scattering by a perfectly conducting sphere. The purpose is to get analytical expressions for the HEFIE operator coefficients in a basis of the orthogonal vectorial spherical harmonics and then to study the operator norms in particular the coupling between the subspaces of divergent and solenoidal surface currents.

One of the objectives of this chapter is to give a completely explicit representation of the HEFIE operator in the vectorial spherical harmonics basis in the previously given factorised form. Since the EFIE operator, $\mathcal{E}$, is diagonal in that basis, we can take advantage of the relation $\mathcal{H} = \Psi^{-1}\mathcal{E}\Psi$ developed in Chapter 2 to get a full representation of $\mathcal{H}$. Therefore, the essential difficulty is to find a representation of Ψ (or Ψ^{-1}) in the basis of vectorial spherical harmonics.

With a representation of Ψ and Ψ^{-1} in the basis of the vectorial spherical harmonics and using the similarity relation between the EFIE and the HEFIE, we get an explicit representation of $\mathcal{H}$. We shall see that these transformation matrices are essentially band-matrices and using the

fact that the EFIE has a diagonal matrix representation, we obtain a band matrix representation of the HEFIE.

This chapter is split into five parts. First we recall the problem using spherical coordinates, which appears to be the more appropriate system regarding the scene. Then, we present the spherical harmonics and the different relations they respect. In a third part, we give a description of the EFIE operator on the spherical harmonic basis. We do the same operation for the phase function Ψ in order to get in the last section a representation of $\mathcal{H}$ and an estimation of its norms.

6.1 The scattering problem in spherical coordinates

By introducing the decomposition of the total electric field E^{tot} into the given incident fields E^{inc} and a scattered field E^s, i.e., $E^{\text{tot}} = E^i + E^s$, and using the boundary condition $\tau^*(E^{\text{tot}}) = 0$, we have shown that the scattering problem can be reduced to a boundary value problem. We also established that this leads to the Electric Field Integral Equation (EFIE) which is an integral equation satisfied by the boundary value of the total magnetic field, $j_S = \tau^*(H)$, on the sphere.

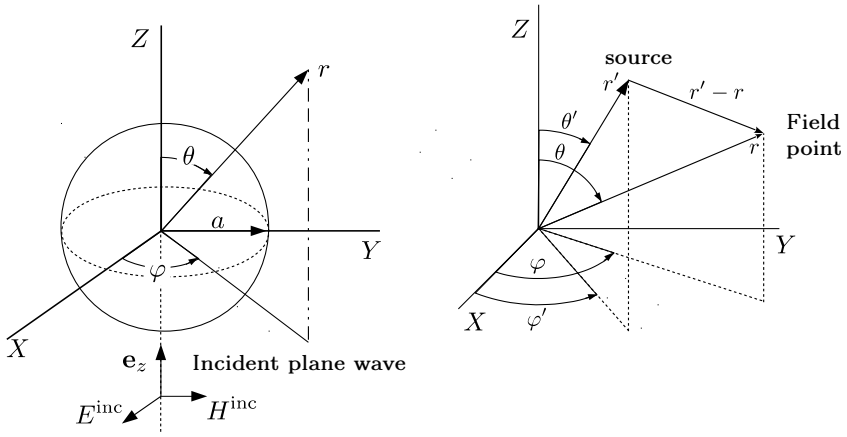

Figure 6.1 – Graphical representation of spherical coordinates.

As usual, we choose the Cartesian spatial coordinates (x, y, z) adapted to the incident plane wave such that the propagation direction is parallel to the z-coordinate axis and the polarisation of the electric field is parallel to the x-coordinate axis. Since there is complete rotational symmetry, we also introduce spherical coordinates (r, θ, φ) (see Figure 6.1). The Euclidean metric in the cotangent spaces in the spherical coordinates is given by

$$g = dr \otimes dr + r^2 d\theta \otimes d\theta + r^2 \sin^2(\theta) d\varphi \otimes d\varphi$$

and the corresponding metric in the cotangent spaces is then given by

$$g = \partial_r \otimes \partial_r + r^{-2} \partial_\theta \otimes \partial_\theta + r^{-2} \sin^{-2}(\theta) \partial_\varphi \otimes \partial_\varphi.$$

In order to make easier the comparison of our presentation with the vector analysis version, we shall not use the natural basis in the cotangent spaces, i.e., the basis of differentials $\{dr, d\theta, d\varphi\}$, but an orthonormal basis $\{\rho, \Theta, \Upsilon\}$ defined by

$$\begin{aligned} \rho &= dr, \\ \Theta &= r d\theta, \\ \Upsilon &= r \sin(\theta) d\varphi. \end{aligned}$$

With this choice, the metric coefficients are unitary.

The incident plane wave, with propagation direction θ and transverse electric polarisation E_0, is then given by

$$E^i : \mathbb{R}^3 \ni (x, y, z) \mapsto E_0 \psi(x, y, z)$$

where the phase function and the polarisation are given by

$$\begin{aligned} \psi(x, y, z) &= e^{i\kappa z}, \\ E_0 &= dx, \end{aligned}$$

or, in spherical coordinates,

$$\begin{aligned} \psi(r, \theta, \varphi) &= e^{i\kappa r \cos(\theta)}, \\ E_0 &= \sin(\theta)\cos(\theta)dr + r\cos(\theta)\sin(\varphi)d\theta - r\sin(\theta)\sin(\varphi)d\varphi, \end{aligned}$$

where $\kappa = 2\pi f/c$ is the wave number as usual. This reduces to

$$E_0 = \sin(\theta)\cos(\theta)\rho + \cos(\theta)\sin(\varphi)\Theta - \sin(\varphi)\Upsilon$$

in the orthonormal basis.

6.2 The basis of *1-form* spherical harmonics

The vectorial spherical harmonics we use for the expansion of the 1-forms E and H on the sphere are derived from the scalar spherical harmonics using the fact that the Hodge decomposition on the sphere ($\ker(\Delta) = \emptyset$) allows the representation of each 1-form v through the relation $v = \mathbf{d}\,\alpha + \star\,\mathbf{d}\,\beta$, where α and β are 0-forms, i.e., scalar functions. We present here a construction of those harmonics and the main relations to consider to work with them.

6.2.1 Definitions

. Scalar spherical harmonics

The scalar spherical harmonics are defined as the set

$$\mathscr{H}^s = \{\ h_n^m \mid n \in \mathbb{N}^*,\ m \in \mathbb{Z},\ |m| \leq n\ \}$$

with

$$\begin{aligned} h_n^m(\theta, \varphi) &= b_{n,m} P_n^m(\cos(\theta)) e^{im\varphi}, \\ b_{n,m} &= (-1)^{\frac{1}{2}(m+|m|)} \sqrt{\frac{2n+1}{4\pi n(n+1)} \frac{(n-|m|)!}{(n+|m|)!}} \end{aligned}$$

where P_n^m denotes the associated Legendre polynomial of degree n and of order m (n and m restricted to positive integers) defined by (see [70, Section 7.3] and [71, Appendix E]):

$$P_n^m(\eta) = \frac{(1-\eta^2)^{\frac{m}{2}}}{2^n n!} \frac{d^{n+m}(\eta^2-1)^n}{d\eta^{n+m}}.$$

The properties of the associated Legendre functions, which constitute a subset of hyper-geometric functions, have been greatly exploited in the past and various representations have been proposed. For the purpose of this study, the main relations are the indispensable recurrence formula and the description of the product and the integral of the product of two associated Legendre polynomials (see [70, Section 7.3], [71, Appendix E] or again [72, 73]).

Proposition 6.1 : **Associated Legendre Polynomials: recurrence relations**

$$
\begin{aligned}
(n-m+1)P_{n+1}^m(\eta) - (2n+1)\eta P_n^m(\eta) + (n+m)P_{n-1}^m(\eta) &= 0,\\
P_{n-1}^m(\eta) &= \eta P_n^m(\eta) - (n-m+1)\sqrt{1-\eta^2}P_n^{m-1}(\eta),\\
P_{n+1}^m(\eta) &= \eta P_n^m(\eta) - (n+m)\sqrt{1-\eta^2}P_n^{m-1}(\eta),\\
\sqrt{1-\eta^2}P_n^{m+1}(\eta) &= (n+m+1)\eta P_n^m(\eta) - (n-m+1)P_{n+1}^m(\eta),\\
\sqrt{1-\eta^2}P_n^{m+1}(\eta) &= (n+m+1)\eta P_n^m(\eta) - (n-m+1)P_{n+1}^m(\eta),\\
\sqrt{1-\eta^2}P_n^{m+1}(\eta) &= 2m\eta P_n^m(\eta) - (n+m)(n-m+1)\sqrt{1-\eta^2}P_n^{m-1}(\eta),\\
\sqrt{1-\eta^2}P_n^m(\eta) &= \frac{1}{2n+1}(P_{n+1}^{m+1}(\eta) - P_{n-1}^{m+1}(\eta)).
\end{aligned}
$$

□

Proposition 6.2 : **Associated Legendre Polynomials: integral relations**

For $n \neq l$ or $m \neq l$ respectively, we have:

$$\int_{-1}^{1} P_n^m(\eta)P_l^m(\eta)d\eta = 0, \quad \int_{-1}^{1} \frac{1}{1-\eta^2}P_n^m(\eta)P_n^l(\eta)d\eta = 0.$$

Furthermore, we have:

$$\int_{-1}^{1} [P_n^m(\eta)]^2\, d\eta = \frac{2}{2n+1}\frac{(n+m)!}{(n-m)!}, \qquad \int_{-1}^{1} \frac{1}{1-\eta^2}\,[P_n^m(\eta)]^2\, d\eta = \frac{1}{m!}\frac{(n+m)!}{(n-m)!}.$$

□

By the way, the function $\cos(m\varphi)P_n^m(\cos(\theta))$ and $\sin(m\varphi)P_n^m(\cos(\theta))$ are periodic on the surface of a unit sphere and their indices (n, m) determine the number of nodal lines, i.e., the lines where the function changes its sign. The number and the position of these nodal lines can be determined by studying the zeros of the functions $\cos(m\varphi)$, $\sin(m\varphi)$ and $(1-\cos(\theta)^2)^{m/2}$ (see [70, Section 7.3 and Appendix IV] for more details). As an example we draw the representation of the nodal lines of the function $\sin(3\varphi)P_5^3(\cos(\theta))$ in Figure 6.2.

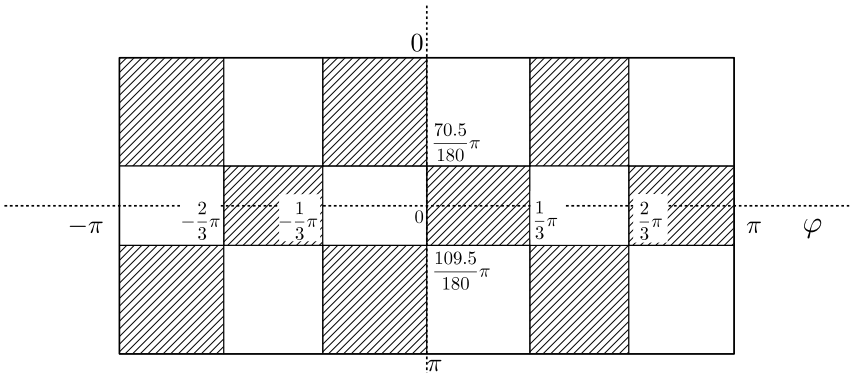

Figure 6.2 – Nodes of the function $\sin(3\varphi)P_5^3(\cos(\theta))$. The function has negative values over the shaded areas and positive on the white.

. Vectorial spherical harmonics

From the scalar basis we get the 1-form spherical harmonics $\{\mathbf{D}_n^m, \mathbf{S}_n^m\}$ by derivation

$$\begin{aligned}\mathbf{D}_n^m &= \mathbf{d}\, h_n^m = \partial_\theta h_n^m d\theta + \partial_\varphi h_n^m d\varphi,\\ &= \partial_\theta h_n^m \Theta + \frac{1}{\sin(\theta)}\partial_\varphi h_n^m \Upsilon,\\ \mathbf{S}_n^m &= \star\mathbf{D}_n^m = \star\mathbf{d}\, h_n^m = -\partial_\varphi h_n^m d\theta + \partial_\theta h_n^m d\varphi,\\ &= -\frac{1}{\sin(\theta)}\partial_\varphi h_n^m \Theta + \partial_\vartheta h_n^m \Upsilon.\end{aligned}$$

Note that, by definition $\mathbf{d}\, D_n^m \equiv 0$ and $\boldsymbol{\delta}\, S_n^m \equiv 0$. In terms of the derivatives we obtain the explicit expression for the form components

$$\begin{aligned}\mathbf{D}_n^m(\theta,\varphi) &= \left(-a_{n,m}\sin^2(\theta)P_n^{m\prime}(\cos(\theta))e^{im\varphi}\right)\xi + \left(\frac{a_{n,m}(im)}{\sin(\theta)}P_n^m(\cos(\theta))e^{im\varphi}\right)\eta,\\ \mathbf{S}_n^m(\theta,\varphi) &= \left(\frac{a_{n,m}(im)}{\sin(\theta)}P_n^m(\cos(\theta))e^{im\varphi}\right)\xi + \left(a_{n,m}\sin^2(\theta)P_n^{m\prime}(\cos(\theta))e^{im\varphi}\right)\eta\end{aligned}$$

where $a_{n,m}$ is defined as

$$a_{n,m} = a_n^m = (-1)^{\frac{1}{2}(m+|m|)}\sqrt{\frac{1}{4\pi}\frac{(n-|m|)!}{(n+|m|)!}\frac{2n+1}{n(n+1)}} = \frac{1}{\sqrt{n(n+1)}}b_{n,m}$$

and where $P_n^{m\prime}$ denotes the derivative of P_n^m. This derivative can also be expressed by means of recurrence relations (see [73, section 8.7], [74] or [70, Section 7.3]).

Proposition 6.3 : **Associated Legendre Polynomials: derivative**

$$\begin{aligned}(1-\eta^2)\frac{dP_n^m}{d\eta} &= (n+1)\eta P_n^m - (n-m+1)P_{n+1}^m,\\ (1-\eta^2)\frac{dP_n^m}{d\eta} &= (n+m)P_{n-1}^m - n\eta P_n^m.\end{aligned}$$

□

6.2.2 Orthogonality relations

Let S_a^2 denote the sphere of radius a. We define the L^2 inner product of two 1-forms, say α and β, on S_a^2 by

$$\langle\alpha\ ;\ \beta\rangle = \int_{S_a^2}\alpha\wedge\star\beta$$

where here $\star$ is the Hodge duality operator for the metric induced on S_a^2 by the Euclidean metric on $\mathbb{E}^3$.

We shall make use of the fact that the 1-form spherical harmonics are orthogonal in the following two ways. Firstly, we have orthogonality within one component of the Hodge decomposition:

$$\begin{aligned}\langle\mathbf{S}_n^m\ ;\ \mathbf{S}_q^p\rangle &= \delta^{(m-p)}\delta_{(n-q)},\\ \langle\mathbf{D}_n^m\ ;\ \mathbf{D}_q^p\rangle &= \delta^{(m-p)}\delta_{(n-q)}.\end{aligned}$$

Secondly, we have the orthogonality of the Hodge decomposition itself

$$\langle \mathbf{S}_n^m \ ; \ \mathbf{D}_q^p \rangle = 0 = \langle \mathbf{D}_n^m \ ; \ \mathbf{S}_q^p \rangle$$

for any index tuple m, n, p, q. The first orthogonality is due to the orthogonality of the scalar spherical harmonics as eigenfunctions of the symmetric Laplacian on the sphere.

$$\langle h_n^m \ ; \ h_q^p \rangle = \int_{S_a^2} h_n^m \wedge \star \overline{h_q^p} = \delta^{(m-p)} \delta_{(n-q)}$$

together with the definition of the inner product

$$\langle \mathbf{D} \ ; \ \mathbf{S} \rangle = \int_{S_a^2} \mathbf{D} \wedge \star \overline{\mathbf{S}}$$

and the reductions

$$\int_{S_a^2} \mathbf{d}\, \alpha \wedge \star \mathbf{d}\, \overline{\beta} = \int_{S_a^2} \alpha \wedge \star \boldsymbol{\delta}\, \mathbf{d}\, \overline{\beta} = \int_{S_a^2} \alpha \wedge \star \Delta \overline{\beta}$$

which yield

$$\langle \mathbf{d}\, h_n^m \ ; \ \mathbf{d}\, \overline{h}_q^p \rangle = \lambda_q^p \langle h_n^m \ ; \ h_q^p \rangle$$

with $\lambda_q^p = \frac{q(q+1)}{a^2}$ the non-zero eigen-value of h_q^p and

$$\langle h_n^m \ ; \ h_q^p \rangle = \delta^{mp} \delta_{nq} \int_{\varphi=0}^{2\pi} \int_{\theta=0}^{\pi} |h_n^m|^2 a^2 \sin(\theta) d\theta \wedge d\varphi.$$

Using

$$|h_n^m|^2 = a_{n,m}^2 P_n^m(\cos(\theta))^2$$

and a change of coordinate $z = \cos(\theta)$, we get

$$\begin{aligned} \langle \mathbf{d}\, h_n^m \ ; \ \mathbf{d}\, \overline{h}_q^p \rangle &= \delta^{mp} \delta_{nq} a_{n,m}^2 \frac{q(q+1)}{a^2} 2\pi a^2 \int_{z=1}^{z=-1} P_n^m(z)^2 dz, \\ &= \delta^{mp} \delta_{nq} a_{n,m}^2 q(q+1) 2\pi 2 \frac{(n+m)!}{(2n+1)(n-m)!}, \\ &= \delta^{mp} \delta_{nq}. \end{aligned}$$

6.3 Representation of the EFIE on the sphere in spherical harmonics

After describing the vectorial spherical harmonics, we present now the solution of the scattering problem through the EFIE in the basis of *1-form* vectorial spherical harmonics. The idea is, in a first step, to give all the necessary elements to build a full representation of the EFIE problem, and in a second step, to obtain a representation of the HEFIE through a representation of the operator Ψ.

6.3.1 The incident plane wave

We begin with the right-hand side. The expansion in Legendre polynomials of the incident wave's phase function, ψ, restricted to a sphere of radius a, is given by (see [70, Chapter 7] and [71, Section 6.7-6.8]):

$$\psi(\theta,\varphi) = \sum_{n=0}^{+\infty} i^n(2n+1)j_n(\kappa a)P_n(\cos(\theta)). \tag{6.1}$$

Note that, in this expression, the dependence on the radius a of the sphere is expressed through the Bessel coefficient $j_n(\kappa a)$ ($j_n(\rho) = \sqrt{\pi/(2\rho)}J_{n+1/2}(\rho)$). The incident wave's polarisation restricted to the sphere of radius a is given by

$$\mathbf{p}_E(\theta,\varphi) = cos(\theta)\cos(\varphi)\Theta - \sin(\varphi)\Upsilon. \tag{6.2}$$

This means that the incident electric field restricted to the sphere is given by

$$\tau^* E^i(\theta,\varphi) = \sum_{n=0}^{+\infty} i^n(2n+1)j_n(\kappa a)P_n(\cos(\theta))\left(cos(\theta)\cos(\varphi)\Theta - \sin(\varphi)\Upsilon\right).$$

Therefore, we can expand the incident electric field as the sum of vectorial spherical harmonics:

$$E^{\text{inc}} = \sum_{n,m} \alpha_{n,m}\mathbf{S}_n^m + \beta_{n,m}\mathbf{D}_{n,m}.$$

However, some considerations about the azimuthal harmonics can reduce the effort of the decomposition to the case $m = 1$. In fact, if we consider for example the expansion of E^{inc} on $\{\mathbf{S}_n^m\}$, we have

$$\langle E^{\text{inc}} \ ; \ \mathbf{S}_n^m\rangle = \sum_{p=0}^{+\infty} i^p(2p+1)j_p(\kappa)a_{n,m}\left(I_\varphi^1 I_\theta^1 + I_\varphi^2 I_\theta^2\right)$$

where I_θ denotes the integral over θ including Legendre polynomials and

$$I_\varphi^1 = \int_0^{2\pi} e^{-im\varphi}\cos(\varphi)d\varphi = \int_0^{2\pi} \cos(m\varphi)\cos(\varphi) - i\sin(m\varphi)\cos(\varphi) = \pi\delta_m^{\pm 1},$$
$$I_\varphi^2 = im\int_0^{2\pi} e^{-im\varphi}\sin(\varphi)d\varphi = \int_0^{2\pi} \cos(m\varphi)\sin(\varphi) - i\sin(m\varphi)\sin(\varphi) = \pi\delta_m^{\pm 1},$$

which restrict the decomposition to $m = \pm 1$. Furthermore, considering the relation

$$P_l^{-m} = (-1)^m\frac{(l-m)!}{(l+m)!}P_l^m,$$

we can reduce the work to the case $m = 1$. The case $m = -1$ being then given through a simple relation. We can use this result for the decomposition on $\{\mathbf{D}_n^m\}$, but also by anticipation for all our future developments.

After simplification, we get for the incident electric field reduced to the sphere, the following expansions:

$$\langle E^i \ ; \ \mathbf{S}_n^m\rangle = \frac{2\pi}{-iZ_0}i^{n+1}\ \alpha_{n,1}n(n+1)j_n(\kappa a),$$
$$\langle E^i \ ; \ \mathbf{D}_n^m\rangle = \frac{2\pi}{-iZ_0}i^n\ \alpha_{n,1}\frac{n(n+1)}{2n+1}\ \left((n-1)j_{n+1}(\kappa a) - (n+2)j_{n-1}(\kappa a)\right).$$

To complete and illustrate these expansions, we represent in Figure 6.3 the modulus of the coefficients obtained for $\kappa a = 0.2$.

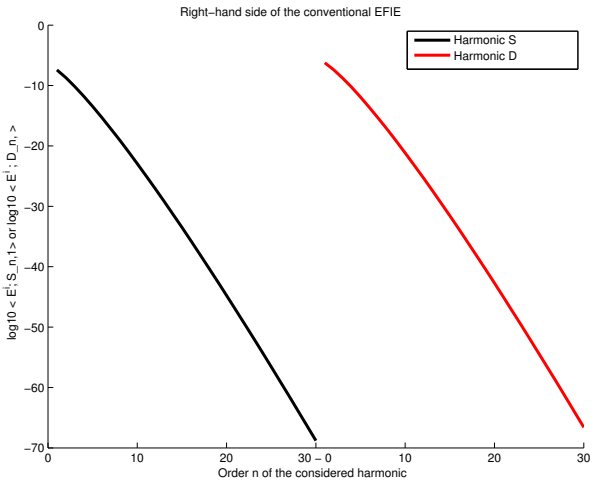

Figure 6.3 – Representation of the decreasing modulus of the coefficients of the right-hand side of the EFIE for $\kappa a = 0.2$.

6.3.2 The EFIE operator

After having presented the right-hand side, we now consider the EFIE operator. Let us recall that the EFIE problem is

$$\text{to find } j_S \text{ such that } \forall j',\ \langle \mathcal{E}[j_S]\ ;\ j' \rangle = -\langle \tau^* E^{\text{inc}}\ :\ j' \rangle.$$

To be precise, for some particular reasons we do not develop here, we have chosen to consider the EFIE problem where $\mathcal{E}[j] = \tau^*(\mathcal{A}[j] - \frac{1}{\kappa^2}\,\mathbf{d}\,\boldsymbol{\delta}\,\mathcal{A}[j])$ and the corresponding right-hand side. Therefore, since the solution of this problem, j_S, can be represented as a sum of vectorial spherical harmonics

$$j_S = \sum_{n,m} \alpha_{n,m}\mathbf{S}_n^m + \beta_{n,m}\mathbf{D}_{n,m}, \tag{6.3}$$

the operator $\mathcal{E}$ in this basis brings all the necessary information to find the solution. Furthermore, it appears that in the spherical harmonics basis the EFIE operator is an infinite dimensional diagonal matrix where each coefficient on the diagonal corresponds to the EFIE operator in a one dimensional subspace.

To get these coefficients, the main thing to consider is the expansion of the Green function G into the spherical coordinates and associated Legendre polynomials. For this, consider the field of a point source at r'

$$h_0^{(1)}(|r - r'|) = \frac{e^{i|r-r'|}}{i|r - r'|}$$

where r and r' are defined in Figure 6.1. We desire to express this function, which is nearly the Green function up to a constant, in terms of scalar harmonic functions. On the sphere, following [71, p.290-292], we have the following expansion:

$$h_0^{(1)}(|r - r'|) = \sum_{n=0}^{+\infty} (2n+1) h_n^{(1)}(r) j_n(r) P_n(\cos(\xi)) \tag{6.4}$$

where $h_n^{(1)}$ denotes the spherical Hankel function of order n and the angle ξ is defined by

$$\cos(\xi) = \cos(\theta)\cos(\theta') + \sin(\theta)\sin(\theta')\cos(\varphi - \varphi'). \tag{6.5}$$

The zonal harmonics $P_n(\cos(\xi))$ can also be expressed in terms of scalar harmonics through the identity:

$$P_n(\cos(\xi)) = \sum_{m=1}^{n} \varepsilon_m \frac{(n-m)!}{(n+m)!} P_n^m(\cos(\theta)) P_n^m(\cos(\theta')) \cos(m(\varphi - \varphi')) \tag{6.6}$$

where ε_m is Neumann's number (1 for $m = 0$, 2 for $m > 0$).

Finally, using the expansion of the Green function given above, the main difficulty to get the coefficients of the EFIE, is to correctly express the integral over the product of two associated Legendre polynomials appearing in the expression of

$$\langle \mathcal{E}[\mathbf{S}_n^m] \ ; \ \mathbf{S}_n^m \rangle \quad \text{and} \quad \langle \mathcal{E}[\mathbf{D}_n^m] \ ; \ \mathbf{D}_n^m \rangle.$$

Once again some considerations can allow the restriction to $m = 1$ and the elimination of $\langle \mathcal{E}[\mathbf{S}_n^m] \ ; \ \mathbf{D}_n^m \rangle$ and $\langle \mathcal{E}[\mathbf{D}_n^m] \ ; \ \mathbf{S}_n^m \rangle$. At the end, as expressed in [70, p.401-404] and [71, p.290-295], we get:

$$\langle \mathcal{E}[\mathbf{S}_n^1] \ ; \ \mathbf{S}_n^1 \rangle = \frac{2i\pi\kappa a}{2n+1} j_n(ka) h_n^{(1)}(\kappa a)(n(n+1))^2,$$
$$\langle \mathcal{E}[\mathbf{D}_n^1] \ ; \ \mathbf{D}_n^1 \rangle = \frac{2i\pi\kappa a}{(2n+1)^2} (n(n+1))^2 \left((n-1) j_{n+1}(ka) - (n+2) j_{n-1}(\kappa a)\right) h_n^{(1)'}(\kappa a).$$

To illustrate this expansions, we represent in Figure 6.4 the modulus of the coefficients obtained for $\kappa a = 0.2$.

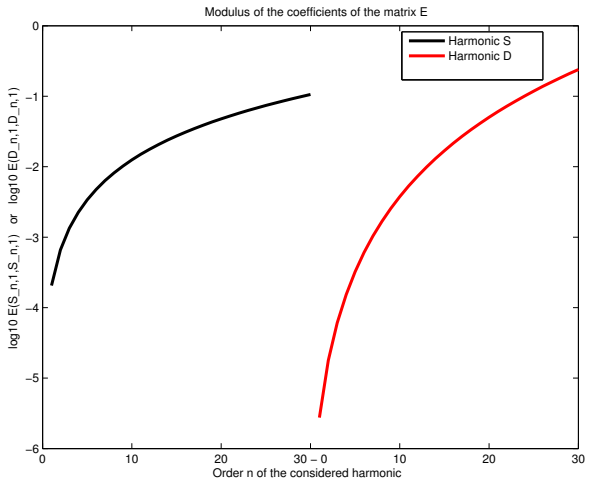

Figure 6.4 – The modulus of the coefficients of the EFIE operator in a spherical harmonics basis for $\kappa = 0.2$.

6.3.3 The solution of the EFIE

After developing the operator and the incident plane wave on the basis of the vectorial spherical harmonics, we easily get the solution (see [75, 70, 71]):

$$\langle j_S \ ; \ \mathbf{S}_n^1 \rangle = \frac{i^{n+1}}{\kappa a Z_0} \frac{2n+1}{n(n+1)} \frac{\alpha_{n,1}}{h_n^{(1)}(\kappa a)},$$
$$\langle j_S \ ; \ \mathbf{D}_n^1 \rangle = \frac{-i^n}{\kappa a Z_0} \frac{2n+1}{n(n+1)} \frac{\alpha_{n,1}}{h_n^{(1)'}(\kappa a)}.$$

Once again, as an illustration, we represent in Figure 6.5 the modulus of the coefficients obtained for $\kappa a = 0.2$.

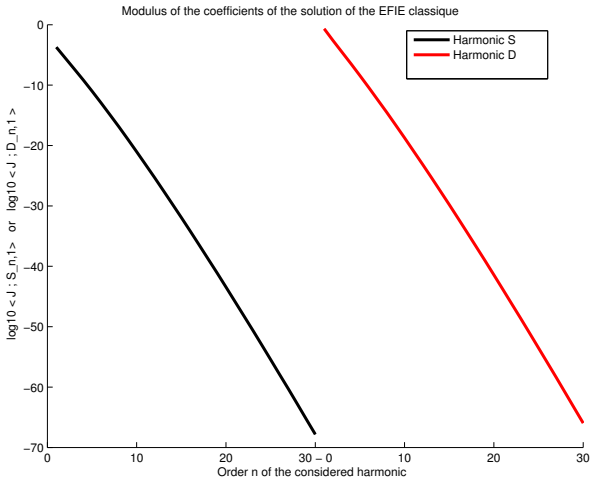

Figure 6.5 – Representation of the decreasing coefficients of the solution of the EFIE in spherical harmonics.

6.4 Representation of the phase conjugation operator in spherical harmonics

6.4.1 Analytical developments

In this paragraph, we present the computation of the matrix $\mathcal{P}$ representing the function Ψ on the spherical harmonic basis and study its structure. In the basis of divergent and solenoidal spherical harmonics $\{\mathbf{S}_n^m, \mathbf{D}_n^m\}$, we represent $\mathcal{P}$ as an infinite dimensional 2×2 block matrix:

$$\mathcal{P} = \begin{bmatrix} P^{SS}_{mn;pq} & P^{SD}_{mn;pq} \\ \\ P^{DS}_{mn;pq} & P^{DD}_{mn;pq} \end{bmatrix}$$

where we have for the various combinations of polarisation types

$$P^{XY}_{mn;pq} = \langle X_n^m \ ; \ \psi Y_q^p \rangle$$

for all $X, Y \in \{\mathbf{S}, \mathbf{D}\}$.

The essential computations for the coefficients of the matrix representation of the similarity transformation concern the following two inner products:

$$\langle \mathbf{S}_{n_1}^{m_1} \ ; \ \psi \mathbf{S}_{n_2}^{m_2} \rangle \quad \text{and} \quad \langle \mathbf{S}_{n_1}^{m_1} \ ; \ \psi \mathbf{D}_{n_2}^{m_2} \rangle \, .$$

In this document, we shall not develop the complete computation of these coefficients, but present the basic ideas which lead to the expression of $\mathcal{P}$. The computation of $\langle \mathbf{S}_{n_1}^{m_1} \ ; \ \psi \mathbf{S}_{n_2}^{m_2} \rangle$ can be performed in two steps. First, considering the expansion of the incident phase in associated Legendre polynomials series and its multiplication with a vectorial spherical harmonics, we begin with the integration over the azimuthal angle φ. This integration gives a condition on the indices m_1 and m_2 to warrant that the scalar product is non-zero. Then we consider the integral over the angle θ. As before, we work only on $m = 1$, since the solution can be expressed with only $\{\mathbf{D}_n^1, \mathbf{S}_n^1\}$.

We compute $\langle \mathbf{S}_{n_1}^{m_1} \ ; \ \psi \mathbf{D}_{n_2}^{m_2} \rangle$ by using the definition of $\mathbf{D}_{n_2}^{m_2}$ as the differential of a scalar harmonic and transposing the derivative to the other factor in the integrand. Formally, we

write:

$$\begin{aligned}\langle \mathbf{S}_{n_1}^{m_1} \ ; \ \psi \mathbf{D}_{n_2}^{m_2} \rangle &= \langle \bar{\psi} \mathbf{S}_{n_1}^{m_1} \ ; \ a_{n,m} r \, \mathbf{d} \, h_{n_2}^{m_2} \rangle, \\ &= -\langle \sqrt{n_2(n_2+1)} \, \mathbf{d}(\bar{\psi} \mathbf{S}_{n_1}^{m_1}) \ ; \ r h_{n_2}^{m_2} \rangle, \\ &= -\langle \sqrt{n_2(n_2+1)} \, \mathbf{d}(\bar{\psi}) \mathbf{S}_{n_1}^{m_1} \ ; \ r h_{n_2}^{m_2} \rangle \, .\end{aligned}$$

The computations of both $\langle \mathbf{S} \ ; \ \mathbf{D} \rangle$ and $\langle \mathbf{S} \ ; \ \mathbf{S} \rangle$ involve the integral of products of three associated Legendre polynomials in $\cos(\theta)$. To deal with it, the main strategy is to describe the product of two Legendre polynomial as a finite sum of Legendre polynomials and then to play judiciously with the recurrence relation presented in Section 6.2 to get a tractable integral (see also [76]). After some simplifications, we end up with:

$$\langle \mathbf{S}_{n_1}^{m_1} \ ; \ \psi \mathbf{S}_{n_2}^{m_2} \rangle = \sum_{p=0}^{+\infty} i^p (2p+1) j_p(\kappa a) a_{n_1}^{m_1} a_{n_2}^{m_2} \pi \delta_{m_1}^{m_2} \left(\sum_{|n_1-p| \leq k}^{n_1+p} \left(2A_{n_1,n_2}^{m,p}(k) + \chi_{n_1}^{m} \chi_{n_2}^{m} A_{n_1,n_2}^{m-1,p}(k) - A_{n_1,n_2}^{m+1,p}(k) \right) \delta_{n_2}^{k} \right),$$

$$\langle \mathbf{S}_{n_1}^{m_1} \ ; \ \psi \mathbf{D}_{n_2}^{m_2} \rangle = \sum_{p=0}^{+\infty} i^{p+1} j_p(\kappa a) a_{n_1}^{m_1} b_{n_2}^{m_2} (2\pi) \delta_{m_1}^{m_2} mp(p+1) \left(\sum_{|n_1-p+1| \leq k}^{n_1+p-1} B_{n_1,n_2}^{m,p-1}(k) \delta_{n_2}^{k} - \sum_{|n_1-p-1| \leq k}^{n_1+p+1} B_{n_1,n_2}^{m,p+1}(k) \delta_{n_2}^{k} \right).$$

Since their definition is tedious, the different coefficients A, B and χ which represent the integrals over the products of associated Legendre polynomials, are defined in Appendix B. We note that we have now an infinite sum of a number of finite sums with rather complicated summands that notably involved Wigner-$(3-j)$ symbols (see [77] and [78] for fast and accurate computation of those coefficients) and factorials.

It is necessary to work on the infinite summation over p. One idea consists of looking at the terms between parentheses and to note that the Kronecker symbol plays an important role here because for fixed n_1, n_2 and m, there exists a p_0 such that

$$(p \ > \ p_0) \Longrightarrow \sum_{|n_1-p+1| \leq k}^{n_1+p-1} B_{n_1,n_2}^{m,p-1}(k) \delta_{n_2}^{k} = 0.$$

By working a bit on the limits of the sums, we readily observe that when $p > n_1 + n_2 + 1$ all the terms within the parentheses are zero because $(p > n_1 + n_2 + 1) \Longrightarrow (k > n_2)$. In this way, we can truncate the sum over p without introducing any error. We then obtain:

$$\langle \mathbf{S}_{n_1}^{m_1} \ ; \ \psi \mathbf{S}_{n_2}^{m_2} \rangle = \sum_{p=0}^{n_1+n_2} i^p (2p+1) j_p(\kappa a) a_{n_1}^{m_1} a_{n_2}^{m_2} \pi \delta_{m_1}^{m_2} \left(\sum_{|n_1-p| \leq k}^{n_1+p} \left(2A_{n_1,n_2}^{m,p}(k) + \chi_{n_1}^{m} \chi_{n_2}^{m} A_{n_1,n_2}^{m-1,p}(k) - A_{n_1,n_2}^{m+1,p}(k) \right) \delta_{n_2}^{k} \right),$$

$$\langle \mathbf{S}_{n_1}^{m_1} \ ; \ \psi \mathbf{D}_{n_2}^{m_2} \rangle = \sum_{p=0}^{n_1+n_2+1} i^{p+1} j_p(\kappa a) a_{n_1}^{m_1} b_{n_2}^{m_2} (2\pi) \delta_{m_1}^{m_2} mp(p+1) \left(\sum_{|n_1-p+1| \leq k}^{n_1+p-1} B_{n_1,n_2}^{m,p-1}(k) \delta_{n_2}^{k} - \sum_{|n_1-p-1| \leq k}^{n_1+p+1} B_{n_1,n_2}^{m,p+1}(k) \delta_{n_2}^{k} \right).$$

Now that we have these analytical expressions for $\langle \mathbf{S}_{n_1}^{m_1} \ ; \ \psi \mathbf{S}_{n_2}^{m_2} \rangle$ and $\langle \mathbf{S}_{n_1}^{m_1} \ ; \ \psi \mathbf{D}_{n_2}^{m_2} \rangle$, it is rather easy to access the remaining relations for computing $\mathcal{P}$. Indeed, it suffices to remark that we have the following relations:

$$\langle \mathbf{D}_{n_1}^{m_1} \ ; \ \psi \mathbf{D}_{n_2}^{m_2} \rangle = \langle \mathbf{S}_{n_1}^{m_1} \ ; \ \psi \mathbf{S}_{n_2}^{m_2} \rangle,$$

$$\langle \mathbf{D}_{n_1}^{m_1} \ ; \ \psi \mathbf{S}_{n_2}^{m_2} \rangle = \overline{\langle \psi \mathbf{S}_{n_2}^{m_2} \ ; \ \mathbf{D}_{n_1}^{m_1} \rangle} = \overline{\langle \mathbf{S}_{n_2}^{m_2} \ ; \ \bar{\psi} \mathbf{D}_{n_1}^{m_1} \rangle} \, .$$

The first relation is easily obtained from $\mathbf{S}_{n_1}^{m_1} \cdot \mathbf{S}_{n_2}^{m_2} = \mathbf{D}_{n_1}^{m_1} \cdot \mathbf{D}_{n_2}^{m_2}$. The second one, relies on a property of the scalar product. To complete this last relation, one has to use the expansion in Legendre polynomials of $\bar{\psi}$,

$$\bar{\psi}(\theta) = \sum_{p=0}^{+\infty} \bar{i^p}(2p+1) j_p(\kappa a) P_p^{(0)}(\cos(\theta)),$$

and observe that only some minor changes are needed (the major part of the integrations remains unchanged). In the same way, one obtains the matrix $\mathcal{P}^{-1}$ by means of the following relations

$$\begin{aligned}
\langle \bar{\psi}\mathbf{S}_{n_1}^{m_1} \ ; \ \mathbf{S}_{n_2}^{m_2} \rangle &= \langle \mathbf{S}_{n_1}^{m_1} \ ; \ \psi\mathbf{S}_{n_2}^{m_2} \rangle, \\
\langle \bar{\psi}\mathbf{D}_{n_1}^{m_1} \ ; \ \mathbf{D}_{n_2}^{m_2} \rangle &= \langle \mathbf{D}_{n_1}^{m_1} \ ; \ \psi\mathbf{D}_{n_2}^{m_2} \rangle, \\
\langle \bar{\psi}\mathbf{S}_{n_1}^{m_1} \ ; \ \mathbf{D}_{n_2}^{m_2} \rangle &= \langle \mathbf{S}_{n_1}^{m_1} \ ; \ \psi\mathbf{D}_{n_2}^{m_2} \rangle, \\
\langle \bar{\psi}\mathbf{D}_{n_1}^{m_1} \ ; \ \mathbf{S}_{n_2}^{m_2} \rangle &= \langle \mathbf{D}_{n_1}^{m_1} \ ; \ \psi\mathbf{S}_{n_2}^{m_2} \rangle .
\end{aligned}$$

Modulo a few details we skipped, we are now able to give a completely explicit expression for each coefficient of the matrices $\mathcal{P}$ and $\mathcal{P}^{-1}$. We observe, by the way, that these matrices are in principle dense.

6.4.2 Numerical construction

. Decomposition of ψh_n^1

.

Having presented the formal computation of the matrix P, we shall now delve a bit more into the numerical implementation. In a first instance, we concentrate on the scalar problem to expand the product of a single spherical harmonic and the plane wave phase function into the basis of spherical harmonics. Basically, this concerns the computation of the quantities

$$\langle \psi h_n^m \ ; \ h_k^m \rangle.$$

Starting with the expansion of ψ in associated Legendre polynomials and using the expansion of the product of two associated Legendre polynomials, one of order 0 the other of order m, as a finite sum in the basis of associated Legendre polynomials:

$$P_{j_1}^{m_1}(z) P_{j_2}^{m_2}(z) = (-1)^{m_1} \sqrt{\frac{(j_1+m_1)!}{(j_1-m_1)!}\frac{(j_2+m_2)!}{(j_2-m_2)!}} \sum_{|j_1-j_2|\leq k}^{j_1+j_2} G(k) \sqrt{\frac{(k-m_2+m_1)!}{(k+m_1-m_1)!}} P_k^{-m_1+m_2}(z)$$

with

$$G(k) = (-1)^{-m_1+m_2}(2k+1) \begin{pmatrix} j_1 & j_2 & k \\ 0 & 0 & 0 \end{pmatrix} \begin{pmatrix} j_1 & j_2 & k \\ -m_1 & m_2 & m_1-m_2 \end{pmatrix}$$

where $\begin{pmatrix} j_1 & j_2 & j_3 \\ m_1 & m_2 & m_3 \end{pmatrix}$ is the 3-j Wigner symbol, we get in a few steps

$$\psi h_n^m = \sum_{p=0}^{+\infty} i^p (2p+1) j_p(\kappa a) \sum_{|n-p|\leq k}^{n+p} (-1)^m \sqrt{2n+1}\sqrt{2k+1} \begin{pmatrix} p & n & k \\ 0 & 0 & 0 \end{pmatrix} \begin{pmatrix} p & n & k \\ 0 & m & -m \end{pmatrix} h_k^m .$$

In this intermediate result, we change the order of the summations over p and k and get the following equality:

$$\langle \psi h_n^m \ ; \ h_k^m \rangle = (-1)^m \sqrt{2n+1}\sqrt{2k+1} \sum_{|n-k|\leq p}^{n+k} i^p (2p+1) j_p(\kappa a) \begin{pmatrix} k & p & n \\ 0 & 0 & 0 \end{pmatrix} \begin{pmatrix} k & p & n \\ -m & 0 & m \end{pmatrix} .$$

At this point, we would like to be able to estimate the asymptotic behaviour of this latter coefficient as a function of k.

We can reasonably expect a rapid decay of $\langle \bar{\psi} h_n^m \ ; \ h_k^m \rangle$ when $k \to \infty$, i.e.,

$$\lim_{k \to 0} |\langle \bar{\psi} h_n^m \ ; \ h_k^m \rangle| = 0$$

Indeed, through this function $f(k) = \langle \bar{\psi} h_n^m \ ; \ h_k^m \rangle$, we observe the harmonic spectrum of the product of two functions: one very regular (having a Dirac spectrum) and the other one less regular with a spectrum determined by the Bessel coefficients j_p:

$$\langle \psi \ ; \ h_k^m \rangle = 4\pi i^k \ j_k(\kappa a) \delta_m^0.$$

This leads us to believe that the spectrum of the product is close to the spectrum of $\bar{\psi}$.

From the numerical point of view, leaving the implementation aside for the moment, we observe a number of interesting things. First, as we can see in Figure 6.6, numerically, ψh_n^m, is expanded in terms of a relatively small number of harmonics (of identical azimuthal order $m = 1$). By analogy with Fourier analysis, we can observe here the spectrum of a very smooth function.

We also note that we have no decay as function of n, i.e., for each n we find the same form of the harmonic spectrum (we could use the term "sliding spectrum").

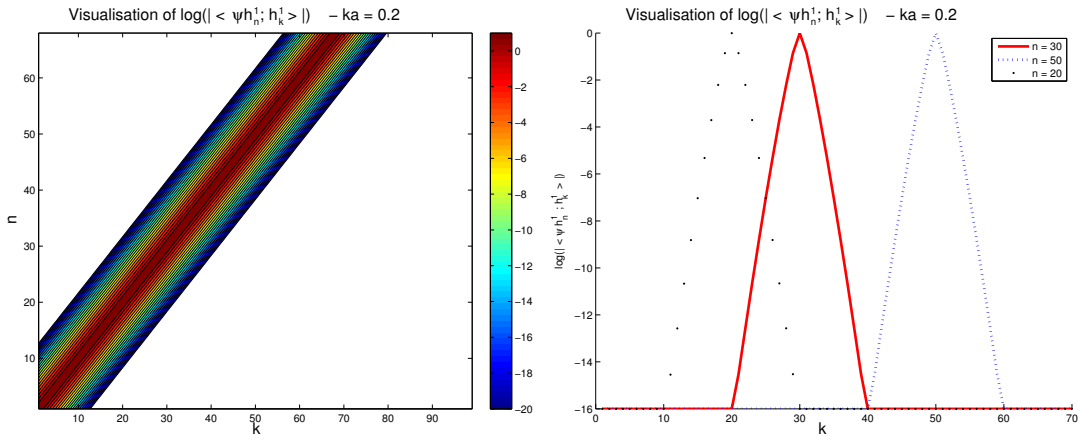

Figure 6.6 – Graphical representation of $\langle \psi h_n^1 \ ; \ h_k^1 \rangle$ for $\kappa a = 0.2$.

Another important point is the influence of κa in the width of the observed spectra. We have tested different configurations and we observe, see Figure 6.7, that with the increasing of κa the width of the spectrum increases too, to be precise, the spectral approximation of ψh_n^m requires more and more harmonics. In order to explain this, we look at the definition of ψ:

$$\psi(\theta) = \sum_{p=0}^{+\infty} i^p (2p+1) j_p(\kappa a) P_p^{(0)}(\cos(\theta))$$

and the behaviour of the coefficients $j_p(\kappa a)$. When κa tends to 0 all coefficients $j_p(\kappa a)$ tend to 0 excepting the term $j_0(\kappa a)$ which tends to 1. In short, the smaller κa is, the closer ψ is to the unit function. In that case, we obtain

$$\lim_{\kappa a \to 0} \langle \psi h_n^m \ ; \ h_k^m \rangle = \langle \lim_{\kappa a \to 0} \psi h_n^m \ ; \ h_k^m \rangle = \langle h_n^m \ ; \ h_k^m \rangle.$$

In the opposite case, when κa increases, the other coefficient j_p also increase and become dominant, perturbing the harmonic h_n^m and hence requiring a larger spectral support (although still restricted due to the regularity of ψh_n^m).

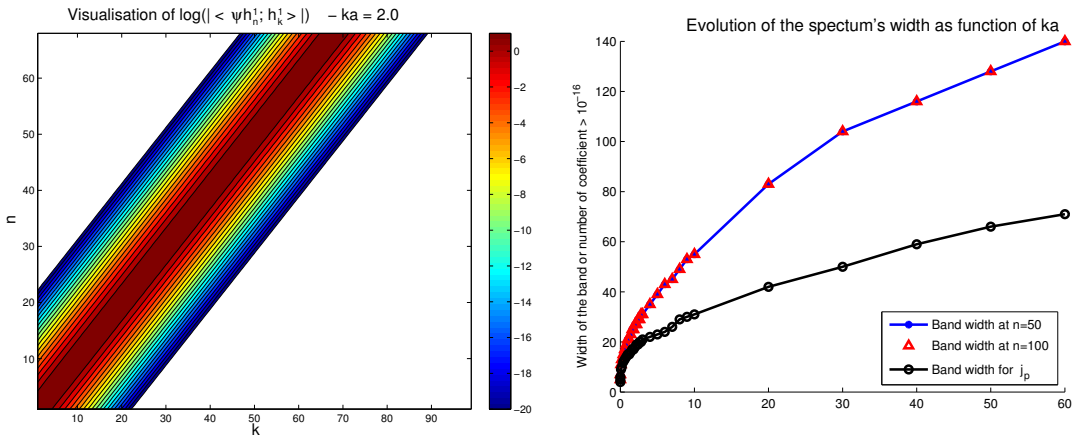

Figure 6.7 – On the left: $\langle \psi h_n^1 \ ; \ h_k^1 \rangle$ for $\kappa a = 2.0$. On the right: evolution of the spectral width as a function of κa and the number of Bessel coefficients $j_p(\kappa a) > 10^{-16}$.

. Decomposition of $\psi\mathbf{D}$ and $\psi\mathbf{S}$

Having looked at the details of the scalar case, i.e., the decomposition in scalar spherical harmonics of ψh_n^m, we can do the same operations for $\psi\mathbf{S}_n^m$. As indicated before, there are a few relations which allow us to obtain from $\langle \mathbf{S}_n^m \ ; \ \psi\mathbf{S}_k^m \rangle$ and $\langle \mathbf{S}_n^m \ ; \ \psi\mathbf{D}_k^m \rangle$ all blocks of the matrices $\mathcal{P}$ and $\mathcal{P}^{-1}$. We therefore only handle these two decompositions.

In both cases, considering the decomposition of $\psi\mathbf{S}_n^m$ on the harmonics $\vec{\mathbf{S}}$ or on the harmonics $\vec{\mathbf{D}}$, we find the same properties found for $\bar{\psi} h_n^m$.

First, as we can see in Figures 6.8 and 6.9, we find a relatively limited spectrum, meaning that $\psi\mathbf{S}_n^m$ can be spectrally approximated by a not too large number of harmonics $\vec{\mathbf{S}}$ and $\vec{\mathbf{D}}$. In the second place, as for the scalar function's case, we observe a sliding spectrum, i.e., a spectrum non-decreasing with the increasing of n. Finally, we obtain the same dependence of the band width as a function of κa as we can see in Figure 6.10.

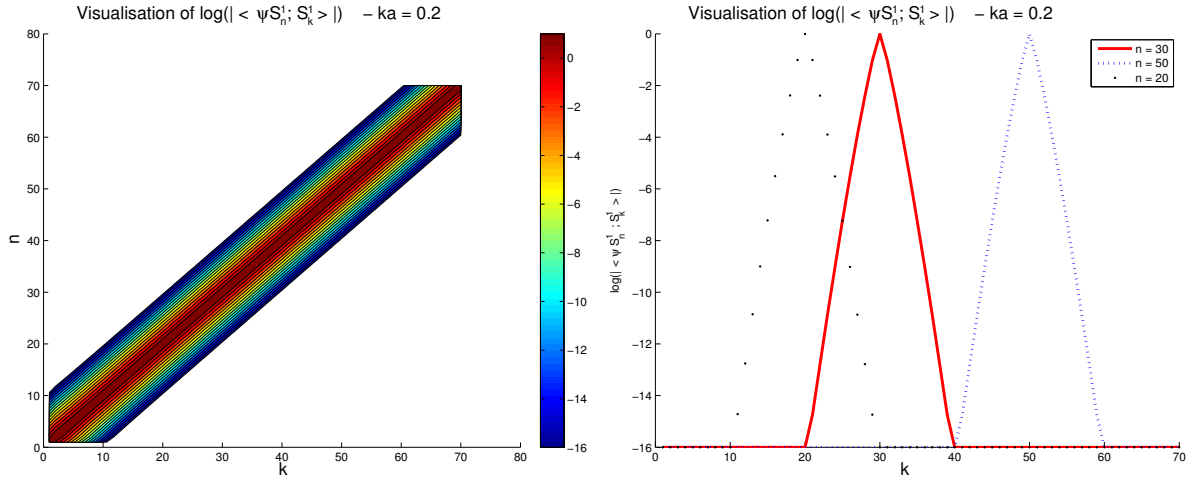

Figure 6.8 – Representation of $\langle \psi\mathbf{S}_n^1 \ ; \ \mathbf{S}_k^1 \rangle$ for $\kappa a = 0.2$.

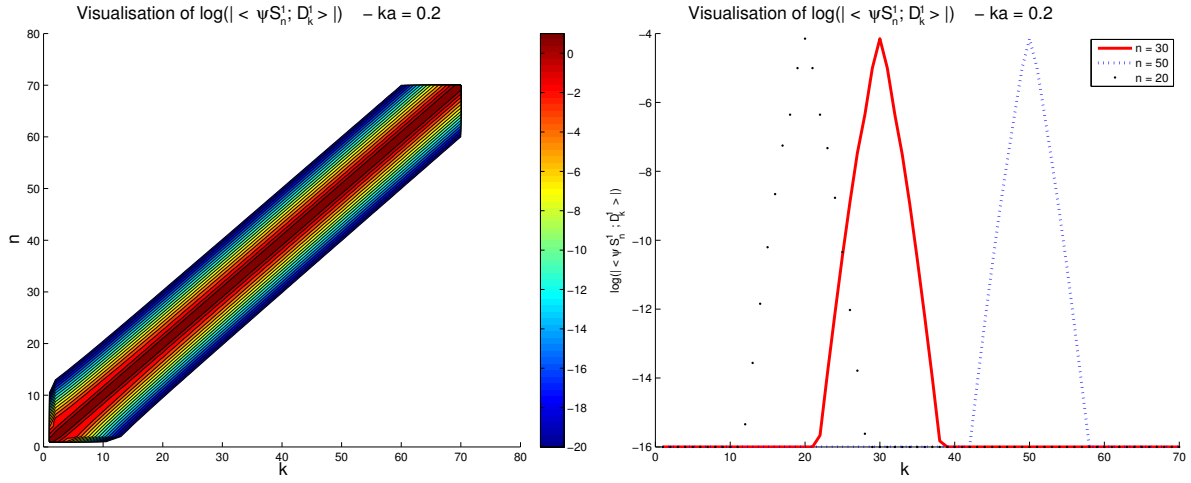

Figure 6.9 – Representation of $\langle \psi \mathbf{S}_n^1 \ ; \ \mathbf{D}_k^1 \rangle$ for $\kappa a = 0.2$.

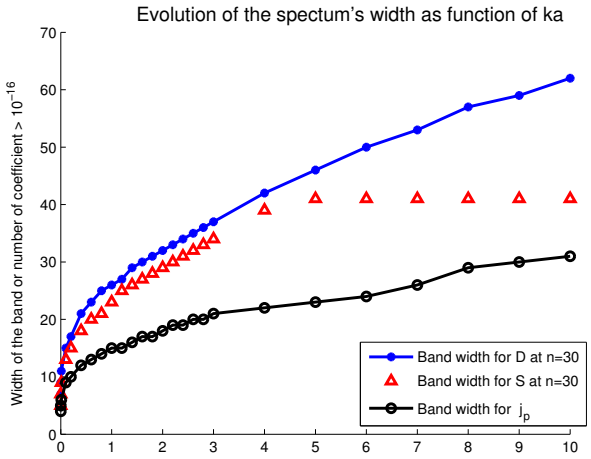

Figure 6.10 – Evolution of the extension of the spectrum of $\psi \mathbf{S}_n^1$ (on the harmonics $\vec{\mathbf{S}}$ and $\vec{\mathbf{D}}$) as a function of κa. For each value of κa we show the number of Bessel coefficients $j_p(\kappa a) > 10^{-16}$.

. Validation of the analytical results

To validate the various results obtained, and to be sure that the numerous developments are correctly done, we have applied a second method based on numerical integration of the decompositions $\langle \psi \mathbf{S}_n^m \ ; \ \mathbf{S}_k^m \rangle$ and $\langle \psi \mathbf{S}_n^m \ ; \ \mathbf{D}_k^m \rangle$ (in fact, a simple uniform discrete integration rule in θ and φ on the sphere). It appears, regarding the result presented in Figure 6.11, that the obtained results are reasonably equivalent, i.e.,

$$\forall k, \ \frac{\left| \langle \psi \mathbf{S}_n^m \ ; \ \mathbf{S}_k^m \rangle_{\text{analytical}} - \langle \psi \mathbf{S}_n^m \ ; \ \mathbf{S}_k^m \rangle_{\text{numerical}} \right|}{\left| \langle \psi \mathbf{S}_n^m \ ; \ \mathbf{S}_k^m \rangle_{\text{analytical}} \right|} \leq 10^{-3},$$

which partly validates our analytical developments. Another supporting element is that for each n the norm of $\sum_k \langle \psi \mathbf{S}_n^m \ ; \ \mathbf{S}_k^m \rangle + \langle \bar{\psi} \mathbf{S}_n^m \ ; \ \mathbf{D}_k^m \rangle$ is indeed 1 (this is required because $\| \psi \mathbf{S}_n^m \| = 1$).

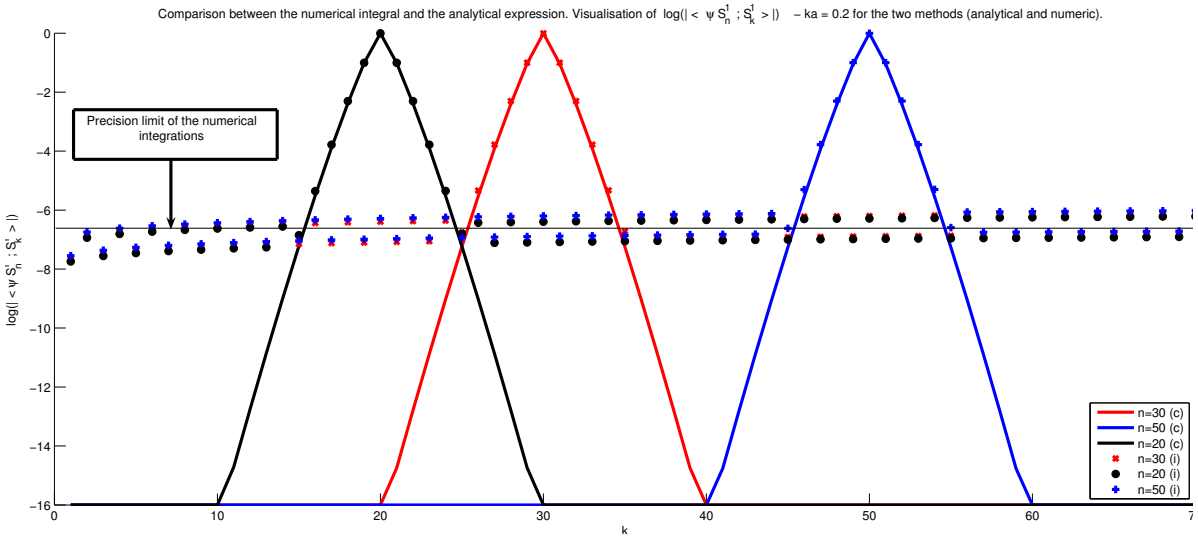

Figure 6.11 – Representation of $\langle \psi \mathbf{S}_n^m \ ; \ \mathbf{S}_k^m \rangle$ for $\kappa a = 0.2$. Comparison between numerical integration and analytical formulas. ((i) numerical integration, (c) analytical computation).

. The matrix $\mathcal{P}$

As we indicated, the matrix $\mathcal{P}$ can be put in the following form (by organising the spherical harmonics appropriately)

$$\mathcal{P} = \left(\begin{array}{c|c} \left(\langle \mathbf{S}_k^\ell \ ; \ \psi \mathbf{S}_n^m \rangle \right)_{n,m} & \left(\langle \mathbf{S}_k^\ell \ ; \ \psi \mathbf{D}_n^m \rangle \right)_{n,m} \\ \hline \left(\langle \mathbf{D}_k^\ell \ ; \ \psi \mathbf{S}_n^m \rangle \right)_{n,m} & \left(\langle \mathbf{D}_k^\ell \ ; \ \psi \mathbf{D}_n^m \rangle \right)_{n,m} \end{array} \right).$$

Regarding the results of the numerical computation of the decomposition of $\psi \vec{\mathbf{S}}$, we can propose the complete representation of the operator Ψ. As we can see in Figure 6.12, its matrix representation on vector spherical harmonics of an order $n \leq N$ (N fixed) has four blocs with a band structure.

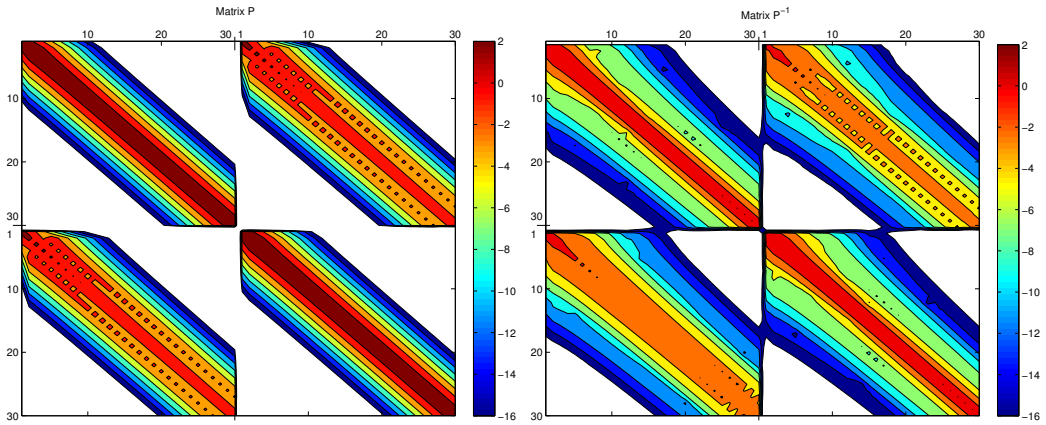

Figure 6.12 – Representation of the modulus in logarithmic scale of the matrix $\mathcal{P}$ coefficients on the left and its inverse $\mathcal{P}^{-1}$ on the right.

6.5 Representation of the HEFIE operator on the sphere in spherical harmonics

6.5.1 Construction

Having seen the matrix P and its inverse, we can now construct the matrix H. The operators $\mathcal{E}$ and $\mathcal{H}$ being related by

$$\mathcal{H} = \Psi^{-1}\mathcal{E}\Psi,$$

we have the matrix relation

$$H = \mathcal{P}^{-1}E\mathcal{P}.$$

With a diagonal matrix E and two matrices $\mathcal{P}$ and $\mathcal{P}^{-1}$ having a 2×2 band block structure, the resulting H matrix has the same structure as $\mathcal{P}$ (see Figure 6.13) and can be view as a 2×2 block matrix with a band block structure:

$$H = \begin{pmatrix} H^{SS} & H^{SD} \\ H^{DS} & H^{DD} \end{pmatrix}. \tag{6.7}$$

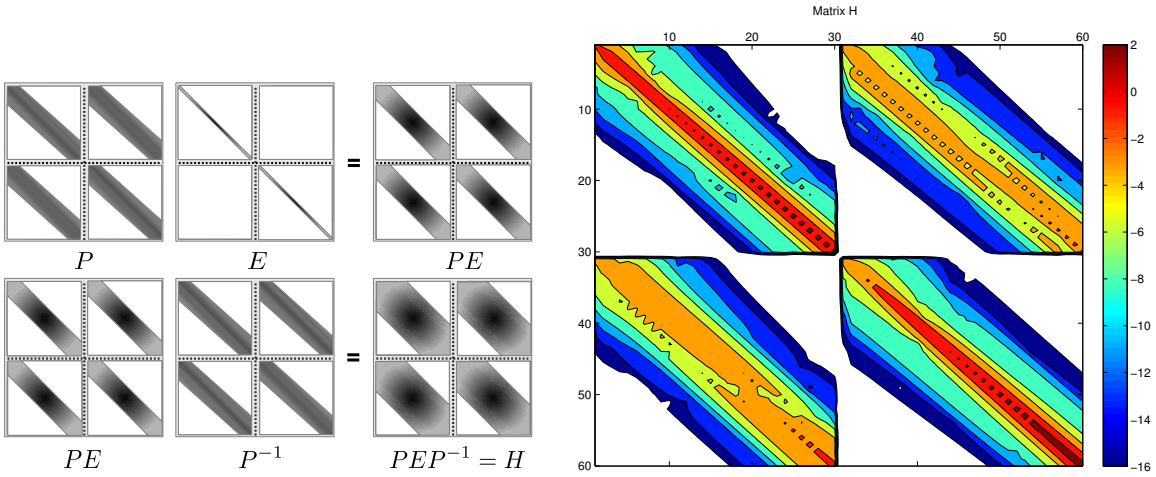

Figure 6.13 – On the left, the geometrical "scheme" of the matrix H. On the right, the representation of the modulus (in logarithmic scale) of the matrix coefficients of H.

6.5.2 Norm estimates

As suggested in the preceding sections, notably through the shape of the matrix $\mathcal{P}$ and H, the HEFIE, working on a pseudo current (the physical current multiplied by the conjugate phase of the incident wave), introduces a coupling between the divergent and the solenoidal part, which was totally absent in the EFIE with the physical current. The idea now is to give a good estimation of this coupling by looking at the anti-diagonal blocks of the HEFIE matrix. As we already wrote, for some particular reasons, we have considered the operator $\mathcal{E}[j] = \tau^*(\mathcal{A}[j] - \frac{1}{\kappa^2}\,\mathbf{d}\,\boldsymbol{\delta}\,\mathcal{A}[j])$. We then observe increasing norms and not decreasing norms as it was presented in Chapter 5. It is just a normalization choice. The important thing is still the ratio between the norm of the various blocks.

In this section we compare the spectral norm, i.e., the largest singular value, of the four blocks constituting the HEFIE operator. We compute these norms as a function of the frequency between $\kappa a = 10^{-4}$ and $\kappa a = 20$. These computations reveal a few interesting elements.

First, as we can see in Figures 6.14 and 6.15, we observe that at the lower frequencies, i.e., for $\kappa a < 10^{-1}$, the norms of the diagonal blocks are asymptotically proportional to the first order spherical Bessel coefficients $j_1(\kappa a)$. In the same way, asymptotically, the norms of the extra-diagonal blocks follow the Bessel coefficients $j_2(\kappa a)$. These two coefficients appear naturally in the expansions of the matrices E and P.

We also note that for the lower frequencies, the diagonal blocks have larger norms than the extra-diagonal blocks. This implies that at low frequencies the coupling between the divergent (**D**) and the solenoidal (**S**) current distributions remains relatively weak.

For the higher frequencies, the norms of the blocks H^{DS}, H^{SD} et H^{SS} tend to be of the same order of magnitude. A possible explanation for this is that at high frequencies the phase of the incident plane wave expands over a large number of harmonics. This makes that the expansion of $\psi\mathbf{D}$ (resp. $\psi\mathbf{S}$) extends also over a larger number of harmonics, which can cause the matrix norms to increase.

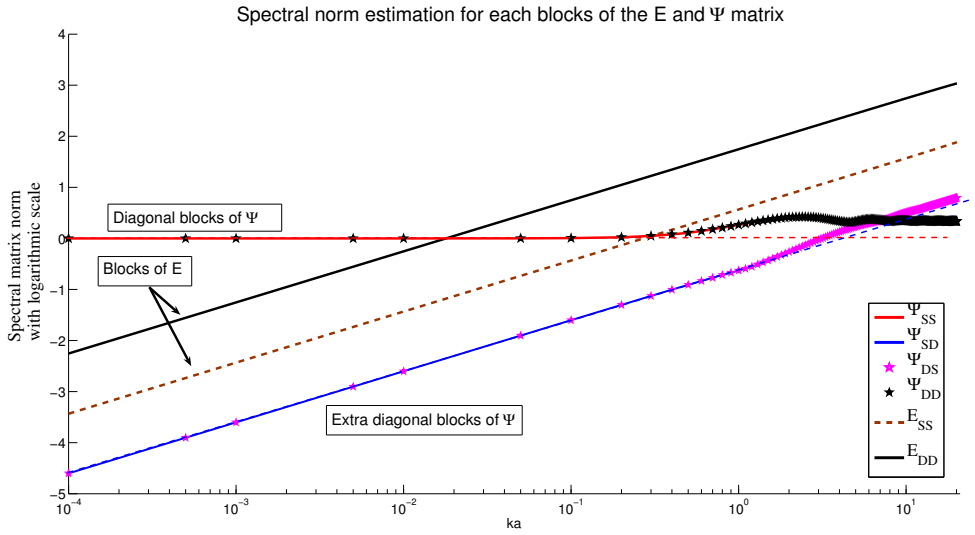

Figure 6.14 – Evolution of the L^∞ norms of the matrices E and $\mathcal{P}$ as a function of κa.

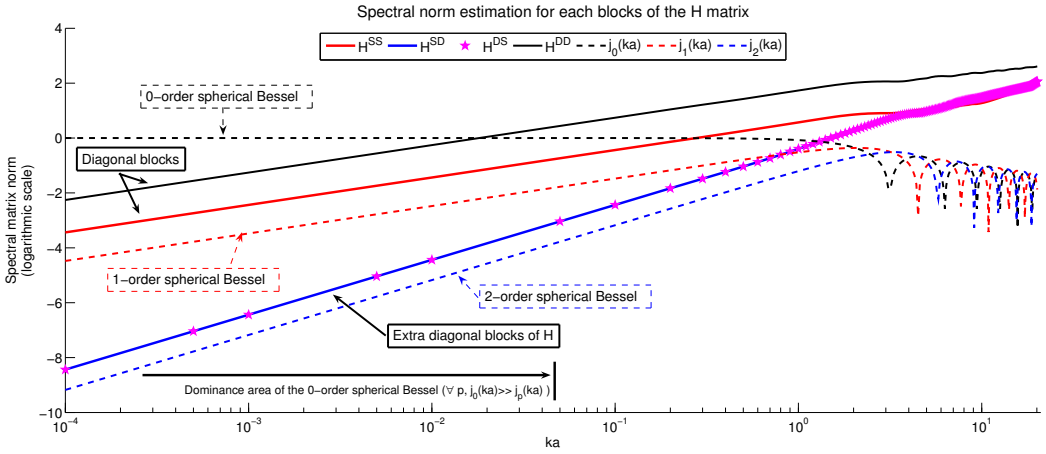

Figure 6.15 – Evolution of the L^∞ norms of the four blocks of H and of the first three Bessel coefficients as a function of κa.

To conclude this section, it is interesting to make a link between the results obtained here and those presented in Chapter 3. In fact, besides re-normalization, we perceive through the analytical developments that, at low frequencies, the coupling is weak between the solenoidal and divergent parts of the current, whereas in the context of the use of a edge functions, the coupling appears pretty strong. This can be explained by the fact that we have two approximations. The first is the approximation made by the choice of edge functions and the second is the choice of method used to establish the Helmholtz decomposition on this functional space. Both approximations then makes it difficult to achieve a weak coupling between solenoidal and divergent currents. However, as we show in Chapter 3, the construction method of the loop functions has a huge impact on the norms of the discrete operator. Therefore, the existence of a matrix D_H able to re-obtain this decoupling is highly possible. However, as for higher frequencies the coupling is strong, it is unlikely to find a method of construction that would lead to weak norms for extra-diagonal blocks.

Conclusions and Perspectives

Conclusions

Herberthson's equations. In this thesis, we studied Herberthson's integral equations dedicated to the scattering of a plane wave by a perfectly conducting object. The general idea of these new equations is to work not on the physical surface currents induced by the incident wave but on a pseudo-current, defined as the physical current multiplied by the conjugate phase of the incident wave. Whereas the presentation of Herberthson was a mix of differential forms and the more usual vector analysis, we took up the challenge to use exterior differential forms all the way through (see Chapters 1 and 2). The original work of Herberthson was specific for some surface topologies where a Helmholtz decomposition allows a representation of the pseudo current via two scalar potentials. In order to treat more general topologies, we did not use that specialization and worked on another orthogonal decomposition splitting the pseudo current into a solenoidal and a divergent constituent.

Study of an analytical case. We have studied the general problem from the mathematical and the numerical point of view, but also, for the particular case of a perfectly conducting sphere, by means of a completely analytical approach. This analytical study allowed us, in particular, to establish the coupling between solenoidal and divergent current distributions. While, initially, the special form of the new equations inspired some hope to reduce the modelling essentially to the non-solenoidal part of the current distributions, this analytical study clearly indicated that this is not generally possible (see Chapter 6).

A well-posed problem. The mathematical analysis of the general problem concerned the first requirement of any model: to be well-posed. That means that we have to provide a proof of unique existence of a solution in a well-defined large class of configurations. We have shown that the new equations are algebraically equivalent to the conventional equations, which are for almost every frequency well-posed indeed. This was done using the phase conjugation operator as a similarity transformation (see Section 2.4).

The situation is now satisfactory from the mathematical point. Indeed, we provided a proof of existence and uniqueness of a solution in a well-defined large class of configurations, additionally proving that the problem was well-posed.

Implementations. Although, we also wanted to see whether the potential advantages of the new equations could be turned into a concrete reduction of the computational cost. Therefore, we constructed an edge element implementation of the new integral equations (see Chapter 3). The essential difficulty here was to account for the modified kernel distribution and to implement the Hodge-Helmholtz decomposition. In fact, the computation of the coefficients of the perturbation with respect to the conventional integral equation needed only few new developments.

For the Helmholtz decomposition, we used a graph based algorithm, which is specific for the edge elements used in the discretization, and a change of basis matrix representation.

Solution. We could then perform comparisons between computations with the conventional and the new equations. All numerical experiments are done comparing the EFIE to Herberthson's EFIE (HEFIE) for the scattering of a plane wave by a sphere and by an airplane. In all numerical experiments, the complete Galerkin matrix is computed and a GMRES iterative solver is used with various preconditioning.

Reduction of degrees of freedom. Apart from the analysis of linear systems and their proper resolution, we were interested in another important property: the possibility to reduce the number of degrees of freedom required to get an accurate solution of the problem. To benefit from this property, we built a reduced system allowing a reduction by a factor four of the number of degrees of freedom without any loss of the quality of the computed surface current.

The global conclusion of these experiments can be summarized as follows.
The HEFIE, with model reduction, presents an advantage over the EFIE because the reduction in the number of degrees of freedom makes the iterative solution of the equations faster and this weighs up against the increased computational cost of the construction of the perturbation of the Galerkin matrix (which has to be redone for each specific direction of incidence).

In this global conclusion, the Helmholtz-Hodge decomposition and the various preconditioners are not explicitly mentioned. In fact, the Helmholtz-Hodge decomposition could serve in specific preconditioning techniques such as those based on a Schur complement. In the experiments done, the cost of the construction of such preconditioners outweighed the gain in iteration count for the solver. In the Perspectives section below, we make a few suggestions on future developments on this.

Perspectives

The work done in this thesis opens some interesting perspectives. From a theoretical point of view, we mention an interesting further development. In this manuscript, we focused on the properties of the HEFIE and provided proofs of existence and uniqueness of a solution. To establish the convergence of a Galerkin method for the new integral equations appeared a more diffcult problem. During the PhD work, a method of proof derived from work by Christiansen [49] has been identified but the proof could not be completed in the given time span.
From a numerical point of view, there are three main axes to develop: the matrix assembly, the preconditioning and the model reduction. We comment on these aspects below.

The assembly of the matrices H (mainly for the HEFIE). As we have seen through Chapters 4 and 5, the main downside of the method was the additional costs induced by the assembly of the perturbation. Since the assembly increases significantly the number of operations, it reduces, sometimes considerably if not completely, the gains offered by the solution. Therefore, it seems important to work on the assembly and appropriate to propose an acceleration method to compute the various matrices faster.
A first track could be the use of hierarchical matrices method ($\mathscr{H}$-matrices, see [79, 80, 81]). The main idea of this kind of method is to create a data-sparse approximation of non-sparse matrices requiring only $O(n^k log(n))$ units of storage, where k is a parameter controlling the accuracy of the approximation for a computational cost of the order of $O(n^{k'} \log(n))$. For the construction of the approximation, we propose for example the use of the combination $\mathscr{H}$-matrix and ACA techniques (ACA for Adaptative Cross Approximation, see [10, 82]) on the matrix $\tilde{H}$ obtained from the discretization of Herberthson's equations (without considering the Helmholtz decomposition). In that case, the additional cost would be automatically reduced.
In the same way, we can also suggest the development of a multipole method (see [7, 8, 9, 23]) on $\tilde{H}$ to reduce the computational cost.

Preconditioning. The second essential point is the development of good preconditioners. In Chapter 4, we tested various preconditioners in order to reduce the number of GMRES iterations. We noted in particular that the Jacobi preconditioner was efficient and the Inverse and Schur blocks were interesting in the sense that these reduce the number of iterations, but were prohibitive, because too costly computationally. Therefore, it appears necessary to construct better preconditioners.
Basically, we think that the idea to focus on the matrix obtained from the discretization, i.e., the matrix $\tilde{H}$, is the better approach. The adaptation to a chosen Helmholtz decomposition and by this way to H is rather straightforward.
In this respect, a first track could be the use of Sparse Inverse Matrix both to approximate the Inverse and the Schur block preconditioners and to find a global preconditioner to $\tilde{H}$ (see [67]). The objective of such an approach would be to create a sparse matrix approximating either the inverse of the block $\tilde{H}_{11}$ and $\tilde{H}_{22}$ or the inverse of $\tilde{H}$ which are easier to compute than the actual inverses.
A second track would be to use Hierarchical matrix methods to create the preconditioners. Formally, the idea would be to construct a coarse approximation of the full matrix $\tilde{H}$, with the combination of a $\mathscr{H}$-matrix and the ACA method for example. Although such an approximation may not be good enough to obtain a good solution, it may yield a good preconditioner with a Hierarchical structure (see for example [83, 84, 85]).

Model reduction. As we explained earlier, the advantage of the HEFIE is the possibility to reduce the number of degrees of freedom required to obtain a good solution. In Chapter 5, dealing with two matching meshes, we have developed a method to construct a reduced system that lets us obtain a good solution in terms of the surface current and RCS with a lower cost than the conventional EFIE and the HEFIE.
This method could be extended in different directions. In the first place, it would be interesting to test this approach for the HMFIE (and the HCFIE) and on less canonical objects (airplane, wind turbine, ...). It would be the occasion to identify the situations where this method can be used and where it appears as the best suited. This study should have for objective to answer the following questions :

- Can we use macro-elements with larger support than the four triangles tested in this thesis?
- Can we use the macro-elements everywhere on the structure or are specific regions (transition between illuminated and shadow regions,...) to be excluded?
- Can we use more general submesh constructions replacing the coarse to fine mapping used in this thesis (see [16, 68, 69, 86, 87])?

Another important remark that could be the starting point of further developments concerns the possibility of reducing again the computational time. Indeed, in our developments, we suppose that everywhere the use of the HEFIE brings some help into the solution of the problem (or at least does not worse the problem). However, in some located area such as the transition zone or locally concave area, the adding of the phase/phase conjugate into the integral equation does not appear really useful. Therefore, it can be interesting to use the conventional EFIE on those area instead of the HEFIE. That is another interest of our formulation where we clearly expressed the perturbation apart, since we can combine the HEFIE and the EFIE, following the area, by simply cancelling the associated perturbation.

Appendix

Appendix A

A short overview of differential forms

Contents

In this chapter, we review the essential elements of differential form calculus. First, we introduce some basic notions from the theory of manifolds and tangent bundles. Then, we specialise to differentiable manifolds with a metric and present the most important properties of the exterior differential operator and the Hodge duality operator on differential forms. We conclude with a summary of the special case of differential forms on three-dimensional Euclidean space and manifolds embedded in it. This presentation of differential form is a rather succinct overview of the theory. More exhaustive, formal and complete presentations can be found in [27, 33, 34, 32].

A.1 Motivations

. Motivations

Despite its centenary existence (E. Cartan, 1899) and its general adoption in fundamental theoretical physics (such as general relativity, quantum field theory, Hamiltonian dynamics, ...), the differential form formulation is still not well established in the world of research in electromagnetic modelling (see [35] for an historic overview). Despite some interesting publications such [27] or [29], for example, the major part of the literature on electromagnetics is still formulated in vector calculus.

In fact, the algebra and calculus of differential forms, due to its convenience, compactness, and many other qualities, is ideally suited to the study of electromagnetics. The calculus and use of differential forms, which has been applied to EM theory by Deschamps [27], Lindell [28], Bossavit [36], Warnick [29, 37, 38, 39] and other authors [40, 41, 42, 43], make main results and equations in EM theory more concise than the usual vector analysis presentations. For example, the differential forms provide a simple, compact and elegant formulation for the Maxwell and

Helmholtz equations using only two operators: the exterior derivative operator **d** and the Hodge star operator $\star$ while vectorial formulation requires the use of the gradient, the curl and the divergence.

The calculus of differential forms offers both algebraic and geometrical advantages over vector analysis. With differential forms, vector identities and theorems are reduced to simpler algebraic properties and manipulations are often more transparent and less tedious than they would be in vector analysis. In particular, the behaviour under coordinate changes of differential is as simple as with scalar functions because, in a certain way, the reference frame makes part of the definition of the differential form. Differential forms also let field quantities and the laws they obey to be manipulated and visualised in a more intuitive manner. In addition, there is a simple correspondence between the formalism of differential forms and classical vector calculus.

A.2 Some notations and reminders

In this section, we define some basic notational tools and some concepts of topology and linear algebra. See [88, 33, 28, **?**, 89, 90] or [44, Chapter 4].

. Notations

We start with the Kronecker symbol.

Definition A.1 : **The Kronecker symbol**

The Kronecker symbol is a function of two integers, that takes the value 1 if the two integers are equal and 0 otherwise. We denote it by an indexed letter δ with some variations depending on the context:

$$\delta_{ij} = \delta_i^j = \delta^{ij} = \begin{cases} +1 & \text{if } i = j, \\ 0 & \text{if } i \neq j. \end{cases}$$

□

In the presentation of exterior forms of any degree, will also need permutations of index sets. We will briefly recall what a permutation is, its parity and the Levi-Civita symbol of order N.

Definition A.2 : **Permutation. Parity of a permutation**

Let $A = \{\alpha_1, ..., \alpha_p\}$ be an ordered set (of natural numbers, for example). Every permutation σ can be broken down into the composition of elementary permutations called transpositions. Each transposition consists of the commutation of two neighbouring (successive) elements. We call σ

- an even permutation, if it can be expressed as the composition of an even number of transpositions,
- an odd permutation, if it can be expressed as the composition of an odd number of transpositions.

We write $\mathfrak{S}_A$ for the set of permutations of A. □

Definition A.3 : The Levi-Civita symbol

Let $A = \{\alpha_1, ..., \alpha_p\}$ be an ordered set. The Levi-Civita symbol of a permutation σ, written $\varepsilon(\sigma)$, is the mapping defined by

$$\begin{aligned} \varepsilon : \mathfrak{S}_A &\longrightarrow \{1, -1\}, \\ \sigma &\longmapsto \varepsilon(\sigma) = \begin{cases} +1 & \text{if } \sigma \text{ is an even permutation of } A, \\ -1 & \text{if } \sigma \text{ is an odd permutation of } A. \end{cases} \end{aligned} \tag{A.1}$$

$\varepsilon(\sigma)$ is called the sign (or the parity) of σ. □

. Topological manifolds and vector bundles

In this section, we present some definitions related to topological spaces such as manifolds and vector bundles.

Definition A.4 : Topological Manifold

A topological manifold of dimension n is a topological space M such that for each point $p \in M$, there exists an open neighbourhood $U_p \subset M$ and a homeomorphism $\phi : U_p \to \mathbb{R}^n$. □

In short, we ask for a topological manifold to look, at least locally, like an open set in $\mathbb{R}^n$. This definition is related to the definition of a chart.

Definition A.5 : Charts

A chart ϕ on a topological manifold M of dimension n is a homeomorphism (a bijective continuous mapping with continuous inverse) from an open set $U \subset M$ to an open set V in $\mathbb{R}^n$, $\phi : U \subset M \to V \subset \mathbb{R}^n$. For example, we can define the chart x^k, the k-th coordinate function, by:

$$\begin{aligned} x^k : M &\longrightarrow \mathbb{R}, \\ p &\longmapsto x^k(p) = \phi^k(p). \end{aligned} \tag{A.2}$$

We note (ϕ, U) for $\phi : U \subset M \to V \subset \mathbb{R}^n$. □

In the above definition of a topological manifold M with charts, it is assumed that charts can be defined and continuity can be proven. However, this requires that a topology of M has already been defined. This is indeed the case when, for example, the manifold is defined as a subspace of an existing topological space like $\mathbb{R}^3$ with the standard Cartesian product topology. If this is not the case, the manifold can be defined by a collection of open sets called an atlas, $A = \{U_k\}$, and transition maps between the elements of the atlas.

Definition A.6 : Atlas and transition maps

Given U, V two chart from the atlas A, a transition map between U and V is a homeomorphism

$$\tau : W \subset U \to V.$$

Note that a transition map between U and V must be defined when the corresponding subsets of M (are supposed to) intersect. In the general case, a topological manifold is then defined as an equivalence class of atlases. Two atlases are equivalent if they can be combined into a single atlas with transition functions satisfying the homeomorphy constraint.
Note that, in general, the open set of an atlas are the only spaces on which we have to define functions. The associated charts are also called the charts of the atlas and points in a chart are only implicitly identified with points in the underlying manifold. We can still use (A.2) for the coordinate functions, forgetting the map ϕ, as the standard coordinate functions of $\mathbb{R}^n$. □

In order to prepare the analysis of vector fields on a manifold, we introduce the notion of vector bundle.

Definition A.7 : Vector bundle

Let M be a topological manifold. A real vector bundle ξ of rank n over M consists of real vector spaces ξ_p of dimension n, associated to every point p of M. The vector spaces ξ_p depend continuously on p. In other words, to define a vector bundle, we define a topological space E, called the "total space of the bundle", and a continuous mapping $\pi : E \longrightarrow M$, a projection from E onto M, and a vector space structure on the inverse images, $\xi_p = \pi^{-1}(p)$, that is locally constant in the following sense: for each point $p \in M$, there exists a neighbourhood U of p and a homeomorphism

$$h : U \times \mathbb{R}^n \longrightarrow \pi^{-1}(U) := E(\xi_{|U}) \tag{A.3}$$

such that every $h_p : \mathbb{R}^n \longrightarrow h(p, U)$ is an isomorphism of vector spaces. □

A.3 The tangent, cotangent and *1-forms* spaces

We now focus on the concept of tangent space and present some of the properties of a tangent space. For this, we need to specialise to differentiable manifolds. A differentiable manifold is defined like a topological manifold, but the homeomorphisms are replaced by diffeomorphisms. In what follows, we assume the class of infinitely smooth of C^∞-manifolds. We will use the qualification "smooth" for functions on a C^∞-manifold to indicate that we suppose that they have enough regularity to justify every operations.

Definition A.8 : Tangent space

Let M be a differentiable manifold of dimension n. The tangent space to M in p, written T_pM is, by definition, the set of p-derivations of the algebra on $C^\infty(M,\mathbb{R})$, i.e. the set of the mappings h defined as:

$$\begin{aligned} h: \qquad C^\infty(M,\mathbb{R}) &\longrightarrow \mathbb{R}, \\ f &\longmapsto h(f) \end{aligned} \tag{A.4}$$

which satisfy the following relation:

$$\forall f \in C^\infty(M,\mathbb{R}),\ \forall g \in C^\infty(M,\mathbb{R}), \quad h(fg) = h(f)g(p) + f(p)h(g). \tag{A.5}$$

□

Proposition A.9 : Basis of a tangent space

Let M be a manifold of dimension n and p a point in M. Let $(\mathbf{x}, U)$ a coordinate chart on a neighbourhood U of p. Let x^k be the coordinate function (see (A.2)). Using the restriction operator $\restriction_p \circ f = f(p)$ we can define the p-derivation $\restriction_p \circ \partial_k = \left(\restriction_p \circ \frac{\partial}{\partial x^k}\right)$. The set $\{\restriction_p \circ \partial_k : k \in [\![1;n]\!]\}$ is a basis for T_pM. □

Differential forms of degree 1 on differentiable manifolds are in a first instance defined as linear maps on tangent spaces and, therefore, can be identified with elements of the dual of the tangent spaces.

Definition A.10 : Dual of a vector space

Let V be a vector space ($\mathbb{R}^n$ or $\mathbb{C}^n$ with the usual linear structure). We define the dual space, written V^*, as the space of linear functions on V. More explicitly:

$$V^* = \left\{\omega : V \to \mathbb{R} \mid \forall (a,b) \in \mathbb{R}^2 \text{ and } \forall (v,w) \in V^2, \omega(av+bw) = a\omega(v) + b\omega(w)\right\}. \tag{A.6}$$

□

Proposition A.11 :

If V has finite dimension ($\dim(V) < \infty$), then V^* is finite dimensional too and

$$\dim(V) = \dim(V*).$$

□

. The relation between vectors and *1-forms*

We start with the construction of the space of 1-forms by an explicit construction of a basis. In a second step, we show which relations can be made between vector-valued fields and 1-form valued fields. Some objects (functions, vector fields,...) will be indexed with p when the evaluation at a point p is meant. This index will not be used as the label of a value component.

Definition A.12 : Cotangent vector and *1-forms*

Let p be a point in a manifold M and f a function locally defined on an open neighbourhood U of p ($p \in U$). We suppose that f is a smooth function and define $\restriction_p \circ df$ as the following operator:

$$\begin{aligned} \restriction_p \circ df : T_pM &\longrightarrow \mathbb{R}, \\ v &\longmapsto \restriction_p \circ df(v) = \restriction_p [v(f)] = \sum_k v^k(\partial_k) f(p). \end{aligned} \tag{A.7}$$

This defines $\restriction_p \circ df_{|p}$ as a linear form on T_pM, and it is an element of the dual space of T_p^*M (the cotangent space at p). This operator is called the differential of f in p. The elements of T_p^*M are called cotangent vectors or *1-forms*. □

Suppose, now, that we have a smooth function g and a smooth chart dg given by the mapping $p \mapsto dg_{|p} \in T_p^*M$. We could then try to assemble a bundle T^*M consisting of all cotangent spaces T_p^*M in order to obtain for any vector field $\mathbf{x}$ over M a well-defined, even point-wise, of dg by $dg_{|p}(\mathbf{x}_p)$.

As an illustration, choosing a coordinate function $g = \mathbf{x}$, we can make an explicit construction of the dual basis.

Proposition A.13 : Coordinates and a dual basis

Let $(\mathbf{x}, U)$ be a local coordinate chart on a manifold M of dimension n. Let $dx^k_{|p}$ be the differential of the coordinate function x^k. Then, $\restriction_p \circ dx^k$ is a base for T_p^*M, dual to the base $\restriction_p \circ \frac{\partial}{\partial x^k}$ in T_pM. In other words

$$\restriction_p \circ dx^k \left(\restriction_p \circ \frac{\partial}{\partial x^j} \right) = \delta^k_j. \tag{A.8}$$

For any smooth functions on U, we have:

$$\begin{aligned} \restriction_p \circ df &= \restriction_p \left(\sum_{k=1}^n \frac{\partial f}{\partial x^k} dx^k \right), \\ &= \sum_{k=1}^n \frac{\partial f}{\partial x^k}(p) \ \restriction_p \circ dx^k. \end{aligned}$$

This is usually written as

$$df = \sum_{k=1}^n \frac{\partial f}{\partial x^k} dx^k \quad \text{or} \quad df(p) = \sum_{k=1}^n \frac{\partial f}{\partial x^k}(p) dx^k(p)$$

if the value in a point p is wanted.

Proof A.14 :

By definition, cf. A.12, we have:

$$\forall k, \ \forall j, \quad \restriction_p \circ dx^k \left(\restriction_p \circ \frac{\partial}{\partial x^j} \right) = \restriction_p \circ \restriction_p \frac{\partial}{\partial x^j}(x^k) = \frac{\partial x^k}{\partial x^j}(p) = \delta^k_j. \tag{A.9}$$

In addition, because of the duality between the spaces, $\dim(T_pM) = \dim(T_p^*M) = n$. So we have n linearly independent elements (cotangent vectors) as of their action on the basis of T_pM. This means that with $\left\{ dx^k_{|p} \right\}$ we have a basis of T_p^*M. ⊠

We obtain two corollaries which emphasize essential properties of differential forms under change of coordinates

Corollary A.15 :

Let $(\mathbf{x}, U)$ and $(\mathbf{y}, V)$ be two coordinate systems on open sets U and V in a manifold M. Let $p \in U \cap V$. The basis cotangent vectors in T_p^*M ($\left(dx^k_{|p}\right)_k$ and $\left(dy^j_{|p}\right)_j$) satisfy the following transformation:

$$dx^j(p) = \sum_{k=1}^{n} \frac{\partial x^j}{\partial y^k}(p) dy^k(p). \tag{A.10}$$

□

Proof A.16 :

This results immediately from proposition A.13 by taking $f = x^k$ in the coordinates $(\mathbf{y}, V)$.

⊠

Corollary A.17 :

Let $(\mathbf{x}, U)$ be a local coordinate system in an open neighbourhood of $p \in M$. Following proposition A.13, any element $\alpha \in T_p^*M$ is given by

$$\alpha = \sum_{k=1}^{n} \alpha_k dx^k_{|p} \tag{A.11}$$

where α_k is a smooth function on M with values in $\mathbb{R}$. □

A.4 Differentiable manifolds with a metric

So far, we have spoken of scalar functions and vector or 1-form valued functions on a manifold and by choosing a chart we could do analysis as usual. We have seen that the transition from one chart to another one goes by and by with changes of the functions via the derivatives of the coordinate transition maps (i.e., old coordinates given as functions of the new ones). But there was, as yet, no constraint on the choice of coordinates. Hence our analysis of functions on a manifold was entirely local and, until now, we could not see any difference between analysis on a sphere or on an ellipsoid or even on an infinite plane. In the applications we are interested in, in the context of this thesis, we have to do with metric spaces which represent physical spaces where distances and angles are supposed to have a meaning. The simplest form of a metric manifold is a linear space, i.e., a manifold with a vector space structure, and an inner product defined by a symmetric and positive bi-linear form.

Definition A.18 : Metric

A metric g is a symmetric positive bilinear form $TM \times TM \to \mathbb{R}$. If $\{e_i\}_{i\in[\![1;n]\!]}$ is a basis of TM, then g can be defined by :

$$\begin{aligned} g : (TM \times TM) &\longrightarrow \mathbb{R}, \\ (X,Y) = \left(\sum_{i=1}^{n} x^i e_i, \sum_{j=1}^{n} y^i e_j\right) &\longmapsto g(X,Y) = \sum_{i=1}^{n}\sum_{j=1}^{n} x^i g(e_i,e_j) y^i, \\ &= \sum_{i,j=1}^{n} x^i g_{ij} y^j \end{aligned} \tag{A.12}$$

where the set $(g_{ij})_{i,j\in[\![1;n]\!]}$ defines an $n \times n$ matrix. We call g a non-degenerate metric if $[\forall Y \in TM,\ g(X,Y) = 0]$ implies $X = 0_{TM}$ and positive if $\forall X \in TM,\ g(X,X) \geq 0$.
In a given chart the metric is represented in terms of differentials

$$g = \sum_{i,j} g_{ij} dx^i \otimes dx^j.$$

Note that the $\otimes$ is the standard tensor product and this representation does not use the symmetry of the matrix of coefficients. □

Definition A.19 : Musical isomorphisms

Let g be a non-degenerate metric on a vector space V with a dual V^*. We define the metric on the V^* as the inverse of the metric on V and write the matrix coefficients of the metric in the dual space as g^{ij}. Note that we have $g^{ik}g_{kj} = \delta^i_j$. We introduce two isomorphisms, $\flat$ (flat) and $\sharp$ (sharp), defined as follows

1. ≪The index-lowering map≫

$$\begin{aligned} \flat : V &\longrightarrow V^*, \\ v &\longmapsto v^\flat = g(v,\cdot). \end{aligned} \tag{A.13}$$

   such that for $v \in V$, $\forall w \in V$, we have $v^\flat(w) = g(v,w)$ or, in components, $v^\flat_i = \sum_j g_{ij} v^j$.

2. ≪The index-raising map≫

$$\begin{aligned} \sharp : V^* &\longrightarrow V, \\ \alpha &\longmapsto \alpha^\sharp = g^{-1}(\alpha,\cdot). \end{aligned} \tag{A.14}$$

   such that for $\alpha \in V^*$, $\forall w \in V$, we have $\alpha(w) = g(\alpha^\sharp, w)$ or, in components, $\alpha^{\sharp,i} = \sum_j g^{ij}\alpha_j$.

□

These transposition mappings define an isomorphism between TM and T^*M and we shall use them to translate expressions from differential form analysis into expressions from vector analysis. Note that $(X^\flat)^\sharp = X$ and reciprocally (or equivalently $(X^\sharp)^\flat = X$).
Therefore, using the metric on T^*M (space also denoted by Λ^1), we can define a inner product between elements of T^*M. We use the shorthand notation $\langle \cdot\ ;\ \cdot \rangle_{\Lambda^1}$. If $\{dx^i\}_{i\in[\![1;n]\!]}$ is a a basis of $T^*M = \Lambda^1$, $a = \sum_{i=i}^n \alpha_i dx^i$ and $b = \sum_{i=j}^n \beta_j dx^j$, the inner product between a and b is given

by

$$\langle a \ ; \ b \rangle_{\Lambda^1} = \sum_{i,j=1}^{n} \alpha_i g^{ij} \beta_j$$

The classical model for physical space without gravity is the Euclidean 3-dimensional space $\mathbb{E}^3$ with a canonical chart $\mathbb{R}^3$ in which the metric coefficients are given by

$$g_{ij} = \delta_{ij}. \tag{A.15}$$

All other charts are defined with respect to this canonical chart. In Figure A.1 the relations between tangent vectors and 1-forms are illustrated for linear Euclidean spaces. We denote by $.^\tau$ the canonical isomorphism between $\mathbb{R}^3$ and $T\mathbb{R}^n$

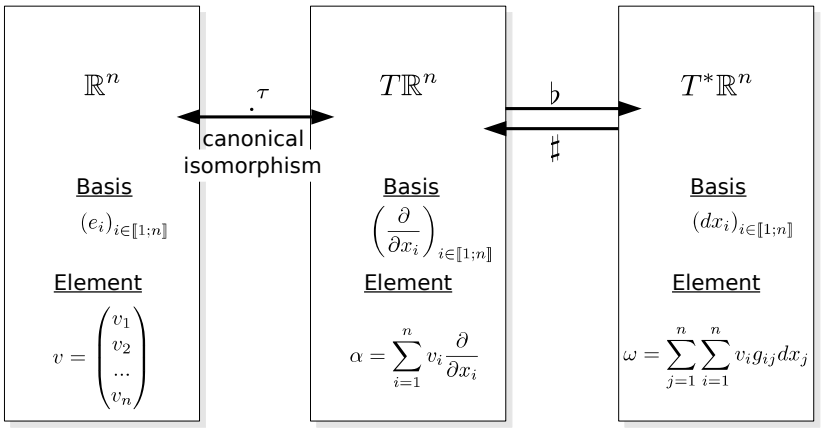

Figure A.1 – Symbolic representation of the various spaces and their isomorphisms for the case of a canonical chart $\mathbb{R}^n$ on a linear manifold with a metric.

A.5 The exterior product and the space of *p-forms*

In this section, we introduce the forms of degree p, called p-forms.

Definition A.20 : **Exterior product of co-vectors**

Let V be a vector space and V^* its dual. The exterior product of two co-vectors ω and ξ in V^* is defined as the mapping:

$$\begin{aligned} \omega \wedge \xi : V \times V &\longrightarrow \mathbb{R}, \\ (u, v) &\longmapsto (\omega \wedge \xi)(u, v) = \omega(u)\xi(v) - \xi(u)\omega(v). \end{aligned} \tag{A.16}$$

□

Properties A.21 :

The exterior product has the following properties:

- $\forall \alpha \in V^*$, $\alpha \wedge \alpha = [V \times V \longrightarrow \mathbb{R}, (u,v) \longmapsto O_{\mathbb{R}}]$,
- $\forall (\alpha, \beta) \in (V^*)^2$, $\alpha \wedge \beta = -\beta \wedge \alpha$,
- $\forall (\alpha, \beta, \gamma) \in (V^*)^3$, $\forall (\lambda, \mu) \in \mathbb{R}^2$,

$$(\lambda\alpha + \mu\beta) \wedge \gamma = \lambda(\alpha \wedge \gamma) + \mu(\beta \wedge \gamma). \tag{A.17}$$

- $\forall (\alpha, \beta, \gamma) \in (V^*)^3$, $\forall (\lambda, \mu) \in \mathbb{R}^2$,

$$\alpha \wedge (\lambda\beta + \mu\gamma) = \lambda(\alpha \wedge \beta) + \mu(\alpha \wedge \gamma). \tag{A.18}$$

□

We observe that the bi-linear form $\omega \wedge \xi$ is necessarily antisymmetric.

Definition A.22 :

Let M be a manifold of dimension n. A k-linear form ω on TM is called a k-form if it is completely anti-symmetric, i.e., if

$$\omega(v_1, ..., v_i, v_{i+1}, ...v_k) = -\omega(v_1, ..., v_{i+1}, v_i, ...v_k) \tag{A.19}$$

for all i and for any k vectors $v_1, ..., v_k$ o TM. □

The space of all k-forms over M is written, $\Lambda^p(M)$. By extension, the 0-forms are the $\mathbb{R}$-valued functions such that $\Lambda^0(M) = C^\infty(M)$.

Definition A.23 :

Let α be a p-form and β a q-form. We define the exterior product of α and β by:

$$(\alpha \wedge \beta) : V^p \times V^q \longrightarrow \mathbb{R},$$
$$(v_1, \ldots, v_p, v_{p+1}, \ldots, v_{p+q}) \longmapsto \frac{1}{p!q!} \sum_{\sigma \in \mathfrak{S}_{p+q}} \varepsilon(\sigma)\alpha(v_{\sigma(1)}, \ldots, v_{\sigma(p)})\beta(v_{\sigma(p+1)}, \ldots, v_{\sigma(p+q)})$$

where $\varepsilon(\sigma)$ gives the sign of the permutation. □

Proposition A.24 :

If α is a p-form and β a q-form then $\alpha \wedge \beta$ is a $(p+q)$-form. □

Properties A.25 : **Associativity of the exterior product**

$\forall T$ t-form, $\forall R$ r-form and $\forall S$ s-form we have

$$T \wedge (R \wedge S) = (T \wedge R) \wedge S. \tag{A.20}$$

□

Proposition A.26 :

If R is an r-form and T a t-form, then

$$R \wedge T = (-1)^{rt} T \wedge R. \tag{A.21}$$

□

Proposition A.27 :

The space Λ^p of p-forms on a vector space V of dimension n ($p \leq n$), is a vector space of dimension $\binom{n}{p}$ □

A.6 The Hodge star operator

The Hodge star (or duality) operator defines a bijection between the p-forms and the $(n-p)$-forms on a metric manifold of dimension n. Consider a manifold M with finite dimension n, TM its tangent bundle with a basis $\{e_i\}_{i\in[\![1;n]\!]}$ and cotangent bundle T^*M with basis $\{a^i\}_{i\in[\![1;n]\!]}$. The definition of the basis of T^*M is such that $a^i(e_j) = \delta^j_i$. Let g be the metric on TM defined by its n^2 coefficients $g_{ij} = g(e_i, e_j)$. Let Λ^p denote the space of p-forms on M.

From the results presented in the preceding sections we observe that

$$\dim(\Lambda^p) = \binom{n}{p} = \binom{n}{n-p} = \dim(\Lambda^{n-p}) \tag{A.22}$$

which shows that the point-wise vector spaces are isomorphic. In order to establish Hodge's duality, we need a metric on the spaces of p-forms. We have already introduced the metric on T^*M

Proposition A.28 : **Scalar product of p-forms**

The scalar product of two p-forms written as $\langle\cdot\,;\cdot\rangle_{\Lambda^p}$ is defined by:

$$\begin{aligned} \langle\cdot\,;\cdot\rangle_{\Lambda^p} : \quad & \Lambda^p \times \Lambda^p \longrightarrow \mathbb{R}, \\ & (\alpha, \beta) \longmapsto \langle\alpha;\beta\rangle_{\Lambda^p} \end{aligned} \tag{A.23}$$

where, for any p-tuple $\{m_i\}_{i\in[\![1;p]\!]}$ and $\{k_i\}_{i\in[\![1;p]\!]}$, we have:

$$\langle a^{m_1} \wedge ... \wedge a^{m_p}; a^{k_1} \wedge ... \wedge a^{k_p}\rangle_{\Lambda^p} = \det\left(\left(\langle a^{m_i}; a^{k_j}\rangle_{\Lambda^1}\right)_{i\in[\![1;p]\!],j\in[\![1;p]\!]}\right). \tag{A.24}$$

□

This definition only involves p-fold exterior products of 1-forms (i.e. $p-1$ exterior product operator $\wedge$ and p *1-forms*). A general p-form is a linear combination of such terms in particular when the factors are the chosen basis 1-forms. The scalar product for such general forms are found using the bilinearity of the scalar product.

Assuming an orthogonal basis in T^*M, $\{a^1, \ldots, a^n\}$, we can now define Hodge's star operator written as $\underline{\star}$.

Definition A.29 : **Hodge's star operator**

$$\begin{aligned} \underline{\star} : \quad & \Lambda^p \longrightarrow \Lambda^{n-p} \\ & \omega \longmapsto \underline{\star}\omega \end{aligned} \tag{A.25}$$

such that

$$\forall(\alpha, \beta) \in \Lambda^p \times \Lambda^p,\ \alpha \wedge \underline{\star}\beta = \langle\alpha;\beta\rangle_{\Lambda^p}\ \sigma \tag{A.26}$$

where $\sigma = a^1 \wedge \ldots a^n$. □

This definition is implicit. For practical computations the following result is more convenient.

Proposition A.30 : Computing the Hodge dual of a p-form

Let ω be a p-form which is the p-fold product of 1-forms

$$\omega = a^{m_1} \wedge ... \wedge a^{m_p} \tag{A.27}$$

and g^* the metric on T^*M. Let $\{m_1, ...m_p, k_1, ..., k_{n-p}\}$ a permutation of $[\![1; n]\!]$ then the Hodge dual of ω is given by

$$\underline{\star}\omega = \langle a^{m_1} \wedge \dots a^{m_p}; a^{m_1} \wedge \dots a^{m_p} \rangle_{\Lambda^p} \, \varepsilon_{m_1,...,m_p,k_1,...,k_{n-p}} \bigwedge_{r=1}^{n-p} a^{k_r}. \tag{A.28}$$

This definition extends to the cases, $p = 0$ and $p = n$:

$$\underline{\star}1 = |g^*|^{-1} a^1 \wedge ... \wedge a^n \text{ and } \underline{\star}(a^1 \wedge ... \wedge a^n) = |g^*| \tag{A.29}$$

where $|g^*|$ is the determinant of the metric on T^*M. □

Properties A.31 : Properties of the Hodge star operator

1. If α and β are p-forms, then
$$\alpha \wedge \underline{\star}\beta = \beta \wedge \underline{\star}\alpha. \tag{A.30}$$

2. If $\alpha \in \Lambda^p$, then
$$\underline{\star}\,\underline{\star}\alpha = (-1)^{p(n-p)} s\alpha \tag{A.31}$$
where s is the signature of the metric.

3. The inverse star operator, $\underline{\star}^{-1}$, is defined by
$$\underline{\star}^{-1} : \Lambda^p \longrightarrow \Lambda^{(n-p)} \tag{A.32}$$
$$\eta \longmapsto (-1)^{k(n-k)} s \underline{\star}\eta \tag{A.33}$$
where s is the signature of the metric (as a reminder, the signature of a metric is the sign of the product of the metric tensor's eigenvalues).

□

A.7 Exterior derivative and the co-derivative

In the context of differential forms, there is essentially one differential operator: the exterior differential operator $\underline{\mathbf{d}}$. Via the Hodge star operator $\underline{\star}$, one additional differential operator is introduced called the co-differential operator $\underline{\boldsymbol{\delta}}$.

. The exterior differential operator

Recall that any $\omega \in \Lambda^p$ has a representation

$$\omega = \sum_{\substack{m_1,...,m_p=1 \\ m_1<...<m_p}}^{n} \omega_{m_1,...,m_p} a^{m_1} \wedge ... \wedge a^{m_p}, \tag{A.34}$$

the exterior differential operator, $\underline{\mathbf{d}}$, is an operator defined by:

$$\begin{aligned}\underline{\mathbf{d}}: \qquad & \Lambda^p \longrightarrow \Lambda^{p+1}, \\ & \omega \longmapsto \underline{\mathbf{d}}\,\omega = \sum_{\substack{m_1,\ldots,m_p=1 \\ m_1<\ldots<m_p}}^{n} d(\omega_{m_1,\ldots,m_p}) a^{m_1} \wedge \ldots \wedge a^{m_p}, \\ & \qquad = \sum_{\substack{m_1,\ldots,m_p=1 \\ m_1<\ldots<m_p}}^{n} \sum_{j=1}^{n} \frac{\partial \omega_{m_1,\ldots,m_p}}{\partial x_j} a^j \wedge a^{m_1} \wedge \ldots \wedge a^{m_p}.\end{aligned} \tag{A.35}$$

This definition implies :

1. for any function f,
$$\underline{\mathbf{d}}\, f = \sum_i \frac{\partial f}{\partial x^i} dx^i \quad ,$$
2. $\forall \omega$, $\underline{\mathbf{d}}(\underline{\mathbf{d}}\,\omega) = 0$,
3. $\underline{\mathbf{d}}(\omega + \eta) = \underline{\mathbf{d}}\,\omega + \underline{\mathbf{d}}\,\eta$,
4. $\underline{\mathbf{d}}(\lambda \wedge \mu) = (\underline{\mathbf{d}}\,\lambda) \wedge \mu + (-1)^{\deg(\lambda)} \lambda \wedge (\underline{\mathbf{d}}\,\mu)$.

. The co-differential operator

The co-differential operator is defined by

$$\underline{\boldsymbol{\delta}}: \qquad \Lambda^{p+1}(U) \longrightarrow \Lambda^p(U), \tag{A.36}$$

$$\omega \longmapsto \underline{\boldsymbol{\delta}}\,\omega = \underline{\star}^{-1}\, \underline{\mathbf{d}}\, \underline{\star}\, \omega. \tag{A.37}$$

The co-differential operator is the adjoint of the exterior differential operator in the following context. For all sufficiently smooth $\eta \in \Lambda^p$ and $\xi \in \Lambda^{p+1}$, we have the following relation

$$\int_{\mathbb{R}^n} \eta \wedge \underline{\star}(\underline{\boldsymbol{\delta}}\,\xi) = \langle \eta, \underline{\boldsymbol{\delta}}\,\xi \rangle_{{}^p\bigwedge_0^\infty(\mathbb{R}^n)} = \langle \underline{\mathbf{d}}\,\eta, \xi \rangle_{{}^p\bigwedge_0^\infty(\mathbb{R}^n)} = \int_{\mathbb{R}^n} \underline{\mathbf{d}}\,\eta \wedge \underline{\star}\,\xi \tag{A.38}$$

where ${}^p\bigwedge_0^\infty(\mathbb{R}^n)$ indicates that the relation applies to p-forms with $C_0^\infty(\mathbb{R}^n)$ coefficients.

Appendix B

Notations for the study of the scattering of an electromagnetic plane by a PEC sphere

$$a_{n,m} = a_n^m = (-1)^{\frac{1}{2}(m+|m|)} \sqrt{\frac{1}{4\pi} \frac{(n-|m|)!}{(n+|m|)!} \frac{2n+1}{n(n+1)}}$$

$$b_{n,m} = (-1)^{\frac{1}{2}(m+|m|)} \sqrt{\frac{2n+1}{4\pi} \frac{(n-|m|)!}{(n+|m|)!}}$$

$$j_n(ka) = \frac{i^{-n}}{2} \int_{\theta=0}^{\pi} e^{-ikr\cos(\theta)} P_n^{(0)}(\cos(\theta)) d\theta$$

$$\tilde{j}_n(ka) = \frac{i^{-n}}{2} \int_{\theta=0}^{\pi} e^{+ikr\cos(\theta)} P_n^{(0)}(\cos(\theta)) d\theta$$

$$\gamma_n^m = \sqrt{\frac{(n+m)!}{(n-m)!}}$$

$$l_n^m = \sqrt{\frac{(n-m)!}{(n+m)!}}$$

$$\Big) \begin{matrix} j_1 & j_2 & j_3 \\ m_1 & m_2 & m_3 \end{matrix} \Big(= (-1)^{j_1-j_2-m_3} \left[\frac{\prod_{i=1}^{3}(j_{i+1}+j_{i+2}-j_i)!(j_i+m_i)!(j_i-m_i)!}{(j_1+j_2+j_3+1)!} \right]$$
$$\times \left[\sum_k \frac{(-1)^k}{k!(j_1+j_2-j_3-k)!(j_1-m_1-k)!(j_2+m_2-k)!} \right.$$
$$\left. \frac{1}{(j_2+m_2-k)!(j_3-j_2+m_1+k)!(j_3-j_1-m_3+k)!} \right]$$

$$G_{j_1,j_2}^{m_1,m_2}(k) = (-1)^{-m_1+m_2}(2k+1) \Big) \begin{matrix} j_1 & j_2 & k \\ 0 & 0 & 0 \end{matrix} \Big(\Big) \begin{matrix} j_1 & j_2 & k \\ -m_1 & m_2 & m_1-m_2 \end{matrix} \Big($$

$$u_n^m = \int_{X=-1}^{+1} \frac{P_n^m(X) P_n^m(X)}{1-X^2} dX = \frac{(n+m)!}{m(n-m)!}$$

$$\omega_n^m = \int_{X=-1}^{X=1} P_n^m(X) P_n^m(X) dX = \frac{2}{2n+1} \frac{(n+m)!}{m(n-m)!}$$

$$\chi_n^m = (n+m)(n-m+1)$$
$$A_{n_1,n_2}^{m,p}(k) = \gamma_{n_1}^m G_{p,n_1}^{0,m}(k) l_k^m \omega_{n_2}^m$$
$$B_{n_1,n_2}^{m,p}(k) = \gamma_{n_1}^m G_{p,n_1}^{0,m}(k) l_k^m u_{n_2}^m$$

Appendix C

Analyse mathématique et numérique de l'équation intégrale de Herberthson dédié à la diffraction électromagnétique d'onde plane

C.1 Le contexte

La simulation des phénomènes de diffraction électromagnétique et le calcul des signatures radars de structures de grande taille sont un enjeu important pour les applications industrielles. Les domaines d'application de telles simulations sont variés; parmi eux, on peut trouver les technologies de furtivité radar, de reconnaissance et d'identification d'aéronef ou encore la modélisation des effets électromagnétiques d'une éolienne sur un champ électromagnétique. Comme les méthodes numériques utilisées pour caractériser de tels phénomènes requièrent toujours plus de ressources, tant en mémoire qu'en puissance de calcul, la simulation de ces phénomènes a constitué un domaine de recherche très actif ces dernières décennies.

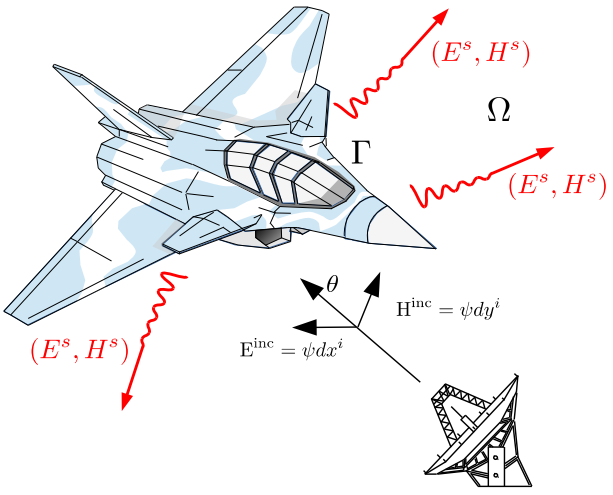

Figure C.1 – Représentation d'une scène de diffraction électromagnétique.

D'un point de vue général, un problème de diffraction électromagnétique est un problème de

radiation où la distribution locale de courant à calculer est induite par un courant ou un champ extérieur. Pour être plus concret, considérons un objet, un avion par exemple (voir Figure C.1), plongé dans un espace libre et soumis à une onde incidente. Cette onde incidente crée une distribution de courant à travers l'objet diffractant, courant qui à son tour va générer un champ diffracté dans l'espace environnant.

C.2 Méthodes classiques de résolution

D'un point de vue mathématique, pour formaliser et modéliser un phénomène de diffraction, le premier outil à notre disposition est le système des équations de Maxwell:

$$\mathbf{d} \star(\mu H) = \rho_m/\mu_0 \qquad \text{La Loi de Gauss,} \tag{C.1}$$
$$\mathbf{d} \star(\varepsilon E) = \rho/\varepsilon_0 \qquad \text{La Loi de Gauss,} \tag{C.2}$$

$$\mu\partial_t \star H + \mathbf{d}\, E = -m \qquad \text{l'équation de Lenz-Faraday,} \tag{C.3}$$
$$\varepsilon\partial_t \star E - \mathbf{d}\, H = -j \qquad \text{la loi de Maxwell-Ampère,} \tag{C.4}$$

$$\partial_t\rho + \mathbf{d}\, j = 0 \qquad \text{la loi de conservation de la charge,} \tag{C.5}$$
$$\partial_t\rho_m + \mathbf{d}\, j_m = 0 \qquad \text{la loi de conservation de la charge.} \tag{C.6}$$

. Équations aux dérivées partielles

À partir des équations de Maxwell et de l'établissement de conditions aux limites, on peut résoudre le problème de diffraction. Techniquement, à partir de ce point, nous pouvons soit rechercher une expression analytique de la solution soit discrétiser les équations aux dérivées partielles (EDP) qui constituent les équations de Maxwell. Il existe diverses méthodes pour discrétiser ces EDP; parmi elles, on peut citer deux classes importantes: la discrétisation par différences finies, principalement utilisée dans le domaine temporel, et la discrétisation par éléments finis, principalement utilisée dans le domaine fréquentiel.
La discrétisation des EDP est intéressante pour la simulation à la fois dans les domaines temporel et fréquentiel, mais aussi pour des objets et des milieux hétérogènes. L'avantage des méthodes temporelles est d'obtenir le comportement de l'objet pour une gamme de fréquences à partir des résultats d'un seul calcul. Cependant, en général, ces méthodes souffrent de difficultés théoriques très sérieuses (voir [1] par exemple).

. Équations intégrales

Comme les méthodes de discrétisation des EDP peuvent souffrir de certaines difficultés, d'autres approches, fondamentalement différentes, peuvent aussi être considérées. En fait, dans des milieux homogènes, il est possible d'établir une représentation intégrale des champs électromagnétiques dans le domaine au moyen de leurs valeurs à la frontière du domaine (i.e., au moyen des courants surfaciques électrique j_S et magnétique m_S par exemple).
Dès lors, le problème de la diffraction d'objets homogènes, comme des objets parfaitement conducteurs (PEC), peut être réduit à une équation intégrale sur la frontière de l'objet. Les principales équations intégrales sont établies au Chapitre 1. Pour des objets PEC, par exemple, les méthodes d'équation intégrale impliquent le calcul du courant électrique j_S à la surface de l'objet diffractant (le courant magnétique m_S étant connu dans ce cas), calcul passant par la

résolution d'une équation intégrale telle que l'EFIE :

$$\forall x \in \Gamma,\ \mathcal{E}[j_S] = \tau^* \left(\zeta \mathcal{A}[j_S] + \frac{1}{\eta} \mathbf{d}\, \boldsymbol{\delta}\, \mathcal{A}[j_S] \right) = -\tau^*(E^{\text{inc}}) \tag{C.7}$$

où $\mathcal{A}$ est défini par

$$\mathcal{A}[j](x) = \int_{y \in \Gamma} \tau^*(\mathbf{G}(x,y)) \wedge \star\, j(y)$$

et où $\mathbf{G}$ désigne la fonction de Green suivante

$$\mathbf{G}(x,y) = \sum_{i=1}^{3} G(x,y) dx^i \otimes dy^i = \sum_{i=1}^{3} \frac{e^{i\kappa|x-y|}}{4\pi|x-y|} dx^i \otimes dy^i, \tag{C.8}$$

$\zeta = i\omega\mu$ et $\eta = -i\omega\varepsilon$.
Ce problème est strictement équivalent au calcul des champs électrique E et magnétique H dans l'espace environnant Ω. À partir des courants j_S et m_S, au moyen de représentations intégrales, les champs diffractés E^S et H^S (ou totaux E^{tot} et H^{tot}) peuvent être déterminés à travers tout l'espace (respectant de par le fait les équations de Maxwell et les conditions de radiations à l'infini). De plus, comme le domaine extérieur n'a pas besoin d'être maillé, les méthodes intégrales, lorsqu'elles peuvent être utilisées, s'avèrent généralement plus précise que les méthodes discrétisant les EDP et sont pour cette raison souvent utilisées comme méthodes de référence (voir [3, 4, 5]).

D'un point de vue technique, tout courant surfacique peut être développé sur une base de fonctions vectorielles tangentes à la surface. De telles fonctions ont généralement un support réduit (de l'ordre de $\lambda/10$ où λ est la longueur d'onde). La principale difficulté repose sur le fait que tout courant local, représenté par une fonction de cette base, rayonne à travers tout l'espace environnant et interagit avec tous les autres éléments de base. Cette forte interaction mène à la résolution d'un système linéaire

$$EX = S \tag{C.9}$$

impliquant une matrice E à valeurs complexes, dense et pouvant être être mal conditionnée.

Pour les objets de très grandes tailles, la résolution de ce système linéaire est un problème majeur qui demande beaucoup de ressources de calcul. Dans l'espoir de réduire celles-ci, il est couramment fait usage de solveurs itératifs comme CG, BiCG, QMRES, GMRES or TFQMR (cf. [6]). Bien que ces derniers ne requièrent que des produits matrice-vecteurs, le mauvais conditionnement de la matrice E met en difficulté ces méthodes numériques, augmentant significativement les coûts CPU et les besoins en mémoire. Dès lors, il apparaît nécessaire de les coupler à des méthodes d'accélération et de préconditionnement (cf. [7, 8, 9, 10]).
À l'heure actuelle, il n'existe pas de solution définitive; même combinés à des méthodes de préconditionnement et d'accélération, les solveurs itératifs peuvent encore souffrir d'une faible vitesse de convergence pour des objets réalistes, et ce pour de multiples raisons: complexité de la géométrie, sur-maillage local, ...

C.3 Couplage des méthodes assymptotiques et des équations intégrales

S'il existe déjà un grand nombre de méthode de résolution, le problème de diffraction pour les hautes fréquences constitue toujours un domaine de recherche très actif. Depuis quelques dizaines d'années, différents auteurs ont proposé de combiner différents types de méthodes de

résolution, en particulier les équations intégrales et les méthodes asymptotiques.
Ces dernières, justifiées par une analyse pseudo-différentielle de l'opérateur, consistent à considérer une approximation particulière de la solution, à localiser la propagation des ondes selon des directions privilégiées et à proposer un problème plus simple. Cette famille de méthodes comprend diverses méthodes telles que l'optique physique ou la théorie de la diffraction géométrique. Ces méthodes ont été pendant longtemps les seules à donner des résultats pour les hautes fréquences, car elles ont l'avantage de présenter une complexité qui n'augmente pas avec la fréquence. Cependant, elles souffrent de plusieurs limitations, parmi elles, citons la difficulté d'implémentation pour des surfaces non convexes ou dans le cas de multiples réflexions.
À l'opposé, les équations intégrales sont en mesure de prendre en compte toute la géométrie de l'objet diffractant et sont assez simples à mettre en œuvre dans les cas non convexes. Les principales limitations sont une complexité qui augmente avec la fréquence et la nécessité de résoudre un système linéaire plein, de grande taille avec des valeurs complexes, parfois mal conditionné. Par conséquent, l'idée est de combiner ces deux méthodes pour réduire les difficultés inhérentes à chacune d'entre elles, en particulier réduire le nombre de coefficients de la matrice résultant des équations intégrales.

Parmi les nombreuses propositions, l'une des formulations les plus intéressantes est celle proposée par T. Abboud, J.-C. Nédélec et B. Zhou, voir [16, 17, 18]. Celle-ci est basée sur une configuration où la surface diffractante $\Gamma \subset \mathbb{R}^3$, surface régulière et convexe, est éclairée par une onde plane $\mathbf{E}^{\text{inc}}$. Comme expliqué dans [16], la difficulté majeure des problèmes hautes fréquences provient de l'approximation de la phase du courant physique $\mathbf{J}$. Le courant physique ayant la forme d'une fonction oscillante sur la surface de diffusion, en prenant en compte l'onde plane incidente, l'idée consiste à trouver une solution $\mathbf{J}$ sous la forme

$$\mathbf{J}(x) = \tilde{\mathbf{J}}(k, x)e^{ik\phi(x)} \tag{C.10}$$

où $\tilde{\mathbf{J}}$ et ϕ sont deux inconnues décrivant respectivement le module et la phase du courant physique. Au travers un développement asymptotique, pour tout objet diffractant convexe, il est possible de donner une première approximation de la phase sous la forme:

$$\phi(x) = ik\phi_0(x) + k^{1/3}\phi_1(x) = ik\theta\cdot\mathbf{x} + k^{1/3}\phi_1(x). \tag{C.11}$$

Dans la zone éclairée, voir Figure C.2, le courant physique sera décrit par:

$$\mathbf{J}(x) = \tilde{\mathbf{J}}(k, x)e^{ik\phi_0(x)}, \tag{C.12}$$

oscillant de la même manière que l'onde incidente, alors que dans la zone de transition ou dans la zone non éclairée, le développement asymptotique nous donne:

$$\mathbf{J}(x) = \tilde{\mathbf{J}}(k, x)e^{ik\phi_0(x)+k^{1/3}\phi_1(x)}. \tag{C.13}$$

Compte tenu de ces différentes expressions, Zhou propose d'approcher la phase du courant par la phase de l'onde incidente sur Γ arguant que, même si, par le fait, nous commettons une erreur dans les zones de transition et non éclairées, le module y diminue de façon exponentielle. Dès lors si nous écrivons que

$$\mathbf{J} = e^{ik\phi_0(x)}\hat{\mathbf{J}}(x), \tag{C.14}$$

avec ϕ_0 la phase de l'onde incidente, la nouvelle fonction $\hat{\mathbf{J}}$ apparaît moins oscillante dans la mesure où nous avons déjà isolé la partie la plus oscillante de la phase du courant.

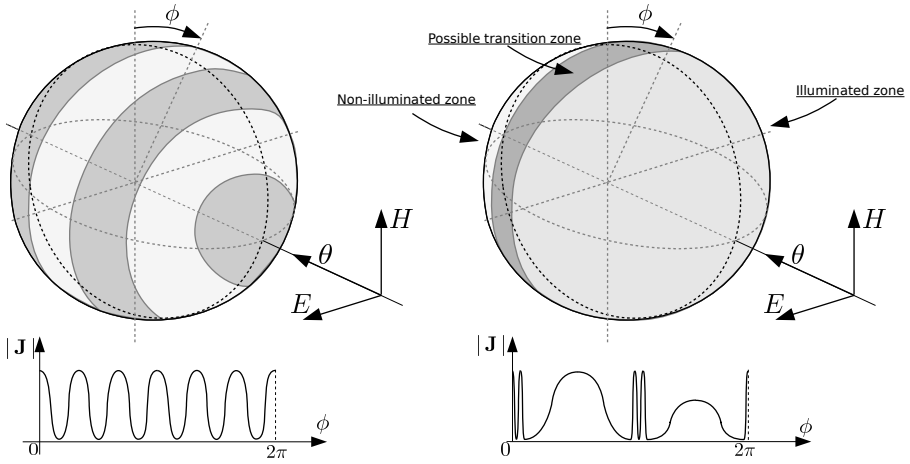

Figure C.2 – Représentation symbolique des oscillations du courant phyisque $\mathbf{J}$ (à gauche) et du pseudo-courant $\hat{\mathbf{J}}$ (à droite).

De là, Zhou propose de coupler cette approximation avec la méthode des équations intégrales dans le but de réduire le nombre de degrés de liberté nécessaires pour obtenir le courant physique. Cependant, d'un point de vue numérique, pour travailler sur un maillage plus grossier, il est nécessaire de calculer plus finement les intégrales impliquées dans le calcul de la matrice de Galerkin. Pour cela, il propose la construction d'un système technique de double maillage, appelé discrétisation micro-locale, nécessitant un certain effort de programmation, avec un maillage grossier pour représenter le courant et un maillage fin pour calculer correctement les intégrales.

C.4 Point de départ de la thèse

Le point de départ de cette thèse est le travail de M. Herberthson, publié entre 2008 et 2010 (cf. [24, 25, 26]). Herberthson y propose une nouvelle formulation des trois principales équations intégrales, c'est-à-dire pour l'équation intégrale de champ électrique (EFIE), magnétique (MFIE) et combinée (CFIE). L'idée de base est la même que celle qui a inspiré les travaux de Zhou: adapter les équations intégrales classiques à la diffusion des ondes planes en supposant que la fonction de phase de l'onde plane incidente détermine, en grande partie, la fonction de phase de la distribution de courant induite à la surface de l'objet:

$$\mathbf{J} = e^{ik\phi_0(x)}\hat{\mathbf{J}}(x). \tag{C.15}$$

La deuxième idée était de multiplier chacun des membres de l'équation intégrale par la phase conjugée de l'onde incidente, réduisant ainsi le second membre de l'équation à la trace d'un vecteur de polarisation constante. Typiquement, pour le problème électrique, on obtient l'équation suivante:

$$\forall x \in \Gamma,\ \mathcal{H}[\hat{\mathbf{J}}] = \tau^*\left(\bar{\psi}(x)\zeta\mathcal{A}[\psi\hat{\mathbf{J}}] + \frac{1}{\eta}\bar{\psi}(x)\,\mathbf{d}\,\boldsymbol{\delta}\,\mathcal{A}[\psi\hat{\mathbf{J}}]\right) = -\tau^*(\bar{\psi}(x)E^{\text{inc}}) = -\tau^*(\mathbf{p}_E)\,. \tag{C.16}$$

Une fois discrétisée avec des éléments d'arêtes classiques, cette équation mène à un système linéaire équivalant à celui proposé par Zhou où l'équation classique est discrétisée au moyen de fonctions particulières (définies comme des éléments d'arêtes multipliés par la fonction de phase). À la fin, nous nous obtenons un système linéaire :

$$\tilde{H}\tilde{J} = \tilde{C}. \tag{C.17}$$

A cela, Herberthson propose d'utiliser la décomposition de Helmholtz pour décomposer le pseudo-courant en deux parties : une composante divergente et une composante solénoïdale

$$\hat{\mathbf{J}} = J^D + J^S = \mathbf{d}\, f^d + \boldsymbol{\delta} \star f^s, \tag{C.18}$$

afin de transformer plus tard l'équation intégrale d'origine définie avec une distribution vectorielle $\hat{\mathbf{J}}$ en une équation intégrale définie avec deux distributions scalaires f^d et f^s. Cette dernière étape, qui est possible pour des surfaces topologiques particulières, n'est pas abordée dans cette thèse.

C.5 La thèse

C.5.1 Le formalisme employé

Comme indiqué précédemment, le point de départ des méthodes intégrales est le système des équations de Maxwell. Pour répondre à l'invitation de M. Herberthson dans ses articles, nous avons choisi de reprendre ces équations dans le formalisme des formes différentielles et d'offrir une modélisation complète du phénomène de diffraction en utilisant ce même formalisme. Malgré son existence centenaire (E. Cartan, 1899) et son adoption générale dans la physique théorique fondamentale, les formes différentielles ne sont pas courantes dans le milieu de la modélisation électromagnétique. Toutefois, l'algèbre et le calcul des formes différentielles sont idéalement adaptés à l'étude de l'électromagnétisme. Comme nous le montrons dans le Chapitre 1 (et l'Annexe A), ce formalisme fournit une formulation simple, compacte et élégante des équations de l'électromagnétisme. Dans ce même chapitre, les équations intégrales de frontières conventionnelles, à savoir l'EFIE (voir l'équation C.7), la MFIE et la CFIE, sont formellement dérivées des équations de Maxwell.

C.5.2 Adaptation de l'EFIE et de la MFIE à la diffraction d'ondes planes

Dans le Chapitre 2, nous étudions les équations intégrales des frontières d'un point de vue mathématique, c'est-à-dire que nous considérons un ensemble d'espaces fonctionnels cohérent pour représenter les grandeurs physiques (les champs incident et diffracté, les courants surfaciques,...) et les différents opérateurs. Pour chaque équation (EFIE/MFIE), la littérature nous fournit un jeu d'espaces fonctionnels pour établir l'existence et l'unicité d'une solution au problème de diffraction. Notre objectif est de décrire, au sens mathématique, la solution du problème afin de donner pour chaque équation intégrale, classique ou modifiée d'Herberthson, une formulation forte et faible dans des espaces fonctionnels appropriés. On montre alors que les versions modifiées des équations intégrales, dénotées HEFIE et HMFIE, sont strictement équivalentes d'un point de vue algébrique, puisque:

$$\mathcal{H} = \Psi^{-1}\mathcal{E}\Psi \tag{C.19}$$

où Ψ est l'opérateur de phase (dans l'espace approprié). Au travers l'équivalence des deux opérateurs, on obtient alors les conditions d'existence et d'unicité d'une solution. On montre ensuite que l'opérateur HEFIE $\mathcal{H}$ peut être décrit comme la somme de l'opérateur EFIE $\mathcal{E}$ et d'une perturbation $\mathcal{K}$ telle que:

$$\mathcal{H} = \mathcal{E} + \mathcal{K}. \tag{C.20}$$

Cette représentation s'avère très avantageuse dans le cadre d'une implémentation numérique.

C.5.3 Mise en œuvre numérique

Dans le Chapitre 3, nous commençons par la mise en œuvre pratique de l'équation intégrale. L'objectif ici est de donner tous les éléments nécessaires pour construire les matrices de Galerkin et former les systèmes linéaires. Tout d'abord, nous considérons la mise en œuvre pratique de l'HEFIE dans un espace d'éléments d'arête. L'originalité de notre mise en œuvre repose sur la possibilité de profiter de l'expérience acquise sur l'EFIE, en termes de mise en œuvre et de code éléments finis, en ne se concentrant pas sur l'opérateur HEFIE $\mathcal{H}$ lui-même, mais sur l'opérateur de perturbation $\mathcal{K}$. Cette approche nous conduit à introduire une nouvelle matrice pour représenter la perturbation:

$$H = E + K. \tag{C.21}$$

Nous adoptons la même stratégie pour l'HMFIE.

Dans une deuxième partie, nous étudions la mise en œuvre de la décomposition d'Helmholtz sur l'espace des éléments d'arêtes. L'objectif est de passer du système HEFIE décrit sur la base des éléments d'arêtes à celui suggéré par Herberthson, où la distribution de courant est décomposée en une partie divergente et une partie solénoïdale. À terme, le système final se présente sous la forme d'un 2×2 avec un second membre possédant beaucoup de termes nuls:

$$HJ = C \Longleftrightarrow \begin{pmatrix} H^{DD} & H^{DS} \\ H^{SD} & H^{SS} \end{pmatrix} \begin{pmatrix} J^D \\ J^S \end{pmatrix} = \begin{pmatrix} C^D \\ 0 \end{pmatrix}. \tag{C.22}$$

Pour cela, nous étudions notamment le lien entre les cycles sur le graphe face-arrête du maillage, les combinaisons linéaires de fonctions d'arêtes formant un cycle et éléments appartenant au noyau de la divergence. Finalement, nous formalisons cette décomposition au moyen une matrice de changement de base, creuse et obtenons le système désiré au travers la relation:

$$H = D_H \tilde{H} D_H^{-1} = D_H (E + K_e) D_H^{-1}\,. \tag{C.23}$$

Grâce à cette implémentation, nous avons réalisé deux études distinctes.

- La première concerne l'étude des nouveaux systèmes linéaires (HEFIE / HMFIE) et leur résolution (voir Chapitre 4). Le but était ici d'évaluer s'il est possible, en utilisant une décomposition d'Helmholtz, d'accélérer la résolution en ne se concentrant que sur un sous-espace, à savoir la partie divergente ou la partie solénoïdale du pseudo-courant . Afin de corroborer les résultats de cette étude numérique, nous avons mené une étude analytique détaillée de l'HEFIE en décrivant l'opérateur sur la base des harmoniques sphériques vectorielles dans le cas de la diffraction d'une onde plane par une sphère PEC (voir Chapitre 6).

- La deuxième étude (voir Chapitre 5) porte sur la réduction du nombre de degrés de liberté rendue possible par le fait que le pseudo-courant n'est que faiblement oscillant. Dans cette partie, nous montrons notamment les avantages qu'il peut y avoir à calculer séparément l'opérateur de perturbation. En effet, comme l'opérateur HEFIE H dépend de la direction de l'incidence, lorsque l'on souhaite traiter une ou plusieurs directions d'incidence, en combinant la réduction du nombre de degrés de liberté et un calcul judicieux de la partie perturbation K (qui est la seule partie dépendante de la direction de l'incidence), nous montrons que l'HEFIE peut s'avérer moins coûteuse que l'EFIE.

C.5.4 Résolution des systèmes linéaires

Après l'implémentation des versions modifiées de l'EFIE, de la MFIE et de la CFIE, nous présentons dans le Chapitre 4 certaines propriétés numériques des matrices de Galerkin obtenues et certains aspects de la résolution des systèmes linéaires associés. Pour ce faire, nous avons considéré la diffraction d'une onde plane sur deux objets parfaitement conducteurs: une sphère et un avion.

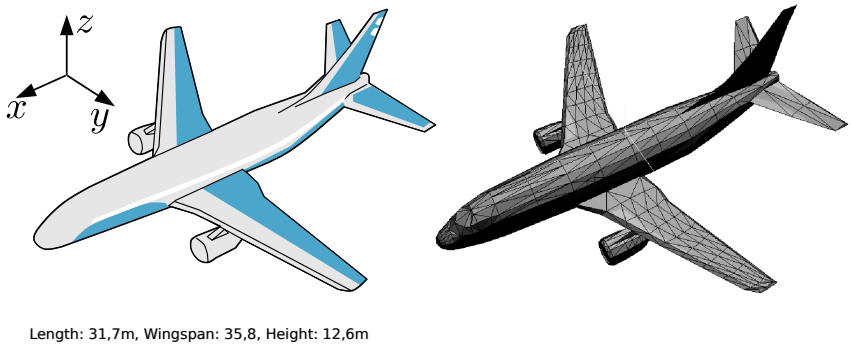

Figure C.3 – L'avion considéré (un Boeing 737) et son maillage.

Afin de choisir une méthode de résolution appropriée (complément Schur, système réduit, ...), il est rapidement apparu nécessaire d'examiner les interactions entre courants divergents et solénoïdaux, qui se reflètent dans les normes de certains blocs de la matrice.

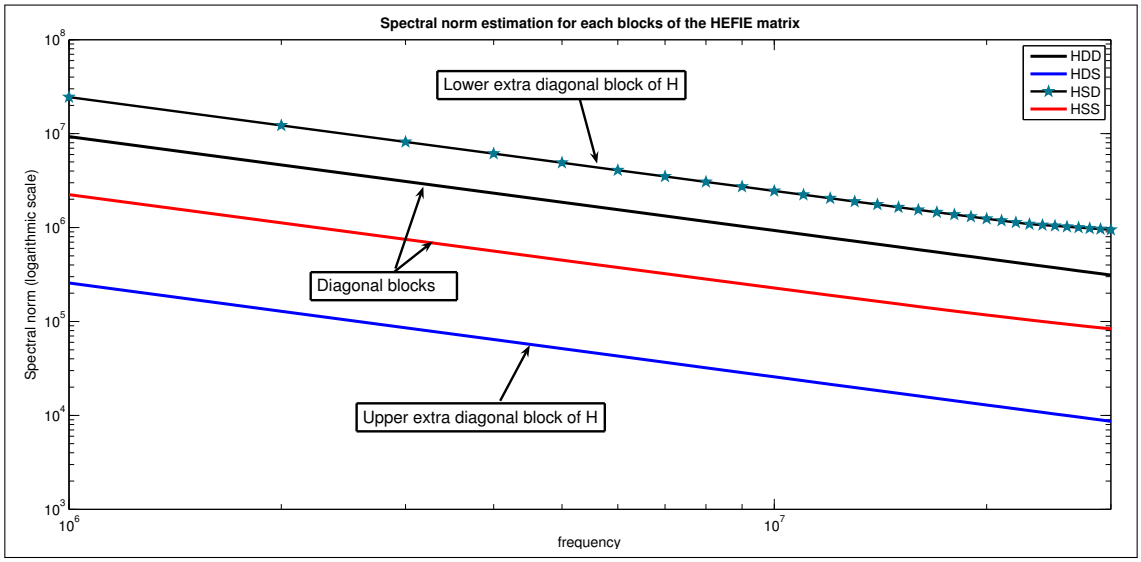

Figure C.4 – Estimation de la norme spectrale de chaque bloc de la matrice H (HEFIE) sur une plage de fréquence pour l'avion (échelle logarithmique).

.

Grâce à l'étude des normes des différents blocs de la matrice (voir par exemple la Figure C.4), on observe, pour les hautes fréquences, un couplage fort entre les parties divergentes et solénoïdales du pseudo-courant, qui est clairement exprimé par la norme élevée des blocs extra-diagonaux inférieurs et supérieurs de la matrice. Ce couplage fort est assez ennuyeux puisqu'il

ne permet pas d'utiliser un système réduit ou un système basé sur le complément Schur pour obtenir une première estimation de la solution. En fait, si nous essayons de résoudre le système formé par le complément Schur :

$$S_e J^D = \left(H^{DD} - H^{DS}(H^{SS})^{-1}H^{SD}\right) J^D = C^D \tag{C.24}$$

avec une méthode de Krylov, comme GMRES, nous observons que la méthode ne converge pas et atteint presque toujours le nombre maximal d'itérations (même en utilisant l'inverse de H^{DD} pour préconditionner le système).

Ensuite, nous examinons la résolution des systèmes linéaires et surtout les préconditionneurs algébriques possibles. Dès lors, pour évaluer les avantages de nos méthodes de résolution, nous commençons par l'analyse des coûts supplémentaires engendrés par la construction de l'HEFIE à partir de l'EFIE (et, de même, pour obtenir l'HMFIE à partir de la MFIE), c'est-à-dire le coût de calcul de la perturbation.

N_G	Algorithmic cost for E		Algorithmic cost for K	
3	$\sim 2.600F^2$	$\sim 1.150N^2$	$\sim 1.482F^2$	$\sim 659N^2$
7	$\sim 13.200F^2$	$\sim 5.850\ N^2$	$\sim 5.694F^2$	$\sim 2.531\ N^2$

Table C.1 – Coût algorithmique du calcul de E et coût supplémentaire pour le calcul de la matrice H. (F: nombre de faces, N: nombre d'arêtes internes, N_G: nombre de points de Gauss utilisés pour les intégrations numériques).

En choisissant le solveur itératif GMRES comme référence, il est possible de traduire ces coûts en un nombre équivalent d'itérations GMRES, afin de voir si les versions de Herberthson sont compétitives. Ensuite, nous proposons divers préconditionneurs, en fonction de nos études et expériences antérieures, et comparons, pour les deux configurations choisies, le nombre d'itérations GMRES nécessaires pour résoudre le système.

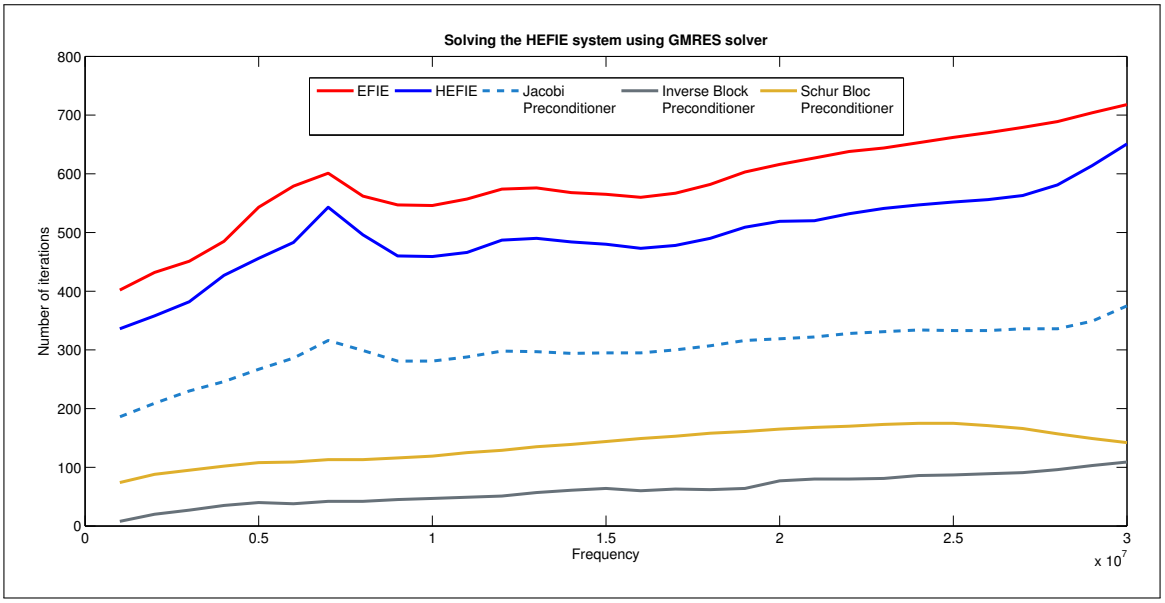

Figure C.5 – Nombre d'itérations requis pour atteindre une erreur résiduelle de 10^{-4}, en fonction de la fréquence pour le système EFIE et le système HEFIE (préconditionné ou non).

.

Nous avons observé que, dans le cas de la sphère, les différents systèmes linéaires sont assez similaires en terme de difficultés, c'est-à-dire pour les deux systèmes, le solveur GMRES a besoin

d'environ le même nombre d'itérations pour atteindre la solution. Il s'est également avéré que les différents préconditionneurs étaient inefficaces dans cette configuration. Ensuite, dans le cas de l'avion, nous avons noté que les versions modifiées étaient plus faciles à résoudre que leurs homologues classiques. Nous avons notamment noté que l'HEFIE exigeait moins d'itérations que l'EFIE et que les préconditionneurs décrits ont un énorme impact, bénéfique, sur le nombre d'itérations. En sommant les différents coûts, il apparait que la combinaison de l'HEFIE et du préconditionneur Jacobi développé coûte un peu moins que l'EFIE conventionnel et que les autres préconditionneurs doivent être approximés (avec par exemple une structure éparse) pour être efficaces en terme de coût CPU.

C.5.5 Réduction du nombre de degrés de liberté

Outre l'analyse des systèmes linéaires et de leur résolution, nous nous sommes intéressés à une autre propriété importante offerte par les équations de Herberthson: la possibilité de réduire le nombre de degrés de liberté requis pour obtenir une solution précise du problème. Dans le Chapitre 5, nous développons cet aspect des équations modifiées. Si l'on considère les équations conventionnelles et la diffraction d'une onde plane de fréquence f_0, une bonne approximation du courant de surface nécessite que les arêtes du maillage aient une taille maximale, h, plus petit que $\lambda_0/7$. Par conséquent, il semblait intéressant de voir si le HEFIE souffre de la même contrainte. Pour tester cela, nous avons étudié la qualité du courant obtenu à partir du HEFIE avec des maillages conformes et non conformes à cette contrainte.

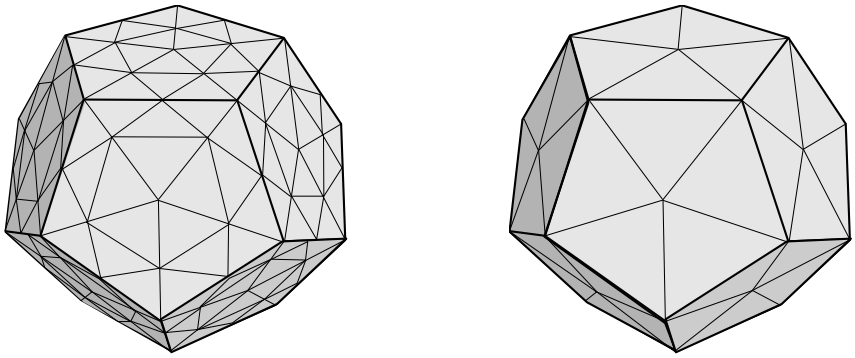

Figure C.6 – À gauche, le maillage requis pour travailler à $f > f_0$. À droite, le maillage sur lequel on pourrait espérer travailler avec l'HEFIE à $f > f_0$.

Il apparaît que les limites du HEFIE soient identiques à celles de l'EFIE, mais pour différentes raisons. Alors que l'EFIE originale souffre à la fois de mauvaises intégrations numériques et d'un maillage non adapté pour la représentation du courant physique, le HEFIE souffre uniquement de mauvaises intégrations numériques.

Afin d'obtenir une bonne solution en termes de courant, nous avons montré qu'il fallait travailler sur un maillage fin. Cependant, à mesure que la taille du système linéaire associé augmente, il est utile de rechercher une alternative. Dès lors, notre objectif fût de créer un système linéaire avec une taille aussi petite que possible qui puisse donner une solution de bonne qualité. L'idée fût alors de considérer deux maillages: un maillage grossier adapté à la représentation du pseudo-courant, mais pas nécessairement conforme à la contrainte " $h < \lambda/7$", et un maillage fin se conformant à cette contrainte et ayant une taille de maille h_{fin} un facteur deux plus petit que le maillage grossier. Notant que les interactions entre les courants locaux définis sur le maillage grossier sont mal décrites, nous proposons de calculer les coefficients de la matrice de Galerkin associée au maillage grossier en utilisant les règles d'intégration associées

au maillage fin.
Pour une raison pratique, nous implémentons cette réduction avec une matrice de projection R. Dans les implémentations futures, cette projection sera intégrée directement dans l'assemblage de la matrice. Notons que, à partir de sa définition, la matrice R est une matrice creuse de taille $N \times 4N$ (où N est le nombre d'inconnus du plus petit système) et seulement 8 coefficients sur chaque ligne. Nous définissons alors:

$$H_{\mathrm{RED}} = RH_{\mathrm{FIN}}R^T, \tag{C.25}$$

$$H_{\mathrm{RED},alt} = RE_{\mathrm{FIN}}R^T + K_{\mathrm{COA}} \tag{C.26}$$

où E_{FIN} et H_{FIN} désignent respectivement les matrices EFIE et HEFIE obtenues à partir du maillage fin et K_{COA} la matrice de perturbation construite à partir du maillage grossier.

Nous avons ensuite évalué les différents systèmes réduits H_{RED} et $H_{\mathrm{RED},alt}$ en termes de qualité du courants obtenus, du coût CPU et du nombre d'itérations requis par GMRES pour la résolution.

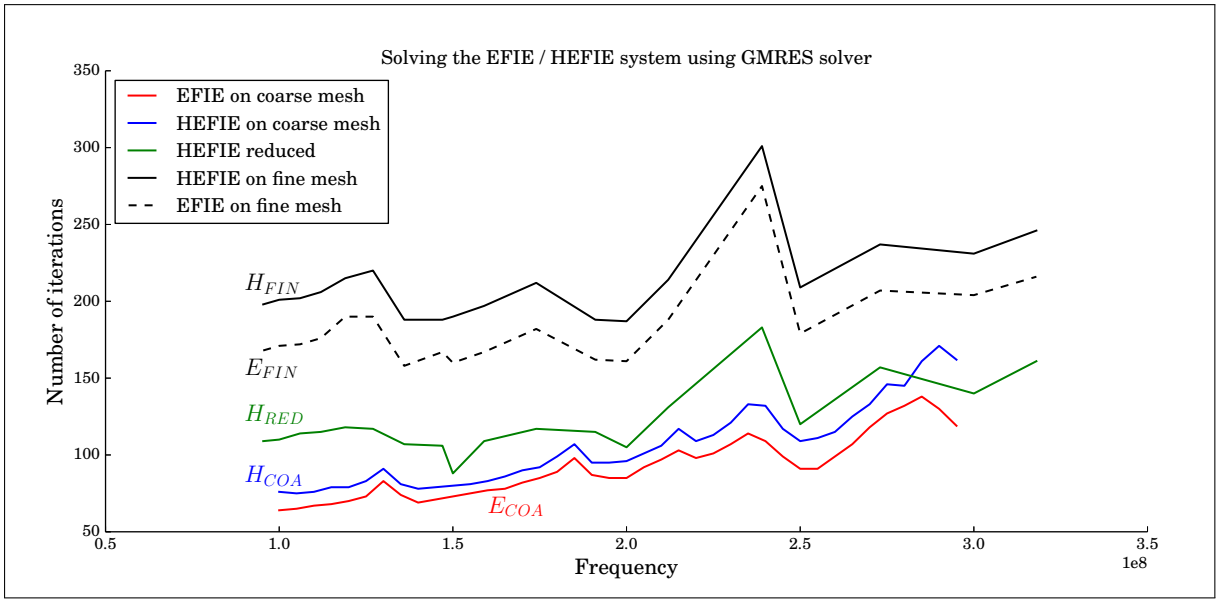

Figure C.7 – Nombre d'itérations requis pour atteindre une erreur résiduelle de 10^{-4} en fonction de la fréquence pour les différents systèmes (non préconditionné) pour la sphère.

.

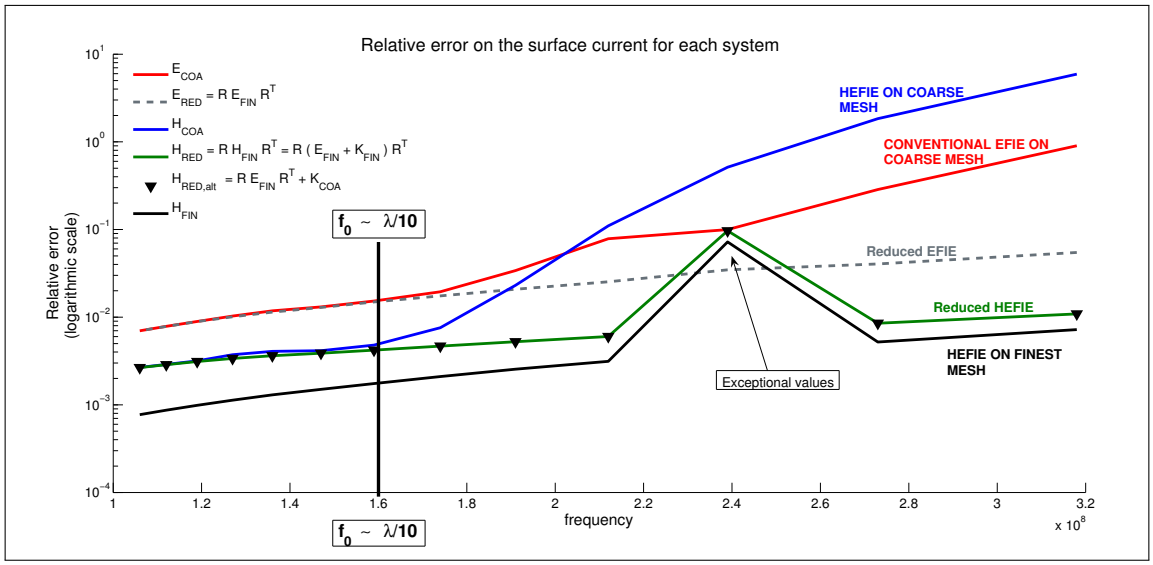

Figure C.8 – Évolution de l'erreur relative commise sur le courant pour chaque système proposé (réduit, conventionnel sur le maillage grossier ou sur le maillage).

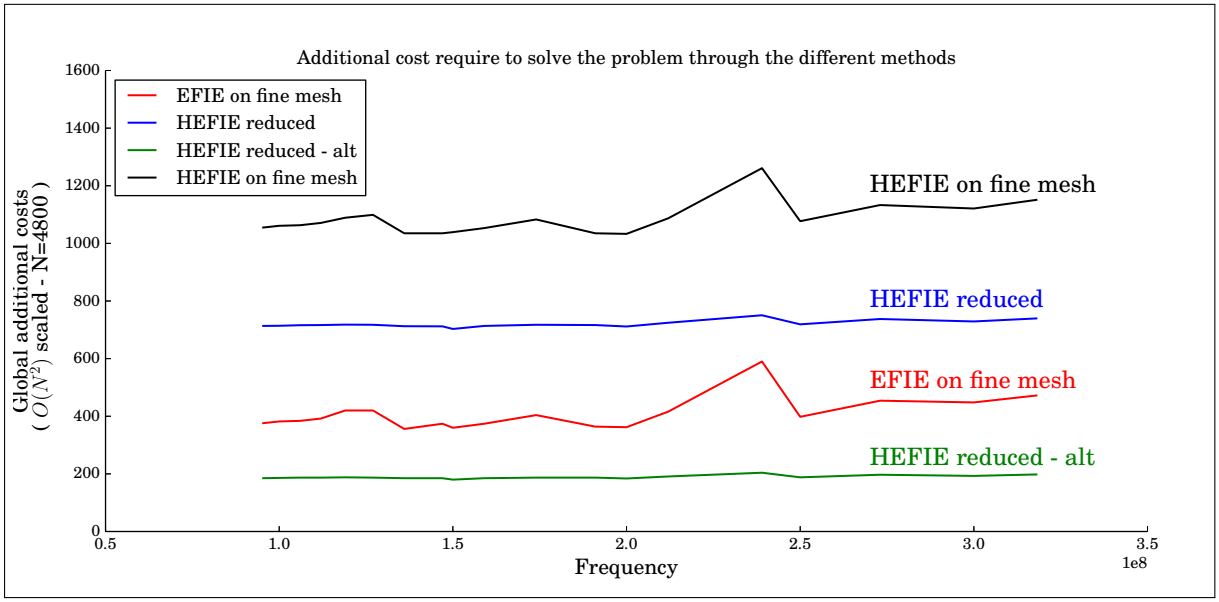

Figure C.9 – Évaluation des coûts supplémentaires, i.e., des coûts totaux moins le coût de calcul de la matrice E_{FIN}, pour les différentes méthodes (coûts supplémentaires = assemblage de K (si nécessaire) + résolution) .

La conclusion tirée des différents tests effectués est que l'HEFIE est utile lorsque le coût d'assemblage de la matrice de perturbation K est faible par rapport au coût de la résolution (typiquement quand le système EFIE est difficile à résoudre). Ensuite, il semble avantageux d'utiliser le système HEFIE réduit, avec K calculé sur un maillage grossier. Cela permet d'obtenir une bonne solution à un coût de calcul inférieur à celui de l'EFIE qui nécessite toujours une discrétisation sur un maillage fin. Cependant, ces perspectives doivent être confirmées par une étude numérique pour un objet de plus grande taille et devraient également être comparées lors de l'utilisation de techniques d'accélération comme FMM ou H-Matrix. De toute évidence, la même stratégie pourrait être appliquée à l'HMFIE (et à l'HCFIE).

Un autre avantage à calculer calculer K séparément apparaît lorsque l'on considère plusieurs directions d'incidence. Si nous voulons gérer un grand nombre d'ondes incidentes différentes, avec l'EFIE, nous devrions envisager la résolution d'un certain nombres de systèmes linéaires:

$$\forall i \in [\![1; N_{RHS}]\!] \; E_{\text{FIN}} X_i = b_i, \tag{C.27}$$

où b_i représente le second membre pour une direction d'incidence donnée θ_i. Dans de nombreux cas d'intérêt, N_{RHS} est un grand nombre. Avec l'EFIE, le problème n'est qu'un système linéaire avec de multiples seconds membres. Avec l'HEFIE, nous devons calculer pour chaque direction une nouvelle matrice H.

Si nous sommes intéressés par plusieurs directions d'incidence, il apparaît rapidement que le coût d'assemblage des matrices H_{RED} est très important par rapport aux autres coûts et que, par conséquent, cette méthode n'est pas adaptée à la résolution de ce type de problème. Pour $H_{\text{RED,alt}}$, nous distinguons deux options.

\+ $H^{+}_{\text{RED,alt}}$
La première consiste à assembler toutes les matrices K_{COA} en même temps que la matrice E_{RED} pour réduire les coûts de construction au détriment d'un coût de stockage devenant important (voir Tableau 5.4).

* $H^{*}_{\text{RED,alt}}$
La deuxième option consiste à assembler chacune des matrices K_{COA} indépendamment (chacune d'elles ayant un coût d'assemblage $\sim 1300N^2$) et à mettre à jour la matrice $H_{\text{RED,alt}}$ à chaque incidence.

Dans les deux cas, le coût d'assemblage est supérieur au coût d'assemblage de E_{FIN}. Cependant, nous sommes amenés à résoudre des systèmes plus petits, potentiellement 16 fois moins coûteux à résoudre. Pour les systèmes alternatifs réduits et EFIE, le coût de la résolution devient vite prédominant lorsque le nombre d'itérations requis pour résoudre le système avec GMRES devient important.

	Assembly cost	Solution cost	Total cost
E_{FIN}	$\simeq 18.400\ N^2$	$32N_E^{iter}N^2$	$(18.400 + 32N_E^{iter})N^2$
H_{RED}	$\simeq 27500\ N^2$	$2N_{RED}^{iter}N^2$	$(27.500 + 2N_{\text{RED}}^{iter})N^2$
$H_{\text{RED,alt}}$	$\simeq 19000\ N^2$	$2N_{RED,alt}^{iter}N^2$	$(19.000 + 2N_{RED,alt}^{iter})N^2$

Table C.2 – Coût algorithmique, nombre d'inconnues et coût de la résolution pour chaque système pour une direction d'incidence (N: nombre de bords internes du maillage grossier).

	Assembly cost	Solution cost	Total cost
E_{FIN}	$18.400\ N^2$	$180 \times 32N_E^{iter}N^2$	$(18.400 + 5760 * N_E^{iter})N^2$
H_{RED}	$(18.400 + 180 \times 9100)\ N^2$	$180 \times 2N_{RED}^{iter}N^2$	$(1.656.400 + 360 * N_{RED}^{iter})N^2$
$H^{+}_{\text{RED,alt}}$	$(18.400 + 180 \times 650)\ N^2$	$180 \times 2N_{RED,alt}^{iter}N^2$	$(135.400 + 360 * N_{RED,alt}^{iter})N^2$
$H^{*}_{\text{RED,alt}}$	$(18.400 + 180 \times 1300)\ N^2$	$180 \times 2N_{RED,alt}^{iter}N^2$	$(234.000 + 360 * N_{RED,alt}^{iter})N^2$

Table C.3 – Coût algorithmique de l'assemblage et de la résolution du problème pour chaque méthode, pour $N_{RHS} = 180$ directions d'incidence (N: nombre d'arêtes internes du maillage grossier). Dans ce tableau, N^{iter} doit être interprété comme un nombre moyen d'itérations requises pour obtenir une erreur résiduelle fixée et unique.

C.5.6 Un cas de référence : la diffraction d'une onde plane par une sphère parfaitement conductrice

En complément des travaux présentés ci-dessus, nous avons également étudié analytiquement l'HEFIE et son opérateur dans le cas particulier de la diffraction d'une onde plane par une sphère parfaitement conductrice. Le but du Chapitre 6 est d'obtenir les expressions des coefficients de l'opérateur HEFIE sur la base des harmoniques sphériques vectorielles, puis d'étudier les normes de l'opérateur, en particulier celles liées au couplage entre les parties divergentes et solénoïdales du pseudo-courant.
Étant donné que l'opérateur EFIE est diagonal dans cette base d'harmonique, nous profitons de la relation de similarité développée dans le Chapitre 2, pour obtenir une représentation complète de l'HEFIE. La principale difficulté est alors de trouver une représentation de l'opérateur Ψ sur la base des harmoniques sphériques vectorielles.
Avec une représentation de l'opérateur Ψ (et de son inverse) sur la base des harmoniques sphériques vectorielles et en utilisant la relation de similarité entre l'EFIE et l'HEFIE, nous obtenons une représentation explicite de l'HEFIE. Étant donné que ces matrices de transformation sont essentiellement des matrices bandes, et en utilisant le fait que l'EFIE a une représentation matricielle diagonale, on obtient une représentation matricielle de l'HEFIE. Cette dernière représentation nous donne alors un autre point de vue sur certains aspects de l'HEFIE et de la décomposition d'Helmholtz.

Bibliography

[1] A. Taflove and S.C. Hagness. *Computational Electrodynamics: The Finite-Difference Time-Domain Method, Third Edition.* Artech House, 2005.

[2] J.M. Jin. *The Finite Element Method in Electromagnetics.* Wiley, 2015.

[3] A. Bendali. Numerical Analysis of the Exterior Boundary Value Problem for the Time-Harmonic Maxwell Equations by a Boundary Finite Element Method Part 1: The Continuous Problem. *Mathematics of Computation*, 43(167):29–46, 1984.

[4] A. Bendali. Numerical Analysis of the Exterior Boundary Value Problem for the Time-Harmonic Maxwell Equations by a Boundary Finite Element Method Part 2: The Discrete Problem. *Mathematics of Computation*, 43(167):47–68, 1984.

[5] Walton C. Gibson. *The Method of Moments in Electromagnetics.* Chapman and Hall/CRC, 2007.

[6] Y. Saad. *Iterative Methods for Sparse Linear Systems, 2nd Edition.* EngineeringPro collection. Society for Industrial and Applied Mathematics, 2003.

[7] Eric Darve. *Méthodes multipôles rapides : résolution des équations de Maxwell par formulations intégrales.* PhD thesis, Paris 6, 1999.

[8] Pascal Havé . *Fast Multipole Methods for electromagnetism : Parallelism and low frequencies.* PhD thesis, Université Pierre et Marie Curie - Paris VI, May 2004.

[9] Guillaume Sylvand. *La méthode multipôle rapide en électromagnétisme. Performances, parallélisation, applications.* PhD Thesis, Ecole des Ponts ParisTech, June 2002.

[10] S. Rjasanow and O. Steinbach. *The Fast Solution of Boundary Integral Equations.* Mathematical and Analytical Techniques with Applications to Engineering. Springer US, 2007.

[11] Levadoux, David and Michielsen, Bas. *A New Class of Integral Equations for Scattering Problems*, pages 227–232. Mathematical and Numerical Aspects of Wave Propagation WAVES 2003, Springer Berlin Heidelberg, 2003.

[12] S. Borel F. Alouges and D.P. Levadoux. A stable well-conditioned integral equation for electromagnetism scattering . *Journal of Computational and Applied Mathematics* , 204(2):440 – 451, 2007. Special Issue: The Seventh International Conference on Mathematical and Numerical Aspects of Waves (WAVES'05).

[13] Snorre H. Christiansen and Jean-Claude Nédélec. A Preconditioner for the Electric Field Integral Equation Based on Calderon Formulas. *SIAM Journal on Numerical Analysis*, 40(3):1100–1135, 2002.

[14] V. Rokhlin. Rapid Solution of Integral Equations of Scattering Theory in Two Dimensions. *J. Comput. Phys.*, 86(2):414–439, February 1990.

[15] F.X. Canning. The impedance matrix localization (IML) method for moment-method calculations. *IEEE Antennas and Propagation Magazine*, 32(5):18–30, Oct 1990.

[16] Bin Zhou. *Méthode des équations intégrales pour la résolution des problèmes de diffraction à hautes frequences.* PhD thesis, Paris 11, 1995.

[17] T. Abboud, J.-C. Nédélec and B. Zhou. Méthodes des équations intégrales pour les hautes fréquences. *C. R. Acad. Sci. Paris*, (318):165–170, 1994.

[18] T. Abboud, J.-C. Nédélec and B. Zhou. Improvement of the integral equation method for high frequency problems. *Third International Conference on Mathematical and Numerical Aspects of Wave Propagation*, pages 178–187, 1995.

[19] Marc Tolentino. *Résolution hautes fréquences d'équations intégrales par une méthode de discrétisation microlocale.* Theses, Ecole des Ponts ParisTech, December 1997.

[20] Armel de La Bourdonnaye. High frequency approximation of integral equations modeling scattering phenomena. *ESAIM: Mathematical Modelling and Numerical Analysis - Modélisation Mathématique et Analyse Numérique*, 28(2):223–241, 1994.

[21] Eric Darrigrand. *Couplage Methodes Multipoles - Discretisation Microlocale pour les Equations Integrales de l'Electromagnetisme.* PhD Thesis, Université Sciences et Technologies - Bordeaux I, Sep 2002.

[22] Alain Bachelot, Eric Darrigrand and Katherine Mer-Nkonga . Coupling of a multilevel fast multipole method and a microlocal discretization for the 3-D integral equations of electromagnetism. *Comptes Rendus Mathematique*, 336(6):505 – 510, 2003.

[23] Eric Darrigrand. Coupling of Fast Multipole Method and Microlocal Discretization for the 3-D Helmholtz Equation, 2001. Rapport interne n 0119 du LRC-CEA MAB.

[24] M. Herberthson. Validation of the Potential Method ; Comparing measurements of a dihedral with calculations . *Scientific Computing in Electrical Engineering conference, Zurich*, 2012.

[25] Magnus Herberthson. EM Scattering Calculations Using Potentials. *Scientific Computing in Electrical Engineering SCEE 2008*, pages 375–382, 2010.

[26] Magnus Herberthson. Application of the Potential Method to the Combined Field Integral Equation. *Scientific Computing in Electrical Engineering SCEE 2010 (Abstract book)*, pages 103–104, 2012.

[27] G.A. Deschamps. Electromagnetics and differential forms. *Proceedings of the IEEE*, 69:676–96, June 1981.

[28] Ismo V. Lindell. *Differential Forms in Electromagnetics.* Wiley-IEEE Press, 2004.

[29] K.F. Warnick. *A Differential Forms Approach to Electromagnetics in Anisotropic Media.* PhD thesis, Brigham Young University, United States, 2003 (first publication : 1997).

[30] David J. Griffiths. *Introduction to Electrodynamics (3rd Edition).* Prentice Hall, 1999.

[31] John L. Volakis and Kubilay Sertel. *Integral Equation Methods for Electromagnetics (Electromagnetics and Radar)*. SciTech Publishing, 2012.

[32] H. Flanders. *Differential Forms with Applications to the Physical Sciences*. Dover books on advanced mathematics. Dover Publications, 1963.

[33] Stephen C. Preston . An introduction to Differential Geometry. , :, April 2013.

[34] Manfredo P. Do Carmo. *Differential Forms and Applications (Universitext)*. Springer, 2013.

[35] Hans Samelson. Differential Forms, the Early Days; or the Stories of Deahna's Theorem and of Volterra's Theorem. *The American Mathematical Monthly*, 108(6):522–530, 2001.

[36] A. Bossavit. Differential forms and the computation of fields and forces in electromagnetism. *European Journal of Mechanics, B/Fluids*, pages 474–488, 1991.

[37] Karl F. Warnick and David V. Arnold. Electromagnetic Green functions using differential forms. *Journal of Electromagnetic Waves and Applications*, 10(3):427–438, 1996.

[38] K.F. Warnick, R.H. Selfridge and D.V. Arnold. Teaching electromagnetic field theory using differential forms. *IEEE Transactions on Education*, 40(1):53–68, Feb 1997.

[39] K.F. Warnick, R.H. Selfridge and D.V. Arnold. Electromagnetic boundary conditions and differential forms. *IEE Proceedings - Microwaves, Antennas and Propagation*, 142(4):326–332, Aug 1995.

[40] Masao Kitano. *Reformulation of Electromagnetism with Differential Forms*. InTech, dr. victor barsan (ed.) edition, 2012.

[41] Stefan Kurz and Bernhard Auchmann. *Differential Forms and Boundary Integral Equations for Maxwell-Type Problems*, pages 1–62. Springer Berlin Heidelberg, Berlin, Heidelberg, 2012.

[42] Robin W. Tucker. Differential form valued forms and distributional electromagnetic sources. *Journal of Mathematical Physics*, 50(3), 2009.

[43] R. Hiptmair. Finite elements in computational electromagnetism. *Acta Numerica*, 11:237–339, 1 2002.

[44] J.E. Marsden and Tudor Ratiu. *Introduction to Mechanics and Symmetry: A Basic Exposition of Classical Mechanical Systems (Texts in Applied Mathematics)*. Springer, 2002.

[45] K.F. Warnick and D.V. Arnold . Green Forms for Anisotropic, Inhomogeneous Media. *Journal of Electromagnetic Waves and Applications*, 11(8):1145–1164, 1997.

[46] D. Baldomir. Differential forms and electromagnetism in 3-dimensional Euclidean space R3. *IEE Proceedings A - Physical Science, Measurement and Instrumentation, Management and Education - Reviews*, 133(3):139–143, May 1986.

[47] Roger Petit. *Ondes électromagnétiques en radioélectricité et en optique*. Dunod, 1997.

[48] J.A. Stratton and L. J. Chu. Diffraction Theory of Electromagnetic Waves. *Phys. Rev.*, 56:99–107, Jul 1939.

[49] Snorre H. Christiansen. Discrete Fredholm properties and convergence estimates for the electric field integral equation. *Mathematics of computation*, 73(245):143–168, 2004.

[50] J.C. Nédélec. *Acoustic and Electromagnetic Equations: Integral Representations for Harmonic Problems*. Number vol. 144 in Acoustic and electromagnetic equations: integral representations for harmonic problems. Springer, 2001.

[51] Cyril Safa. *Résolution rapide d'équations intégrales pour un problème d'antennes par des méthodes d'ondelettes*. PhD thesis, Université de Rennes 1, Septembre 2001.

[52] Harsh Bhatia, Gregory Norgard, Valerio Pascucci and Peer-Timo Bremer. The Helmholtz-Hodge Decomposition : A Survey. *IEEE Transactions on Visualization and Computer Graphics*, 19(8):1386–1404, August 2013.

[53] R. Hiptmair and C. Schwab. Natural Boundary Element Methods for the Electric Field Integral Equation on Polyhedra. *SIAM J. Numer. Anal.*, 40(1):66–86, January 2002.

[54] A. Buffa, M. Costabel and D. Sheen. On traces for $H(curl, \Omega)$ in Lipschitz domains. *Journal of Mathematical Analysis and Applications*, 276(2):845 – 867, 2002.

[55] S. Sauter and C. Schwab. *Boundary Element Methods*. Springer Series in Computational Mathematics. Springer Berlin Heidelberg, 2010.

[56] S. Rao, D. Wilton and A. Glisson. Electromagnetic scattering by surfaces of arbitrary shape. *IEEE Transactions on Antennas and Propagation*, 30(3):409–418, May 1982.

[57] Jin-Fa Lee, R. Lee and R. J. Burkholder. Loop star basis functions and a robust preconditioner for EFIE scattering problems. *IEEE Transactions on Antennas and Propagation*, 51(8):1855–1863, Aug 2003.

[58] F.P. Andriulli. Loop-Star and Loop-Tree Decompositions: Analysis and Efficient Algorithms. *IEEE Transactions on Antennas and Propagation*, 60(5):2347–2356, May 2012.

[59] G. Vecchi. Loop-star decomposition of basis functions in the discretization of the EFIE. *IEEE Transactions on Antennas and Propagation*, 47(2):339–346, Feb 1999.

[60] F. P. Andriulli and G. Vecchi. A Helmholtz-Stable Fast Solution of the Electric Field Integral Equation. *IEEE Transactions on Antennas and Propagation*, 60(5):2357–2366, May 2012.

[61] John Adrian Bondy and U.S.R. Murty. *Graph Theory With Applications*. Elsevier Science Ltd/North-Holland, 1976.

[62] Adrian Bondy and U.S.R. Murty. *Graph Theory (Graduate Texts in Mathematics)*. Springer, 2008.

[63] Reinhard Diestel. *Graph Theory (Graduate Texts in Mathematics)*. Springer, 2010.

[64] Shimon Even. *Graph Algorithms*. Cambridge University Press, 2011.

[65] T.F. Eibert. Iterative-solver convergence for loop-star and loop-tree decompositions in method-of-moments solutions of the electric-field integral equation. *IEEE Antennas and Propagation Magazine*, 46(3):80–85, June 2004.

[66] M. B. Stephanson and J.F. Lee. Preconditioned Electric Field Integral Equation Using Calderon Identities and Dual Loop/Star Basis Functions. *IEEE Transactions on Antennas and Propagation*, 57(4):1274–1279, April 2009.

[67] Michele Benzi and Miroslav Tûma. A comparative study of sparse approximate inverse preconditioners. *Applied Numerical Mathematics*, 30(2):305 – 340, 1999.

[68] F. Vipiana, G. Vecchi and P. Pirinoli. A Multiresolution System of Rao-Wilton-Glisson Functions. *IEEE Transactions on Antennas and Propagation*, 55(3):924–930, March 2007.

[69] F. Vipiana, P. Pirinoli and G. Vecchi. A multiresolution method of moments for triangular meshes. *IEEE Transactions on Antennas and Propagation*, 53(7):2247–2258, July 2005.

[70] J.A. Stratton. *Electromagnetic Theory*. IEEE Antennas and Propagation Society. Wiley, 2007.

[71] R.F. Harrington. *Time-Harmonic Electromagnetic Fields*. IEEE Press Series on Electromagnetic Wave Theory. Wiley, 2001.

[72] S. J. Claessens. New relations among associated Legendre functions and spherical harmonics. *Journal of Geodesy*, 79:398–406, 2005.

[73] I.S. Gradshteyn and I.M. Ryzhik. *Table of Integrals, Series, and Products*. Table of Integrals, Series, and Products Series. Elsevier Science, 2007.

[74] Felipe Vico, Leslie Greengard and Zydrunas Gimbutas. Boundary Integral Equation Analysis on the Sphere. *Numer. Math.*, 128(3):463–487, November 2014.

[75] R. W. Scharstein. Helmholtz decomposition of surface electric current in electromagnetic scattering problems. In *System Theory, Proceedings of the Twenty-Third Southeastern Symposium*, pages 424–426, Mar 1991.

[76] H.A. Mavromatis and R.S. Alassar. A generalized formula for the integral of three associated Legendre polynomials . *Applied Mathematics Letters* , 12(3):101 – 105, 1999.

[77] James H. Luscombe and Marshall Luban. Simplified recursive algorithm for Wigner $3j$ and $6j$ symbols. *Phys. Rev. E*, 57:7274–7277, Jun 1998.

[78] Billy C. Brock. Using Vector Spherical Harmonics to Compute Antenna Mutual Impedance from Measured or Computed Fields . pages 45–62, Appendix III, April 2001.

[79] W. Hackbusch. A Sparse Matrix Arithmetic Based on H-matrices. Part I: Introduction to H-matrices. *Computing*, 62(2):89–108, May 1999.

[80] Wolfgang Hackbusch. *Hierarchical Matrices: Algorithms and Analysis (Springer Series in Computational Mathematics)*. Springer, 2015.

[81] Mario Bebendorf. *Hierarchical Matrices: A Means to Efficiently Solve Elliptic Boundary Value Problems (Lecture Notes in Computational Science and Engineering)*. Springer, 2008.

[82] L. Grasedyck. Adaptive Recompression of H-Matrices for BEM. *Computing*, 74(3):205–223, 2005.

[83] Guillaume Alléon, Michele Benzi and Luc Giraud. Sparse approximate inverse preconditioning for dense linear systems arising in computational electromagnetics. *Numerical Algorithms*, 16(1):1–15, 1997.

[84] M. Bebendorf. Hierarchical LU decomposition-based preconditioners for BEM. *Computing (Vienna/New York)*, 74(3):225–247, 2005. cited By 58.

[85] Steffen Börm, Lars Grasedyck and Wolfgang Hackbusch. Hierarchical matrices. Technical report, Max Planck Institute for Mathematics in the Sciences, 2003.

[86] M. Bluck, N. Cinosi and S. Walker. A multilevel hierarchical preconditioner technique for multiscale and complex EM scattering bodies. In *Electromagnetics in Advanced Applications (ICEAA), 2013 International Conference on*, pages 1519–1522, Sept 2013.

[87] F.P. Andriulli, F. Vipiana and G. Vecchi. Hierarchical Bases for Nonhierarchic 3-D Triangular Meshes. *IEEE Transactions on Antennas and Propagation*, 56(8):2288–2297, Aug 2008.

[88] John Lee. *Introduction to Smooth Manifolds (Graduate Texts in Mathematics, Vol. 218)*. Springer, 2012.

[89] Yvonne Choquet-Bruhat and Cecile DeWitt-Morette. *Analysis, Manifolds and Physics, Part 1: Basics*. North Holland, 1982.

[90] Y. Choquet-Bruhat and C. DeWitt-Morette. *Analysis, Manifolds and Physics, Part 2*. Elsevier, 2000.

[91] T. Kato. *Perturbation Theory for Linear Operators*. Classics in Mathematics. Springer Berlin Heidelberg, 1995.

[92] V. I. Ivakhnenko, Yu G. Smirnov and E. Tyrtyshnikov. The electric field integral equation: theory and algorithms. In *Approximations and numerical methods for the solution of Maxwell's equations (Oxford, 1995)*, pages 251–262. Clarendon Press New York, 1998.

[93] A. Buffa and P. Ciarlet. On traces for functional spaces related to Maxwell's equations Part II: Hodge decompositions on the boundary of Lipschitz polyhedra and applications. *Mathematical Methods in the Applied Sciences*, 24(1):31–48, 2001.

[94] S.N.Chandler-Wilde, D.P. Hewett, and A. Moiola. Interpolation of Hilbert and Sobolev Spaces: Quantitative Estimates and Counterexamples. *ArXiv e-prints*, April 2014.

[95] G. Hsiao and W.L. Wendland. *Boundary Integral Equations*. Applied Mathematical Sciences. Springer Berlin Heidelberg, 2008.

[96] Gabriel N. Gatica. *Raviart-Thomas Spaces*, pages 61–91. A Simple Introduction to the Mixed Finite Element Method: Theory and Applications, Springer International Publishing, Cham, 2014.

[97] Snorre H. Christiansen. *Résolution des équations intégrales pour la diffraction d'ondes acoustiques et électromagnétiques - Stabilisation d'algorithmes itératifs et aspects de l'analyse numérique*. Theses, Ecole Polytechnique X, January 2002.

[98] L. Todjihounde. *Calcul différentiel 2e édition*. éditions cépaduès.

[99] Robert Dautray and Jacques-Louis Lions. *Mathematical Analysis and Numerical Methods for Science and Technology: Volume 2 Functional and Variational Methods*. Springer, 2013.

[100] J.E. Roberts and J.-M. Thomas. Mixed and hybrid methods . In *Finite Element Methods (Part 1)*, volume 2 of *Handbook of Numerical Analysis*, pages 523 – 639. Elsevier, 1991.

[101] Christine Bernardi, Claudio Canuto and Yvon Maday. Generalized Inf-Sup Conditions for Chebyshev Spectral Approximation of the Stokes Problem. *SIAM Journal on Numerical Analysis*, 25(6):1237–1271, 1988.

[102] Y. Goldman, P. Joly, M. Kern and J.-C. Nédélec. The electric field in the conductive half space as a model in mining and petroleum prospecting. *Mathematical Methods in the Applied Sciences*, 11(3):373–401, 1989.

[103] L. Demkowicz. Asymptotic convergence in finite and boundary element methods: part 1: theoretical results. *Computers and Mathematics with Applications*, 27(12):69 – 84, 1994.

[104] I. Babuška. Error-Bounds for Finite Element Method. *Numerische Mathematik*, 16:322–333, 1970/71.

[105] H. Brézis, P.G. Ciarlet and J.L. Lions. *Analyse fonctionnelle: théorie et applications*. Collection Mathématiques appliquées pour la maîtrise. Dunod, 1999.